High Capacity Multiuser Multiantenna Communication Techniques

By

Walid Al-Hussaibi

A Thesis Submitted for the Degree of Doctor of Philosophy

School of Engineering and Informatics

University of Sussex

September 2011

Declaration

I hereby declare that this thesis has not been submitted, either in the same or different form, to this or any other University for a degree and the work produced here is my own except stated otherwise.

Signature: .....

Walid Al-Hussaibi
Date:

University of Sussex

Thesis Submitted in Fulfilment of the Requirements for the Degree of
Doctor of Philosophy

High Capacity Multiuser Multiantenna Communication Techniques

By: Walid Al-Hussaibi

Summary

One of the main issues involved in the development of future wireless communication systems is the multiple access technique used to efficiently share the available spectrum among users. In rich multipath environment, spatial dimension can be exploited to meet the increasing number of users and their demands without consuming extra bandwidth and power. Therefore, it is utilized in the multiple-input multiple-output (MIMO) technology to increase the spectral efficiency significantly. However, multiuser MIMO (MU-MIMO) systems are still challenging to be widely adopted in next generation standards. In this thesis, new techniques are proposed to increase the channel and user capacity and improve the error performance of MU-MIMO over Rayleigh fading channel environment.

For realistic system design and performance evaluation, channel correlation is considered as one of the main channel impurities due its severe influence on capacity and reliability. Two simple methods called generalized successive coloring technique (GSCT) and generalized iterative coloring technique (GICT) are proposed for accurate generation of correlated Rayleigh fading channels (CRFC). They are designed to overcome the shortcomings of existing methods by avoiding factorization of desired covariance matrix of the Gaussian samples. The superiority of these techniques is demonstrated by extensive simulations of different practical system scenarios.

To mitigate the effects of channel correlations, a novel constellation constrained MU-MIMO (CC-MU-MIMO) scheme is proposed using transmit signal design and maximum likelihood joint detection (MLJD) at the receiver. It is designed to maximize the channel capacity and error performance based on principles of maximizing the minimum Euclidean distance (d_{min}) of composite received signals. Two signal design methods named as unequal power allocation (UPA) and rotation constellation (RC) are utilized to resolve the detection ambiguity caused by correlation. Extensive analysis and simulations demonstrate the effectiveness of considered scheme compared with conventional MU-MIMO. Furthermore, significant gain in SNR is achieved particularly in moderate to high correlations which have direct impact to maintain high user capacity.

A new efficient receive antenna selection (RAS) technique referred to as phase difference based selection (PDBS) is proposed for single and multiuser MIMO systems to maximize the capacity over CRFC. It utilizes the received signal constellation to select the subset of antennas with highest d_{min} constellations due to its direct impact on the capacity and BER performance. A low complexity algorithm is designed by employing the Euclidean norm of channel matrix rows with their corresponding phase differences. Capacity analysis and simulation results show that PDBS outperforms norm based selection (NBS) and near to optimal selection (OS) for all correlation and SNR values. This technique provides fast RAS to capture most of the gains promised by multiantenna systems over different channel conditions.

Finally, novel group layered MU-MIMO (GL-MU-MIMO) scheme is introduced to exploit the available spectrum for higher user capacity with affordable complexity. It takes the advantages of spatial difference among users and power control at base station to increase the number of users beyond the available number of RF chains. It is achieved by dividing the users into two groups according to their received power, high power group (HPG) and low power group (LPG). Different configurations of low complexity group layered multiuser detection (GL-MUD) and group power allocation ratio (η) are utilized to provide a valuable tradeoff between complexity and overall system performance. Furthermore, RAS diversity is incorporated by using NBS and a new selection algorithm called HPG-PDBS to increase the channel capacity and enhance the error performance. Extensive analysis and simulations demonstrate the superiority of proposed scheme compared with conventional MU-MIMO. By using appropriate value of η, it shows higher sum rate capacity and substantial increase in the user capacity up to two-fold at target BER and SNR values.

Acknowledgements

A few words mention here cannot adequately capture all my appreciation to those who supported me during the development of this thesis.

First of all, I would like to express my sincere gratitude and obligation to my supervisor Dr. Falah Ali for his support, guidance and encouragement during the period of my study in UK. The contributions of this thesis are the results of numerous discussions we had on multiuser wireless systems. His insights and innovative thinking have the main influence to give a solid shape to this thesis.

My special thanks to Dr. Elias Stipidis for his help and support throughout my study. It was a great privilege and joy to work under the guidance of my supervisors in communication research group (COMMS), which enriched the path towards research project completion. I would like to express my deep gratitude and great thanks to all my friends and colleagues in UK and outside for their valuable support and encouragement. Some of them in no particular order are: Cai, Indu, Shahin, Bilal, Marwan, Saif, James, Periklis, Georege, Ian, Najeeb, Fadhil, Yaseen, and Hameed.

My sincere gratitude must go to my parents whose life inspired and nourished me for higher levels of education. Their love and prayers smoothed my way for better future. In the same line, the unlimited support and encouragements of my brothers and sisters have the direct impact on the success in my life. I must extend my thanks and obligations to them and their family members.

Last but not least, all my love and sincere gratitude go to my dear wife and lovely kids Khaldoon, Reem and Rose. I would not be able to reach this step without their patience to see me spending most of the time building this work. I would like to take this opportunity to dedicate this thesis to them and those who pray for me to be in success all the time.

"*It is dangerous to put limits on wireless*."

Guglielmo Marconi (1932)

List of publications

- W. Al-Hussaibi, F. Ali and E. Stipidis, "A Simple 2-User Multiple Access Technique Using Fading Signatures and Space Diversity," *Proc. LAPC2009*, Loughborough, UK, vol. 1, pp. 433-436, Nov. 2009.
- W. Al-Hussaibi, and F. Ali, "On the Generation of Correlated Rayleigh Fading Envelopes for Multi-Antenna Systems," *Proc. 7th Innovations'11*, Al Ain and Abu Dhabi, UAE, pp. 12- 17, April 2011.
- W. Al-Hussaibi, and F. Ali, "On the Capacity Region of Promising Multiple Access Techniques," *Proc. 12th PGNet2011*, Liverpool, UK, pp. 403-408, June 2011.
- W. Al-Hussaibi, and F. Ali, "Iterative Coloring Technique for the Generation of Correlated Rayleigh Fading Envelopes for Multi-Antenna and Multicarrier Systems," *Proc. 12th PGNet2011*, Liverpool, UK, pp. 103-108, June 2011.
- W. Al-Hussaibi, and F. Ali, "Receive Antenna Selection for Uplink Multiuser MIMO Systems over Correlated Rayleigh Fading Channels," *Proc. 14th WPMC'11*, Brest, France, pp. 388-392, 3-7 October 2011.
- W. Al-Hussaibi, and F. Ali, "Generation of Correlated Rayleigh Fading Channels for Accurate Simulation of Promising Wireless Communication Systems," *Submitted in May 2011 to Elsevier: Simulation Modelling Practice and Theory, Revised in Nov.2011.*
- W. Al-Hussaibi, and F. Ali, "Fast Receive Antenna Selection for Spatial Multiplexing MIMO over Correlated Rayleigh Fading Channels," *Submitted to Springer: Wireless Personal Communications, Sep. 2011.*
- W. Al-Hussaibi, and F. Ali, "Low Complexity Receive Antenna Selection for Uplink Multiuser MIMO Systems over Correlated Rayleigh Fading Channels," *Submitted to IEEE Transaction on Vehicular Technology, Sep. 2011.*
- W. Al-Hussaibi, and F. Ali, "Constellation Constrained MU-MIMO System for Higher Sum Rate Capacity and Error Performance over Correlated Channels," *To be submitted in Nov. 2011 to Wiley: Wireless Communication and Mobile Computing.*
- W. Al-Hussaibi, and F. Ali, "High User Capacity Group Layered Multiuser Multiantenna System with Low Complexity Detection and Receive Antenna Selection Diversity," *To be submitted in Dec. 2011 to: IEEE Transaction on Wireless Communications.*

Table of Contents

List of Abbreviations

3G	Third Generation
3GPP	Third Generation Partnership Project
4G	Fourth Generation
AWGN	Additive White Gaussian Noise
BC	Broadcast Channel
BD	Block Diagonalization
BER	Bit Error Rate
BPSK	Binary Phase Shift Keying
BS	Base Station
CBS	Correlation Based Selection
CCMA	Collaborative Coding Multiple Access
CC-MU-MIMO	Constellation Constrained Multiuser Multiple-Input Multiple-Output
CDMA	Code Division Multiple Access
CEO	Cross Entropy Optimization
CRFC	Correlated Rayleigh Fading Channel
CSI	Channel State Information
CSIR	Channel State Information at the Receiver
CSIT	Channel State Information at the Transmitter
DFT	Discrete Fourier Transform
DL	Downlink
d_{min}	Minimum Euclidean Distance
DoF	Degree of Freedom
DPC	Dirty Paper Coding
DSA	Decremental Selection Algorithm
DS-SS	Direct Sequence Spread Spectrum
EGC	Equal Gain Combining
EPA	Equal Power Allocation
FDMA	Frequency Division Multiple Access
GA	Genetic Algorithm
GICT	Generalized Iterative Coloring Technique
GL-MUD	Group Layered Multiuser Detection
GL-MU-MIMO	Group Layered Multiuser Multiple-Input Multiple-Output
GPRS	General Packet Radio Service
GSC	Generalized Selection Combining

GSCT	Generalized Successive Coloring Technique
GSD	Generalized Sphere Decoding
GSIC	Group Successive Interference Cancellation
GSM	Global System for Mobile Communications
HPG	High Power Group
HPG-MUD	High Power Group Multiuser Detection
HPG-PDBS	High Power Group Phase Difference Based Selection
i.i.d	independently identically distributed
IC	Identical Constellation
IC-BPSK	Identical Constellation Binary Phase Shift Keying
IC-QAM	Identical Constellation Quadrature Amplitude Modulation
IC-QPSK	Identical Constellation Quadrature Phase Shift Keying
ICSI	Instantaneous Channel State Information
ICT	Iterative Coloring Technique
IMT	International Mobile Telecommunication
ISA	Incremental Selection Algorithm
ISI	Inter Symbol Interference
ITU	International Telecommunication Union
LDPC	Low Density Parity Check Codes
LOS	Line-of-Sight
LPG	Low Power Group
LPG-MUD	Low Power Group Multiuser Detection
LS	Least Squares
LTE	Long Term Evolution
MAC	Multiple Access Channel
MAI	Multiple Access Interference
MBER	Minimum Bit Error Rate
MC-CDMA	Multicarrier Code Division Multiple Access
MIMO	Multiple-Input Multiple-Output
MIMO-CDMA	Multiple-Input Multiple-Output Code Division Multiple Access
MIMO-MC-CDMA	Multiple-Input Multiple-Output Multicarrier Code Division Multiple Access
MIMO-OFDM	Multiple-Input Multiple-Output Orthogonal Frequency Division Multiplexing
MIMO-OFDMA	Multiple-Input Multiple-Output Orthogonal Frequency Division Multiple Access
MISO	Multiple-Input Single-Output
ML	Maximum Likelihood
ML/ML-MUD	Maximum Likelihood / Maximum Likelihood Multiuser Detection
ML/ZF-MUD	Maximum Likelihood / Zero Forcing Multiuser Detection

MLJD	Maximum Likelihood Joint Detection
MMSE	Minimum Mean Squares Error
MRC	Maximum Ratio Combining
MSE	Mean Squares Error
MUD	Multiuser Detection
MUI	Multiple User Interference
MUMA	Multiuser Multiantenna
MU-MIMO	Multiuser Multiple-Input Multiple-Output
NBS	Norm Based Selection
NLOS	No Line-of-Sight
NOWMA	Nonorthogonal Wave Multiple Access
OCDMA	Orthogonal Code Division Multiple Access
OFDM	Orthogonal Frequency Division Multiplexing
OFDMA	Orthogonal Frequency Division Multiple Access
OS	Optimal Selection
OWMA	Orthogonal Wave Multiple Access
PAM	Pulse Amplitude Modulation
PDBS	Phase Difference Based Selection
PDF	Probably Density Function
PIC	Parallel Interference Cancellation
PN	Pseudo-Noise
PN-CDMA	Pseudo-Noise Code Division Multiple Access
PSK	Phase Shift Keying
QAM	Quadrature Amplitude Modulation
QoS	Quality of Service
QPSK	Quadrature Phase Shift Keying
RAS	Receive Antenna Selection
RC	Rotated Constellation
RC-BPSK	Rotated Constellation Binary Phase Shift Keying
RC-QAM	Rotated Constellation Quadrature Amplitude Modulation
RC-QPSK	Rotated Constellation Quadrature Phase Shift Keying
RF	Radio Frequency
RSMA	Rate Splitting Multiple Access
SC	Selection Combining
S-C	Superposition Coding
SCBS	Spatial Correlation Based Selection
SCT	Successive Coloring Technique

SD	Sphere Decoding
SDMA	Space Division Multiple Access
SER	Symbol Error Rate
SIC	Successive Interference Cancellation
SIMO	Single-Input Multiple-Output
SINR	Signal-to-Interference-plus-Noise-Ratio
SIR	Signal-to-Interference-Ratio
SISO	Single-Input Single-Output
SM	Spatial Multiplexing
SNR	Signal-to-Noise-Ratio
SO	Successive Optimization
SSD	Slab Sphere Decoding
STBC	Space-Time Block Code
STC	Space-Time Coding
STTC	Space-Time Trellis Code
SU-MIMO	Single User Multiple-Input Multiple-Output
SVD	Singular Value Decomposition
TAS	Transmit Antenna Selection
TDMA	Time Division Multiple Access
THP	Tomlinson-Harashima Precoding
UL	Uplink
UPA	Unequal Power Allocation
UPA-BPSK	Unequal Power Allocation Binary Phase Shift Keying
UPA-QAM	Unequal Power Allocation Quadrature Amplitude Modulation
UPA-QPSK	Unequal Power Allocation Quadrature Phase Shift Keying
V-BLAST	Vertical-Bell Labs Layered Space-Time
VP	Vector Perturbation
WBE	Welch Bound Equality
WH	Walsh Hadamard
WiMAX	Worldwide Interoperability for Microwave Access
ZF	Zero Forcing
ZF/ML-MUD	Zero Forcing / Maximum Likelihood Multiuser Detection
ZF/ZF-MUD	Zero Forcing / Zero Forcing Multiuser Detection
ZFBF	Zero Forcing Beamforming

List of Notations

$\|A\|$	Total number of elements in set A
$\|h\|$	Magnitude of complex value h
$\|\mathbf{h}\|$	Magnitude of vector
$\|\|\mathbf{h}\|\|$	Vector Euclidean norm
$\|\mathbf{H}\|$	Determinant of matrix
$\|\|\mathbf{H}\|\|_F$	Matrix Frobenius norm
$[.]^H$	Conjugate transposition
$[.]^T$	Transposition
$\mathrm{abs}(.)$	Absolute value
$\mathcal{C}^{m\times u}$	Complex $m \times u$ matrix
$\mathrm{E}\{.\}$	Expectation value
$E_i\{x\}$	Complete elliptic integral of the second kind with modulus x
$\mathbf{H}^{\dagger}$	Moore-Penrose inverse of matrix $\mathbf{H}$
$\mathcal{H}(x)$	Entropy of x
I_m	$m \times m$ Identity matrix
$I_0(.)$	First-kind modified Bessel function of zero order
$J_0(.)$	First-kind Bessel function of zero order
$\min(a, b)$	The minimum elements
$\mathcal{O}(m)$	Order of m
$\mathcal{R}^{m\times u}$	Real $m \times n$ matrix
$\mathrm{tr}(.)$	Matrix trace
$\mathrm{Var}\{.\}$	Variance

List of Figures

List of Tables

Chapter 1

Introduction

1.1 Motivations

Wireless communication systems are rapidly expanding worldwide and became an essential technology with crucial impact for modern life. For example, smartphones and broadband enabled portable devices such as tablets and laptops are used nowadays in extremely large scale to get advantages of various wireless services such as mobile internet and media rich applications. As a result, global mobile data traffic is expected to be growing aggressively. Therefore, efficient use of the limited available spectrum is a challenging task to meet the increasing number of clients and their demands. Furthermore, power and complexity constraints add more difficulties on the development of next generation mobile systems.

One of the key issues involved in the advancement of future wireless communications is the multiple access technique used to share the accessible bandwidth between users efficiently. In rich scattering environment, spatial dimension can be utilized to increase the number of users and transmission rate without consuming extra bandwidth and power. Therefore, it is employed in the multiple-input multiple-output (MIMO) technology to increase the spectral efficiency considerably with high quality of service (QoS). This technique plays an essential role in the evolving standards of Worldwide Interoperability for Microwave Access (WiMAX) and Third Generation Partnership Project (3GPP), represented by IEEE 802.16m and Long Term Evolution advanced (LTE)-Advanced, respectively. These standards are targeting fourth generation (4G) requirements of 100 Mb/s in high mobility and 1Gb/s for low mobility applications as defined by the International Telecommunication Union (ITU) for International Mobile Telecommunication (IMT)-Advanced [1-5].

Currently, MIMO schemes have been widely adopted in many applications and represent one of the most crucial features for the migration towards 4G systems [2, 6]. Furthermore, the hybrid combination of MIMO with orthogonal frequency division multiple access (OFDMA) [7-9], orthogonal frequency division multiplexing (OFDM) [10-12], code division multiple access (CDMA) [13, 14], or multicarrier CDMA (MC-CDMA) [15, 16] are promising solutions for flexible and spectrally efficient data services. However, the paradigm shift from single user MIMO (SU-MIMO) to multiuser MIMO (MU-MIMO) of uplink (UL) and downlink (DL) channels is a challenging task to be broadly covered [3, 17]. In the existing IEEE 802.16m and

LTE-Advanced standards, up to 4×4 antenna configuration (four transmit antennas and four receive antennas) is supported for UL channel of SU-MIMO and up to 8×8 for DL channel. For MU-MIMO with user equipments equipped with 1, 2, or 4 antennas, up to 4 users can be supported in both UL and DL channel of 802.16m. In LTE Release 9, the supported number of users is up to 4 for DL and up to 8 for UL while LTE-Advanced specifications are still under development [1-3].

The practical emergence of MU-MIMO systems has opened up the possibility of allowing multiple users equipped with one antenna or more to access the base station (BS) receiver simultaneously without subdivision in the scarce resources of time, frequency and codes [17-19]. Since the multiple antennas at users' side can be considered as "*virtual*" transmit antennas, developments in this field appears as extension to SU-MIMO concepts for the multiple access channel (MAC) and able to increase the spectral efficiency by exploiting the rich multipath environment, spatial difference among users and total degree of freedom (DoF) represented by BS antennas associated with the available number of radio frequency (RF) chains [20]. Therefore, multiple users can be served as in space division multiple access (SDMA) systems with appropriate tradeoff between performance and complexity [21]. This leads to substantial increase in channel and user capacity with high QoS and much reduction in latency for each user compared with time division multiple access (TDMA) systems [2, 3, 17, 22]. However, it is seriously affected by channel correlations due to insufficient antenna separation at the communication terminals and/or poor scattering environment [23]. As a result, the channel capacity and bit error rate (BER) performance are significantly degraded and users with highly correlated channels may not be served which reduces the user capacity. Furthermore, maximum number of users with multiple antennas that can be supported is critically limited by the available DoF represented by costly RF chains and the high complexity burden of multiuser detection (MUD) methods. Therefore, innovative and practical techniques are required to address these key problems of MU-MIMO before it becomes widely adopted in future communication systems.

1.2 Research Aims and Objectives

To provide effective solutions for the requirements and problems of future wireless system, this thesis aims to improve the channel and user capacity and error performance of MU-MIMO techniques in realistic channel conditions. To achieve these targets, the following objectives are defined:

- Investigate efficient techniques for accurate generation of correlated Rayleigh fading channels (CRFC) to overcome the shortcomings of existing methods and to assess the improvement of new system designs in realistic propagation environment precisely.

- Utilize simple transmit signal design methods with maximum likelihood joint detection (MLJD) to maximize the capacity and error performance of MU-MIMO systems over CRFC.
- Investigate new low complexity receive antenna selection (RAS) method to maximize the channel capacity of single and multiuser MIMO systems over CRFC.
- Explore high user and sum rate capacity approach for overloaded MU-MIMO systems with affordable complexity by employing user grouping, group layered MUD (GL-MUD) with interference cancellation, and RAS techniques for the available RF chains.

1.3 Contributions of the Thesis

The work in this thesis is categorized into two major areas of contributions to achieve the outlined objectives as channel modeling and high capacity MU-MIMO techniques. Summary of each contributing area is given below:

1) In the first contribution area (channel modeling), two simple techniques referred to as generalized successive coloring technique (GSCT) and generalized iterative coloring technique (GICT) are proposed for accurate generation of equal and unequal power CRFC after intensive analysis of the existing methods. They are designed for multiantenna and multicarrier systems to overcome the shortcomings and high computational complexity of conventional methods by avoiding factorization of desired covariance matrix. The simplicity and accuracy of these methods enable accurate evaluation of various existing and future wireless communication systems over realistic channel environment. Furthermore, they facilitate efficient design and integration of new techniques into feasible applications.
2) In the second major contribution area (high capacity MU-MIMO techniques), the following schemes are proposed:
   - Constellation constrained MU-MIMO (CC-MU-MIMO) scheme is designed to maximize the channel and user capacity and error performance over CRFC without need of additional receive antenna diversity. Constellation constrained using unequal power allocation (UPA) and rotation constellation (RC) transmit signal design methods with maximum likelihood joint detection (MLJD) at the receiver are utilized to provide robust performance even in severe correlation levels. The idea is based on maximizing the minimum Euclidean distance (d_{min}) of composite received signals to resolve the detection ambiguity caused by channel correlation.
   - Low complexity phase difference based selection (PDBS) technique for RAS diversity is introduced to maximize the channel capacity of single and multiuser MIMO systems over CRFC. The design is based on maximizing d_{min} of composite received signals by employing Euclidean norm of channel matrix rows with their corresponding phase

differences to achieve near optimal selection (OS) results with significant reduction in complexity. Moreover, PDBS improves the error performance and enables high user capacity for multiuser systems even in severe conditions of channel correlation.

- Group layered MU-MIMO (GL-MU-MIMO) scheme is considered to increase the user capacity beyond the limit of available RF chains with affordable complexity. It takes the advantages of spatial difference among users and power control at BS to exploit the available spectrum efficiently by dividing the active users into two groups according to their received power, high power group (HPG) and low power group (LPG). Different configurations of low complexity GL-MUD and group power allocation ratio (η) are utilized to provide a valuable tradeoff between complexity and overall system performance. The proposed scheme is utilized to increase the sum rate capacity with efficient and fair rate among served users. Additionally, RAS diversity is integrated by using NBS and a new selection technique named as HPG-PDBS to maximize the sum rate capacity and improve the error performance.

1.4 Outline of the Thesis

The thesis is organized as follows. Technical background theory and literature review of the related work are presented in Chapter 2. Classification and modeling of fading channels for mobile communication systems are given first followed by brief review of the diversity methods used to mitigate the effects of fading. Next, the importance of multiple access techniques for wireless communications is discussed and brief review of different methods is provided. The chapter includes sufficient study on the capacity of multiuser communication systems. For this purpose, main capacity definitions in the communication theory are presented and followed by discussion on the capacity region of Gaussian MAC. Extensive analysis and simulations of capacity region for 2-user Gaussian multiple access techniques are provided to investigate the capacity reaching methods in both Gaussian and fading channels. MIMO systems are reviewed in this chapter. The SU-MIMO is considered first. Basic concepts and technical details are given followed by brief review of spatial multiplexing (SM) technique and information theoretic capacity. Capacity-diversity tradeoff and the main practical considerations are discussed also. Similarly, basic concept and technical details of MU-MIMO are presented with the main advantages and disadvantages compared with SU-MIMO. UL and DL channel models with brief review of precoding, scheduling, and MUD techniques are presented. In addition, capacity-diversity tradeoff and practical considerations of most challenging problems are investigated.

The main contributions of this thesis to achieve the outlined objectives are contained in Chapter 3-6 with more specific literature review of the related work. Chapter 3 is focused on the

generation methods for CRFC to utilize them in the rest of the thesis. In this chapter, literature review on the generation methods of correlated fading channels is provided first. Next, intensive analysis of previous techniques for the generation of CRFC is given. To overcome the shortcomings and high complexity of previous methods, GSCT and GICT techniques are proposed for accurate generation of equal and unequal power CRFC for multiantenna and multicarrier systems. For these methods, principles, generalized algorithms, complexity analysis and extensive simulations of practical scenarios are provided.

The next three contributing chapters are focused on the area of high capacity MU-MIMO techniques. In Chapter 4, CC-MU-MIMO scheme is proposed. Literature review on multiuser multiantenna (MUMA) systems is presented first. Next, system model, MLJD and signal design methods of CC-MU-MIMO are given. Furthermore, channel capacity analysis including the ergodic sum rate capacity and constellation constrained capacity is introduced. To validate and show the effectiveness of CC-MU-MIMO scheme, simulation results of capacity and BER performance of proposed signal design methods compared with identical constellation (IC) are carried out over CRFC environment.

In Chapter 5, PDBS is introduced for single and multiuser MIMO systems. The chapter starts with literature review of receive signal combining methods for wireless communications and antenna selection techniques for SU-MIMO and MU-MIMO systems. RAS for SU-MIMO is considered first. This part includes system model and channel capacity analysis followed by low complexity PDBS algorithm. Extensive simulations are demonstrated to validate and show the superiority of proposed method over CRFC. In the second part of this chapter, RAS for MU-MIMO is investigated. System model and analysis of sum rate capacity are introduced followed by PDBS algorithm for multiuser case. Complexity analysis and simulation results are presented also. In the last section, impact of imperfect channel estimation on the capacity and BER performance of MIMO systems employing PDBS is investigated.

In Chapter 6, novel GL-MU-MIMO scheme is presented. First, literature review on SM multiantenna systems and overloaded MU-MIMO systems are given. Next, signal model of proposed scheme and different GL-MUD configurations with its complexity analysis are given. Capacity analysis including user capacity, sum rate capacity, and capacity region are presented. To integrate RAS diversity with the proposed scheme, NBS and new HPG-PDBS algorithms are introduced with their complexity analysis. Simulation results over uncorrelated channel environment are demonstrated to show the effectiveness of GL-MU-MIMO with/without RAS. It includes the evaluation of sum rate capacity, capacity region, and BER performance. After that, it is investigated over CRFC and simulation results for sum rate capacity and BER performance are given.

Finally, Chapter 7 concludes the thesis and provides some important recommendations for future work on MUMA technology and related topics.

Chapter 2

Multiuser Mobile Communications

2.1 Introduction

This chapter provides technical background and literature review of the related works of the thesis (more specific literature reviews are presented in the contribution chapters also). It is organized as follows. Classification and modeling of fading channels for mobile communication systems are presented in Section 2.2. A brief review of different diversity techniques conventionally employed to mitigate the fading effects is given in Section 2.3. It includes the well known time, frequency, space, and cooperative diversity methods. In Section 2.4, the importance of multiple access techniques for wireless systems and a brief discussion of different orthogonal and nonorthogonal methods are provided.

Section 2.5 is dedicated for the capacity of multiuser communication systems. It starts with the main capacity definitions in communication theory and followed by detailed discussion on the capacity region of Gaussian MAC. Due to the importance of MAC in the development of future wireless systems, an intensive study on the capacity region of some multiple access techniques is provided in subsection 2.5.3 to investigate the capacity reaching methods. The benchmark results of 2-user Gaussian MAC are presented in subsection 2.5.4 to clarify the path for higher capacity multiuser systems in both Gaussian and fading channels. It is demonstrated that spatial dimension can increase the channel capacity significantly and hence, it becomes the best competitive direction to fulfil the requirement of high data rate applications in modern and future communications. Furthermore, superposition coding (S-C) and successive interference cancellation (SIC) are examples of promising techniques which can be integrated with other multiple access methods for further improvement in the capacity and error performance with low complexity requirements.

In Section 2.6, MIMO communication systems that exploit spatial dimension to increase the capacity and reliability in rich scattering environments are reviewed. In subsection 2.6.1, SU-MIMO systems are considered. It starts with the basic concepts and technical details followed by brief review of SM technique for transmitted signals and information theoretic capacity. Capacity-diversity tradeoff and the main practical considerations are discussed also. In subsection 2.6.2, MU-MIMO systems are reviewed. The basic concepts and technical details are given first with the main advantages and disadvantages compared with SU-MIMO schemes. UL

and DL channel models with brief review of precoding, scheduling, and MUD techniques utilized in MU-MIMO systems are presented. Furthermore, capacity-diversity tradeoff and practical considerations of most challenging problems are addressed.

Finally, chapter conclusions are withdrawn in the last Section.

2.2 Fading Channels

The most frequently assumed model for a transmission channel in digital communication theory is the additive white Gaussian noise (AWGN) channel. However, it represents a poor channel model for many communication systems. Therefore, more precise and complicated models are needed. One basic type of non-Gaussian channel, which frequently occurs in practice, is the fading channel [24-33]. A typical example is the mobile radio fading channel. Radio waves of transmitted signals propagate from transmit antenna to receive antenna through free space channel and hence may undergo different situations such as reflection, diffraction, and scattering. Therefore, the characteristic features of received signals depend on these physical phenomena due to the effects of ground terrain, atmosphere, and objects on the transmitted signals as shown in Fig. 2.1 [26, 27].

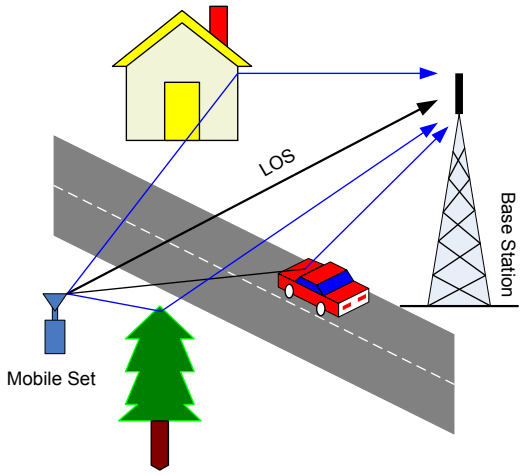

Figure 2.1: A typical multi-path fading channel.

Due to the small height of antennas in most of mobile systems compared with the surrounding objects and structures, the dominant propagation line-of-sight (LOS) path between transmit and receive ends is absent in most cases. Therefore, communication link in such a case is mainly due to signal reflection and scattering. As a result, signal over several paths with random amplitudes and phases will be received at the destination in different time delays generating the so called multipath channel. Accordingly, the combined received signal will

fluctuate randomly in time and space dimensions. For example, a moving mobile at one location may receive signal amplitude that is much different at another location due to the phase change of incoming radio waves. This random fluctuation in the received signal amplitude is termed in communication theory as *fading channel* where maintaining reliable communication links in such a situation becomes an important issue [27, 28].

2.2.1 Classification of Fading Channels

In fading channels, the long term variation in the mean signal amplitude is termed as *large-scale fading* (*shadowing*). It is assumed to be slow process representing the movement result over large distances causing gross variations in the overall signal path and usually modelled as lognormal statistics. On the other hand, short-term fluctuation in the signal level observed over approximately half wavelength ($0.5\lambda_c$) distances and caused by the local multipath is termed as *small-scale fading*. It is also denoted as *Rayleigh fading* if the number of multiple reflective paths is large with no dominant LOS (NLOS) or *Rician fading* when there is a dominant LOS path. The reason behind these names is when the combined received signal envelope includes large number of paths, it will described by Rayleigh or Rician probability density function (PDF) [3-6] as

$$f_{Rayleig\ h}(r) = \frac{r}{\sigma_o^2}\ exp\left(\frac{-r^2}{2\sigma_o^2}\right) \quad ; r \geq 0 \tag{2.1}$$

$$f_{Rice}(r) = \frac{r}{\sigma_o^2}\ exp\left[\frac{-(r^2+\varrho^2)}{2\sigma_o^2}\right] I_o\left(\frac{r\varrho}{\sigma_o^2}\right) \quad ; r \geq 0 \tag{2.2}$$

where ϱ is the amplitude of specular component (i.e. LOS component) and $I_o(.)$ is the zero-order modified Bessel function of the fist kind. The Rician $\mathcal{K}$ factor is given by

$$\mathcal{K} = \frac{\varrho^2}{2\sigma_o^2} \tag{2.3}$$

The best and worst case Rician fading channels associated with the Rician factors $\mathcal{K}$ of $\mathcal{K} = \infty$ and $\mathcal{K} = 0$ are the Gaussian and Rayleigh channels with strong LOS and NLOS path, respectively.

Coherence bandwidth of the fading channel (f_o) is the maximum frequency separation for which the signals from different paths are still correlated. For signals separated in frequency by more than f_o , then they would face different fading and can be considered as independent paths as shown in Fig. 2.2. The maximum time delay between the first and last received signals of

significant power in the channel is called the multipath *delay spread* and denoted by σ_τ. The relation between multipath delay spread of the channel and the coherence bandwidth is usually approximated by [26-29]

$$f_o \approx \frac{1}{\sigma_\tau} \tag{2.4}$$

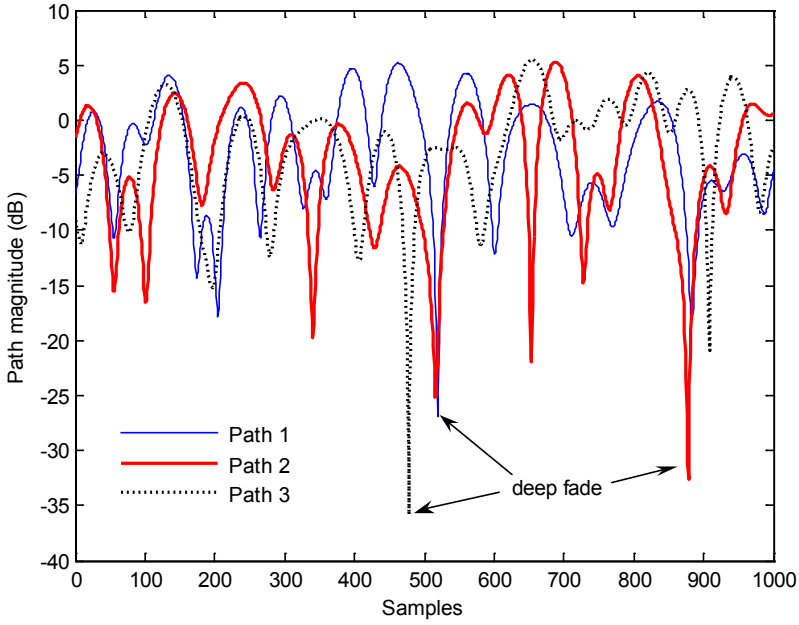

Figure 2.2: Typical example of multiple independent Rayleigh fading paths.

Small-scale fading channels such as Rayleigh and Rician is also classified as flat or frequency selective and slow or fast. If the fading channel has a constant amplitude and linear phase response over bandwidth f_o greater than baseband signal bandwidth B, the received signal is said to be affected by *flat fading*. In such a case, the received signal amplitude will fluctuate due to the random changes in channel amplitude over the time caused by multipath while the spectral characteristics of transmitted signal remain undistorted. On the other side, *frequency selective* occurs when the fading channel has constant amplitude and linear phase response over bandwidth f_o less than B. In this situation, the received signal will be distorted and dispersed since it consists of different versions of transmitted signal that exhibit delay and attenuation. Thus, intersymbol interference (ISI) is introduced due to time dispersion of transmitted signals within the channel caused by different time delays [26-29].

Doppler frequency shift (f_d) from the carrier frequency (f_c) is arising in the spectrum of received signal when a relative motion between transmit and receive ends occur. The received signal undergo *fast fading* when the Doppler shift is significant compared with B. On the other side, *slow fading* will happen if the Doppler shift is much less than B. The magnitude of Doppler frequency shift is given by [6]

$$f_d = \frac{v_m \, f_c}{c} \tag{2.5}$$

where v_m is mobile unit velocity and the light speed is $c = 3 \times 10^8 \, m/sec$.

Coherence time ($T_d \approx 1/f_d$) of the fading channel is the time over which the channel response to a sinusoid is essentially invariant. The Doppler power spectral density $S(f)$ of the mobile channel is often expressed as [6]

$$S(f) = \frac{1}{\pi f_d \sqrt{1 - (f/f_d)^2}} \quad ; \; f - f_d < f < f + f_d \tag{2.6}$$

2.2.2 Modelling Fading Channel

Performance of wireless digital communication systems is most likely to be affected by small-scale fading [24-29]. The complex-valued Rayleigh distributed fading sequence can be obtained as

$$z(n) = z_c(n) + jz_s(n) \tag{2.7}$$

where $|z(n)|$ is the fading amplitude (envelope) at n^{th} time instant, $z_c(n)$ and $z_s(n)$ are uncorrelated in-phase and quadrature samples of zero mean stationary Gaussian random processes each with σ_o^2 variance. Another method for generating complex-valued Rayleigh fading process is called *the improved sum of sinusoids* where a Gaussian noise is approximated by a finite sum of weighted and properly designed sinusoids as given by [33]

$$z(t) = z_c(t) + jz_s(t) = \alpha(t)e^{-j\emptyset(t)} \tag{2.8}$$

where $\alpha(t)$ and $\emptyset(t)$ are the fading amplitude and phase, respectively. The quadrature components of this process are given by

$$z_c(t) = \sqrt{\frac{2}{G}} \sum_{i=1}^{G} \cos(w_d t \cos(\beta_i) + \psi_i) \quad , i = 1, \dots, G \tag{2.9}$$

$$z_s(t) = \sqrt{\frac{2}{G}} \sum_{i=1}^{G} \cos(w_d t \sin(\beta_i) + \varphi_i) \quad , i = 1, \dots, G \tag{2.10}$$

where ψ_i and φ_i are waves' initial phase related to the quadrature components, β_i is the angle of incoming wave i and given by

$$\beta_i = \frac{2\pi i - \pi + \theta_i}{4G} \tag{2.11}$$

G is the number of sinusoids, w_d is the angular Doppler frequency, and all of ψ_i , φ_i and θ_i are statistically independent and uniformly distributed on $[-\pi, +\pi]$, $\forall\, i \in \{1, \dots, G\}$.

The generated process $z(t)$ has Rayleigh PDF for the envelope and uniform PDF on $[-\pi, +\pi]$ as depicted in Fig 2.3. Autocorrelation and cross-correlation functions of the quadrature components are shown in Fig 2.4 and given by

$$R_{z_c z_c}(\tau) = R_{z_s z_s}(\tau) = J_o(w_d \tau) \tag{2.12}$$

$$R_{z_c z_s}(\tau) = R_{z_s z_c}(\tau) = 0 \tag{2.13}$$

where, $J_o(.)$ is the zero-order Bessel function of first kind. As shown in [33], the desired statistics of Clarke's reference model [32] is achieved as the number of sinusoids G increased.

In case of LOS appearance with uniform phase distribution of ϑ on the range$[-\pi, +\pi]$, the Rician distributed fading sequence without showing the time index can be obtained from

$$\mathcal{Z} = \sqrt{\frac{\mathcal{K}}{\mathcal{K}+1}} e^{j\vartheta} + \sqrt{\frac{1}{\mathcal{K}+1}}\, z \tag{2.14}$$

where z is complex-valued Rayleigh distributed fading sequence given previously, $\vartheta = 2\pi d/\lambda_c$ and d is the link distance [24, 26]. For this process, PDF of the envelope are depicted in Fig. 2.5 for two different values of Ricin factor ($\mathcal{K} = 2$ and 10). Furthermore, by incorporating the effects of path loss and shadowing to $\mathcal{Z}$, a general form of the channel modelled as

$$\acute{Z} = \sqrt{c\frac{\mathcal{S}}{d^{\gamma}}}\left\{\sqrt{\frac{\mathcal{K}}{\mathcal{K}+1}}e^{j\vartheta} + \sqrt{\frac{1}{\mathcal{K}+1}}\,z\right\} \tag{2.15}$$

where γ is path loss exponent (e.g., 2 for free space and 2.7~3.5 for urban microcell), $\mathcal{S} = 10^{(\mathcal{s}/10)}$ is shadow fading of log-normal distribution and $\mathcal{s}$ is zero mean Gaussian random variable with standard deviation of $\sigma_{\mathcal{s}}$ [34].

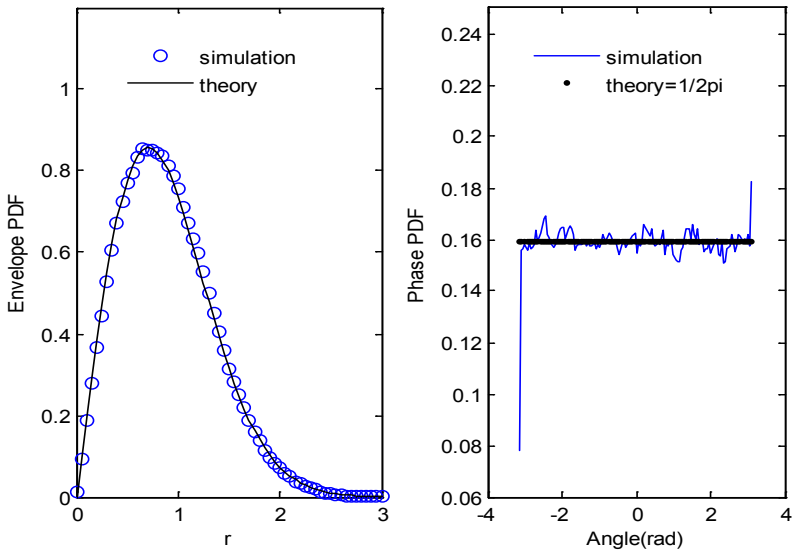

Figure 2.3: Simulation results of envelope PDF and phase PDF for unite power Rayleigh fading process.

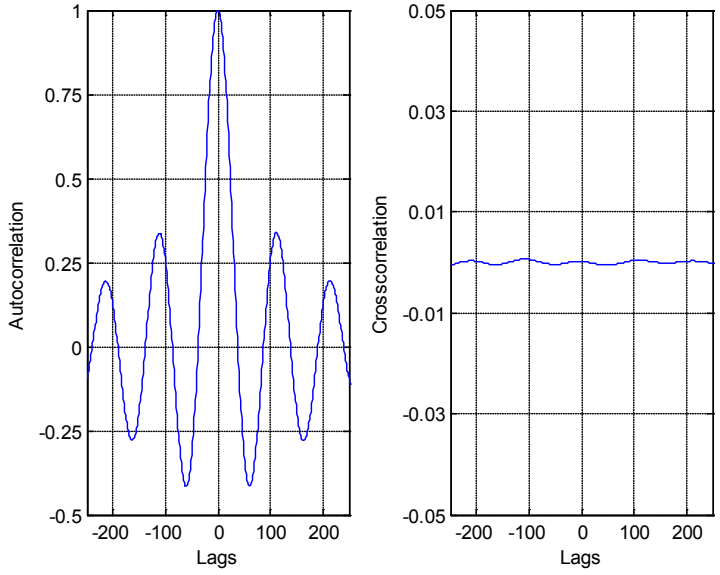

Figure 2.4: Simulation results of autocorrelation and crosscorrelation of the quadrature components for Rayleigh fading process.

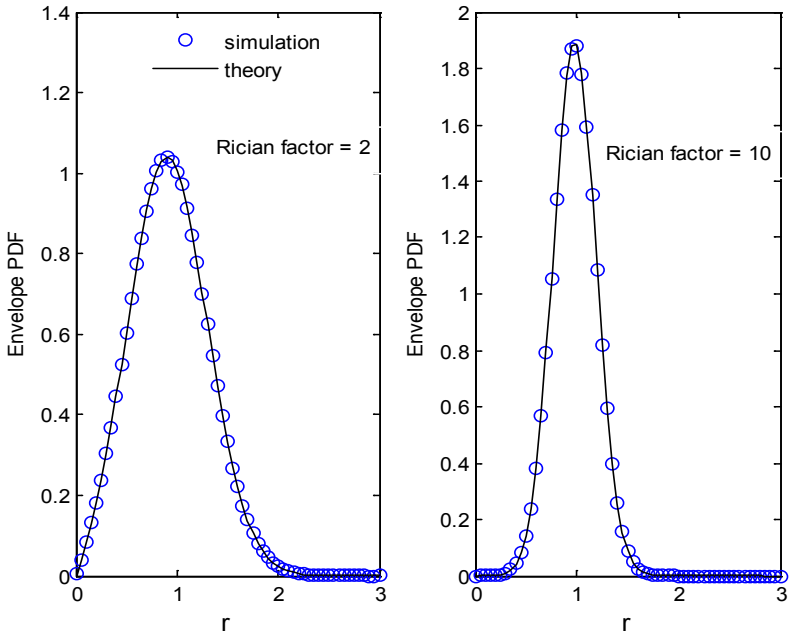

Figure 2.5: Simulation results of envelope PDF for unite power Rician fading process using $\mathcal{K} = 2$ and 10.

2.3 Diversity Techniques for Fading Channel Mitigations

Diversity techniques can be used to improve the system performance over fading channels where reliable communication mainly depends on signal path strength which may cause a poor performance in case of deep fade [24-26, 30, 34-36]. It is possible to obtain L different copies of the desired signal through independent multiple signal paths instead of transmitting and receiving through one signal path [35, 37]. The idea is while some copies may undergo deep fades, others may not. So by combining several copies of the transmitted signal, the overall received power will be increased to make the correct decision leading to performance improvement.

Probability of error in decision P_e can be shown as a function of SNR and the number of diversity branches as [24]

$$P_e = \left(\frac{1-\mu}{2}\right)^L \sum_{l=1}^{L} \binom{L-1+l}{l} \left(\frac{1+\mu}{2}\right)^l \; ; \; \mu = \sqrt{\frac{SNR}{1+SNR}} \tag{2.16}$$

For example, BER performance of coherent BPSK signal over fading channel using L diversity orders is shown in Fig. 2.6 where the use of L diversity order will improve the performance in L^{th} power of SNR.

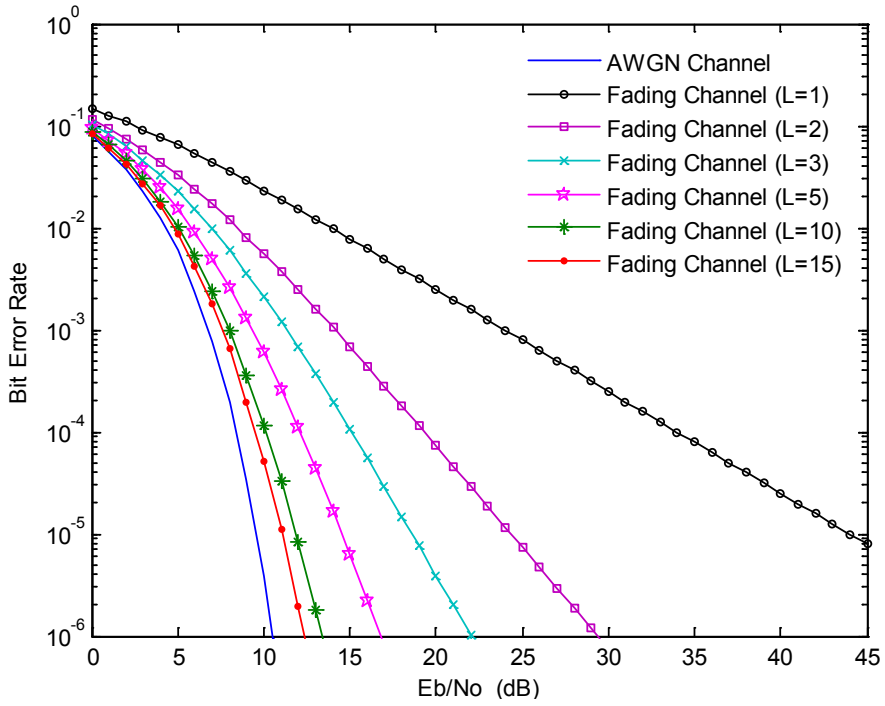

Figure 2.6: BER performance of coherent BPSK signal over fading channel using L diversity orders.

In the literature [37-39], many combining methods at the receive side are used for different diversity techniques such as selection combining (SC), equal gain combining (EGC) and maximum ratio (MRC) combining. The latest has the best performance and highest complexity while EGC has close performance to MRC without need for channel gain estimation. Among them, SC has the lowest performance and least complexity.

There are different kinds of diversity which are commonly used in wireless communication such as time diversity, frequency diversity, space diversity and user cooperation diversity. A brief review of these techniques is given next.

2.3.1 Time Diversity

Time diversity is achieved by transmitting the desired signal in L different periods of time, hence we have averaging the channel fading over time. The intervals between transmissions of the same symbol should be at least the coherence time of the channel so that different copies of the transmitted symbol undergo independent fading. By sending same symbol L times is like applying repetition coding. Typically, coherence time of the channel is of order tens to hundreds of transmitted symbols [29, 37]. Error control coding such as convolutional codes or linear

block codes together with interleaving can be an effective way to combat time selective fading while MRC can give the optimal combining in the receiver side [24-26, 36].

2.3.2 Frequency Diversity

Frequency diversity can be used efficiently to combat frequency selective fading. In wideband channels where signal bandwidth is greater than coherence channel bandwidth, the transmitted signal arrives at end link antenna over multiple symbol times. Hence, multipaths signals can be resolved and detected at the receiver. Due to the wideband nature of communication channel, frequency diversity is achieved by resolving multipaths signals at the receiver without distortion. For channel response having L independent taps, the delayed copies of transmitted signal provides diversity order L by sending data symbol every L times of symbol duration. As in time diversity, the degree of freedom (DoF) are wasted where only one information symbol can be transmitted during every channel delay spread σ_τ. By trying to transmit data symbols more frequently, ISI problem occurs where the delayed copies of previous transmitted symbols interfere with the current symbol [24-26]. To exploit the frequency diversity inherent in the wireless channel with efficient mitigation of ISI, there are three different and popular techniques given as follows [24, 36].

First: by using single-carrier systems with equalization. In this method ISI can be mitigated by using linear and nonlinear processing at the receiver and typically used for small number of taps. The complexity of the nonlinear algorithms such as the optimal Viterbi algorithm is increased exponentially with the available number of taps. Linear equalizers have lower complexity and attempt to detect the current received symbol while suppressing the interference from the rest linearly.

Second: by using direct sequence spread spectrum (DS-SS) where the data symbols are modulated using pseudonoise sequence and transmitted over a channel bandwidth W greater than data rate. In this method, the achieved symbol rate is very low leading to small ISI which simplify the structure of receiver. Using this technique will allow multiple users to share the total DoF by considering users' signals as pseudonoise to each other.

Third: by using multicarrier systems such as OFDM [11, 12]. To convert the ISI channel into a set of non-interfering sub-channels, orthogonal sub-carriers are used where each one experiences a narrow-band flat fading. Each sub-carrier should be separated from the others by at least the channel coherence bandwidth so that different signal replicas undergo independent fading. In the receiver side, optimal combining by using MRC are performed for L independently faded copies to have a correct decision.

2.3.3 Space Diversity

Space diversity can be achieved by employing multiple antennas at communication ends to receive different copies of transmitted signal as shown in Fig. 2.7. Independent signal paths can be created if the antennas are placed sufficiently far apart where the fading channel gains between different transmit and receive antenna pairs will fade independently.

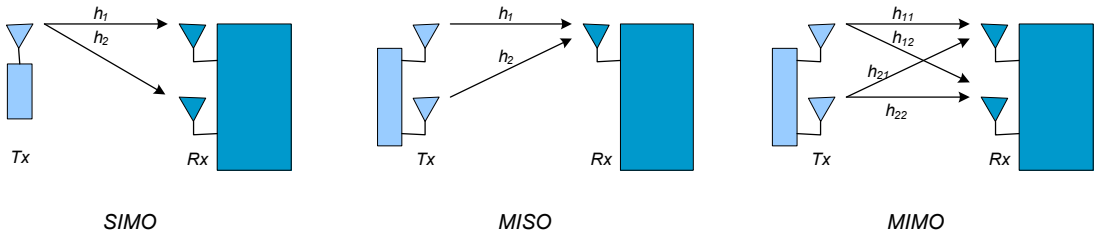

Figure 2.7: Space diversity for single user communicating with one receiver.

The required separation distance between antennas is depending mainly on the carrier frequency f_c and the local scattering environment. For mobile equipment close to the ground level and surrounded by many scatterers, the typical antenna separation is 0.5~1.0 of carrier wavelength λ_c. However, for BS antennas placed on high towers, larger antenna separation around 10's of wavelengths may be required. Different than frequency diversity and time diversity, no additional work needed in the transmit/receive side and no extra bandwidth or transmission time required [24, 26]. Receive diversity is achieved using multiple receive antennas as in single-input multi-output (SIMO) scheme while transmit diversity is achieved using multiple transmit antennas as in multi-input single-output (MISO) scheme. When multiple transmit and receive antennas are used such as MIMO, the achieved diversity is increased significantly.

2.3.4 Cooperative Diversity

Generally, transmit diversity requires more than one antenna at transmit end to allow independent faded copies of signal at the receive end. MIMO systems have many well known advantages such as high capacity and reliability [24]. In these schemes, Alamouti signalling is a well known transmit diversity method [40]. However, many wireless devices such as cellular handsets and communication nodes in wireless sensor network are limited by one antenna due to size or hardware complexity. Therefore, a new class of diversity referred to as cooperative communication has been proposed [41-45] based on the work of Cover and El- Gamal on the

relay channels [26]. This method enables mobiles equipped with single antenna in a multiuser communication environment to share their antennas and construct a virtual multiple antennas to achieve transmit diversity. In Fig. 2.8, two mobile users are communicating with one receiver and are not able to generate diversity individually. However, it may be possible for one mobile to receive the other's data, in which case it can forward some information for his partner along with its own data. Spatial diversity is achieved when fading channel paths from two mobiles are statistically independent. In a cooperative communication system, it is assumed that each mobile user act as a cooperative agent for other users in addition to his task as information source.

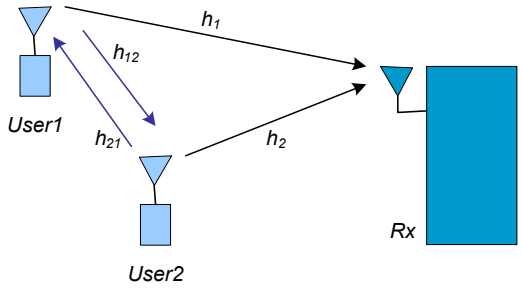

Figure 2.8: 2-user cooperative diversity.

2.4 Multiple Access Techniques

One of the most challenging topics in next generation wireless communications such as cellular systems is the multiple access technique which allows multiple users to share a communication channel efficiently. Users in any multiple access method send their signals to one common receiver via different channels (each user has his own channel). Signals from user k in the MAC must be within the total system bandwidth W and has power constraint of P_k. If the synchronization is required, the transmitters must be coordinated in the UL transmission [47-49]. Multiple access techniques can be classified into two distinct classes in terms of the total number of accommodated users on a given channel [34-36, 47, 50].

The first class is referred to as *orthogonal waveform multiple access* (OWMA) [47]. It includes TDMA, frequency division multiple access (FDMA), CDMA with orthogonal spreading sequences (OCDMA), SDMA, OFDMA, collaborative coding multiple access (CCMA), and any hybrid combinations of these schemes or other multiple access which assign orthogonal signal waveforms. Multiple access techniques that utilize orthogonal channels for each user as shown in Fig. 2.9 are effective methods which have been the primary choice for voice and low rate data traffic. The receiver demodulates signals of each user separately without

any interference from others. Thus, the error performance of such a technique resembles that of single user systems [24-26]. In these techniques, channels with bandwidth W larger than the individual user signals bandwidth B by N times can accommodate N users without any interference. Therefore, N is the upper limit of system capacity which cannot be exceeded without reducing user bit rates.

The second class is referred as *nonorthogonal waveform multiple access* (NOWMA) [47]. It includes CDMA with pseudo-noise (PN) spreading sequences (PN-CDMA) and frequency hopping based multiple access techniques. The system capacity of PN-CDMA schemes does not have a hard limit on the number of accommodated users. However, it is subject to multiuser interference which grows linearly as the number of users increased. Therefore, it depends on the receiver type and the tolerable performance degradation.

In the following, the main characteristics of some important multiple access techniques are briefly reviewed.

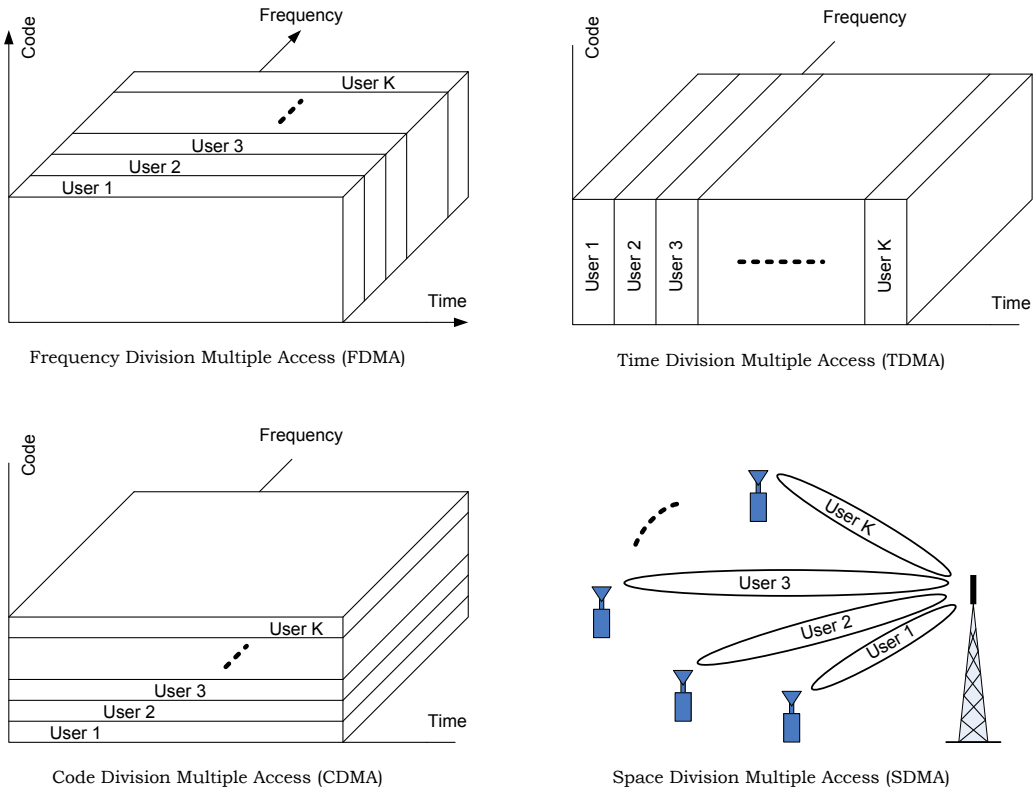

Figure 2.9: Orthogonal waveform multiple access techniques.

2.4.1 Time Division Multiple Access (TDMA)

TDMA is a very attractive multiple access technique used in many international standards and systems such as Global System for Mobile Communications (GSM) and General Packet Radio Service (GPRS) [24, 26, 47, 51]. It is also considered for 3G wireless cellular networks for providing full duplex capabilities. TDMA uses single carrier frequency and consists of transmission time slots from users' signals occupying the entire system bandwidth W. As shown in Fig. 2.9, this scheme formats the composite signal into frames of N time slots. The k^{th} time slot of each frame is assigned to the k^{th} user. Time guard intervals as well as accurate time synchronization are required while the bit rate of composite signal is shared between the N active users. Compared with the signal bandwidth of single user case (B) and by neglecting the framing overhead, the multiplexed signal bandwidth is NB. TDMA is more efficient than FDMA in the sense that it supports asymmetric user data traffic in UL and DL by varying the time slot periods that is assigned to each user. However, in a system that provides time-limited services, TDMA technique can only support few users in order to maintain high QoS. Increasing user's number requires longer waiting time for others which leads to drop in user's data rate in each transmission period. To compensate long waiting periods, TDMA system uses high data transmission rate during a given time slot, which may leads to ISI.

2.4.2 Frequency Division Multiple Access (FDMA)

FDMA is widely used in satellite systems, cable communications, and radio networks to multiplex information signals [24, 26, 47, 51-53]. It is the most classic multiple access technique and consists of assigning different carrier frequencies for the served users. Therefore, the available bandwidth W is divided into N separated channels, each allocated to one of the served users as shown in Fig. 2.9. Frequency spacing of the user channels (sub-channels) is required to avoid the overlap between adjacent signals' spectra. By neglecting the guard bands, FDMA of N modulated carriers with an individual signal bandwidth B will occupy NB of spectrum. Therefore, $K \leq N$ users can be accommodated at cost of larger bandwidth requirement to allow more users in the system.

The basic problems of classic FDMA are: Firstly, the requirement of N modulators and demodulators at the base station to serve N users simultaneously. This leads to excessive cost and complexity where the BS must handle large number of users (hundreds to thousands). Secondly, FDMA is conventionally suffers from not being flexible in handling users with varying transmission rate requirements due to the rigid allocation of narrowband channels. Thirdly, it suffers from inefficient usage of the bandwidth where no sub-channel is reallocated to other user if it is not in use by the assigned user.

In FDMA, each user occupies $(1/N)^{th}$ of the total system bandwidth W. Therefore, channel equalization is simpler compared with those used in other multiple access schemes or not required. This represents one of the main advantages of FDMA over other OWMA schemes.

2.4.3 Orthogonal Code Division Multiple Access (OCDMA)

CDMA is derived from DS-SS communication systems originally implemented for military applications [24, 26, 36, 47, 52, 54, 55]. In DS-SS systems, the main interesting properties are: Firstly, transmitted information signal is virtually buried in the background noise after spreading in time and frequency domains. Secondly, the transmitted signal becomes more immune against jamming. At the receiver, despreading operation improves the signal-to-interference ratio (SIR) by gain factor of $10\ \log_{10}(N)$, where N denotes the spreading factor.

In OCDMA, a set of orthogonal sequences such as Walsh-Hadamard (WH) sequences is employed for spectral spreading. These sequences are deterministic and repeated during the transmission process from one symbol to the next. For spreading and despreading signals, one sequence from orthogonal set will be assigned to each user. All users are able to transmit their signals simultaneously in the same channel as shown in Fig. 2.9 where for each user, the other signals are considered as cochannel interference.

The orthogonality of spreading sequences guarantees interference free between users if the signals are well synchronized. The maximum number of accommodated users K on a given channel with equal bit rate is limited by the number of orthogonal sequences N. Therefore, OCDMA is equivalent to TDMA and FDMA in terms of system capacity (users for given DoF).

2.4.4 Space Division Multiple Access (SDMA)

SDMA technique is used to maximize the system capacity and transmission gain by exploiting the space dimension through uniform linear antenna arrays consisting of several antenna elements at the base station receiver [24, 26, 34, 36, 56]. These elements are placed in a given space such as to ensure good array response towards desired direction. The composite response of the whole array is controlled by weighting each element separately. This beamforming is used to steer the higher gain beams towards desired users and low gain beams or nulls towards interfering users as shown in Fig. 2.9. By using N antenna arrays, SDMA can support simultaneous transmission of up to $N-1$ users in a given system bandwidth W without subdivision in time, frequency or orthogonal codes. In other side, the transmission gain by focusing the energy into a narrow beam can be used to increase the maximum distance of the communication link.

2.4.5 Orthogonal Frequency Division Multiple Access (OFDMA)

The use of a novel approach to FDMA which is called orthogonal FDMA (OFDMA) with channel coding is a promising technique for broadband wireless communications [7-9]. It has been adopted in many standards such as digital video broadcasting, cable networks and 4G wireless networks [3, 5, 24, 26, 34, 47, 52]. High speed data communications over realistic channels may incur severe ISI due to longer delay spread of channels that spans over several symbol periods. This ISI leads to irreducible error floor and in such case, channel equalization becomes inevitable. Since most equalization techniques requires complex algorithm, OFDMA is now becoming more popular for broadband wireless communications. In this technique, each user is assigned one or more flat fading subcarriers that preserve orthogonality even when the signals are transmitted through frequency selective fading channels. This considerably reduce the computational complexity required for multi tap equalization of the wideband signals and user signal demodulation is performed through efficient discrete Fourier transform (DFT) at the receiver. In terms of system capacity, OFDMA is similar to FDMA, TDMA, and OCDMA since accommodating N users requires NB system bandwidth.

2.4.6 Collaborative Coding Multiple Access (CCMA)

CCMA technique [57-63] achieves the multiple access function without subdivision in time frequency or orthogonal codes. It exploits the unique decidability property of composite received signal formed by superposition of transmitted collaborative user codes to achieve sum rate much higher than unity. In this scheme, each user transmits a binary codeword of length n chosen from his unique codebook $C_k;\ k = 1, \dots, K$ of $|C_k|$ codewords such that the composite received signal will be uniquely decodable. For example, codewords of length $n = 2$ are used for encoding binary data signals of two users CCMA. Two codewords are assigned to user1 as $C1 = \{00, 11\}$ and three codewords $C2 = \{00, 01, 10\}$ are assigned to user2. These codewords are capable of encoding binary or ternary data symbols and the set of received combined codewords are $\{00, 01, 10\ ; 11, 12, 21\}$. The sum rate of this scheme is $R_{sum} = \log_2\{(|C_1| \times |C_2|)/n\} = 1.292$ bits per channel use. Therefore for the same signal bandwidth B and transmit power P_k , the CCMA offers much higher sum rate than other OWMA schemes. The user capacity of this scheme is defined by the number of users K whose composite codeword signals are uniquely decodable.

2.4.7 Pseudo-Noise Code Division Multiple Access (PN-CDMA)

Asynchronous data transmission, near-far signals, different users' fading channels and overloading conditions are the main characteristics of uplink mobile wireless communications.

So, the use of orthogonal sequences in CDMA which is considered for synchronous transmission does not guarantee interference free detection. For such environment where the uplink synchronization is a challenging task, the NOWMA offers his attractive advantages to tackle this problem. One of the most popular nonorthogonal multiple access technique is PN-CDMA. This asynchronous technique uses the second property of DS-SS systems to share a common communication channel between multiple users. PN spreading sequence is assigned to each active user for signal spreading and despreading. For normalized signal power to 1 and given spreading factor N, the interference power from each other user at the receiver after despreading is $1/N$. Therefore, the total power of signal interference is proportional to the number of interfering users in the system. The system capacity depends on the average BER degradation that can be tolerated. For a system of $K = N$ active users and single user detector, the interference power $[(N-1)/N] \approx 1$ is prohibitive. In such a case and for interference level 6dB below signal level, the system capacity using PN-CDMA is only $N/4$.

System capacity can be maximized by using MUD [50, 52] which cancels the interference components from other users. However, it is still to be verified that PN-CDMA can reach a system capacity of N users with acceptable performance and low complexity detection methods. To maximize the capacity, user's sequences have to be carefully designed to create least interference to other users in the system such as Welch Bound Equality (WBE) Sequences. However, due to higher complexity and other practical limitations of WBE sequences, suboptimal sequences are used in practice.

2.4.8 Hybrid Multiple Access Techniques

In the literature, many hybrid combinations of multiple access methods have been used to increase the spectral efficiency and reliability of communication systems over different fading channel conditions [1-16, 47, 79-81]. The most important examples are; combination of CDMA with OFDM to form MC-CDMA [15] and MIMO schemes with OFDMA [7-9], OFDM [10-12], CDMA [13, 14], MC-CDMA [15, 16]. In addition, several methods are employed along with conventional multiple access schemes to improve the performance of wireless links and maximize the capacity. Such methods as; S-C [51, 64-69], SIC detection [12, 24, 50, 52, 70], low density parity check codes (LDPC) [71-73], and rate splitting multiple access (RSMA) [74-78]. In the following, a brief review of the most important methods, S-C and SIC detection is given.

A. Superposition Coding (S-C)

S-C technique can be used to improve the system capacity and throughput in different scenarios. It is particularly appropriate for applications in which there are spatial or temporal

disparities in received SNR of multiple users. It is shows in [51, 64, 65] that, higher than time-division and frequency-division rates can be send from several transmitters over AWGN channel by using superposition scheme that pools the time, bandwidth and power allocation of the transmitters. The transmitted signal is the sum of users' signals as depicted in Fig. 2.10. In the receiver side, the strongest signal is decoded first, and estimated signal is subtracted then from the received signal, followed by decoding of the intended signal and so on. Higher difference in power level of the users' signals gives better performance which outperforms the orthogonal schemes. Combining S-C with different multiple access techniques has been investigated by many researchers. In [67], S-C of the downlink OCDMA is used. It involves pairing of each two users with different power requirement using S-C to reduce the total average power. By taking the advantage of power disparities that are created by power control, the system can transmit to a larger number of users by using single spreading sequence for multiple users. Transmission of two level signals with different rates using S-C by sharing the same resources (power, time and bandwidth) has been studied extensively by many researchers such as [66, 68, 69].

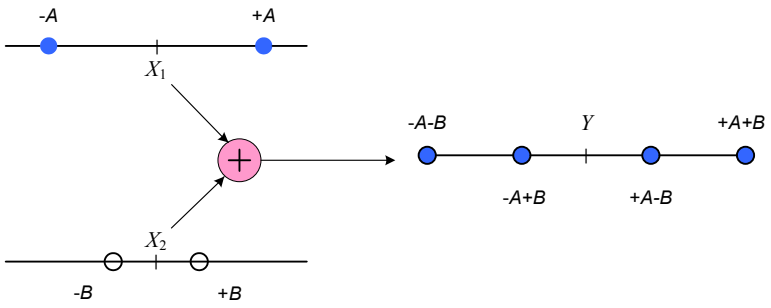

Figure 2.10: Superposition of two signals with different power levels.

B. Successive Interference Cancellation (SIC)

SIC detection is a multiuser receiver which is used to maximize the data rate [1, 27, 29, 47, 48]. The general principle is that SIC receiver can detects one user at a time where estimated strongest user is selected at each detection stage as illustrated in Fig. 2.11. By using this receiver, information of K users can be decoded in K stages. This requires ordering of users' received powers which usually obtained from output of matched filter bank. The notion of SIC is that, the strongest user can be decoded with higher reliability and its cancellation from the received signal will remove significant amount of system multiple access interference (MAI) which improves the detection performance of the later users. However, SIC receiver suffers from error propagation taking place through the consecutive stages of detection due to

inaccurate signal detection of the previous stages leading to performance degradation. Effective SIC operations require each user's received signal to be in different power compared with the others. This property of SIC is well suited in fading channels and near-far user environments. It has been shown that effective power control schemes are very important for SIC receivers to maintain equal BER performance under unequal user power conditions.

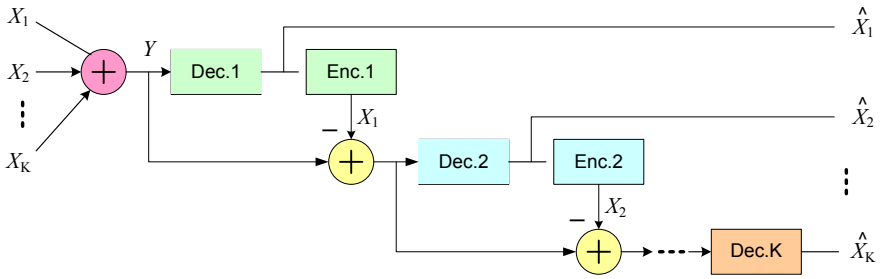

Figure 2.11: Successive decoding where the signal power ordering as; $X_1 > X_2 > \ldots > X_K$.

2.5 Capacity of Multiuser Communication Systems

2.5.1 Capacity Definitions

One of the main performance measures in the point-to-point communication is the *channel capacity* (C) where reliable communication can be attained at any rate $R \leq C$ and impossible at $R > C$. It is given for Gaussian channel as [24]

$$C = \log_2[1 + SNR] \tag{2.17}$$

However, in the multiuser communication case of K users, the performance is often described in terms of *rate region*. Each point in this region represents a set of the achievable users' rates such that all users can simultaneously and reliably communicate with common receiver. The union of all achievable rate sets is known as the *capacity region* $(\mathbb{C})$. Since all users are sharing the available bandwidth, the capacity region characterizes the optimal tradeoff achievable of user's rate by any multiple access techniques [24]. For K-user system, *sum capacity* (C_{sum}) is defined as the sum of each user's maximum information rate that can be reliably transmitted over a unit bandwidth $(W = 1)$ or in other words as the maximum total throughput that can be achieved. It is given for uplink Gaussian MAC in terms of users' rate $R_k; k = 1, \ldots, K$ as

$$C_{sum} := \max_{R_1,\ldots,R_K \in \mathbb{C}} \sum_{k=1}^{K} R_k \tag{2.18}$$

Another performance measure of multiple access techniques is the *user capacity* (C_{user}) which is defined by the ratio of total number of users K to the number of DoF N. The DoF can be non-overlapping frequency bands, time slots or user separating codes. If $C_{user} \leq 1$, Then channel is said to be under-loaded, otherwise it will be overloaded if $C_{user} > 1$. In case of no multiple access scheme is employed and there are K users in the system, then $C_{user} = K$. In practical multiuser systems, several hundreds of users have to be accommodated within a given system bandwidth where each user's signal contribute to noise and interference components of others. For this purpose, the optimum receiver can jointly detect all users' signals and as $C_{user} \to \infty$, it converges asymptotically to the capacity of single user channels [50]. However, it is impractical to implement due to its high computational complexity. Therefore, simple multiple access technique that guarantees interference free between users has become one of the main tasks of practical multiuser wireless systems.

2.5.2 Capacity Region of Gaussian MAC

Consider a single cell of cellular network where K users communicating simultaneously with the BS receiver over an AWGN channel. Each of the users' equipments is equipped with one antenna. Hence, the received signal during every symbol interval is represented as

$$Y = \sum_{k=1}^{K} X_k + Z \tag{2.19}$$

where X_k is the k^{th} user signal under average power constraint of P_k and Z is the independently identically distributed (i.i.d) complex AWGN of zero mean and average power of N_0. At BS receiver, two detection methods are considered, the optimal *joint detection* and the low complexity *independent detection* (single user detection) [24, 50, 56].

Capacity region of 2-user UL AWGN channel is considered in this subsection since the general properties and the relative performance of different multiple access techniques are the same as K increased [64]. Hence, capacity region is a pentagon shown in Fig. 2.12 representing the set of all the possible rate pairs (R_1, R_2) in bit/s/Hz (for normalized system bandwidth, $W = 1$) which satisfies the following conditions [24]

$$R_1 \leq W \log_2\left(1 + \frac{P_1}{WN_0}\right) \tag{2.20}$$

$$R_2 \leq W \log_2\left(1 + \frac{P_2}{WN_0}\right) \tag{2.21}$$

$$R_{sum} = R_1 + R_2 \leq W \log_2\left(1 + \frac{P_1 + P_2}{WN_0}\right) = C_{sum} \tag{2.22}$$

where the total throughput R_{sum} cannot exceed the sum capacity C_{sum} of the individual user's rates. The single user bounds of R_1 and R_2 is represented by the point "B" and "C" while C_{sum} is on the line $\overline{B\ B1\ C1\ C}$.

In the literature, there are many techniques where R_{sum} is achieved and the most fair rate points lies on the line $\overline{B1\ C1}$ [24]. However, when a single-user detection method is employed at the receiver side, the region bounded by $\overline{O\ B2\ A\ C2\ O}$ contains all possible rate pairs (R_1, R_2) that users can reliably transmit. Without C_{sum} constraint, capacity region will be a rectangle shape and point "Q" can be achieved by simultaneous transmission of both as if the other is absent (i.e. no interference). It is very important and challenging point and still attractive to many research communities. But, it is very difficult to achieve practically since multiuser systems incur losses in spectral efficiency compared with the equivalent single user Gaussian channels due to the contribution of MAI. For this purpose, joint detection is optimal at the cost of high computational complexity. Multiuser detection using SIC receiver is another method to maximize the data rate and reduce the MAI [24, 50]. It involves K stages of signal detection for K-users system. For 2-user system, if user 2 detected first treating user 1 as Gaussian interference, the maximum achievable rate will be point "C2" given by

$$R_2 = W \log_2\left(1 + \frac{P_2}{P_1 + WN_0}\right) \tag{2.23}$$

In the second stage, user 1 can be detected after subtracting the contribution of user 2 from the aggregate received signal. Since only background Gaussian noise is left in the system, user 1 can achieve single user bound represented by point "B". If the detection processes is reversed, user 2 can achieve single user bound represented by point "C" while the maximum achievable rate of user 1 will be point "B2" given by

$$R_1 = W \log_2\left(1 + \frac{P_1}{P_2 + WN_0}\right) \tag{2.24}$$

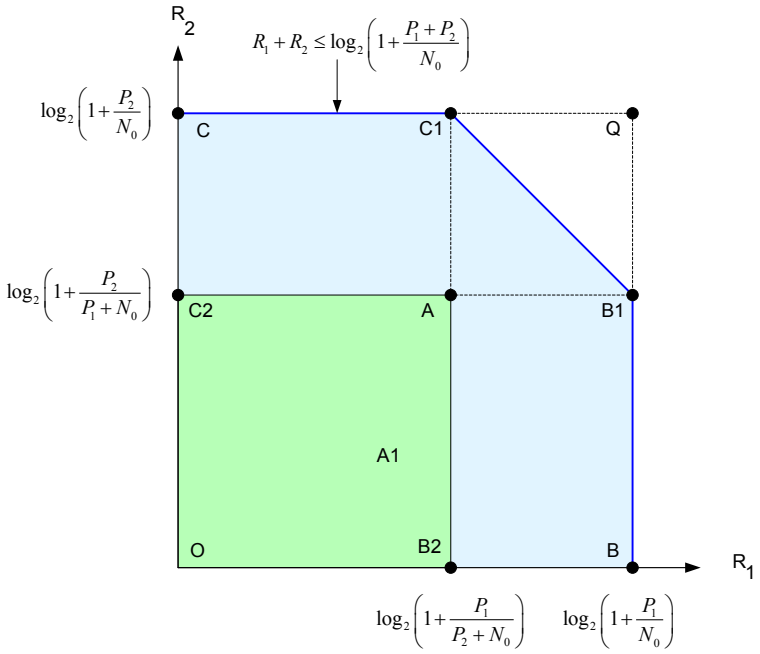

Figure 2.12: Capacity region for 2-user uplink AWGN channel with normalized bandwidth ($W = 1$).

2.5.3 Capacity Region of Promising Multiple Access Techniques

One of the important issues involved in the development of future wireless communication systems is the multiple access technique employed to share the available spectrum among users efficiently. In this section we present intensive study on the capacity region of some multiple access techniques for mobile cellular systems to investigate *capacity reaching* methods [82]. Analysis is carried out for 2-user UL AWGN channel of a single isolated cell represented by the signal model (2.19). The benchmark outcomes can be used to clarify the path for researchers to develop higher capacity multiuser systems in both Gaussian and fading channels of UL and DL.

A. TDMA

In TDMA [51], the available system bandwidth W is allocated to user 1 for a fraction α of the total transmission time and the rest, $1-\alpha$ to user 2. The rate region is represented by all rate pairs (R_1, R_2) for $0 \le \alpha \le 1$ and given by

$$R_1 = \alpha W \log_2\left(1+\frac{P_1}{WN_0}\right)$$
$$R_2 = (1-\alpha) W \log_2\left(1+\frac{P_2}{WN_0}\right) \quad (2.25)$$

B. FDMA

For simultaneous transmission using FDMA, a fraction α of system bandwidth W is allocated to user 1 and the rest, $1-\alpha$ to user 2. The rate region is represented by all rate pairs (R_1, R_2) for $0 \leq \alpha \leq 1$ and given by [53]

$$R_1 = \alpha W \log_2\left(1 + \frac{P_1}{\alpha W N_0}\right)$$
$$R_2 = (1-\alpha) W \log_2\left(1 + \frac{P_2}{(1-\alpha) W N_0}\right) \tag{2.26}$$

C. CDMA

In CDMA [24, 54, 55], users are allowed to simultaneously communicate with the base station receiver over system bandwidth W by using spreading codes such as orthogonal WH sequences. For orthogonal spreading codes of length N (spreading gain), the information bandwidth of each user is W/N. By using conventional single-user detection, the two user rate region is represented by all rate pairs (R_1, R_2) over (P_1, P_2) and given by [24]

$$R_1 = W \log_2\left(1 + \frac{P_1}{P_2 + W N_0}\right)$$
$$R_2 = W \log_2\left(1 + \frac{P_2}{P_1 + W N_0}\right) \tag{2.27}$$

where equal power allocation $(P_1 = P_2)$ provide a practical solution to achieve fair users rates at the cost of low R_{sum}.

To achieve higher rates, multiuser detection using SIC receiver can be employed yielding the following

$$R_1 = W \log_2\left(1 + \frac{P_1}{P_2 + W N_0}\right)$$
$$R_2 = W \log_2\left(1 + \frac{P_2}{W N_0}\right) \tag{2.28}$$

where user 1 is detected first assuming that $P_1 > P_2$. By using SIC, the strongest user can be decoded with higher reliability and its cancellation from the received signal will remove significant amount of MAI which improves the weak user performance.

It should be noted that the rate region of S-C with SIC [51, 65] is described by (2.28) also without subdivision in time, frequency and codes. It requires efficient power allocation $(P_1,\ P_2)$ to maximize the system throughput and can be applied in hybrid combination with any type of multiple access technique [66-69].

D. SDMA

In SDMA [56], users are allowed to simultaneously communicate with the base station over the entire bandwidth W by exploiting the spatial dimension. For 2-user system with M receive antennas (receivers) at BS, the combined received signal is

$$Y = \sum_{i=1}^{M} Y_i = \sum_{i=1}^{M} \left(\sum_{k=1}^{K} X_k + Z_i \right) \tag{2.29}$$

where Y_i is the received signal at the i^{th} antenna and Z_i is i.i.d complex AWGN of zero mean and average power of N_0 at same antenna.

The capacity region of SDMA depends on the users' positions and detection method. Therefore, the inner bound is given for joint detection as [56]:

$$\begin{aligned} R_1 &\leq W \log_2 \left(1 + \frac{MP_1}{WN_0}\right) \\ R_2 &\leq W \log_2 \left(1 + \frac{MP_2}{WN_0}\right) \\ R_1 + R_2 &\leq W \log_2 \left(1 + M\frac{P_1 + P_2}{WN_0}\right) \end{aligned} \tag{2.30}$$

while for independent detection as

$$\begin{aligned} R_1 &\leq W \log_2 \left(1 + \frac{MP_1}{MP_2 + WN_0}\right) \\ R_2 &\leq W \log_2 \left(1 + \frac{MP_2}{MP_1 + WN_0}\right) \end{aligned} \tag{2.31}$$

E. CCMA

For 2-user system using CCMA, the rate pairs $(R_1,\ R_2)$ in bit/channel use are [60]

$$R_1 = \log_2(|\,C_1|)\,/n$$
$$R_2 = \log_2(|\,C_2|)\,/n \tag{2.32}$$

For example, if $C_1 = \{00,\ 11\}$ is assigned for user 1 and $C_2 = \{00,\ 01,\ 10\}$ for user 2, the achieved rates are; $R_1 = 0.5,\ R_2 = 0.792$ and $R_{sum} = R_1 + R_2 = 1.292$.

F. RSMA

In RSMA [74-78], each real user in the K user Gaussian MAC creates a number of virtual users using power/rate splitting mechanism. The transmitted signal of any real user is the superposition of its virtual users' signals. At the receive side, SIC is used for all virtual users decoding to achieve every point in the capacity region and maximum equal rate point. The advantage of this scheme is that only $2K - 1$ of independent point-to-point encoding/decoding processes are required rather than their multiuser counterparts. For the 2-user system, user 1 creates two virtual users (1a and 1b) by splitting its power P_1 to α and $P_1 - \alpha$ while user 2 does not split his power [78]. Hence the rates are given for decoding order of (1a, 2, and then 1b) as

$$R_{1a} = W\log_2\left(1 + \frac{\alpha}{P_1 - \alpha + P_2 + WN_0}\right)$$
$$R_2 = W\log_2\left(1 + \frac{P_2}{P_1 - \alpha + WN_0}\right) \tag{2.33}$$
$$R_{1b} = W\log_2\left(1 + \frac{P_1 - \alpha}{WN_0}\right)$$

Then, $R_1 = R_{1a} + R_{1b}$ and $R_{sum} = R_1 + R_2$. By varying α, any point in the dominant face of capacity region can be achieved.

2.5.4 Results

In this section, we simulate the 2-user capacity region for the multiple access techniques presented in previous section and the results are illustrated in Fig. 2.13 [82]. It is assumed that, $P_1 = P_2 = N_0 = 1$ (i.e. SNR $= 0$ dB for both users). The benchmark results include the following :

- *TDMA (2.25):* Users are sharing the maximum $R_{sum} = 1$ according to the allocated transmission time.

- *FDMA (2.26):* It performs better than TDMA and can achieve the maximum capacity ($R_{sum} = 1.585$) at one point ($R_1 = R_2 = 0.7925$) when $\alpha = P_1/(P_1 + P_2$. Hence, the allocated fraction of bandwidth α to each user is proportional to its received power.
- *Conventional CDMA (2.27):* Using single user detection at the receive side, it is represented by the region bounded by $\overline{O\ B2\ A\ C2\ O}$ and the maximum equal rate point that can be achieved is ($R_1 = R_2 = 0.585$) with $R_{sum} = 1.17$. The capacity provided by this technique is low compared with the others except for a small portion of TDMA scheme.
- *CDMA with SIC (2.28):* Using SIC, the maximum capacity ($R_{sum} = 1.585$) is achieved where user 2 can transmit in full rate ($R_2 = 1$) when user 1 detected first (point "C1") while user 1 can transmit in full rate ($R_1 = 1$) when user 2 detected first (point "B1"). Although using of SIC provides high capacity, it is not preferable in practice due to the error propagation problem [24].
- *S-C with SIC (2.28):* Maximum capacity at point "C1" is achieved if user1 detected first and point "B1" is achieved if user2 detected first. The line $\overline{C\ C1}$ is achieved if user 1 detected first and its signal power P_1 reduced while $\overline{B\ B1}$ is when user 2 detected first and its power P_2 reduced. The rate point ($R_1 = 1.0$, $R_2 = 0.3$) is achieved when a practical moderate block-size LDPC codes are employed [71-73, 79]. If time sharing or joint encoding is incorporated, the dominant face line $\overline{B1\ C1}$ of the capacity region is achieved with $R_{sum} = 1.585$.
- *RSMA (2.33):* This scheme can achieve the dominant face line $\overline{B1\ C1}$ of the capacity region with $R_{sum} = 1.585$ including the equal rate point($R_1 = R_2 = 0.7925$) as FDMA. By employing S-C and SIC, the complexity of RSMA for target capacity performance is lower than other schemes where joint detection is used.
- *CCMA (2.32):* In our best of knowledge, the highest achievable rate points are given in [60] as ($R_1 = 0.597$, $R_2 = 0.72$) and ($R_1 = 0.72$, $R_2 = 0.597$). In [61], it is shown that feedback form receive side to one user enables equal rate point ($R_1 = R_2 = 0.694$) to be achieved while ($R_1 = R_2 = 0.717$) if the two users are exploiting the feedback signal. With feedback to both users and user cooperation, a point ($R_1 = R_2 = 0.791$) very close to the capacity region is achieved where $R_{sum} = 1.582$.
- *SDMA:* When joint detection (2.30) is used at the receiver, this scheme provides a significant increase in the capacity. For 2-receive antennas, the achieved equal rate point is ($R_1 = R_2 = 1.161$) with $R_{sum} = 2.322$. It is clear that adding one extra antenna will increase the sum rate capacity by 46.5% compared with maximum $R_{sum} = 1.585$ when single antenna is used. The receiver gets two replicas of transmitted signal which are combined coherently to boost up the capacity performance. If independent detection is employed with SDMA (2.31), the rate point ($R_1 = R_2 = 0.737$) for 2-receive antennas

lies inside the capacity region while for 3-receive antennas, the rate point ($R_1 = R_2 = 0.807$) with $R_{sum} = 1.614$ lies above the capacity region. This low performance compared with the joint detection is due to inherent problem of noise enhancement in independent receivers. However, it represents a tradeoff between complexity and system performance.

Summary of some important capacity region results is given in Table 2.1. Among all other techniques, results show that SDMA can increase the channel capacity significantly and hence, it becomes the best competitive method to fulfil the requirement of high data rate applications. However, more attention should be made to shrink the gap between the simple independent detection and the complex joint detection methods. RSMA, S-C, SIC, and LDPC codes are another promising techniques which can be used with further improvement to increase the capacity with low complexity requirements. The benchmark results will provide the research community with a useful guide for further development of higher capacity multiuser systems.

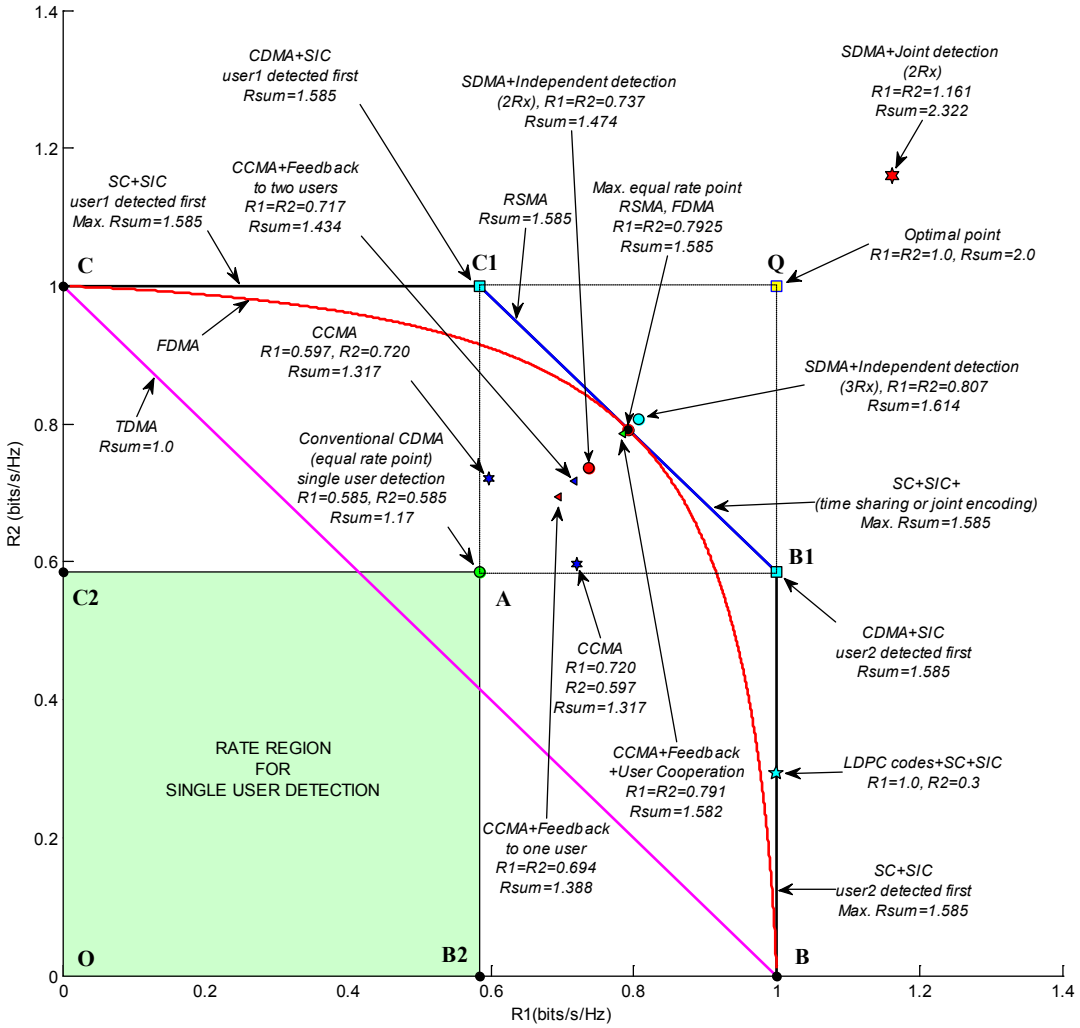

Figure 2.13: Capacity region of different multiple access techniques for the 2-user uplink AWGN channel with normalized bandwidth ($W = 1$) and $P_1 = P_2 = N_0 = 1$ (SNR = 0 dB for both users).

Table 2.1: Summary of some important capacity region results

Multiple Access Technique	R_1	R_2	R_{sum}
SDMA (2Rx and joint detection), (equal rate point)	1.161	1.161	2.322
SDMA (2Rx and independent detection), (equal rate point)	0.737	0.737	1.474
SDMA (3Rx and independent detection), (equal rate point)	0.807	0.807	1.614
RSMA or FDMA or SC+SIC+[time sharing or joint encoding], (equal rate point)	0.7925	0.7925	1.585
CDMA+SIC or SC+SIC (user1detected first, point "C1")	0.585	1.0	1.585
CDMA+SIC or SC+SIC (user2 detected first, point "B1")	1.0	0.585	1.585
CCMA+ Feedback +User cooperation, (equal rate point)	0.791	0.791	1.582
CCMA+ Feedback to two users, (equal rate point)	0.717	0.717	1.434
CCMA+ Feedback to one users, (equal rate point)	0.694	0.694	1.388
CCMA	0.720	0.597	1.317
CCMA	0.597	0.720	1.317
CDMA (independent detection, point "A"), (equal rate point)	0.585	0.585	1.170
TDMA (point "B")	1.0	0.0	1.0
TDMA (point "C")	0.0	1.0	1.0

2.6 Multiple-Input Multiple-Output (MIMO) Communications

In the previous sections, it is shown that exploiting the spatial dimension in mobile communications has the effects to maximize the capacity significantly. By exploiting the multipath signal propagation, digital communications using MIMO has emerged as breakthrough for wireless systems to provide higher data rate and spectral efficiency without consuming extra bandwidth and power [12, 17, 24]. MIMO signals are referred as *multi-dimensional signals* where two or more data streams can be transmitted over the same channel simultaneously in contrast to conventional *one–dimensional signals* even if multiple antennas are used. Since the signals are transmitted through different channel paths, MIMO systems are capable to maintain reliable communications by exploiting both of transmit and receive diversity. MIMO systems have been well investigated in the point-to-point scenario (single user) where multiple antennas can be used to provide *diversity* and/or *multiplexing gains* [83-98]. Moreover, *multiple access gain* can also provided in the multipoint-to-point (multiuser) scenario, where multiple receive antenna can be used to spatially separate the received signals originated from multiple users [18, 21, 99-106]. A brief review of the two aforementioned scenarios is given in the following sections.

2.6.1 Single User MIMO (SU-MIMO)

In SU-MIMO systems, gain in channel capacity and reliability can be achieved by the use of space-time codes combined with SM of data streams [83, 97, 98]. Here, multiple antennas at

transmit and receive sides provide extra DoF which can be exploited for signal detection to improve the system performance at the cost of hardware complexity [84]. General SU-MIMO system model of u transmit and m receive antennas over fading channel with AWGN is shown in Fig. 2.14 where the received signal **r** is given by

$$\begin{bmatrix} r_1 \\ \vdots \\ r_m \end{bmatrix} = \begin{bmatrix} h_{11} & \cdots & h_{u1} \\ \vdots & \ddots & \vdots \\ h_{1m} & \cdots & h_{um} \end{bmatrix} \begin{bmatrix} v_1 \\ \vdots \\ v_u \end{bmatrix} + \begin{bmatrix} n_1 \\ \vdots \\ n_m \end{bmatrix} \tag{2.34}$$

or in a matrix notation form as

$$\mathbf{r} = \mathbf{H}\mathbf{v} + \mathbf{n} \tag{2.35}$$

where $\mathbf{r} \in \mathcal{C}^{m\times 1}$ is $m \times 1$ complex received signal vector which will be decoded to $u \times 1$ estimated data vector $\hat{\mathbf{b}} = [\hat{b}_1 \quad \cdots \quad \hat{b}_u]^T$, $\mathbf{H} \in \mathcal{C}^{m\times u}$ is $m \times u$ complex channel matrix which assumed to be available at the receiver, $\mathbf{v} \in \mathcal{C}^{u\times 1}$ is $u \times 1$ complex transmitted symbol vector and $\mathbf{n} \in \mathcal{C}^{m\times 1}$ is $m \times 1$ vector of i.i.d complex AWGN with each element having σ^2 variance.

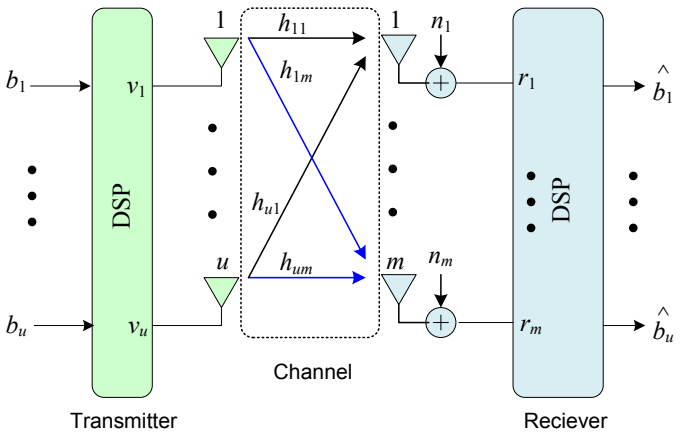

Figure 2.14: $u \times m$ SU-MIMO communication system.

The *rank* of MIMO channel is the algebraic rank of **H** which is the number of independent equations offered by the linear system ($rank \leq \min(u, m)$). It is affected by the presence of LOS and rich scatters environment. In particular, the performance improvement in SU-MIMO systems is due to antenna array, diversity, and SM gains [84, 85].

Antenna array gain can be achieved and results in high increase of average SNR through the processing at transmit and receive ends due to coherent combining [84]. It depends on the number of antennas and channel state information (CSI) at both sides of the system [85]. CSI at the receiver (CSIR) can be calculated using different estimation methods such as training sequences whereas CSI at the transmitter (CSIT) is rather difficult to maintain. Both of CSIT and CSIR are useful to reduce the cochannel interference effects arise due to frequency reuse.

Diversity gain of order um can be achieved if all channel paths are uncorrelated (independently fade) and the channel knowledge is available at both transmission sides. Spatial diversity can be extracted by the use of well designed space-time coding [40] in the absence of CSIT.

SM gain in MIMO systems is the increase of overall data rate which can be achieved by simultaneous transmission of independent data signals from u-transmit antennas without additional increase in power or bandwidth [24, 84-86].

2.6.1.1 Spatial Multiplexing (SM)

SM often referred in literature as Vertical-Bell Labs Layered Space-Time (V-BLAST) is the technique that exploits spatial dimension to increase the capacity rather than diversity in MIMO channels [87, 88]. It offers a linear increase in capacity of $\mathbb{N} = \min(u, m)$ antennas under uncorrelated channel condition by transmitting independent data streams simultaneously using the available power and bandwidth as in Fig. 2.15.

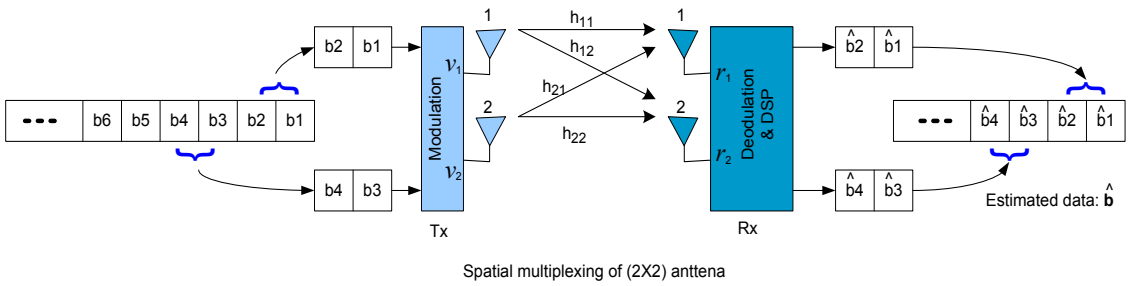

Figure 2.15: Spatial multiplexing in 2×2 SU-MIMO communication system.

An uncorrelated fading channel which relies on the presence of rich multipath and NLOS provide a natural unique signature to each input data stream "*virtual user*". However, the orthogonality among the transmitted streams totally depends on the fading correlation. Hence, the receiver can separate then decode and merge bit streams to the original transmitted data if the channel matrix **H** has independent rows (full rank).

2.6.1.2 Capacity of SU-MIMO

Through the principles of SM and diversity, MIMO can offer higher capacity and QoS [24, 89-91, 99]. Capacity for memoryless SISO systems in bit/s/Hz can be given [1, 63- 65] as

$$C_{SISO} = \log_2(1 + \Gamma|h|^2) \tag{2.36}$$

where Γ is SNR at the receive antenna and h is constant complex fading channel.

In case of SIMO (receive diversity) this capacity improves logarithmically with respect to m receive antennas as

$$C_{SIMO} = \log_2\left(1 + \Gamma\sum_{i=1}^{m}|h_i|^2\right) \tag{2.37}$$

where h_i is constant complex fading channel for i^{th} antenna.

For same transmission power and without array gain, the capacity using MISO (transmit diversity) without CSIT becomes

$$C_{MISO} = \log_2\left(1 + \frac{\Gamma}{u}\sum_{i=1}^{u}|h_i|^2\right) \tag{2.38}$$

Using both transmit and receive diversity in MIMO with constant channel, the capacity in a simple form can be calculated for equal power distribution among *u* antennas without CSIT as

$$C_{MIMO} = \log_2\left|\mathbf{I}_m + \frac{\Gamma}{u}\mathbf{H}\mathbf{H}^{\mathrm{H}}\right| = \log_2\left|\mathbf{I}_m + \mathbf{H}\mathbf{Q}\mathbf{H}^{\mathrm{H}}\right| = \sum_{i=1}^{\mathbb{N}}\log_2\left(1 + \frac{\Gamma}{u}\varepsilon_i\right) \tag{2.39}$$

where $\mathbf{Q} = (\Gamma/u)\mathbf{I}_u$ denote the covariance matrix of signal vector $\mathbf{v}$ under power constrain of $[\mathrm{tr}(\mathbf{Q}) \leq \Gamma]$, $\mathbb{N} = \min(u, m)$ is number of DoF in the channel and $\varepsilon_i;\ i = 1, \ldots, \mathbb{N}$ is nonzero eigenvalues of Wishart matrix $\mathbf{W}$ defined as $\mathbf{W} = \mathbf{H}\mathbf{H}^{\mathrm{H}}$; $m \leq u$ and $\mathbf{W} = \mathbf{H}^{\mathrm{H}}\mathbf{H}$; $m > u$.

The capacity C_{MIMO} grows linearly with $\mathbb{N}$ rather than logarithmically as in C_{SIMO} and C_{MISO}. However, this linear increase in capacity is subject to many assumptions such as "quasi-static" flat Rayleigh fading channel (channel varies randomly from frame to frame of data) and correlation free. When the CSI is available at both transmission sides, the optimal capacity for any channel using *waterfilling* solution (maximizing the capacity over $\mathbf{Q}$ subject to $\mathrm{tr}(\mathbf{Q}) \leq \Gamma$) [85] is given in bit/s/Hz as

$$C_{MIMO}^{wf} = \sum_{i=1}^{\mathbb{N}} \log_2(\mu\varepsilon_i)^+ \tag{2.40}$$

where the plus sign denotes taking positive terms only and μ is chosen to satisfy the condition of $\Gamma = \sum_{i=1}^{\mathbb{N}}(\mu - \varepsilon_i{}^{-1})^+$.

Increasing LOS strength at fixed SNR in Rician channels has the effects of capacity reduction to SISO case due to low channel matrix rank. However, this can happen even if we have rich scatter ring around transmit and receive due to the "pipe" effect as in Fig.2.16 [85].

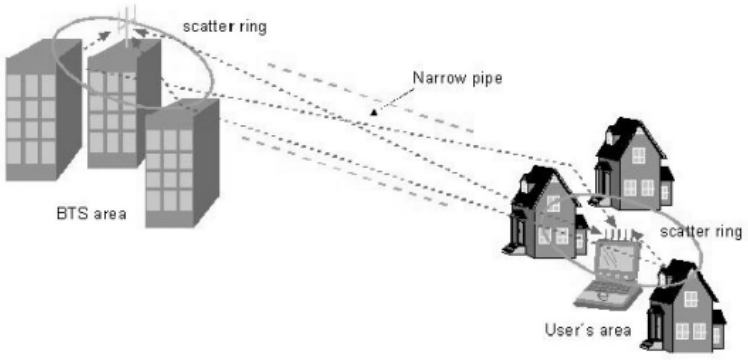

Figure 2.16: Small scatter rings compared to the distance between transmitter and receiver causing low rank channel matrix [85].

2.6.1.3 Capacity-Diversity Tradeoff

Rate and diversity maximizations are the main transmission schemes over SU-MIMO channels. Maximal diversity gain $(L = um)$, is the total number of independent channels between antenna pairs attained when multiplexing gain approaches zero. On the other hand, maximal multiplexing gain $\mathbb{N} = \min(u, m)$ which represents the total number of DoF in the system can be achieved when diversity gain approaches zero [21]. However, space-time coding (STC) such as space-time trellis code (STTC) and space-time block code (STBC) are joint coding schemes used to provide transmit diversity and coding gains without any loss in bandwidth efficiency [84, 85]. STTC offers overall diversity $L \leq um$ at the cost of complex multidimensional Viterbi algorithm at the receiver. Similarly, STBC provides same order of diversity [40] for same number of u antennas but the provided coding gain is minimal or zero. The popularity of STBC over STTC is due to low decoding complexity by using maximum likelihood (ML), zero forcing (ZF), or minimum mean square error (MMSE) techniques [85, 92-94]. Moreover, SM such as V-BLAST can be classified as special class of STBC where

streams of independent data are transmitted over different antennas to maximize the data rate over MIMO channel. Here, signal detection can be done by several methods such as ZF, MMSE, SIC and ML decoding by taking the problem of multiple stream interference into account [84]. The use of those detection methods can provide diversity of $L \leq m$ subject to tradeoff between system complexity and achieved performance. In conclusion, SM offers capacity gain with limited diversity which is not the best choice of transmission for target BER while STC can provide coding and diversity gains which improve the performance. This improvement in the later can be used indirectly to increase the capacity by using higher modulation levels. Moreover, SM and STBC can be combined together in a MIMO system to maximize the average data rate with guarantee of minimum diversity.

2.6.1.4 Practical Considerations

In wireless communication systems, MIMO schemes still have many implementation difficulties [2, 5]. The gain of MIMO systems are well known to be sensitive to channel conditions. Therefore, urban sites are suitable for this case since it provide natural uncorrelated fading channels [84, 85, 95]. However, it comes at cost of receiver complexity in both BS and handsets which affects the wide commercialization of MIMO systems. Channel estimation, correlation amongst antenna elements and high Doppler frequency f_d are other issues which degrade the system performance. Receiver complexity comes from the side of channel model and estimation where full matrix needs to be estimated instead of single coefficient, detection methods, extra RF and hardware circuits, antenna selection algorithms, feedback of CSI to the user transmitter, dual mode of operation to support none MIMO systems and not last, additional processing for equalization or interference cancellation. It is shown that the complexity of 4×4 MIMO is about twice single antenna receiver and more battery life is needed [85]. Design of antenna elements at both communication ends is another important issue where the spacing is a key parameter to avoid fading correlation [95, 96]. At the base station $10\lambda_c$ spacing (1.5m at 2GHz) is enough while $0.5\lambda_c$ at the mobile handset (7.5cm at 2GHz) is a problematic. However, for laptops up to four antenna (maximum number of antenna is envisaged to be four [96]) can be fixed easily.

2.6.2 Multiuser MIMO (MU-MIMO)

By exploiting the spatial dimension in rich fading environment, MU-MIMO technique enables simultaneous communication of multiple users without subdivision in limited resources of time, frequency, and codes [17-19]. It can be considered as and extended version of SU-MIMO for the MAC to increase the spectral efficiency considerably [2-5, 17]. Practically, MU-MIMO with appropriate complexity and performance tradeoff can be implemented by

exploiting the DoF provided by spatial separation of multiple users. However, for the downlink channel there are important needs for precoding techniques, user scheduling and power allocation algorithms. In Fig. 2.17, an example of MU-MIMO system is shown where from all U users, there is a set of K active users each equipped with u_k antennas communicating with m antennas at BS.

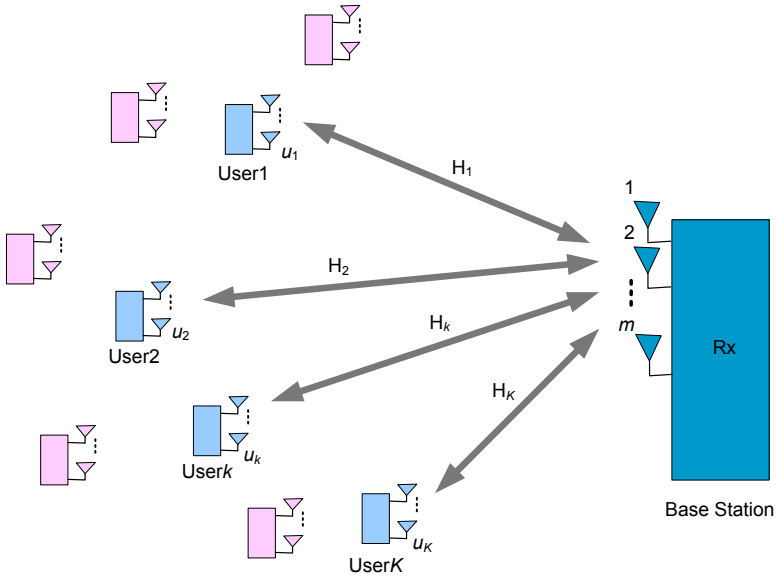

Figure 2.17: MU-MIMO system of one BS having m antennas and U users each has u_k antennas and only K active users out from U are communicating simultaneously.

MU-MIMO has many advantages over SU-MIMO such as [12, 18, 21, 99, 103-106]:

a) Multiple users can be served simultaneously in SDMA fashion by using appropriate precoding technique at the BS.
b) Capacity gain of MAC proportional to the number of BS antennas (m). Hence, the sum rate for K active users will be $R_{sum} = R_1 + R_2 + \cdots + R_K$.
c) Multiuser diversity gain by using proper scheduler to select the best subset of K active users to achieve the highest sum rate.
d) More immune to channel rank loss, appearance of LOS or antenna correlation due to the natural spatial separation between users.
e) Theoretically, a total number of m^2 users each equipped with a single antenna are capable to simultaneously communicate with the BS although simulation results shows numbers between m and m^2 [18].

f) SM gain can be achieved for different data streams from different active users without need for multiple antennas at the terminals.
g) Users' terminals equipped with more than one antenna can get more diversity and/or multiplexing gains at cost of reducing the number of served users.

On the other side, MU-MIMO systems have many disadvantages compared with SU-MIMO which can be summarized as [6, 12, 17, 18, 23, 84, 89, 104, 108]:

a) CSIT is very important for the downlink precoding techniques to achieve user multiplexing gain while it is not essential in the SU-MIMO.
b) Feedback of CSIT reduces the uplink capacity as in wideband systems and high mobility systems.
c) Complex scheduling procedure to select a set of users that will by served simultaneously (exponential relation to the number of served users).
d) Unequal channel conditions among users excite the issues of fairness.
e) Multiple power constraints instead of single.
f) Essential cross-layer design such as power control, user scheduling, antenna combining, and admission control.

In the literature [17, 24, 101, 102, 107, 108], many precoding techniques have been investigated including linear techniques such as MMSE and ZF or non-linear techniques such as dirty paper coding (DPC) or vector perturbation (VP). In addition, many feedback methods are proposed, including dimension reduction, vector quantization, opportunistic SDMA, adaptive feedback, and statistical feed back. Depends upon to precoding and feedback strategies, many scheduling techniques are presented such as max-rate selection, round-robin selection, greedy user selection, and random user selection.

2.6.2.1 Uplink Channel Model

Consider a cellular wireless system of one cell having BS equipped with m antennas and K active users out of U, each of them equipped with u_k antennas as in Fig. 2.17. The received signal vector $\mathbf{r} \in \mathcal{C}^{m\times 1}$ at BS can be written as [17, 18, 99]

$$\mathbf{r} = \sum_{k=1}^{K} \mathbf{H}_k \mathbf{v}_k + \mathbf{n} \tag{2.41}$$

where $\mathbf{v}_k \in \mathcal{C}^{u_k\times 1}$ is transmitted signal vector of k^{th} user. $\mathbf{H}_k \in \mathcal{C}^{m\times u_k}$ is complex Rayleigh flat fading channel matrix of the k^{th} user and assumed to be available at both link sides, and $\mathbf{n} \in \mathcal{C}^{m\times 1}$ is vector of i.i.d complex AWGN with each element having variance of σ_n^2. Each

user is subject to an individual power constraint of P_k which implies $\mathrm{tr}(\mathbf{Q}_k) \leq P_k$; $k = 1, \dots, K$ where the transmit covariance matrix of k^{th} user is defined to be $\mathbf{Q}_k \triangleq \mathrm{E}[\mathbf{v}_k \mathbf{v}_k^{\mathrm{H}}]$.

Capacity of MU-MIMO MAC under constant channel conditions and any set of users' power can be written as [99]

$$C_{MAC}^{const} \triangleq \bigcup_{\substack{\mathbf{Q}_k \geq 0 \\ \mathrm{tr}(\mathbf{Q}_k) \leq P_k}} \left\{ (R_1, \dots, R_K) : \sum_{k=1}^{K} R_k \leq \log_2 \left| \mathbf{I}_m + \sum_{k=1}^{K} \mathbf{H}_k \mathbf{Q}_k \mathbf{H}_k^{\mathrm{H}} \right| \right\} \tag{2.42}$$

For example, in a simplified case of two user system each equipped with one antenna ($u_k = 1;\ k = 1, 2$), the capacity region is equal to $R_1 + R_2 \leq \log_2 \left| \mathbf{I}_m + \mathbf{H}_1 P_1 \mathbf{H}_1^{\mathrm{H}} + \mathbf{H}_2 P_2 \mathbf{H}_2^{\mathrm{H}} \right|$ as shown in Fig. 2.18. Here, the covariance matrices $\mathbf{Q}_1$ and $\mathbf{Q}_2$ are reduced to scalar maximum transmitted powers P_1 and P_2 and the corner point "B1" and "C1" can be achieved by successive decoding.

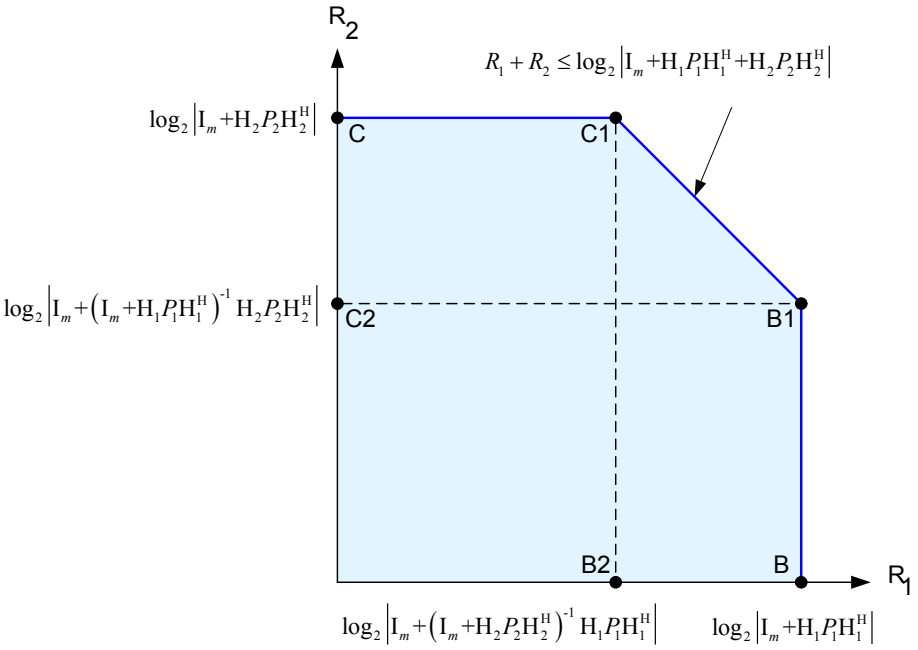

Figure 2.18: Capacity region of two users MIMO MAC communication system where each user has single antenna($u_k = 1$).

For slow fading channel conditions and with the availability of CSI at the transmitters and receiver, the capacity region is found by the time average of capacity at each fading channel instant with constant covariance matrix for each user and given as [99]

$$C_{MAC}^{fad} \triangleq \bigcup_{\substack{\mathbf{Q}_k \geq 0 \\ \mathrm{tr}(\mathbf{Q}_k) \leq P_k}} \left\{ (R_1, \ldots, R_K) : \sum_{k=1}^{K} R_k \leq \mathrm{E}\left[\log_2 \left| \mathbf{I}_m + \sum_{k=1}^{K} \mathbf{H}_k \mathbf{Q}_k \mathbf{H}_k^{\mathrm{H}} \right| \right] \right\} \tag{2.43}$$

The sum capacity of MU-MIMO is found to grow linearly with $\min\left(\sum_{k=1}^{K} u_K\,,\ m\right)$. Thus, increase of receive antennas m will lead to linear growth in capacity while maintaining low cost for users' mobiles.

2.6.2.2 Downlink Channel Model

In the BC of MU-MIMO system, the received signal vector $\mathbf{r}_k \in \mathcal{C}^{u_k \times 1}$ at the receiver of k^{th} user can be written as [17, 99]

$$\mathbf{r}_k = \mathbf{H}_k^{\mathrm{T}} \mathbf{v} + \mathbf{n}_k \ ; \ k = 1, \ldots, K \tag{2.44}$$

where $\mathbf{v} \in \mathcal{C}^{m \times 1}$ is transmitted signal vector from BS. $\mathbf{H}_k \in \mathcal{C}^{m \times u_k}$ is complex Rayleigh flat fading channel matrix of k^{th} user and assumed to be available at both link ends, and $\mathbf{n} \in \mathcal{C}^{u_k \times 1}$ is vector of i.i.d complex AWGN at the receiver of k^{th} user with each element having variance of σ_n^2. The transmitted signal $\mathbf{v} = \sum_{k=1}^{K} \mathbf{v}_k$ is the superposition of modulated users' messages $\mathbf{v}_k \ ; k = 1, \ldots, K$. For power constraint of P, the power allocation needs to maintain the condition of $\sum_{k=1}^{K} P_k \leq P$ which can be written as $\mathrm{tr}(\mathbf{Q}) \leq P$ where $\mathbf{Q} \triangleq \mathrm{E}[\mathbf{v}\mathbf{v}^{\mathrm{H}}]$ is the transmit covariance matrix. Each user will be subject to power constraint of P_k from BS which implies $\mathrm{tr}(\mathbf{Q}_k) = P_k \ ; k = 1, \ldots, K$ where the transmit covariance matrix of k^{th} user is $\mathbf{Q}_k \triangleq \mathrm{E}\left[\mathbf{v}_k \mathbf{v}_k^{\mathrm{H}}\right]$.

The capacity region for a given realization of BC channel matrix can be optimized over each possible ordering of users' power and written as [100]

$$C_{BC} \triangleq \bigcup_{\sum_{k=1}^{K} P_k \leq \mathrm{P}} \left\{ (R_1, \ldots, R_K);\ R_k \leq \log_2 \frac{\left| \mathbf{I}_{u_k} + \mathbf{H}_k^{\mathrm{H}} \left[\sum_{j \geq k} \mathbf{Q}_j \right] \mathbf{H}_k \right|}{\left| \mathbf{I}_{u_k} + \mathbf{H}_k^{\mathrm{H}} \left[\sum_{j > k} \mathbf{Q}_j \right] \mathbf{H}_k \right|} \right\} \tag{2.45}$$

In fact, it is difficult to calculate this capacity region. However, by using the duality between MAC and BC this problem will be simplified. Thus, BC capacity region can be found through the union of all MAC regions assuming that all uplink power allocations satisfies the sum power constraint of $\sum_{k=1}^{K} P_k \leq P$.

2.6.2.3 Precoding Techniques

Precoding techniques are an important issue in the DL of MU-MIMO to achieve higher sum rate based on a good knowledge of CSIT (i.e. BS). It is classified into two categories, linear and nonlinear [17, 24, 101, 102].

A. Linear Precoding

This type of precoding can be seen as a generalization of the conventional SDMA, where different precoding matrices $\mathbf{W}_k \; ; k = 1, \dots , K$ are assigned to K active users at the BS transmitter. Based on CSIT, precoders are designed jointly in different methods such as ZF and MMSE to maximize the performance metrics such as sum rate, BER and signal to interference-plus-noise ratio (SINR) for each data stream. For K selected users by the scheduler from U, the transmitted signal for each user $\mathbf{s}_k \; ; k = 1, \dots , K$ is pre-multiplied by ZF or MMSE inverse of the multiuser channel matrix. Hence, the received signal vector at k^{th} user mobile is given by

$$\mathbf{r}_k = \mathbf{H}_k^{\mathrm{T}} \mathbf{W}_k \mathbf{s}_k + \mathbf{H}_k^{\mathrm{T}} \sum_{\substack{i=1 \\ i \neq k}}^{K} \mathbf{W}_i \mathbf{s}_i + \mathbf{n}_k \quad ; \quad k = 1, \dots , K \tag{2.46}$$

where the second term represents the multiuser interference and when the K users are not sufficiently separated, this leads to rate loss due to inefficient use of transmit power. Another disadvantage here is the performance degradation when multiple receive antennas or streams are extended. To solve this problem, a generalized ZF beamforming (ZFBF) are used when $\sum_{k=1}^{K} u_k = m$ with equal number of antennas and data streams of all users. Suitable $\mathbf{W}_k$ is used in this method to pre-cancel the interference $\left(\mathbf{H}_i^{\mathrm{T}} \mathbf{W}_k = 0 \; ; \; \forall i \neq k\right)$. Thus, received signal at user k will be $\mathbf{r}_k = \mathbf{H}_k^{\mathrm{T}} \mathbf{W}_k \mathbf{s}_k + \mathbf{n}_k$ at cost of extra signal processing due to need of feedback at the receiver side and iterative solutions at the transmitter (BS) [101, 102].

B. Nonlinear Precoding

Nonlinear precoding involves extra signal processing compared with the linear version for higher performance improvement in case of small number of active users U (leak in user diversity) [17, 24]. The main methods used for nonlinear precoding are based on VP, spatial extension of Tomlinson-Harashima precoding (THP) and the optimal DPC. For example, transmit power enhancement incurred by ZF method are avoided by the use of VP where solving of minimum distance problem are involved for modulo operation at the transmitter. For single antenna receiver and composite multiuser channel matrix $\mathbf{H} \in \mathcal{C}^{m \times K}$, the idea is to

minimize the transmit power P by searching for a perturbation vector $\boldsymbol{p}$ from an extended constellation as

$$\boldsymbol{p} = \arg\left[\min_{\boldsymbol{p}' \in M\mathcal{C}\mathbb{Z}^K} \|\mathbf{G}(\mathbf{s} + \boldsymbol{p}')\|^2 \right] \tag{2.47}$$

where $\mathbf{G}$ represents a transmit channel matrix satisfying $\mathrm{tr}(\mathbf{g}^{\mathrm{H}}\mathbf{g}) \leq P$ by using for example ZF or MMSE precoders, $\mathbf{s}$ is modulated transmit signal vector, M is the original constellation size and $\mathcal{C}\mathbb{Z}^K$ is the K-dimensional complex lattice.

2.6.2.4 Scheduling Techniques

To maximize the throughput of MU-MIMO systems, the best subset of K active users from U should be selected with least computational complexity [17 and references therein], [107], [108]. Many optimal and suboptimal algorithms are proposed to exploit the natural multiuser diversity in MU-MIMO such as max-rate selection, round-robin selection, greedy user selection, and random user selection. The optimal maximum rate method requires search of $\mathcal{O}(U^K)$ possible user sets which is prohibited due to the computational complexity. Therefore, suboptimal technique by using greedy user selection is used by choosing the first user with the highest channel capacity followed by searching for the next user that enables maximum rate and so on till K^{th}user. The complexity of this method is of $\mathcal{O}(U \times K)$ which is much less than the max-rate technique. However, both of them are suffering from the fairness issue among users. One of the methods used to solve this problem is the random user selection which has a drawback of wasting capacity.

2.6.2.5 Multiuser Detection (MUD) Techniques

The most popular MUD techniques for MU-MIMO can be classified into *linear* and *nonlinear* schemes where the attainable performance and complexity are mainly depends on the problem formulation and their objective or the cost function.

Linear MUD techniques such as ZF and MMSE provides limited performance at low detection complexity due to the employment of linear front-ends $\mathbf{G}$ as in Fig. 2.19 to separate data streams firstly followed by individual decoding. On the other hand, nonlinear MUD methods such as ML can achieve optimal performance at cost of high computational complexity increased exponentially with the number of simultaneous K active users. Due to complexity issue, practical implementation of ML in overloaded system scenarios is prohibitive leading to search for suboptimal nonlinear MUD techniques [12, 24, 50, 52, 84].

In the literature, many of suboptimal MUD methods have been proposed such as SIC [24, 50], parallel interference cancellation (PIC) [52, 84], sphere decoding (SD) family [109-112], and MUD based minimum bit error rate (MBER) algorithms [113-115] as well as genetic algorithms (GA) [12, 113]. Practically, the *rank-deficient* scenario (overloaded systems when $K > m$) have attracts the main concerns of MUD developments where channel matrix $\mathbf{H}$ becomes noninvertible reducing the DoF required for signal detection. A brief review of some MUD techniques is given below assuming simultaneous communication of K active users each equipped with one antenna in flat Rayleigh fading channel.

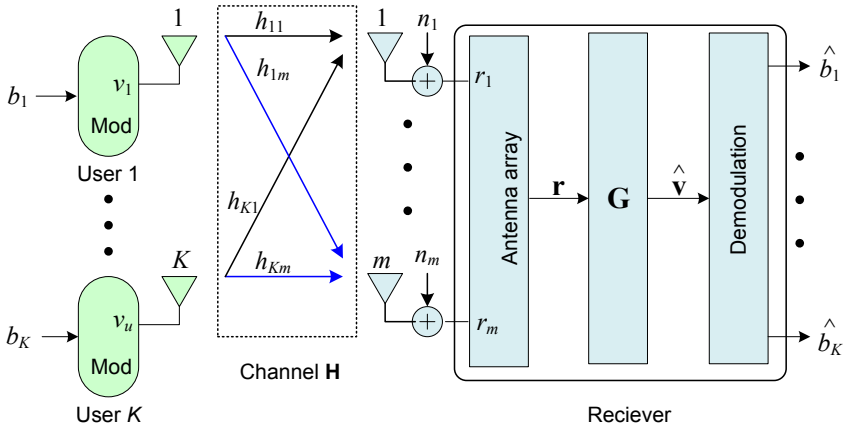

Figure 2.19: Linear receiver for MU-MIMO system of one BS having m antennas and K active users where each user has equipped with one antenna.

A. ZF Receiver

The linear ZF receiver (also known as the *decorrelator* or *interference nulling* receiver) [24, 84, 116, 117] has a front-end $\mathbf{G}_{zf} = \mathbf{H}^{\dagger}$ where $\mathbf{H}^{\dagger} = \left(\mathbf{H}^{\mathrm{H}}\mathbf{H}\right)^{-1}\mathbf{H}^{\mathrm{H}}$ denotes the Moore-Penrose inverse of the channel matrix $\mathbf{H} = [\mathbf{h}_1 \quad \cdots \quad \mathbf{h}_k \quad \ldots \quad \mathbf{h}_K]\,; k = 1, \ldots, K$. The front-end $\mathbf{G}_{zf}$ are constructed from bank of K decorrelators, one decorrelator for each user data stream. Thus, it decouples the matrix channel into parallel scalar channels where k^{th} decorrelator is the k^{th} column in $\mathbf{G}_{zf}$. For special case when $\mathbf{H}$ is square and invertible then, $\mathbf{H}^{\dagger} = \mathbf{H}^{-1}$ and ZF receiver is simply given by channel inversion. In general, the output of ZF receiver with perfect CSIR is given by

$$\hat{\mathbf{v}} = \mathbf{G}_{zf}(\mathbf{H}\mathbf{v} + \mathbf{n}) = \mathbf{v} + \mathbf{H}^{\dagger}\mathbf{n} \tag{2.48}$$

It is obvious that the joint decoding problem is converted to K single stream decoding problem which significantly reduce the decoding complexity and eliminates the multiple user interference (MUI). However, this reduction in complexity comes at cost of noise enhancement (it can be reduced by using proper scheduling to avoid poor channels [116]) causing significant degradation in performance compared with ML receiver. Moreover, it should be noted that each user spatial signature $\mathbf{h}_k = [h_{11} \dots h_{1m}]^T ; k = 1, \dots, K$ is not a linear combination of the others (orthogonal) for successful decoding. Hence, ZF requires $\sum_{k=1}^{K} u_k \leq m$ or $K \leq m$ in case of single antenna per user handset ($u_k = 1 ; k = 1, \dots, K$). The achieved diversity in this case is of order $m - K + 1$ for each user and the maximum achievable rate is

$$R_{zf} = \mathrm{E}\left[\sum_{k=1}^{K} \log_2(1 + \Gamma_k \|\mathbf{h}_k\|^2)\right] \tag{2.49}$$

where $\Gamma_k = P_k / N_o$ is SNR of k^{th} user.

B. MMSE Receiver

The linear MMSE receiver has the functionality of maximizing the output SINR and minimizing the mean square error in estimating the transmitted signals for all range of SNR [24, 50, 52, 118]. It works like the decorrelator for high SNR (MUI is greater than noise level) and like the match filter receiver (receive beamforming) for low SNR values (MUI is less than noise level). The front-end $\mathbf{G}_{mmse}$ of this receiver is constructed from bank of K-MMSE receivers (one for each user data stream) and given by

$$\mathbf{G}_{mmse} = \left(\mathbf{H}^{\mathrm{H}}\mathbf{H} + \boldsymbol{\mathcal{J}}\right)^{-1}\mathbf{H}^{\mathrm{H}} \tag{2.50}$$

where $\boldsymbol{\mathcal{J}}$ is $K \times K$ diagonal matrix with entries of $\mathcal{J}_{kk} = 1/\Gamma_k$, and $\Gamma_k = P_k / N_o$ is SNR of k^{th} user. At low SNR, the MMSE receiver approaches the match filter and outperforms ZF. For high SNR, the performance of MMSE and ZF are close together ($\mathbf{G}_{mmse} = \mathbf{G}_{zf}$). The total throughput R_{mmse} of K active users each equipped with single antenna can be shown as

$$R_{mmse} = E\left[\sum_{k=1}^{K} \log_2\left(1 + P_k \mathbf{h}_k^{\mathrm{H}} \mathbf{N}_k^{-1} \mathbf{h}_k\right)\right] \tag{2.51}$$

where $\mathbf{N}_k$ is invertible covariance matrix of the complex circular symmetric colored noise of k^{th} user.

C. ML Receiver

The optimal nonlinear ML receiver performs signal decoding through exhaustive search for the most likely transmitted signals and hence, minimizing the error probability at the expense of high complexity [12, 50, 52]. For system of K active users each equipped with single antenna and using M alphabet size of constellation (modulation levels), total metric calculations of $D = M^K$ is needed. So, as K increased, the complexity increases exponentially. ML receiver provides receive diversity of order $L = m$ and the signal estimation is formed as

$$\hat{\mathbf{v}} = \arg\left\{ \min_{\mathbf{v}_q \in \boldsymbol{V};\, q=1,\dots,D} \left\| \mathbf{r} - \mathbf{H}\mathbf{v}_q \right\|^2 \right\} ; \;\; \mathbf{v}_q = \left[\boldsymbol{v}_q^{(1)}, \dots, \boldsymbol{v}_q^{(k)}, \dots, \boldsymbol{v}_q^{(K)} \right]^{\mathrm{T}} \tag{2.52}$$

where, $\boldsymbol{V} = \{\mathbf{v}_1, \mathbf{v}_2, \dots, \mathbf{v}_q, \dots, \mathbf{v}_D\}$ is the set of all possible transmitted signals vectors and $\mathbf{v}_q$ is the q^{th} possible vector.

D. SIC Receiver

The SIC receiver is one of the nonlinear MUD methods which invoke an iterative signal processing method that combines signal detection and modulation. For MU-MIMO, SIC can be used with ZF or MMSE front-end ($\mathbf{G}$) to detect users' signal where the arranged individual data streams according to their SINR are decoded successively [6, 12, 24, 50, 52, 84, 119]. This hybrid combination is usually referred to as V-BLAST receiver. As shown in Fig. 2.20, the first decorrelator or MMSE receiver is used to decode the individual data stream $\hat{b}_1$ of highest SINR assuming all the others as interference. Next, the re-encoded data of this user will be subtracted from the received vector. The second data stream will be detected using the same procedure until the last user who has the lowest signal power and no interference to deal with also detected. Since the lowest power users' data is detected last without interference from the others, it will achieve high diversity gain to mitigate the effects of channel fade. However, it has to be noted that SIC is very sensitive to error propagation due to power ordering of users' signals and re-encoding of the estimated data in $K - 1$ stages. Without error propagation (e.g. by using efficient coding), MU-MIMO channel will be converted to parallel SISO channels and the diversity order will be increased at each stage.

This technique can be used for near-far scenarios with the absence of perfect power control to achieve diversity gain at each detection stage. However, it comes at cost of slightly high complexity due to extra computations and comparisons for SINR of the remaining users' streams at each layer.

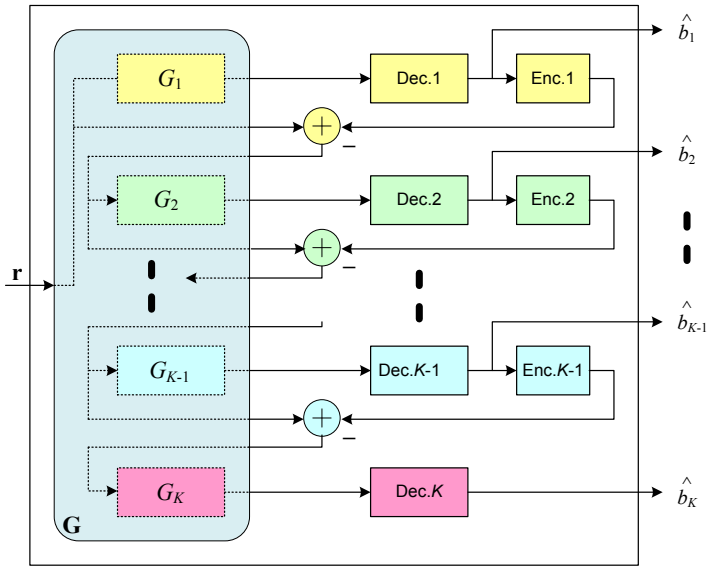

Figure 2.20: MUD using SIC with a bank of decorrelators or MMSE receivers ($G_k; k = 1, \dots, K$) for MU-MIMO system of K active users ordered such that user 1 has highest SINR and user K has the lowest.

E. SD Receiver

One of the powerful receivers is the SD or its generalized form (GSD) in which the performance of ML can be approached with less complexity (polynomial in the number of individual data streams) by controlling the radius of the search sphere. Hence, efficient detection algorithm has to identify the lattice points that surrounded by the decoding sphere of a given relevant radius [109, 110]. However, complexity of GSD is increased (exponentially with difference of transmit and receive antennas) for rank-deficient channels where the total number of transmit antennas are greater than available receive antennas $\sum_{k=1}^{K} u_k > m$. Recently, many researchers such as [111, 112 and references therein] have tried to develop fast and low complexity GSD for overloaded MIMO systems with close performance to ML decoding. For example, efficient MIMO soft decoder with the list-version of slab SD (SSD) is proposed by [111] and capable of generating reliable soft-bit estimates as inputs for iterative soft decoding for higher performance and affordable complexity.

2.6.2.6 Capacity-Diversity Tradeoff

In addition to *diversity* and *multiplexing* gains that can be achieved in SU-MIMO, *multiple access* gain can be achieved in MU-MIMO systems by serving multiple users simultaneously [21]. This can be done by exploiting BS antennas to spatially separate signals originated from different users. Therefore, maximal multiple access gain m can be achieved by selecting the best set of $K = m$ users with highest channel gains using scheduling algorithm. Here, multiuser diversity is attained as well since we have the ability to select the best set of users having

highest SNR at each channel realization to increase the sum rate or user rate while minimizing the transmit power.

Multiplexing gain of the DL is limited by the number of BS antennas m. Hence, the BS can serve up to $\sum_{k=1}^{K} u_k \leq m$ antennas at the users' side. When the user terminals having $\sum_{k=1}^{K} u_k \geq m$ antennas with full user channel matrix rank, the BS may decide to either transmit multiplexed signal to one user or to multiuser achieving same multiplexing gain m [17, 18].

In the symmetric case where all users are equipped with same number of antennas $u_1 = \cdots u_K$, the multiplexing gain for all users in the UL channel are equal and represents the DoF per user $\{\mathbb{N}_k = \min(u_k, m/K),\ k = 1, \ldots, K\}$. In such a case, the total number of DoF for multiuser diversity is $u = \sum_{k=1}^{K} u_k$ and the overall multiplexing gain will be $\min(u, m)$.

2.6.2.7 Practical Considerations

MU-MIMO schemes have not widely adopted in existing and future standards and more concentrated studies are needed to find out the system gain and tradeoffs [2-5, 8, 10, 13, 17, 23, 101, 102]. The most challenging problems can be addressed as:

a) Estimation of very fine CSI for moderate and high mobility systems still difficult with the available technologies.
b) Existence of channel correlation due to poor scattering environment will have the effects to reduce the promised system gains.
c) The lack of simple models for simulating correlated fading channels will lead to inaccurate capacity and BER performance evaluations.
d) For CSIT feedback design metrics, measurement of SINR depends on the number of simultaneous served users and their assigned powers along with the user making the measurement.
e) Opportunistic scheduling requires feedback of CSIT and signalling of the scheduling decision which introduce overhead and latency in the system.
f) Increase of system complexity as the number of served users increases beyoned the number of BS antennas.
g) Difficulties in design low cost mobile handset having multiantenna and complex MUD techniques.
h) The impact of system loading and practical traffic models as in real time services or schemes depending on high user loads.

2.7 Conclusions

In this chapter, a relevant technical background theory and literature review of the basic elements and concepts for the related work in this thesis has been presented. Simple review of fading channels that affects the performance of wireless systems and diversity methods are presented first. After that, it is explained that multiple access techniques represent one of the most challenging topics in the next generation wireless communications such as cellular systems. As a result, new multiple access methods requires efficient use of the limited available spectrum to meet the increasing demands of high data rate applications and admissible number of users per cell in different channel conditions.

Extensive analysis on the capacity region of Gaussian MAC and simulation results of different 2-user multiple access techniques have been demonstrated. The benchmark results show that spatial dimension enables significant increase in the capacity. It represents the best competitive direction to meet the requirement of future mobile communications. Furthermore, S-C and SIC are examples of promising techniques which can be integrated with other multiple access methods for further improvement in the wireless systems such as increasing the capacity with low complexity requirements.

By exploiting the spatial dimension and without consuming extra bandwidth and power resources, MIMO systems enables high capacity and reliability in rich scattering environments. For SU-MIMO, the fundamental concepts, technical details, SM technique, and information theoretic capacity are presented. In addition, capacity-diversity tradeoff and the main practical challenges are highlighted. For MU-MIMO systems, the basic concepts and technical details are discussed first followed by highlighting the main advantages and disadvantages compared with SU-MIMO schemes. Relevant review of precoding, scheduling, and MUD techniques utilized in MU-MIMO systems are presented. Furthermore, capacity-diversity tradeoff and the most challenging problems are addressed.

Modeling of realistic fading channels with different correlation levels is very important for evaluating and developing wireless communication systems. In the next chapter, two novel and simple techniques for the accurate generation of correlated fading channels are proposed.

Chapter 3

Correlated Channel Modeling and Simulations for Wireless Systems

3.1 Introduction

In the last decade, different multiantenna and multicarrier schemes are considered to meet high spectral efficiency demands for wireless communication services and potentially leading to Gigabits communications [2, 3, 5, 9, 11, 12, 84]. However, the typical assumption of uncorrelated fading channels due to simplicity and lack of simple methods for generating any number of fading channels with an arbitrary cross-correlation tends to exaggerate diversity, capacity, and multiplexing gains. Therefore, generation of realistic fading channels is crucial for evaluating the performance improvement of any communication system and important perquisite for design, deployment and integration of new techniques into real wireless applications [120, 121].

In this chapter, two simple techniques are proposed for accurate generation of equal and unequal power CRFC for multiantenna and multicarrier systems after analyzing the shortcomings of previous methods. Spatial and spectral correlation parameters such as Doppler frequency shift, propagation delay spread and subcarriers frequency separation are also considered for different transmission conditions.

The first technique employs successive coloring of fading signals (i.e. making the fading signals correlated [135]) for all successive pairs using real correlation vector of desired signal envelopes rather than complex covariance matrix of the Gaussian samples as in conventional method. It enables simulation of any number of fading signals with any desired correlations of successive envelope pairs. Correlations of all other pairs are determined by the related successive pairs which are in the admissible interval satisfying them. Through extensive simulations of different practical scenarios, it is shown that the proposed technique can overcome the shortcomings of conventional methods particularly as the number of fading signals increased and/or moderate to high correlations is used. For small number of fading signals and/or low correlation levels, it provides high accuracy for successive pairs of signals similar to conventional methods with less computational complexity.

In the second technique, iterative coloring of uncorrelated reference signals is employed to generate any number of fading signals with any correlations using real correlation matrix of

desired signal envelopes. Different practical system scenarios are simulated to show the effectiveness of this technique.

The simplicity and accuracy of these methods will help the research community to study and simulate the impact of channel correlations on the performance evaluation of various multiantenna and multicarrier systems. Moreover, they enable efficient design and integration of new schemes into feasible wireless applications.

This chapter is organized as follows. Literature review on the generation methods of correlated fading channels are presented in Section 3.2. Analysis of previous techniques for the generation of CRFC is given in Section 3.3. In Section 3.4, the proposed successive coloring technique is presented with generalized algorithm, complexity analysis, and simulation of practical system scenarios. In Section 3.5, Iterative coloring technique is given with generalized algorithm, complexity analysis, and simulation of practical system scenarios. Finally, chapter conclusions are withdrawn in the last section.

3.2 Literature Review on the Generation Methods of Correlated Fading Channels

Different multiantenna and multicarrier schemes are adopted to fulfil high data rate and QoS of 4G cellular systems. Such important systems are SU-MIMO [2, 5, 84], MU-MIMO [3, 5, 17], OFDM [1, 52, 122], OFDMA [5, 7], MC-CDMA [11, 52, 123], MIMO-OFDM [4, 10, 12, 88], MIMO-OFDMA [2, 3, 5, 7], MIMO-CDMA [13, 14, 124, 125], and MIMO-MC-CDMA [9, 15, 16, 126]. However, it is well known that propagation channel modelling have a crucial impact on the capacity and error performance evaluations for any wireless communication system. Therefore, realistic channel modelling for different radio propagation conditions has attracted much attention by the research community [23, 33, 120, 121, 127-129].

Typically, in the analysis of multiantenna and multicarrier systems, models of independent fading channels are usually assumed due to the lack of a simple procedure for generating fading signals with an arbitrary cross-correlation. However, it is well known that channels' correlation has direct influence on the diversity, multiplexing and capacity gains [123, 130-132]. It can happen due to insufficient antenna separation at transmit and/or receive ends, poor scattering environment, small coherence bandwidth of the channel or inadequate frequency separation among subcarriers [23, 133, 134].

Based on Jakes' work [31] and for $\mathcal{N} \times \mathcal{N}$ desired covariance matrix of $\mathcal{N}$ correlated Rayleigh fading envelopes, accurate generation methods for $\mathcal{N} = 2$ have been presented by many researchers such as [135, 136]. However, for $\mathcal{N} > 2$ envelopes, many algorithms have been proposed with different limitations that affects their applicability in realistic channel conditions such as [133, 134, 137, 138]. Generation of multiple correlated Rayleigh or Rician process that possess specified cross-correlation and auto-correlation functions are investigated

in [139] using vector autoregressive stochastic model. In [140], Gaussian vector autoregressive process and inverse transform sampling techniques are utilized to generate fading processes with desired cross-correlation, auto-correlation, and heterogeneous probability density functions (Rayleigh, Rician, and Nakagami). The main shortcomings of the aforementioned methods are summarized as follows:

1) The assumption of real covariance matrix in [137] leads to high restriction of use to special cases since covariance matrices are more likely to be complex in reality.
2) The covariance matrix must be *positive definite* (i.e., positive eigenvalues) for successful factorization using Cholesky decomposition as in [138, 139] or *positive semidefinite* (i.e., zero or positive eigenvalues) when Eigenvalue decomposition is utilized [133].
3) The *nonpositive semidefinite* or *unrealizable* covariance matrices produce unstable Gaussian vector autoregressive process as in [139, 140] methods.
4) High computational burden for covariance matrix factorization using Cholesky or Eigenvalue decomposition methods as in [133, 134, 137-139].
5) As $\mathcal{N}$ increased, the desired cross-correlation values will be limited to short interval of operation within the required accuracy tolerance as in [133, 134, 138-140].
6) In [133, 134, 138-140] and for complex covariance matrices, generation of fading processes with high cross-correlation level such as 0.9 is not possible for $\mathcal{N} \geq 3$ and as $\mathcal{N}$ increased, the correlation level that can be simulated will decrease. Therefore, none of these methods can generate any number of fading processes with any desired covariance matrix.

Motivated by the aforementioned shortcomings, simple correlated fading channel models are essentially needed to enable accurate performance analysis of promising communication systems under realistic propagation environments. For efficient models, generation of any number of fading signals with any desired covariance matrices is of high importance. Moreover, *spectral* and *spatial* correlation parameters such as Doppler frequency shift, propagation delay spread, subcarriers frequency separation, antenna spacing, and angular spread should be included.

In this chapter, we are focusing on the generation methods of CRFC due to its popularity of representing radio signals in mobile cellular systems. Therefore, analysis of previous techniques is provided in the next section due its usefulness for new models developments.

3.3 Analysis of Previous Techniques on the Generation of Correlated Rayleigh Fading Channels (CRFC)

Conventionally, a vector of $\mathcal{N}$ complex correlated signals $\mathbf{A} \in \mathcal{C}^{1\times\mathcal{N}}$ with the desired complex covariance matrix $\mathbf{R}_{AA} = \mathrm{E}\{\mathbf{A}\mathbf{A}^H\} \in \mathcal{C}^{\mathcal{N}\times\mathcal{N}}$ is generated by the use of coloring matrix $\mathbf{L}$ [135, 136] and vector $\mathbf{Z} \in \mathcal{C}^{1\times\mathcal{N}}$ of $\mathcal{N}$ predefined samples of unit power uncorrelated complex Gaussian signals that have Rayleigh envelopes. The coloring matrix $\mathbf{L}$ is the lower triangle matrix found by performing factorization of the covariance matrix using Cholesky decomposition as $\mathbf{R}_{AA} = \mathbf{L}\mathbf{L}^H$ [134]. It has the function of correlating the elements of $\mathbf{Z}$ to produce the desired complex Gaussian vector through the transformation $\mathbf{A} = \mathbf{L}\mathbf{Z}$ [137, 138].

Since covariance matrices are more likely to be complex in reality, the assumption of real covariance matrix in [137] leads to high restriction of use to special cases such as the real transmit or receive antenna correlation matrices in multiantenna systems [23, 131]. In this case, *envelopes* and *phases* of the complex signals are correlated in contrast to complex covariance matrices which produce correlation in envelopes only. For example, envelopes and phases of three highly correlated Rayleigh fading signals are shown in Fig. 3.1 using the following *real* covariance matrix [131]

$$\mathbf{R}_{AA} = \begin{bmatrix} 1 & 0.95 & 0.95 \\ 0.95 & 1 & 0.95 \\ 0.95 & 0.95 & 1 \end{bmatrix} \tag{3.1}$$

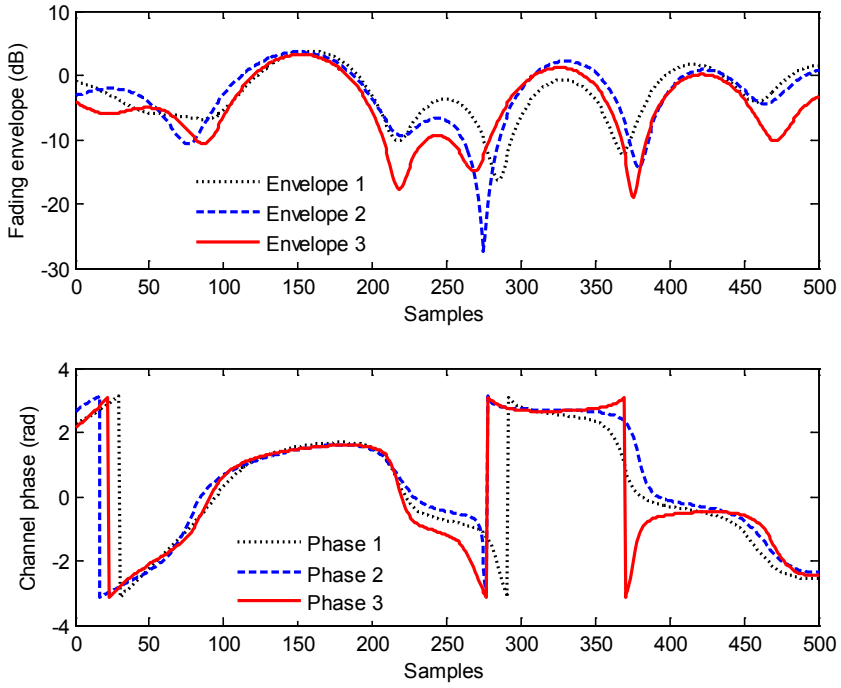

Figure 3.1: Envelopes and phases of three highly correlated Rayleigh fading signals using real covariance matrix.

As can be seen from this figure, all envelopes and phases are very close to each other according to the given desired correlation matrix $\mathbf{R}_{AA}$.

For complex covariance matrices, algorithm of [138] is severely limited by the requirement of positive definite covariance matrix $\mathbf{R}_{AA}$ for successful factorization. Theoretically, covariance matrices are positive definite since the nonpositive definite matrices cannot represent feasible systems where the correlation between any two signal envelopes are not lying in the interval specified by the correlations of all other envelopes. However, covariance matrices formulated empirically for more than two signals can be nonpositive definite [133, 134]. In this situation, the diagonal matrix of eigenvalues $\mathbf{\Lambda}$ resulting from eigenvalue decomposition $\mathbf{R}_{AA} = \mathbf{V}\mathbf{\Lambda}\mathbf{V}$ will have zero or negative values where $\mathbf{V}$ is eigenvector matrix. To overcome this shortcoming, Eigenvalue decomposition is performed in [133] rather than Cholesky decomposition which requires the covariance matrix to be at least positive semidefinite. At cost of accuracy penalty, the procedure performs a replacement of negative eigenvalues in $\mathbf{\Lambda}$ by zeros to produce approximate $\widehat{\mathbf{\Lambda}}$ for coloring matrix calculation as $\mathbf{L} = \mathbf{V}\sqrt{\widehat{\mathbf{\Lambda}}}$. In [134], zero and negative eigenvalues of $\mathbf{\Lambda}$ are replaced by small positive values to find $\widehat{\mathbf{\Lambda}}$ and the approximate covariance matrix $\widehat{\mathbf{R}}_{AA} = \mathbf{V}\widehat{\mathbf{\Lambda}}\mathbf{V}$ is used for coloring matrix calculation using Cholesky decomposition as $\mathbf{L}\mathbf{L}^H = \widehat{\mathbf{R}}_{AA}$.

Complex covariance matrices of the desired correlated signals have direct influence on the performance and limitations of [133, 134, 138] algorithms. To clarify this fact by an example, Monte Carlo simulation results of probability of positive definite covariance matrices as a function of minimum correlation allowed between any pair of signal envelopes $\rho_{kq}, (k \neq q) = 1, \dots, \mathcal{N}$ are illustrated in Fig. 3.2. Different numbers of envelopes $\mathcal{N}$ are used for different values of propagation factor $\mathbb{k}$ which represents the product of frequency separation between adjacent signals and the channel delay spread as will be explained in the next section. From this figure and for all $\mathbb{k}$ values, it is noticed that as $\mathcal{N}$ is increased from 3 to 6, the probability of getting positive definite covariance matrix is decreased sharply. As a result, the algorithm of [138] using Cholesky decomposition can not be applied to generate $\mathcal{N} \geq 5$ envelopes with moderate to high correlations. This is also shown by another example where the desired correlations of all successive envelopes are set to be equal with $\mathbb{k} = 1$ and the range of all other correlations are measured using Monte Carlo simulation.

In Table 3.1, cells marked by "Not Valid" represent the regions where algorithm of [138] is not able to generate the required envelopes. Similarly, results of algorithms given in [133, 134] are shown in Table 3.2 within error tolerance $\varepsilon = \mp 10\%$. The performance is better than [138] but still unfeasible for moderate to high correlations when five or more correlated envelopes are required. As $\mathcal{N}$ is increased from 3 to 6 in the examined algorithms, the range of allowed correlation between any nonsuccessive envelopes shrinks to short interval of operation within

the required accuracy tolerance. Moreover, none of these algorithms is able to generate envelopes $(\mathcal{N} \geq 3)$ with high correlation of 0.9 and more which seriously affects the applicability of these algorithms.

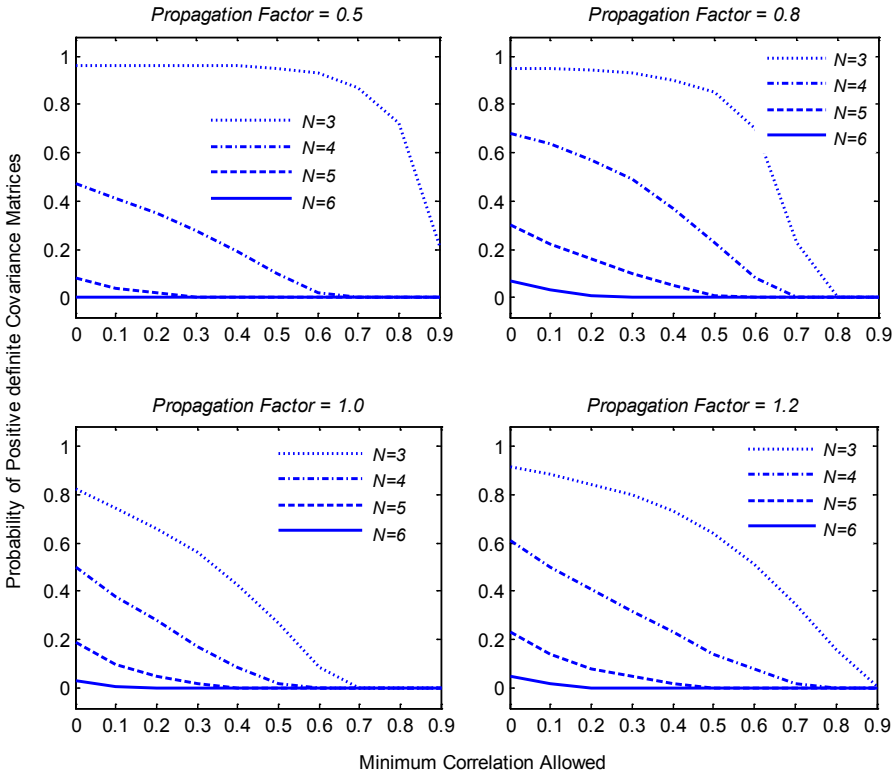

Figure 3.2: Probability of positive definite covariance matrices as a function of number envelopes $\mathcal{N}$, propagation factor $\mathbb{k}$, and minimum correlation allowed between any pair of envelopes $\rho_{kq}, (k \neq q) = 1, \ldots, \mathcal{N}$.

Table 3.1: Desired correlation of all successive envelopes with $\mathbb{k} = 1$ and the range of all other correlations using algorithm of [138]

Desired correlation of all successive envelopes	Correlation range of all other envelopes			
	$\mathcal{N} = 3$	$\mathcal{N} = 4$	$\mathcal{N} = 5$	$\mathcal{N} = 6$
0.0	0.00 - 1.00	0.00 - 0.38	0.00 - 0.22	0.00 - 0.14
0.1	0.00 - 0.97	0.00 - 0.45	0.00 - 0.26	0.00 - 0.18
0.2	0.00 - 0.94	0.00 - 0.45	0.00 - 0.27	0.00 - 0.19
0.3	0.00 - 0.91	0.00 - 0.44	0.00 - 0.27	0.00 - 0.20
0.4	0.00 - 0.86	0.00 - 0.42	0.00 - 0.27	0.05 - 0.20
0.5	0.00 - 0.79	0.00 - 0.39	0.00 - 0.27	0.12 - 0.20
0.6	0.00 - 0.69	0.00 - 0.34	Not Valid	Not Valid
0.7	Not Valid	Not Valid	Not Valid	Not Valid
0.8	Not Valid	Not Valid	Not Valid	Not Valid
0.9	Not Valid	Not Valid	Not Valid	Not Valid
1.0	Not Valid	Not Valid	Not Valid	Not Valid

Table 3.2: Desired correlation of all successive envelopes with $\mathbb{k} = 1$ and the range of all other correlations using algorithms of [133] and [134] within error tolerance $\varepsilon = \mp 10\%$

Desired correlation of all successive envelopes	Correlation range of all other envelopes $\mp\varepsilon$			
	$\mathcal{N} = 3$	$\mathcal{N} = 4$	$\mathcal{N} = 5$	$\mathcal{N} = 6$
0.0	0.00 - 1.00	0.00 - 0.39	0.00 - 0.25	0.00 - 0.16
0.1	0.00 - 1.00	0.00 - 0.48	0.00 - 0.32	0.00 - 0.21
0.2	0.00 - 1.00	0.00 - 0.56	0.00 - 0.35	0.00 - 0.21
0.3	0.00 - 1.00	0.00 - 0.56	0.00 - 0.35	0.00 - 0.21
0.4	0.00 - 1.00	0.00 - 0.52	0.00 - 0.34	0.05 - 0.21
0.5	0.00 - 0.97	0.00 - 0.48	0.00 - 0.33	0.12 - 0.21
0.6	0.00 - 0.93	0.00 - 0.45	0.10 - 0.32	Not Valid
0.7	0.12 - 0.86	0.20 - 0.42	0.20 - 0.30	Not Valid
0.8	0.40 - 0.84	0.25 - 0.35	Not Valid	Not Valid
0.9	Not Valid	Not Valid	Not Valid	Not Valid
1.0	Not Valid	Not Valid	Not Valid	Not Valid

To achieve the diversity, multiplexing, and capacity gains promised by multiantenna systems, the total number of channels between transmit and receive antennas is more likely to be moderate to high [141, 142]. For example, MIMO systems with $M_t = 4$ transmit antennas and $M_r = 4$ receive antennas has $\mathcal{N} = M_t M_r = 16$ channels. Furthermore, in multicarrier systems such as MC-CDMA, the total number of channels is usually high, for example, $\mathcal{N} = 256$ channels (subcarriers) are required to support 256 users. Consequently, hybrid combinations from these two systems will result in large number of fading channels. Therefore, all of the aforementioned promising communication schemes involve large number of fading channels which is difficult to be simulated using existing modelling methods.

In the next sections, two methods with different approaches are proposed for the generation of any number of equal and unequal power CRFC with any desired correlation. The first method is referred to as *Successive Coloring Technique* (SCT) [219] while the second method is called as *Iterative Coloring Technique* (ICT) [141, 142]. In these techniques, the real correlation matrix of fading envelopes is utilized rather than complex covariance matrix which is utilized in conventional methods to reduce the complexity considerably. This matrix is real since it represents the magnitudes (envelopes) of the complex Gaussian signals of desired covariance matrix. Moreover, factorization of the desired covariance matrix is avoided to overcome the shortcomings and high complexity of conventional methods while marinating all required statistical properties. Spectral and spatial correlation parameters are considered also in the proposed methods. For realistic channel modeling, the deterministic sum of sinusoids (SoS) method [129] is utilized in the proposed methods for the generation of uncorrelated reference vector **Z** with normalized auto-correlation function and zero cross-correlation.

3.4 Successive Coloring Technique (SCT)

According to the analysis of previous methods when the number of desired envelopes is increased and/or moderate to high correlations of successive envelopes is required, the admissible correlation ranges of all other nonsuccessive envelopes will be shrinking to specific values. Therefore, correlation factors of the successive envelopes have the main influence on the performance of generation techniques.

In this section, a simple SCT [219] for designing *any* number of correlated fading channels is proposed to overcome the shortcomings of existing methods. It enables generation of equal and unequal power Rayleigh fading envelopes with *any* desired correlation factor for successive pairs in the interval $[0, 1]$. Correlation values of all other pairs of envelopes are determined by the related successive envelopes which are in the admissible interval satisfying them. The proposed method employs successive coloring for the inphase and quadrature components of all successive signal pairs by considering real correlation vector of desired Rayleigh fading envelopes instead of the complex covariance matrix of the Gaussian signals.

3.4.1 Principles of Successive Coloring

Consider a vector $\mathbf{Z}(t) \in \mathcal{C}^{1\times\mathcal{N}}$ of $\mathcal{N}$ equal power uncorrelated complex-valued i.i.d Rayleigh fading signals as

$$\boldsymbol{Z}(t) = [z_1(t) \quad \cdots \quad z_k(t) \quad \cdots \quad z_{\mathcal{N}}(t)] \tag{3.2}$$

where,

$$z_k(t) = w_k(t) + jv_k(t) \tag{3.3}$$

Envelope of $z_k(t)$ is $u_k(t) = |z_k(t)|$ while $w_k(t)$ and $v_k(t)$ are the in-phase and quadrature components of zero mean Gaussian random signals each with $\sigma_z^2/2$ variance. The envelope of $z_k(t)$ has Rayleigh distribution while the phase $\alpha_k(t) = \tan^{-1}(v_k(t)/w_k(t))$ is uniformly distributed over $[-\pi, \pi]$.

For simplicity and notational convenience, the time index will be removed in the rest of this chapter. According to Jakes [31] and for any two uncorrelated Rayleigh fading signals z_k and z_q with $1 \le (k \ne q) \le \mathcal{N}$ assuming $\sigma_z^2 = 1$, the following conditions of inphase and quadrature components must hold:

1) $\mathrm{E}\{w_k^2\} = \mathrm{E}\{v_k^2\} = \mathrm{E}\{w_q^2\} = \mathrm{E}\{v_q^2\} = \sigma_z^2/2$

2) $\mathrm{E}\{w_k\, v_k\} = \mathrm{E}\{w_q\, v_q\} = 0$

3) $\mathrm{E}\{w_k\, w_q\} = \mathrm{E}\{v_k v_q\} = 0$

4) $\mathrm{E}\{w_k\, v_q\} = -\mathrm{E}\{v_k w_q\} = 0$

The required vector $\mathbf{A} \in \mathcal{C}^{1\times\mathcal{N}}$ of $\mathcal{N}$ equal power complex-valued correlated signals having Rayleigh fading envelopes is represented by

$$\mathbf{A} = [a_1 \quad \cdots \quad a_k \quad \cdots \quad a_{\mathcal{N}}] \tag{3.4}$$

where $a_k = x_k + jy_k$, x_k and y_k are the in-phase and quadrature components of zero mean Gaussian random signals each with $\sigma_a^2\ /2$ variance. The Rayleigh distributed envelope of a_k is $r_k = |a_k|$ and the phase $\beta_k = \tan^{-1}(y_k/x_k)$ is uniformly distributed over $[-\pi, \pi]$. The inphase and quadrature components of any pair of correlated signals a_k and a_q for $1 \leq (k \neq q) \leq \mathcal{N}$ assuming $\sigma_a^2 = 1$ must satisfy Jakes conditions [31] as:

1) $\mathrm{E}\{x_k^2\} = \mathrm{E}\{y_k^2\} = \mathrm{E}\{x_q^2\} = \mathrm{E}\{y_q^2\} = \sigma_a^2/2$

2) $\mathrm{E}\{x_k\, y_k\} = \mathrm{E}\{x_q\, y_q\} = 0$

3) $\mathrm{E}\{x_k\, x_q\} = \mathrm{E}\{y_k y_q\} = \mathcal{g}_{kq}$

4) $\mathrm{E}\{x_k\, y_q\} = -\mathrm{E}\{y_k x_q\} = \mathcal{p}_{kq}$

where the statistics $\mathcal{g}_{kq}$ and $\mathcal{p}_{kq}$ are given for isotropic scattering assumption by [31]

$$\mathcal{g}_{kq} = \frac{J_o\left(2\pi f_d \tau_{kq}\right)}{2\left(1 + \mathbb{k}_{kq}^2\right)} \tag{3.5}$$

$$\mathcal{p}_{kq} = -\mathbb{k}_{kq}\, \mathcal{g}_{kq} \tag{3.6}$$

where f_d is the maximum Doppler frequency, τ_{kq} is the arrival time delay between fading signals, $\mathbb{k}_{kq} = 2\pi\left(\Delta f_{kq}\right)\sigma_\tau$ is the propagation factor, $\Delta f_{kq} = f_q - f_k$ is the frequency separation between signals and σ_τ is the wireless channel delay spread.

For desired correlated fading vector $\mathbf{A}$, the corresponding $\mathcal{N} \times \mathcal{N}$ complex covariance matrix $\mathbf{R}_{AA} = \mathrm{E}\{\mathbf{A}\mathbf{A}^H\}$ is given by

$$\mathbf{R}_{AA} = \begin{bmatrix} \gamma_{11} & \gamma_{12} & \cdots & \gamma_{1\mathcal{N}} \\ \gamma_{21}^{*} & \gamma_{22} & \cdots & \gamma_{2\mathcal{N}} \\ \vdots & \vdots & \ddots & \vdots \\ \gamma_{\mathcal{N}1}^{*} & \gamma_{\mathcal{N}2}^{*} & \cdots & \gamma_{\mathcal{N}\mathcal{N}} \end{bmatrix}$$

$$= \begin{bmatrix} \sigma_a^2 & 2\mathcal{g}_{12} - j2\mathcal{p}_{12} & \cdots & 2\mathcal{g}_{1\mathcal{N}} - j2\mathcal{p}_{1\mathcal{N}} \\ 2\mathcal{g}_{21} + j2\mathcal{p}_{21} & \sigma_a^2 & \cdots & 2\mathcal{g}_{2\mathcal{N}} - j2\mathcal{p}_{2\mathcal{N}} \\ \vdots & \vdots & \ddots & \vdots \\ 2\mathcal{g}_{\mathcal{N}1} + j2\mathcal{p}_{\mathcal{N}1} & 2\mathcal{g}_{\mathcal{N}2} + j2\mathcal{p}_{\mathcal{N}2} & \cdots & \sigma_a^2 \end{bmatrix} \tag{3.7}$$

where γ_{kq} , $\forall(k \neq q) = 1, \dots, \mathcal{N}$ is the cross-correlation between k^{th} and q^{th} complex signals (a_k and a_q) and $\gamma_{kk} =, \forall k = 1, \dots, \mathcal{N}$ is the autocorrelation (power) of signal a_k. When $\mathbb{k}_{kq} = 0$; $k, q = 1, \dots, \mathcal{N}$, the covariance matrix will be real and represented as

$$\mathbf{R}_{AA} = \begin{bmatrix} \sigma_a^2 & 2\mathcal{g}_{12} & \cdots & 2\mathcal{g}_{1\mathcal{N}} \\ 2\mathcal{g}_{21} & \sigma_a^2 & \cdots & 2\mathcal{g}_{2\mathcal{N}} \\ \vdots & \vdots & \ddots & \vdots \\ 2\mathcal{g}_{\mathcal{N}1} & 2\mathcal{g}_{\mathcal{N}2} & \cdots & \sigma_a^2 \end{bmatrix} \tag{3.8}$$

The correlation factor ρ_{kq} between the k^{th} and q^{th} envelopes (r_k and r_q) is given by

$$\rho_{kq} = \frac{Cov\{r_k, r_q\}}{\sqrt{Var\{r_k\}Var\{r_q\}}} = \frac{(1+\lambda_{kq})E_i\left[\left(2\sqrt{\lambda_{kq}}\right)/(1+\lambda_{kq})\right] - \frac{\pi}{2}}{2 - \frac{\pi}{2}} \tag{3.9}$$

where $E_i[x]$ is the complete elliptic integral of the second kind with modulus x, and λ_{kq} is the magnitude of correlation between complex Gaussian signals a_k and a_q represented by

$$\lambda_{kq}^2 = \left| \frac{Cov\{a_k, a_q\}}{\sqrt{Var\{a_k\}\ Var\{a_q\}}} \right|^2 = \frac{\mathcal{g}_{kq}^2 + \mathcal{p}_{kq}^2}{\mathcal{b}^2} \tag{3.10}$$

where $\mathcal{b} = \sigma_a^2/2$. In [31], the correlation factor ρ_{kq} is well approximated by λ_{kq}^2 as

$$\rho_{kq} \cong \lambda_{kq}^2 = \frac{\mathcal{g}_{kq}^2 + \mathcal{p}_{kq}^2}{\mathcal{b}^2} \tag{3.11}$$

Therefore, $\mathcal{g}_{kq}$ can be calculated as

$$\mathscr{g}_{kq} \cong \sqrt{\frac{\rho_{kq}}{1+\mathbb{k}_{kq}^2}} \quad \mathscr{b} \tag{3.12}$$

Correlation factors between any pairs of envelopes of $\mathbf{A}$ elements can be given in $\mathcal{N} \times \mathcal{N}$ correlation matrix form $\boldsymbol{\rho} \in \mathcal{R}^{\mathcal{N}\times\mathcal{N}}$ as

$$\boldsymbol{\rho} = \begin{bmatrix} \rho_{11} & \rho_{12} & \rho_{13} & \cdots & \rho_{1\mathcal{N}} \\ \rho_{21} & \rho_{22} & \rho_{23} & \cdots & \rho_{2\mathcal{N}} \\ \rho_{31} & \rho_{32} & \rho_{33} & \cdots & \rho_{3\mathcal{N}} \\ \vdots & \vdots & \vdots & \ddots & \vdots \\ \rho_{\mathcal{N}1} & \rho_{\mathcal{N}2} & \rho_{\mathcal{N}3} & \cdots & \rho_{\mathcal{N}\mathcal{N}} \end{bmatrix} \tag{3.13}$$

where $\rho_{kk} = 1,\ \forall k = 1, \dots, \mathcal{N}$ is the autocorrelation of each signal envelope and $\rho_{kq} = \rho_{qk}$, $\forall (k \neq q) = 1, \dots, \mathcal{N}$. The elements of $\boldsymbol{\rho}$ are real values since they represent the correlation between envelopes (magnitudes of the complex signals).

In SCT, correlation vector $\boldsymbol{\rho_s} \in \mathcal{R}^{1\times(\mathcal{N}-1)}$ of successive pairs from $\boldsymbol{\rho}$ matrix will be considered as

$$\boldsymbol{\rho_s} = [\rho_{12} \quad \rho_{23} \quad \cdots \quad \rho_{(\mathcal{N}-1)\mathcal{N}}] \tag{3.14}$$

To generate $\mathbf{A}$ elements from $\mathbf{Z}$ assuming $\sigma_a^2 = \sigma_z^2 = 1$, the following linear formulation is applied:

$$a_k = \begin{cases} z_k & , k = 1 \\ \mathcal{A}_{(k-1)k}\, a_{k-1} + \mathcal{B}_{(k-1)k}\, z_k & , 2 \leq k \leq \mathcal{N} \end{cases} \tag{3.15}$$

where, $\mathcal{A}_{(k-1)k}$ and $\mathcal{B}_{(k-1)k}$ for $2 \leq k \leq \mathcal{N}$ are the *complex coloring factors* used to insure the required correlation among the inphase and quadrature components of successive envelope pairs which can be calculated directly by satisfying the aforementioned conditions of [31] as follows:

$$\mathcal{A}_{(k-1)k} = \sqrt{\frac{\rho_{(k-1)k}}{1+\mathbb{k}_{(k-1)k}^2}}\ \left[1 + j\mathbb{k}_{(k-1)k}\right] \tag{3.16}$$

$$\mathcal{B}_{(k-1)k} = \sqrt{1-\rho_{(k-1)k}} \tag{3.17}$$

Correlation factors of any nonsuccessive pairs of envelopes ρ_{kq} will be in the range satisfied by the correlation values of all other pairs between k^{th} and q^{th} envelopes and determined by their multiplication result as

$$\rho_{kq} \cong \prod_{i=k}^{q-1} \rho_{i(i+1)} \quad ; k < q-1 \tag{3.18}$$

Note that for conventional methods, the desired correlation parameters must represent a feasible system (i.e. has a positive definite covariance matrix) in order to be simulated accurately. For example, if the desired correlations of three envelopes are $\rho_{12} = \rho_{23} = 0.9$ then as explained in [134], ρ_{13} should be in the interval $[0.64,\ 1.0]$. That is, if there is high correlation between (r_1, r_2) and (r_2, r_3), then there should be high correlation between (r_1, r_3). For this case, ρ_{13} using SCT will be 0.81 which is in the above interval. As the number of desired signals increased and/or moderate to high correlations of successive signal envelopes is required, the admissible correlation ranges of all nonsuccessive envelopes will be shrinking to the specific values of equation (3.18).

3.4.2 SCT Algorithm

For wireless communication system, the desired channel $\mathbf{A}$ of equal power signals ($\sigma_a^2 = 1$) with an arbitrary correlation vector of successive pairs of envelopes $\boldsymbol{\rho_s}$ can be generated as follows:

1) Given the desired correlations $\boldsymbol{\rho_s}$ of successive pairs of envelopes $\rho_{(k-1)k}$ and the propagation factors $\mathbb{k}_{(k-1)k}$ for $2 \le k \le \mathcal{N}$ or calculate them using the available informations.
2) Calculate the coloring factors, $\mathcal{A}_{(k-1)k}$ and $\mathcal{B}_{(k-1)k}$ for $2 \le k \le \mathcal{N}$ using equations (3.16) and (3.17).
3) Generate a reference vector $\mathbf{Z}$ of $\mathcal{N}$ equal power uncorrelated Rayleigh fading signals.
4) For $k = 1, \dots, \mathcal{N}$, use equation (3.15) to calculate the desired signals of correlated fading channel $\mathbf{A}$.

3.4.3 Generalized SCT (GSCT) Algorithm for Equal and Unequal Power CRFC

As shown in the previous section, SCT to generate equal power signals is a simple procedure. However, generation of unequal power signals $\widehat{\mathbf{A}} = [\hat{a}_1 \ \dots \ \hat{a}_k \ \dots \ \hat{a}_{\mathcal{N}}] \in \mathcal{C}^{1\times\mathcal{N}}$ is very useful for many cases such as scattered users in different distances from the base station

receiver with the absence of accurate power control or unequal power transmission from the available transmit antennas. Therefore, GSCT algorithm is presented in this section for the generation of equal and unequal power signals.

Consider a desired correlation matrix $\widehat{\boldsymbol{\rho}}$ of $\mathcal{N}$ signal envelopes with power of $\sigma_{\hat{a}_k}^2$, $k = 1, \ldots, \mathcal{N}$ as;

$$\widehat{\boldsymbol{\rho}} = \begin{bmatrix} \hat{\rho}_{11} & \hat{\rho}_{12} & \hat{\rho}_{13} & \cdots & \hat{\rho}_{1\mathcal{N}} \\ \hat{\rho}_{21} & \hat{\rho}_{22} & \hat{\rho}_{23} & \cdots & \hat{\rho}_{2\mathcal{N}} \\ \hat{\rho}_{31} & \hat{\rho}_{32} & \hat{\rho}_{33} & \cdots & \hat{\rho}_{3\mathcal{N}} \\ \vdots & \vdots & \vdots & \ddots & \vdots \\ \hat{\rho}_{\mathcal{N}1} & \hat{\rho}_{\mathcal{N}2} & \hat{\rho}_{\mathcal{N}3} & \cdots & \hat{\rho}_{\mathcal{N}\mathcal{N}} \end{bmatrix} \tag{3.19}$$

Therefore, correlation vector $\widehat{\boldsymbol{\rho}}_{\boldsymbol{s}} \in \mathcal{R}^{1\times(\mathcal{N}-1)}$ of successive pairs formulated from $\widehat{\boldsymbol{\rho}}$ matrix will be considered in GSCT as

$$\widehat{\boldsymbol{\rho}}_{\boldsymbol{s}} = [\hat{\rho}_{12} \quad \hat{\rho}_{23} \quad \cdots \quad \hat{\rho}_{(\mathcal{N}-1)\mathcal{N}}] \tag{3.20}$$

The desired signals can be generated using the following algorithm where the transformation in steps 2 and 6 are same as in [137].

1) Given the desired correlations $\widehat{\boldsymbol{\rho}}_{\boldsymbol{s}}$ of successive pairs of envelopes $\hat{\rho}_{(k-1)k}$ and the propagation factors $\mathbb{k}_{(k-1)k}$ for $2 \leq k \leq \mathcal{N}$ or calculate them using the available informations.
2) Normalize $\widehat{\boldsymbol{\rho}}_{\boldsymbol{s}}$ to create normalized correlation vector $\boldsymbol{\rho}_{\boldsymbol{s}}$ using the following relation

$$\rho_{(k-1)k} = \frac{\hat{\rho}_{(k-1)k}}{\sqrt{\sigma_{\hat{a}_{(k-1)}}^2 \sigma_{\hat{a}_k}^2}} \tag{3.21}$$

3) Calculate the coloring factors, $\mathcal{A}_{(k-1)k}$ and $\mathcal{B}_{(k-1)k}$ for $2 \leq k \leq \mathcal{N}$ using equations (3.16) and (3.17).
4) Generate a reference vector $\mathbf{Z}$ of $\mathcal{N}$ equal power uncorrelated Rayleigh fading signals.
5) For $k = 1, \ldots, \mathcal{N}$, use equation (3.15) to calculate the equal power signals of correlated fading channel $\mathbf{A}$.
6) For $k = 1, \ldots, \mathcal{N}$, calculate the unequal power signals of desired correlated fading channel $\widehat{\mathbf{A}}$ as

$$\hat{a}_k = \frac{\sigma_{\hat{a}_k}}{\sigma_a} \; a_k \tag{3.22}$$

3.4.4 Complexity Analysis of GSCT

Let's assume that $\mathcal{N}$ is the total number of desired equal power correlated signals. To simulate these signals using GSCT, approximate computational operations of $2\mathcal{N}^2 - 3\mathcal{N} + 2$ are required which is $\mathcal{O}(\mathcal{N}^2)$. This includes additions, subtractions, divisions, multiplications, and square roots. In Table 3.3, the approximate computational effort of the proposed algorithm is compared with the conventional methods that utilize Cholesky or Eigenvalue decomposition.

For comparison purpose, let's consider the generation of $\mathcal{N} = M_t M_r$ signals for $M_t \times M_r$ MIMO system. By using $M_t = 6$ and $M_r = 8$, the required number of signals is $\mathcal{N} = 48$. This means, 4.466×10^3 approximate calculations are needed for GSCT compared with 38.024×10^3 and 109.416×10^3 for Cholesky and Eigenvalue decomposition methods, respectively. When $\mathcal{N} = 256$, such as in MC-CDMA, approximate calculations of 0.13×10^6 are required for GSCT which are significantly less than 5.62×10^6 and 16.74×10^6 for Cholesky and Eigenvalue decomposition methods, respectively. Also, we find that approximately more than 100% reduction in complexity can be achieved at $\mathcal{N} = 9$ compared with Cholesky and at $\mathcal{N} = 4$ compared with Eigenvalue decomposition method. The significant reduction in computations is due to the direct use of $\mathcal{N} - 1$ conditions of successive correlated envelopes rather than $\sum_{n=1}^{\mathcal{N}-1}(n)$ conditions from the covariance matrix $\mathbf{R}_{AA}$ which needs $\mathcal{N}^3/6$ multiplications to be factorized.

For unequal power correlated signals, GSCT requires extra $3(\mathcal{N} - 1)$ calculations for $\widehat{\boldsymbol{\rho}}_{\boldsymbol{s}}$ normalization and $2\mathcal{N}$ for $\widehat{\mathbf{A}}$ elements formulation. Hence, the total extra required computations is $5\mathcal{N} - 3$. Similarly, when Cholesky or Eigenvalue decomposition method is used, extra $3\mathcal{N}^2 + 2\mathcal{N}$ computations are needed. Consequently, GSCT has more significant reduction compared with the other methods.

In addition to the low complexity of proposed method, it provides a high performance compared with the existing methods in terms of accuracy and number of generated signals as we will see in the next section.

Table 3.3: Computational complexity of GSCT to generate equal power correlated fading signals compared with the conventional methods that utilize Cholesky or Eigenvalue decomposition

Algorithm	Total Calculations	Computational Effort
Cholesky	$(2\mathcal{N}^3 + 3\mathcal{N}^2 + \mathcal{N})/6$	$\mathcal{O}(\mathcal{N}^3)$
Eigenvalue	$(6\mathcal{N}^3 - 3\mathcal{N}^2 - 3\mathcal{N})/6$	$\mathcal{O}(\mathcal{N}^3)$
GSCT	$2\mathcal{N}^2 - 3\mathcal{N} + 2$	$\mathcal{O}(\mathcal{N}^2)$

3.4.5 Simulation Results

For the accuracy checking and to demonstrate the effectiveness of GSCT without loss of generality, we consider generation of correlated Rayleigh fading signals using four different representative examples. The first example is for simulating four equal power signals of 2×2 SU-MIMO channel scenario with complex spatial covariance matrix. In the second example, we consider simulation of four equal power signals for 4 receive antenna correlation scenario using real spatial covariance matrix. The third example is for simulating 64 equal power signals of multicarrier channel scenario (OFDM) with spectral correlation. The last example is for simulating unequal power signal needed in many wireless applications that experiencing spectral and/or spatial correlation such as MC-CDMA, MU-MIMO, and MIMO-OFDM. In this study, MATLAB/7.9 is used for all simulations.

Example 1:

Consider generation of $\mathcal{N} = 4$ equal power flat Rayleigh fading signals as $\mathbf{A} = [a_1 \quad a_2 \quad a_3 \quad a_4]$ for 2×2 MIMO scenario using $\sigma_a^2 = 2\mathcal{b} = 1$ and the following empirically formulated covariance matrix.

$$\mathbf{R}_{AA} = \begin{bmatrix} 1 & 0.58 + j0.75 & 0.28 + j0.37 & 0.15 + j0.43 \\ 0.58 - j0.75 & 1 & 0.17 + j0.47 & 0.27 + j0.39 \\ 0.28 - j0.37 & 0.17 + j0.47 & 1 & 0.58 + j0.75 \\ 0.15 - j0.43 & 0.27 - j0.39 & 0.58 - j0.75 & 1 \end{bmatrix} \tag{3.23}$$

The eigenvalues of $\mathbf{R}_{AA}$ are: -0.254 , 0.198 , 1.298 , and 2.756 . Since one of the eigenvalue is negative, $\mathbf{R}_{AA}$ is neither a positive semidefinite nor a positive definite matrix. Besides serving as an illustration of GSCT effectiveness, the given covariance matrix also provides an example of realistic channel conditions where the covariance matrices are not always positive definite. It should be noted that Eigenvalue decomposition method can not be used directly for this example without forcing $\mathbf{R}_{AA}$ to be positive semidefinite by replacing the negative eigenvalue with zero as in [133]. Similarly, Cholesky decomposition method can not be employed without forcing $\mathbf{R}_{AA}$ to be positive definite by replacing the negative eigenvalue with small positive value as in [134]. However, forcing $\mathbf{R}_{AA}$ to be positive semidefinite/definite will affect its structure leading to inaccurate realistic channel simulation and hence the performance evaluation of the considered communication system.

To generate $\mathbf{A}$ using the proposed GSCT, the desired correlation matrix of envelopes $\boldsymbol{\rho}$ can be calculated directly from $\mathbf{R}_{AA}$ using equation (3.11) as

$$\boldsymbol{\rho} = \begin{bmatrix} 1 & \rho_{12} & \rho_{13} & \rho_{14} \\ \rho_{21} & 1 & \rho_{23} & \rho_{24} \\ \rho_{31} & \rho_{32} & 1 & \rho_{34} \\ \rho_{41} & \rho_{42} & \rho_{43} & 1 \end{bmatrix} = \begin{bmatrix} 1 & 0.898 & 0.215 & 0.225 \\ 0.898 & 1 & 0.249 & 0.207 \\ 0.215 & 0.249 & 1 & 0.898 \\ 0.225 & 0.207 & 0.898 & 1 \end{bmatrix} \tag{3.24}$$

Therefore, desired correlation vector $\boldsymbol{\rho_s}$ of successive envelopes is

$$\boldsymbol{\rho_s} = [\rho_{12} \quad \rho_{23} \quad \rho_{34}] = [0.898 \quad 0.249 \quad 0.898] \tag{3.25}$$

Propagation factors of the successive signals are calculated also from $\mathbf{R}_{AA}$ using equation (3.6) as $\mathbb{k}_{12} = \mathbb{k}_{34} = 1.29$ and $\mathbb{k}_{23} = 2.76$. Envelopes (r_1, r_2, r_3, r_4) and phases $(\beta_1, \beta_2, \beta_3, \beta_4)$ of the generated fading signals are depicted in Fig. 3.3 and Fig. 3.4, respectively. It can be seen that envelopes (r_1, r_2) and (r_3, r_4) are very close to each other which reflects the desired high correlations of $\rho_{12} = \rho_{34} = 0.898$ while envelopes (r_1, r_3), (r_1, r_4), (r_2, r_3), and (r_2, r_4) are unrelated to each other due to their low correlation values shown in equation (3.24). In contrast to envelopes, all phases are independent even those related to the high correlated envelopes (r_1, r_2) and (r_3, r_4) which is expected for complex covariance matrices. In Table 3.4, the measured correlation values of fading envelopes are very close to the desired values which validate the accuracy of GSCT. Note that correlations of nonsuccessive envelopes are determined in GSCT by the associated successive envelope correlations using equation (3.18) as $\rho_{13} = \rho_{24} = 0.223$ and $\rho_{14} = 0.2$. PDF of the generated Rayleigh fading envelopes and uniform distributed phases are coincides with the theoretical results as shown in Fig. 3.5 and Fig. 3.6, respectively. The results shown in Figs. 3.3-3.6 demonstrate the effectiveness of simulating the desired correlated fading signals.

Table 3.4: Measured correlations of equal power correlated fading signal envelopes generated using GSCT compared with the desired values of example 1

Correlation	ρ_{12}	ρ_{23}	ρ_{34}	ρ_{13}	ρ_{24}	ρ_{14}
Desired	0.898	0.249	0.898	0.215	0.207	0.225
Measured	0.897	0.250	0.902	0.221	0.201	0.224

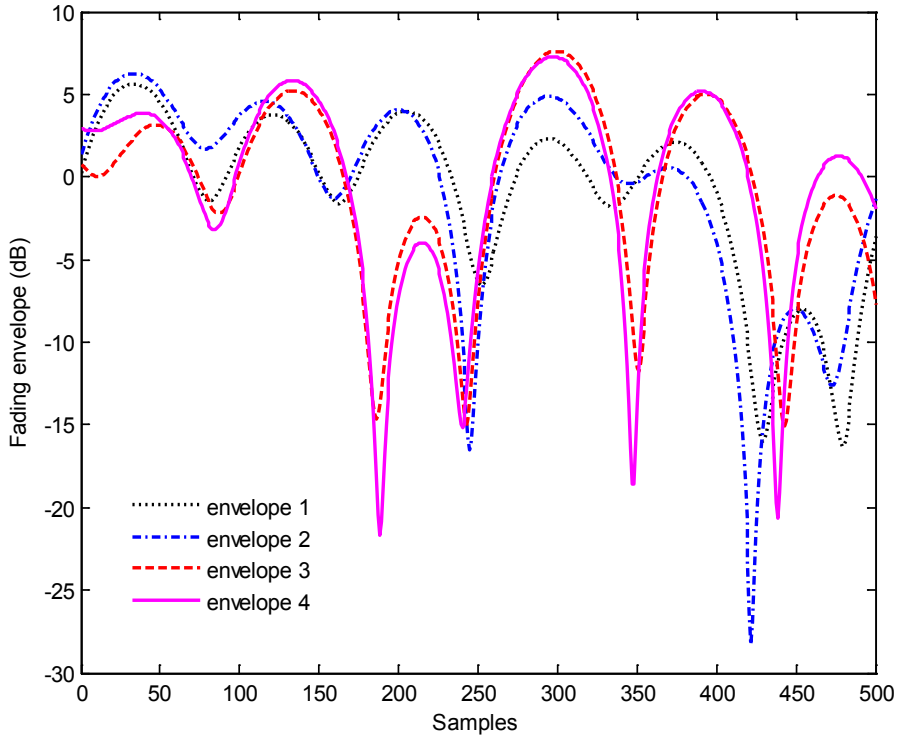

Figure 3.3: Equal power envelopes of **A** generated using GSCT for the parameters given in example 1 as; $\sigma_a^2 = 1$, $\rho_{12} = \rho_{34} = 0.89$, $\rho_{23} = 0.25$, $\mathbb{k}_{12} = \mathbb{k}_{34} = 1.29$, and $\mathbb{k}_{23} = 2.76$ which are related to complex $\mathbf{R}_{AA}$.

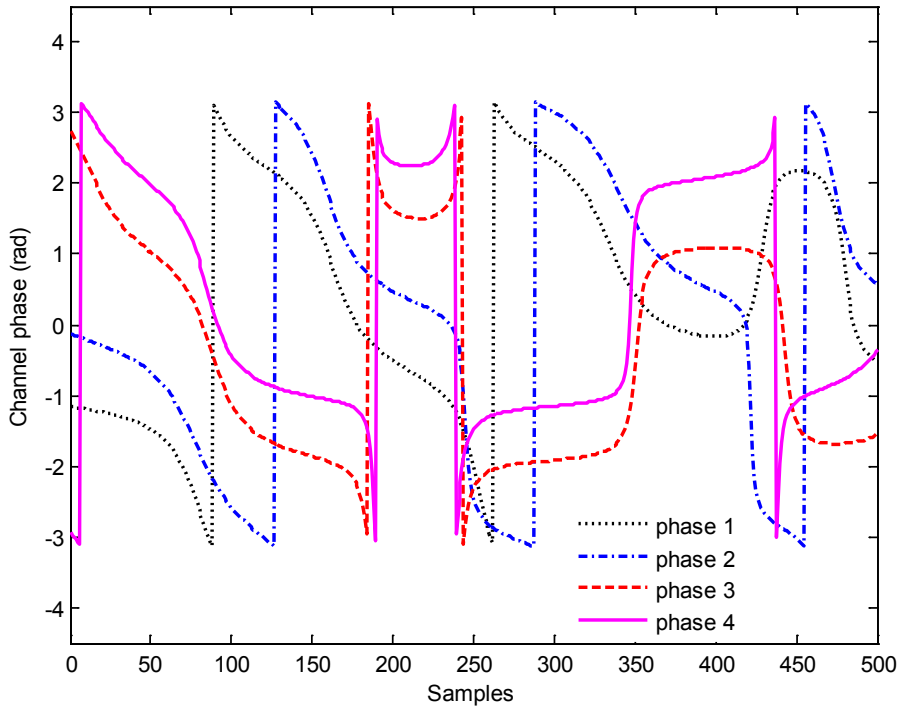

Figure 3.4: Phases of equal power signals of **A** generated using GSCT for the parameters given in example 1 as; $\sigma_a^2 = 1$, $\rho_{12} = \rho_{34} = 0.89$, $\rho_{23} = 0.25$, $\mathbb{k}_{12} = \mathbb{k}_{34} = 1.29$, and $\mathbb{k}_{23} = 2.76$ which are related to complex $\mathbf{R}_{AA}$.

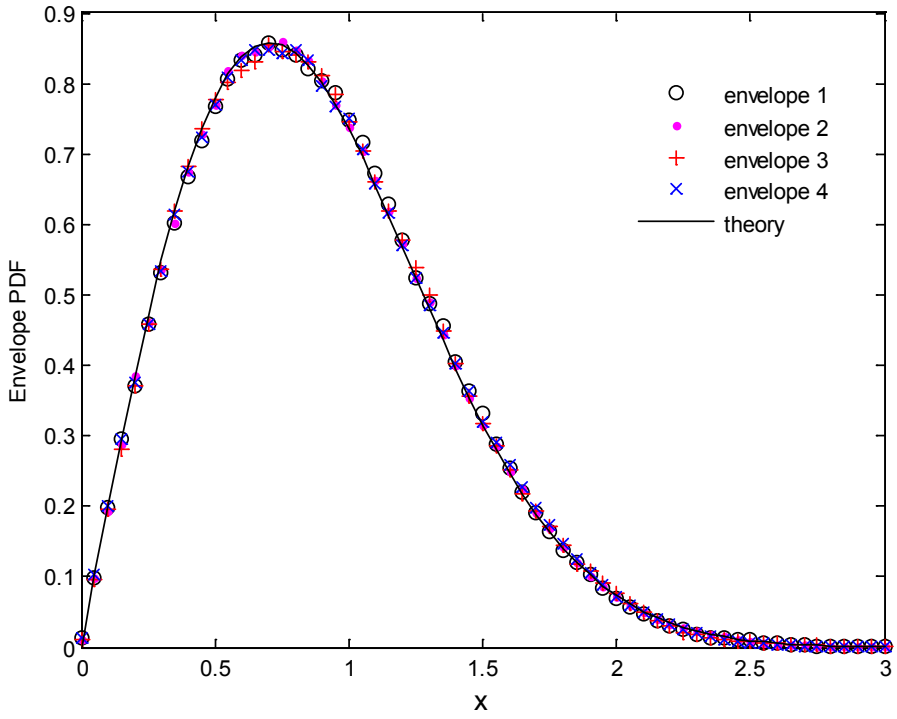

Figure 3.5: PDF of the Rayleigh fading envelopes of **A** signals generated in example 1.

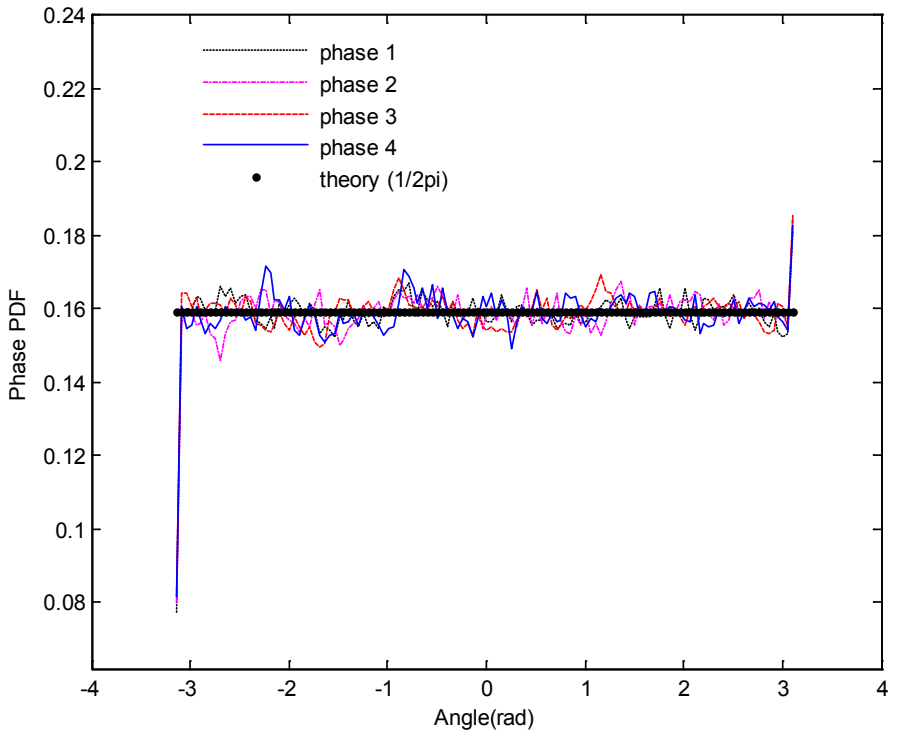

Figure 3.6: PDF of uniform distribution phases of **A** signals generated in example 1.

Example 2:

In this example, we consider generation of $\mathcal{N} = 4$ equal power flat Rayleigh fading signals as $\mathbf{A} = [a_1 \quad a_2 \quad a_3 \quad a_4]$ for 4 receive antenna correlation scenario. The constant spatial correlation model [131] is adopted in this example due its popularity by using the following real constant receive covariance matrix.

$$\mathbf{R}_{AA} = \begin{bmatrix} 1 & \gamma_{12} & \gamma_{13} & \gamma_{14} \\ \gamma_{21}^* & 1 & \gamma_{23} & \gamma_{24} \\ \gamma_{31}^* & \gamma_{32}^* & 1 & \gamma_{34} \\ \gamma_{41}^* & \gamma_{42}^* & \gamma_{43}^* & 1 \end{bmatrix} = \begin{bmatrix} 1 & 0.9 & 0.9 & 0.9 \\ 0.9 & 1 & 0.9 & 0.9 \\ 0.9 & 0.9 & 1 & 0.9 \\ 0.9 & 0.9 & 0.9 & 1 \end{bmatrix} \tag{3.26}$$

Using equation (3.11) with $\sigma_a^2 = 2\mathscr{b} = 1$, the desired correlation matrix of envelopes $\boldsymbol{\rho}$ can be calculated directly from $\mathbf{R}_{AA}$ as

$$\boldsymbol{\rho} = \begin{bmatrix} 1 & \rho_{12} & \rho_{13} & \rho_{14} \\ \rho_{21} & 1 & \rho_{23} & \rho_{24} \\ \rho_{31} & \rho_{32} & 1 & \rho_{34} \\ \rho_{41} & \rho_{42} & \rho_{43} & 1 \end{bmatrix} = \begin{bmatrix} 1 & 0.81 & 0.81 & 0.81 \\ 0.81 & 1 & 0.81 & 0.81 \\ 0.81 & 0.81 & 1 & 0.81 \\ 0.81 & 0.81 & 0.81 & 1 \end{bmatrix} \tag{3.27}$$

Therefore, desired correlation vector $\boldsymbol{\rho_s}$ of successive envelopes is

$$\boldsymbol{\rho_s} = [\rho_{12} \quad \rho_{23} \quad \rho_{34}] = [0.81 \quad 0.81 \quad 0.81] \tag{3.28}$$

In this example, all propagation factors $\mathbb{k}_{kq}, (k \neq q) = 1, \ldots, 4$ are zero since $\mathbf{R}_{AA}$ is a real covariance matrix. Envelopes (r_1, r_2, r_3, r_4) and phases $(\beta_1, \beta_2, \beta_3, \beta_4)$ of the generated fading signals are depicted in Fig. 3.7 and Fig. 3.8, respectively. As can be seen, all phases and envelopes are correlated as expected for real covariance matrices. In this case, the inphase and quadrature components of any two signals a_k and a_q are uncorrelated where $\mathrm{E}\{x_k\, y_q\} = -\mathrm{E}\{y_k x_q\} = 0$ in contrast to $\mathrm{E}\{x_k\, y_q\} = -\mathrm{E}\{y_k x_q\} = \wp_{kq}$ when complex covariance matrices are used. This example demonstrates the applicability and accuracy of simulating signals with real covariance matrices using GSCT with less complexity compared with conventional methods.

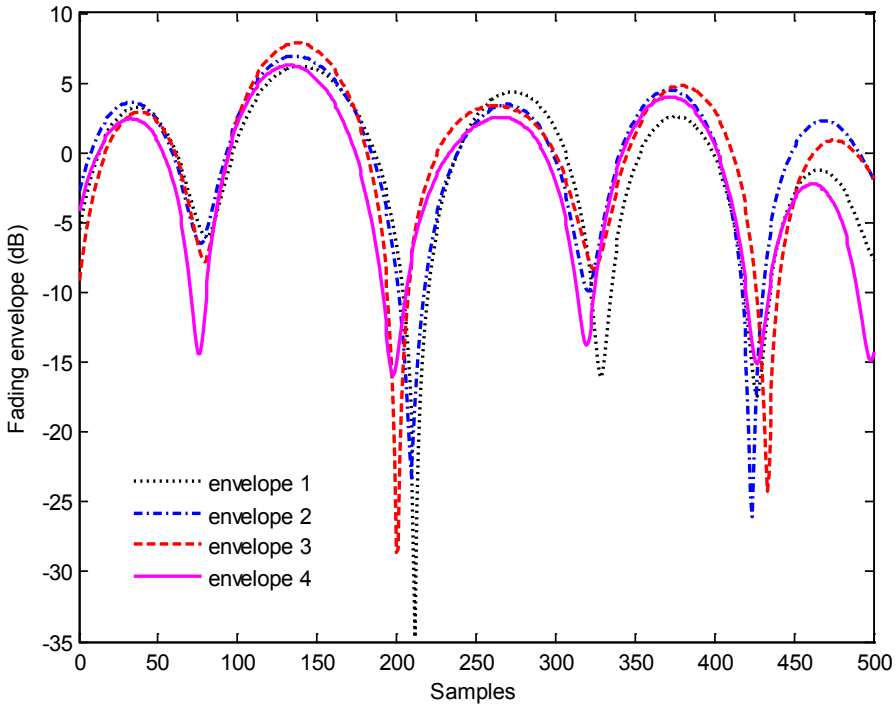

Figure 3.7: Equal power envelopes of **A** generated using GSCT for the parameters given in example 1 as; $\sigma_a^2 = 1, \rho_{12} = \rho_{23} = \rho_{34} = 0.81$ and $\mathbb{k}_{12} = \mathbb{k}_{23} = \mathbb{k}_{34} = 0.0$ which are related to real $\mathbf{R}_{AA}$.

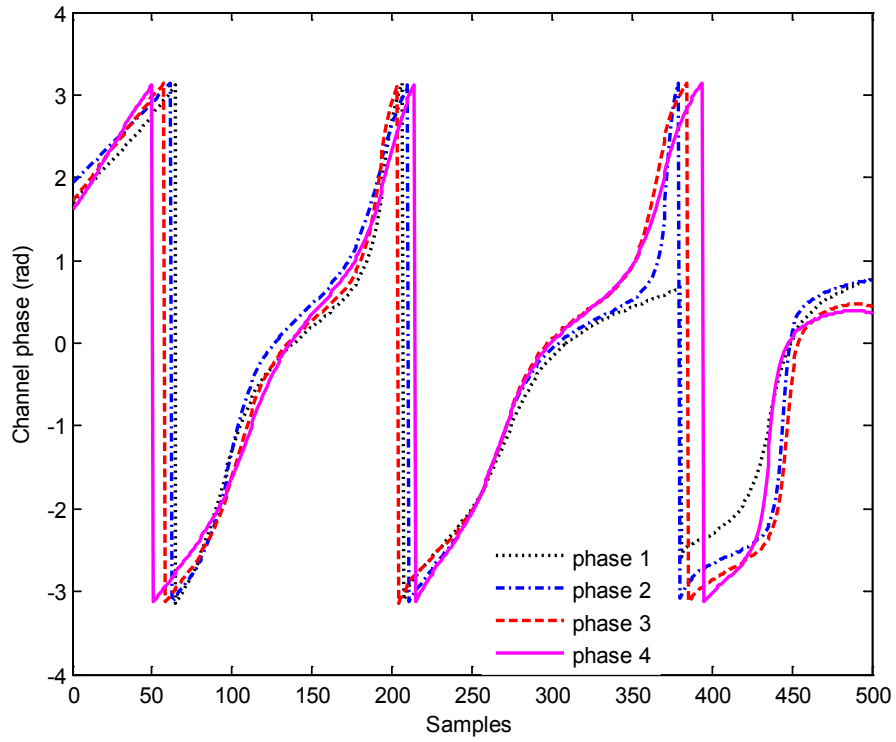

Figure 3.8: Phases of equal power signals of **A** generated using GSCT for the parameters given in example 1 as; $\sigma_a^2 = 1, \rho_{12} = \rho_{23} = \rho_{34} = 0.81$ and $\mathbb{k}_{12} = \mathbb{k}_{23} = \mathbb{k}_{34} = 0.0$ which are related to real $\mathbf{R}_{AA}$.

Example 3:

Channels of many communication systems include large number of correlated fading signals. In this example, we consider generation of $\mathcal{N} = 64$ equal power correlated flat Rayleigh fading signals as $\mathbf{A} = [a_1 \quad a_2 \quad \cdots \quad a_{64}]$ for multicarrier system scenario of 64 subcarriers.

Based on IEEE 802.11a specifications (OFDM) [122, 134], the following parameters are adopted in this example: frequency separation between adjacent frequencies of $\Delta f = 312.5$ kHz, channel delay spread $\sigma_\tau = 0.1\,\mu sec$, maximum Doppler frequency $f_d = 50$ Hz, arrival time delay between any adjacent signals are $\tau_{(k-1)k} = 1\,msec,\ k = 1, \ldots, 64$, and power of each signal is $\sigma_a^2 = 2\mathscr{b} = 1$.

Using equations (3.5), (3.6), and (3.11), the desired correlation vector $\boldsymbol{\rho_s}$ of successive envelopes can be calculated from the given parameters as

$$\boldsymbol{\rho_s} = [\rho_{12} \quad \rho_{23} \quad \cdots \quad \rho_{(63)(64)}] = [0.91 \quad 0.91 \quad \cdots \quad 0.91] \tag{3.29}$$

where the calculated propagation factors are $\mathbb{k}_{(k-1)k} = 0.196,\ k = 1, \ldots, 64$.

From the generated signal of **A** using GSCT, envelopes r_1, r_2, r_3, and r_{64} are shown only in Fig. 3.9 for simplicity. As can be seen, frequency separation between signals is one of the parameters that has great impact on the channel correlation where as Δf decreased, the correlation increased. For example, envelopes r_1, r_2, and r_3 are highly correlated while r_{64} appears independent to them. The measured correlations for these envelopes are; $\rho_{12} = 0.91$, $\rho_{12} = 0.91$, $\rho_{23} = 0.82$, and $\rho_{1(64)} = \rho_{2(64)} = \rho_{3(64)} \cong 0.0$. It should be noted that none of the existing methods can generate the desired signals of this example due to the large number of signals.

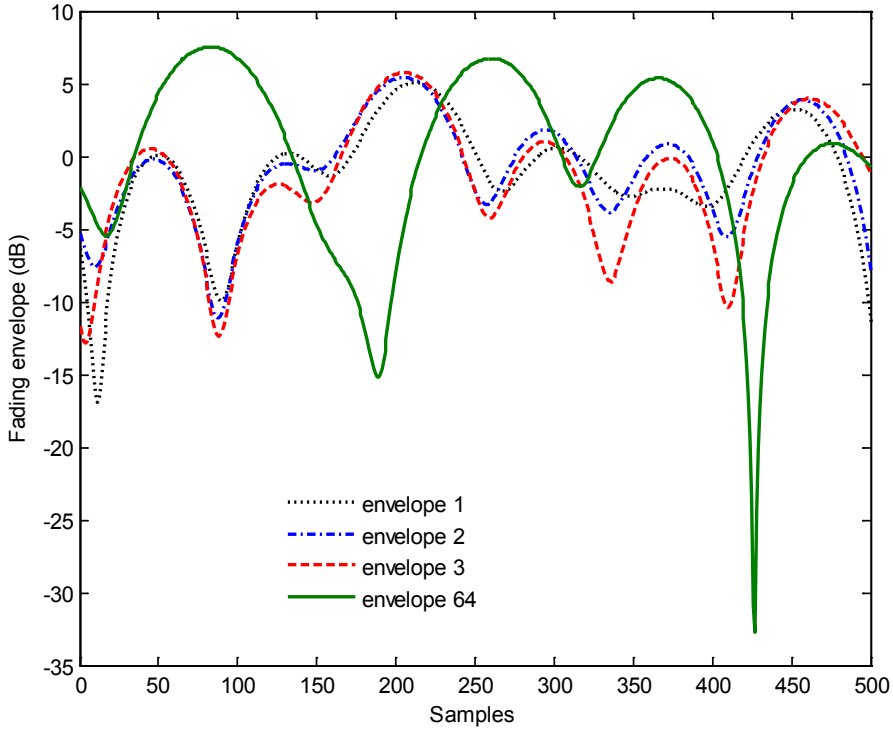

Figure 3.9: Equal power envelopes of **A** generated using GSCT for the parameters given in example 3 as; $\sigma_a^2 = 1, \rho_{12} = \rho_{23} = \rho_{(63)(64)} = 0.91$ and $\mathbb{k}_{(k-1)k} = 0.196,\ k = 1, \ldots, 64$.

Example 4:

In many applications of wireless communication systems such as MC-CDMA and MU-MIMO, the fading channel exhibits unequal power signals due to system design requirement or inaccurate power control. In this representative example, we consider generation of $\mathcal{N} = 4$ correlated flat Rayleigh fading signals as $\widehat{\mathbf{A}} = [\hat{a}_1 \quad \hat{a}_2 \quad \hat{a}_3 \quad \hat{a}_4]$ for unequal power scenario using the following parameters:

Signal power: $\sigma_{\hat{a}_1}^2 = \sigma_{\hat{a}_2}^2 = 1,\ \sigma_{\hat{a}_3}^2 = 2$, and $\sigma_{\hat{a}_4}^2 = 3$

Propagation factors: $\mathbb{k}_{12} = \mathbb{k}_{23} = \mathbb{k}_{34} = 1$

Desired correlation vector $\widehat{\boldsymbol{\rho}}_{\boldsymbol{s}}$ of successive envelopes is

$$\widehat{\boldsymbol{\rho}}_{\boldsymbol{s}} = [\hat{\rho}_{12} \quad \hat{\rho}_{23} \quad \hat{\rho}_{34}] = [0.9 \quad 0.3 \quad 0.7] \tag{3.30}$$

Using GSCT, the first step involves generation of equal unit power correlated Rayleigh fading signals $\mathbf{A} = [a_1 \quad a_2 \quad a_3 \quad a_4]$ with normalized correlation vector $\boldsymbol{\rho}_{\boldsymbol{s}}$ calculated from $\widehat{\boldsymbol{\rho}}_{\boldsymbol{s}}$ using equation (3.21) as

$$\boldsymbol{\rho}_{\boldsymbol{s}} = [\rho_{12} \quad \rho_{23} \quad \rho_{34}] = [0.9 \quad 0.21 \quad 0.28] \tag{3.31}$$

In Fig. 3.10, envelopes (r_1, r_2, r_3, r_4) of the generated signals **A** are shown which reflects the correlation values of $\boldsymbol{\rho_s}$ while all phases $(\beta_1, \beta_2, \beta_3, \beta_4)$ are independent since the corresponding covariance matrix of these signals is complex. In the second step, desired unequal power signals $\widehat{\mathbf{A}}$ are calculated from **A** using equation (3.22).

Unequal power envelopes $(\hat{r}_1, \hat{r}_2, \hat{r}_3, \hat{r}_4)$ of $\widehat{\mathbf{A}}$ are depicted in Fig. 3.11 reflecting the desired signal power and correlations of $\widehat{\boldsymbol{\rho}}_{\boldsymbol{s}}$ while all phases $(\hat{\beta}_1, \hat{\beta}_2, \hat{\beta}_3, \hat{\beta}_4)$ are independent as in the first step. From these figures, it can be seen that envelopes r_3 and r_4 are differ than $\hat{r}_3$ and $\hat{r}_4$ due to the power difference in first and second steps of generation while r_1 and r_2 are same as $\hat{r}_1$ and $\hat{r}_2$ since they have equal powers in both steps. On the other hand, all phases in the first step are similar to that of second step and not affected by the power transformation as expected. Results of this example demonstrate the applicability of designing unequal power correlated fading signals using GSCT.

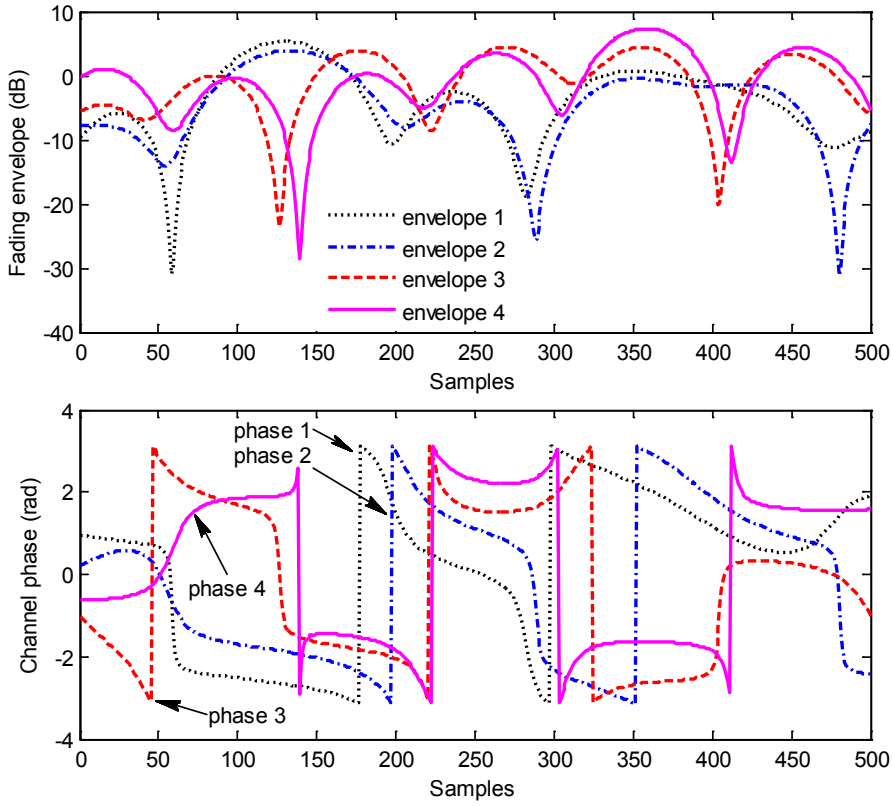

Figure 3.10: Equal unit power envelopes $\left(\sigma_{a_1}^2 = \sigma_{a_2}^2 = \sigma_{a_3}^2 = \sigma_{a_4}^2 = 1\right)$ and phases of **A** generated in the first step of GSCT for the parameters calculated in example 4 as; $\rho_{12} = 0.9$, $\rho_{23} = 0.21$, and $\rho_{34} = 0.28$.

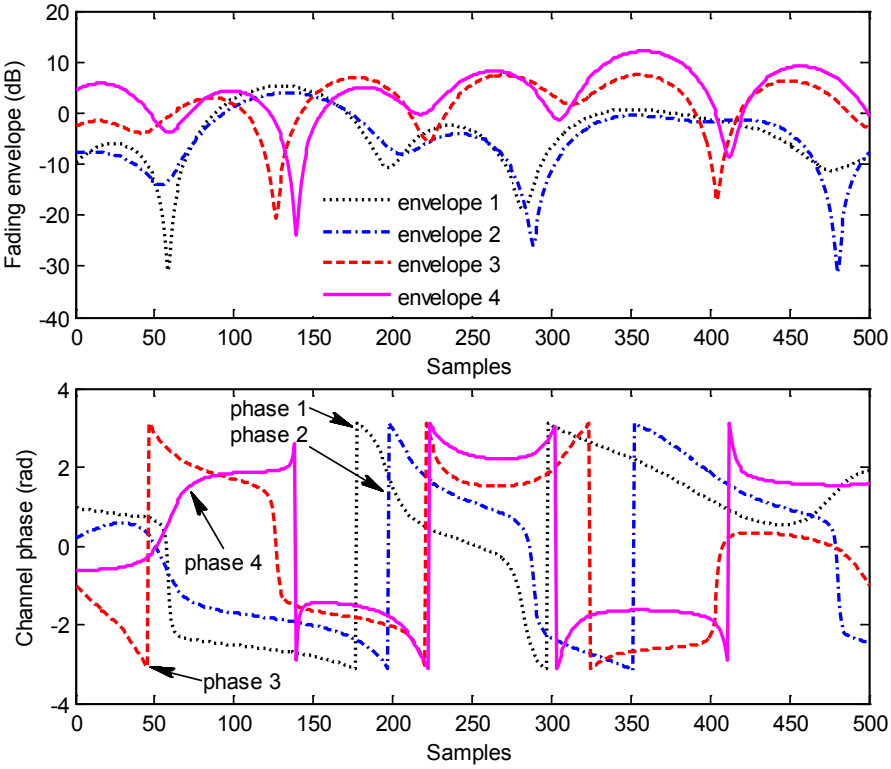

Figure 3.11: Unequal power envelopes and phases of desired $\widehat{\mathbf{A}}$ generated in the second step of GSCT for the parameters given in example 4 as; $\sigma_{\hat{a}_1}^2 = \sigma_{\hat{a}_2}^2 = 1$, $\sigma_{\hat{a}_3}^2 = 2$, $\sigma_{\hat{a}_4}^2 = 3$, $\hat{\rho}_{12} = 0.9$, $\hat{\rho}_{23} = 0.3$, $\hat{\rho}_{34} = 0.7$, and $\mathbb{k}_{12} = \mathbb{k}_{23} = \mathbb{k}_{34} = 1$.

3.5 Iterative Coloring Technique (ICT)

In this section, a simple ICT [141, 142] for designing *any* number of CRFC is proposed to overcome the shortcomings of conventional methods. It enables generation of equal and unequal power Rayleigh fading envelopes with *any* desired correlation factor in the interval $[0, 1]$. The proposed method employs iterative coloring of uncorrelated reference signals using real correlation matrix of envelopes $\boldsymbol{\rho}$ rather than complex covariance matrix of the Gaussian samples $\mathbf{R}_{AA}$ which is employed in conventional methods. Furthermore, correlations of all signal envelope pairs are considered compared with GSCT that utilizes the correlation of successive signal envelopes only.

3.5.1 Principles of Iterative Coloring

In ICT and based largely on the material presented in section 3.4.1, we consider the correlation matrix of envelopes $\boldsymbol{\rho} \in \mathcal{R}^{\mathcal{N}\times\mathcal{N}}$ for generating $\mathbf{A} = [a_1 \quad \cdots \quad a_{\mathcal{N}}] \in \mathcal{C}^{1\times\mathcal{N}}$ of equal power correlated signals from $\mathbf{Z} = [z_1 \quad \cdots \quad z_{\mathcal{N}}] \in \mathcal{C}^{1\times\mathcal{N}}$ of equal power uncorrelated signals using the following linear formulation assuming $\sigma_a^2 = \sigma_z^2 = 1$.

$$a_k = \begin{cases} \alpha_{kk} z_k & , k = 1 \\ \sum_{i=1}^{k-1} (\alpha_{ki} + j\beta_{ki}) z_i + \alpha_{kk} z_k & , 2 \le k \le \mathcal{N} \end{cases} \tag{3.32}$$

where α_{ki} and β_{ki} for $1 \le (i \le k) \le \mathcal{N}$ are *coloring factors* used to insure the required correlation among inphase and quadrature components of complex Gaussian signals which can be calculated directly by satisfying the aforementioned conditions of [31] as follows:

$$\left| \begin{array}{ll} \alpha_{ki} = 1 , & k = i = 1 \\ \alpha_{ki} = 2\mathcal{g}_{ki} , & 2 \le k \le \mathcal{N} \quad , i = 1 \\ \alpha_{ki} = \sqrt{1 - \sum_{j=1}^{k-1} \left(\alpha_{kj}^2 + \beta_{kj}^2 \right)} , & 2 \le i < k \le \mathcal{N} \\ \alpha_{ki} = \dfrac{2\mathcal{g}_{ki} - \sum_{j=1}^{i-1} \left(\alpha_{kj}\, \alpha_{ij} - \beta_{kj}\, \beta_{ij} \right)}{\alpha_{ii}}, & 2 \le i = k \le \mathcal{N} \end{array} \right. \tag{3.33}$$

and,

$$\left| \begin{array}{ll} \beta_{ki} = \mathbb{k}_{ki}\, \alpha_{ki} , & 2 \le k \le \mathcal{N} \quad , i = 1 \\ \beta_{ki} = \dfrac{2\mathcal{p}_{ki} - \sum_{j=1}^{i-1} \left(\beta_{kj}\, \alpha_{ij} - \alpha_{kj}\, \beta_{ij} \right)}{\alpha_{ii}} , & 2 \le i < k \le \mathcal{N} \end{array} \right. \tag{3.34}$$

3.5.2 ICT Algorithm

For wireless communication system, the desired channel **A** of equal power signals with an arbitrary correlation matrix of envelopes $\boldsymbol{\rho}$ can be generated as follows:

1) Given the desired correlations between signal envelopes ρ_{kq} and propagation factors $\mathbb{k}_{kq}$ for $1 \le k \ne q \le \mathcal{N}$ or calculate them using the available informations.
2) Calculate $\mathcal{g}_{kq}$ and $\mathcal{p}_{kq}$ for $1 \le (k \ne q) \le \mathcal{N}$ using equations (3.5), (3.6), (3.11), and (3.12) or directly from $\mathbf{R}_{AA}$ upon the availability.

3) Calculate the coloring factors, α_{ki} and β_{ki} for $1 \leq (i \leq k) \leq \mathcal{N}$ using equations (3.33) and (3.34).
4) Generate a reference vector $\mathbf{Z}$ of $\mathcal{N}$ equal power uncorrelated Rayleigh fading signals.
5) For $k = 1, \ldots, \mathcal{N}$, use equation (3.32) to calculate the desired signals of correlated Rayleigh fading channel $\mathbf{A}$.

3.5.3 Generalized ICT (GICT) Algorithm for Equal and Unequal Power CRFC

Generation of unequal power signals $\widehat{\mathbf{A}} = [\hat{a}_1 \ \ldots \ \hat{a}_k \ \ldots \ \hat{a}_{\mathcal{N}}] \in \mathcal{C}^{1\times\mathcal{N}}$ are very useful for simulating many applications of wireless communications. Therefore, GICT algorithm is presented in this section for the generation of equal/unequal power signals by considering the general correlation matrix $\widehat{\boldsymbol{\rho}} \in \mathcal{R}^{\mathcal{N}\times\mathcal{N}}$ of $\mathcal{N}$ signal envelopes with power of $\sigma^2_{\hat{a}_k}$, $k = 1, \ldots, \mathcal{N}$ as given in equation (3.19).

The desired signals can be generated using the following algorithm where the transformation in steps 2 and 7 are same as in [137].

1) Given the desired correlations between signal envelopes $\hat{\rho}_{kq}$ and propagation factors $\mathbb{k}_{kq}$ for $1 \leq k \neq q \leq \mathcal{N}$ or calculate them using the available informations.
2) Normalize $\widehat{\boldsymbol{\rho}}$ to create normalized correlation matrix $\boldsymbol{\rho}$ using the following relation

$$\rho_{kq} = \frac{\hat{\rho}_{kq}}{\sqrt{\sigma^2_{\hat{a}_k}\sigma^2_{\hat{a}_q}}} \tag{3.35}$$

3) Calculate $\mathscr{g}_{kq}$ and $\mathscr{p}_{kq}$ for $1 \leq (k \neq q) \leq \mathcal{N}$ using equations (3.5), (3.6), (3.11), and (3.12) or directly from $\mathbf{R}_{AA}$ upon the availability.
4) Calculate the coloring factors, α_{ki} and β_{ki} for $1 \leq (i \leq k) \leq \mathcal{N}$ using equations (3.33) and (3.34).
5) Generate a reference vector $\mathbf{Z}$ of $\mathcal{N}$ equal power uncorrelated Rayleigh fading signals.
6) For $k = 1, \ldots, \mathcal{N}$, use equation (3.32) to calculate the equal power signals of correlated fading channel $\mathbf{A}$.
7) For $k = 1, \ldots, \mathcal{N}$, calculate the unequal power signals of desired correlated fading channel $\widehat{\mathbf{A}}$ using equation (3.22).

3.5.4 Complexity Analysis of GICT

Let's assume that $\mathcal{N}$ is the total number of desired equal power correlated signals. To simulate these signals using GICT, approximate computational operations of $3\mathcal{N}^2 - 6\mathcal{N} + 4$ are required which is $\mathcal{O}(\mathcal{N}^2)$. This includes additions, subtractions, divisions, multiplications, and square roots. In Table 3.5, the approximate computational effort of GICT algorithm is compared with GSCT and the conventional methods that utilize Cholesky or Eigenvalue decomposition.

For comparison purpose, let's consider two examples of $\mathcal{N} = 48$ signals for 6×8 MIMO system and $\mathcal{N} = 256$ for MC-CDMA system used in section 3.4.4. For $\mathcal{N} = 48$, approximate calculations of 6.628×10^3 are needed for GICT compared with 4.466×10^3 for GSCT, 38.024×10^3 for Cholesky, and 109.416×10^3 for Eigenvalue decomposition. When $\mathcal{N} = 256$, approximate calculations of 0.19×10^6 are needed for GICT compared with 0.13×10^6 for GSCT, 5.62×10^6 for Cholesky, and 16.74×10^6 for Eigenvalue decomposition. Also, we find that approximately more than 100% reduction in complexity can be achieved at $\mathcal{N} = 14$ compared with Cholesky and at $\mathcal{N} = 5$ compared with Eigenvalue decomposition method. Therefore, GICT requires more computations than GSCT while providing significant reduction in computations compared with Cholesky and Eigenvalue methods due to the direct use of real correlation matrix of envelopes $\boldsymbol{\rho}$ and iterative coloring rather than the complex covariance matrix $\mathbf{R}_{AA}$ which needs $\mathcal{N}^3/6$ multiplications to be factorized.

For unequal power correlated signals, GICT requires extra $3\mathcal{N}^2$ calculations for $\widehat{\boldsymbol{\rho}}_{\boldsymbol{s}}$ normalization and $2\mathcal{N}$ for $\widehat{\mathbf{A}}$ elements formulation. Hence, the total extra required computations are $3\mathcal{N}^2 + 2\mathcal{N}$ similar to Cholesky and Eigenvalue decomposition methods and higher than $5\mathcal{N} - 3$ needed for GSCT algorithm.

Table 3.5: Computational complexity of GICT to generate equal power correlated fading signals compared with GSCT and the conventional methods that utilize Cholesky or Eigenvalue decomposition

Algorithm	Total Calculations	Computational Effort
Cholesky	$(2\mathcal{N}^3 + 3\mathcal{N}^2 + \mathcal{N})/6$	$\mathcal{O}(\mathcal{N}^3)$
Eigenvalue	$(6\mathcal{N}^3 - 3\mathcal{N}^2 - 3\mathcal{N})/6$	$\mathcal{O}(\mathcal{N}^3)$
GSCT	$2\mathcal{N}^2 - 3\mathcal{N} + 2$	$\mathcal{O}(\mathcal{N}^2)$
GICT	$3\mathcal{N}^2 - 6\mathcal{N} + 4$	$\mathcal{O}(\mathcal{N}^2)$

3.5.5 Simulation Results

For the accuracy checking and to show the superiority of GICT without loss of generality, we consider generation of correlated Rayleigh fading signals using MATLAB/7.9 for four different representative examples. The first example is for simulating three equal power signals of multicarrier channel scenario with complex covariance matrix. In the second example, we consider simulation of three equal power signals for 3 receive antenna correlation scenario (real covariance matrix). The third example is for simulating six equal power signals of 2×3 MIMO channel scenario while the last example is for simulating unequal power signal needed in many wireless applications such as MC-CDMA and MU-MIMO.

Example 1:

Consider generation of $\mathcal{N} = 3$ equal power flat Rayleigh fading signals as $\mathbf{A} = [a_1 \quad a_2 \quad a_3]$ for multicarrier system scenario using the following parameters: frequency separation between adjacent frequencies of $\Delta f = 200$ kHz (GSM 900), channel delay spread $\sigma_\tau = 0.5\,\mu sec$, maximum Doppler frequency $f_d = 80$ Hz, arrival time delays between signals in $msec$ are $\tau_{12} = 0.4$, $\tau_{23} = 1$, and $\tau_{13} = 1.4$, power of each signal is $\sigma_a^2 = 2\mathcal{b} = 1$.

Using equations (3.5), (3.6), and (3.7), the considered covariance matrix $\mathbf{R}_{AA}$ of complex signal can be calculated as

$$\mathbf{R}_{AA} = \begin{bmatrix} 1 & \gamma_{12} & \gamma_{13} \\ \gamma_{21}^* & 1 & \gamma_{23} \\ \gamma_{31}^* & \gamma_{32}^* & 1 \end{bmatrix} = \begin{bmatrix} 1 & 0.70 + j44 & 0.34 + j43 \\ 0.70 - j44 & 1 & 0.67 + j42 \\ 0.34 - j43 & 0.67 - j42 & 1 \end{bmatrix} \tag{3.36}$$

where the propagation factors are calculated as $\mathbb{k}_{12} = \mathbb{k}_{23} = 0.628$ and $\mathbb{k}_{13} = 1.256$. The eigenvalues of $\mathbf{R}_{AA}$ are: 0.067 , 0.477 , and 2.455 . Therefore, covariance matrix $\mathbf{R}_{AA}$ is a positive definite since all of the eigenvalue are positive and hence, Cholesky or Eigenvalue decomposition methods can be applied directly for this example.

To generate $\mathbf{A}$ using the proposed GICT, the desired correlation matrix $\boldsymbol{\rho}$ of signal envelopes can be calculated using equations (3.5), (3.6), and (3.11), as

$$\boldsymbol{\rho} = \begin{bmatrix} 1 & \rho_{12} & \rho_{13} \\ \rho_{21} & 1 & \rho_{23} \\ \rho_{31} & \rho_{32} & 1 \end{bmatrix} = \begin{bmatrix} 1 & 0.70 & 0.30 \\ 0.70 & 1 & 0.63 \\ 0.30 & 0.63 & 1 \end{bmatrix} \tag{3.37}$$

Envelopes (r_1, r_2, r_3) and phases $(\beta_1, \beta_2, \beta_3)$ of the generated fading signals are depicted in Fig. 3.12. For comparison, results of signal envelopes and phases using Cholesky decomposition method are shown in Fig. 3.13 and the measured correlations are shown in Table 3.6 with that

of GICT and desired values. It can be seen that the envelopes and phases of a_1 and a_2 signals are identical in both methods while slightly differ for a_3 since the coloring processes are different. This is also shown by the measured correlations where GICT provide very close results for ρ_{23} and ρ_{13} compared with Cholesky decomposition method which prove the accuracy of GICT. In both methods, all phases are independent even those related to high correlated envelopes (r_1, r_2) as expected for complex covariance matrices. PDF of the generated Rayleigh fading envelopes and uniform distributed phases are coincides with the theoretical results as shown in Fig. 3.14 and Fig. 3.15, respectively.

Table 3.6: Measured correlations of example 1 using GICT and conventional Cholesky decomposition method compared with the desired values

Correlation	ρ_{12}	ρ_{23}	ρ_{13}
Desired	0.70	0.63	0.30
GICT	0.70	0.62	0.31
Cholesky	0.70	0.61	0.28

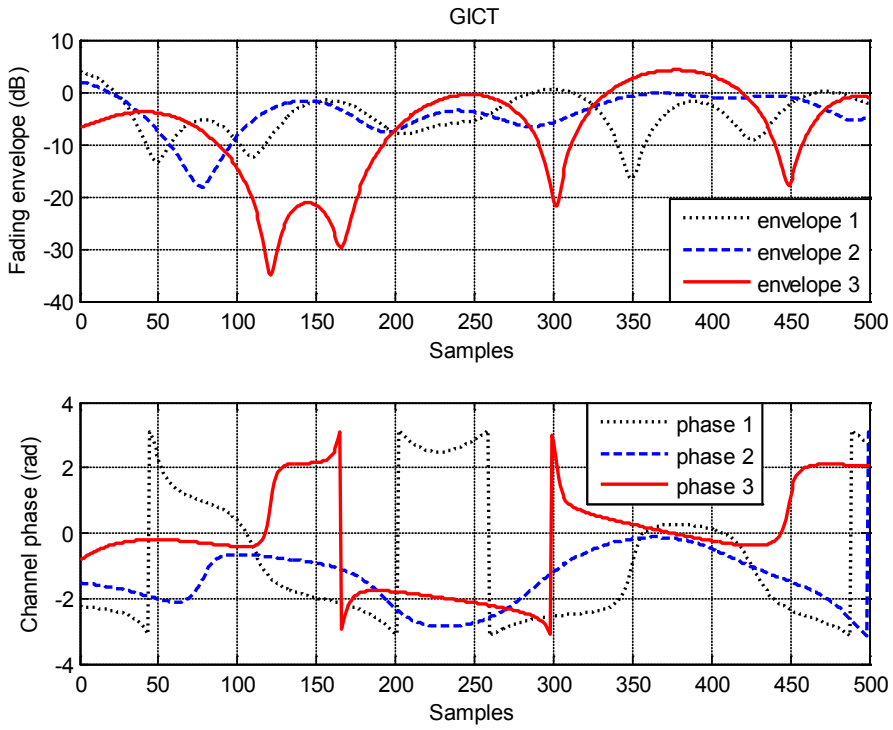

Figure 3.12: Equal power envelopes and phases of **A** signals generated using GICT for the parameters given in example 1 as; $\sigma_a^2 = 1$, $\rho_{12} = 0.7$, $\rho_{23} = 0.63$, $\rho_{13} = 0.3$, $\mathbb{k}_{12} = \mathbb{k}_{23} = 0.628$, and $\mathbb{k}_{13} = 1.256$ which are related to complex $\mathbf{R}_{AA}$.

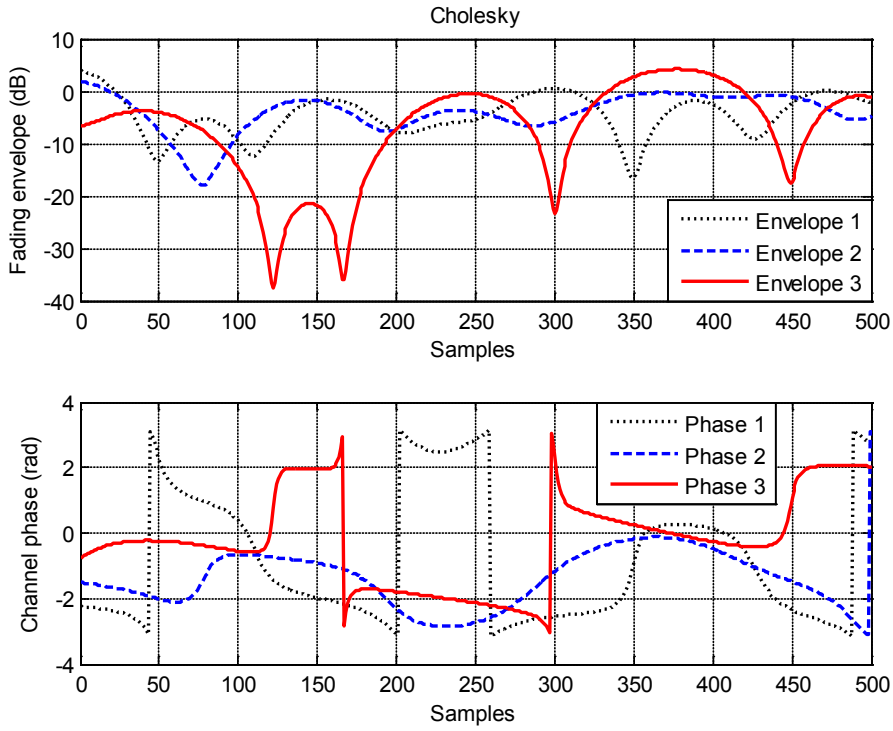

Figure 3.13: Equal power envelopes and phases of **A** signals generated using Cholesky decomposition method for the parameters given in example 1 as; $\sigma_a^2 = 1$, $\rho_{12} = 0.7$, $\rho_{23} = 0.63$, $\rho_{13} = 0.3$, $\mathbb{k}_{12} = \mathbb{k}_{23} = 0.628$, and $\mathbb{k}_{13} = 1.256$ which are related to complex $\mathbf{R}_{AA}$.

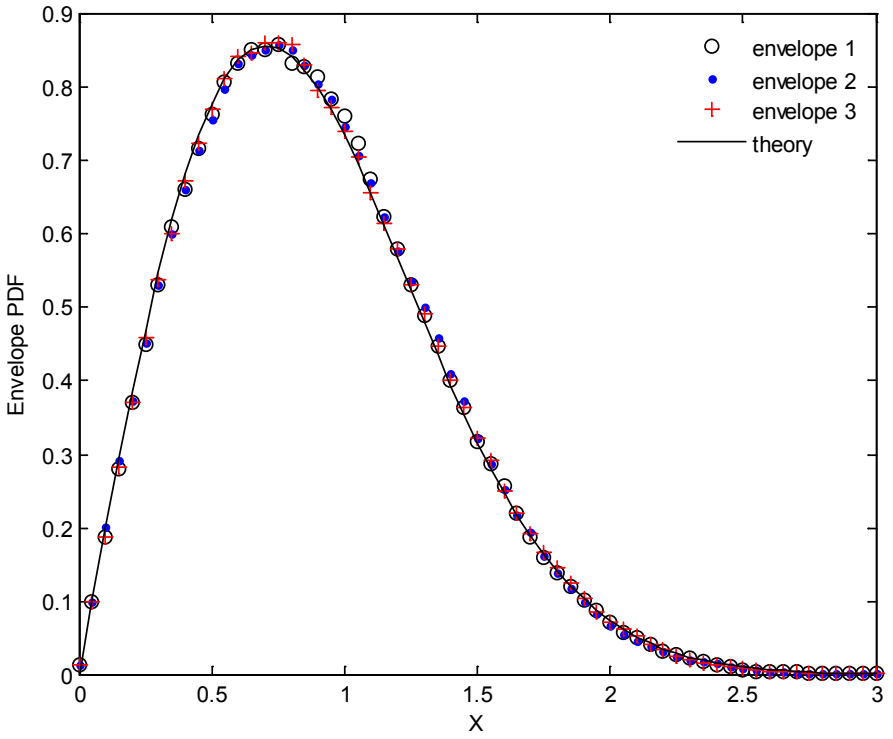

Figure 3.14: PDF of the Rayleigh fading envelopes of **A** signals generated in example 1.

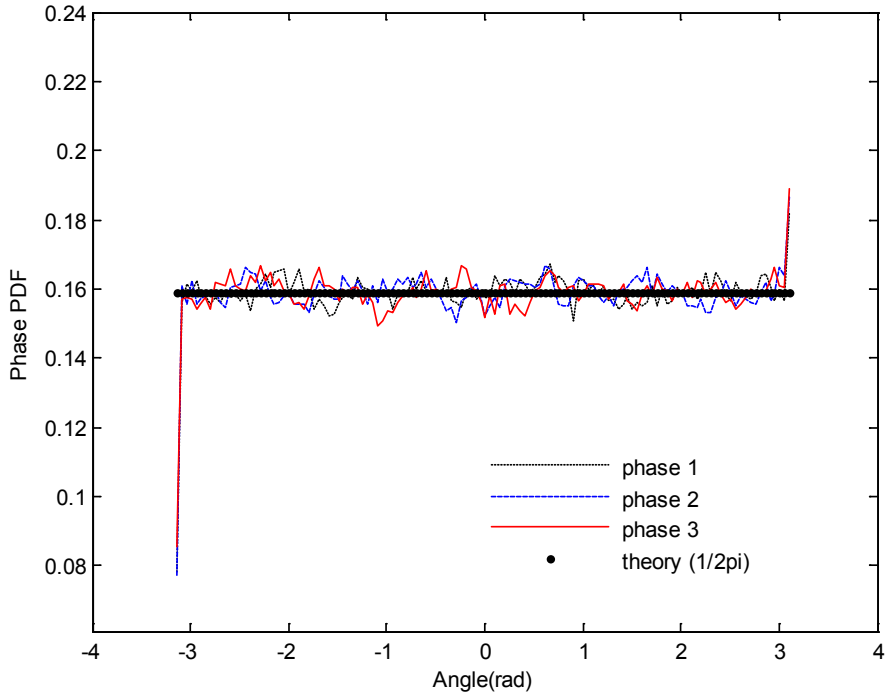

Figure 3.15: PDF of uniform distribution phases of **A** signals generated in example 1.

Example 2:

In this example, we consider generation of $\mathcal{N} = 3$ equal power flat Rayleigh fading signals as $\mathbf{A} = [a_1 \quad a_2 \quad a_3]$ for 3 receive antenna correlation in scenario. The constant antenna correlation model [131] is adopted in this example due its popularity by using the following real constant receive covariance matrix.

$$\mathbf{R}_{AA} = \begin{bmatrix} 1 & \gamma_{12} & \gamma_{13} \\ \gamma_{21}^* & 1 & \gamma_{23} \\ \gamma_{31}^* & \gamma_{32}^* & 1 \end{bmatrix} = \begin{bmatrix} 1 & 0.866 & 0.866 \\ 0.866 & 1 & 0.866 \\ 0.866 & 0.866 & 1 \end{bmatrix} \tag{3.38}$$

Using equation (3.11) with $\sigma_a^2 = 2\mathscr{b} = 1$, the desired correlation matrix of envelopes $\boldsymbol{\rho}$ can be calculated directly from $\mathbf{R}_{AA}$ as

$$\boldsymbol{\rho} = \begin{bmatrix} 1 & \rho_{12} & \rho_{13} \\ \rho_{21} & 1 & \rho_{23} \\ \rho_{31} & \rho_{32} & 1 \end{bmatrix} = \begin{bmatrix} 1 & 0.75 & 0.75 \\ 0.75 & 1 & 0.75 \\ 0.75 & 0.75 & 1 \end{bmatrix} \tag{3.39}$$

In this example, all propagation factors $\mathbb{k}_{12}$, $\mathbb{k}_{23}$, and $\mathbb{k}_{13}$ are zero since $\mathbf{R}_{AA}$ is a real covariance matrix. Envelopes (r_1, r_2, r_3) and phases $(\beta_1, \beta_2, \beta_3)$ of the generated fading signals are depicted in Fig. 3.16. For comparison, results of signal envelopes and phases using Cholesky decomposition method are shown in Fig. 3.17 and the measured correlations are

shown in Table 3.7 with that of GICT and desired values. As can be seen in both methods, all phases and envelopes are correlated as expected for real covariance matrices. In this case, the inphase and quadrature components of any two signals a_k and a_q are uncorrelated where $\mathrm{E}\{x_k\, y_q\} = -\mathrm{E}\{y_k x_q\} = 0$ in contrast to $\mathrm{E}\{x_k\, y_q\} = -\mathrm{E}\{y_k x_q\} = \rho_{kq}$ for complex covariance matrices. Furthermore, envelopes and phases of a_1 and a_2 signals are identical in both methods while slightly differ for a_3 since the coloring processes are different. This is also shown by the measured correlations where GICT provide very close results for ρ_{23} and ρ_{13} compared with Cholesky decomposition method which prove the accuracy of GICT.

Table 3.7: Measured correlations of example 2 using GICT and conventional Cholesky decomposition method compared with the desired values

Correlation	ρ_{12}	ρ_{23}	ρ_{13}
Desired	0.75	0.75	0.75
GICT	0.75	0.74	0.74
Cholesky	0.75	0.74	0.72

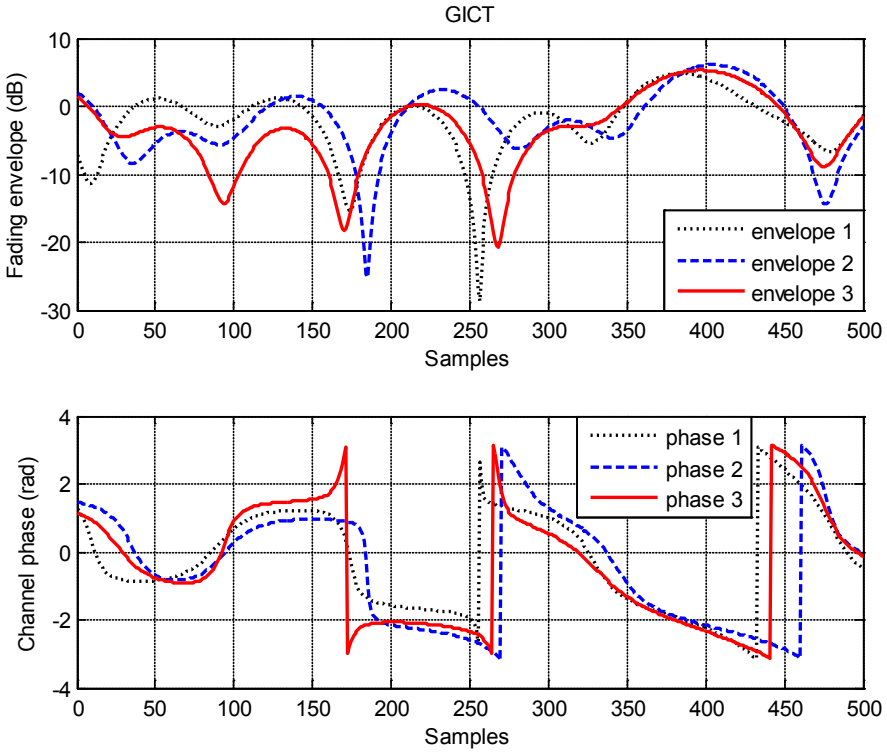

Figure 3.16: Equal power envelopes and phases of **A** signals generated using GICT for the parameters given in example 2 as; $\sigma_a^2 = 1$, $\rho_{12} = \rho_{23} = \rho_{13} = 0.75$, and $\mathbb{k}_{12} = \mathbb{k}_{23} = \mathbb{k}_{13} = 0.0$ which are related to real $\mathbf{R}_{AA}$.

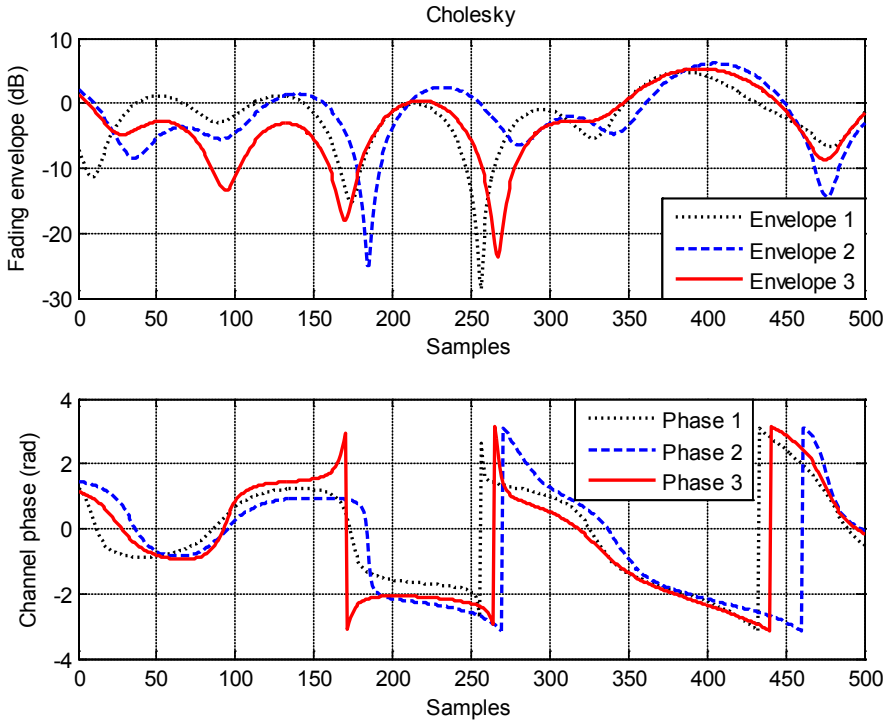

Figure 3.17: Equal power envelopes and phases of **A** signals generated using Cholesky decomposition method for the parameters given in example 2 as; $\sigma_a^2 = 1$, $\rho_{12} = \rho_{23} = \rho_{13} = 0.75$, and $\mathbb{k}_{12} = \mathbb{k}_{23} = \mathbb{k}_{13} = 0.0$ which are related to real $\mathbf{R}_{AA}$.

Example 3:

For large number of fading channels, we consider generation of $\mathcal{N} = 6$ equal power correlated flat Rayleigh fading signals in this example as $\mathbf{A} = [a_1 \quad a_2 \quad \cdots \quad a_6]$ for 2×3 MIMO system scenario. Desired parameters are given by the designer as: $\sigma_a^2 = 1$, $\mathbb{k}_{kq} = 1$, $\forall(k, q) = 1, \ldots, 6$ and the following correlation matrix of signal envelopes.

$$\boldsymbol{\rho} = \begin{bmatrix} 1 & 0.90 & 0.44 & 0.38 & 0.25 & 0.18 \\ 0.90 & 1 & 0.60 & 0.44 & 0.38 & 0.25 \\ 0.44 & 0.60 & 1 & 0.90 & 0.44 & 0.38 \\ 0.38 & 0.44 & 0.90 & 1 & 0.60 & 0.44 \\ 0.25 & 0.38 & 0.44 & 0.60 & 1 & 0.90 \\ 0.18 & 0.25 & 0.38 & 0.44 & 0.90 & 1 \end{bmatrix} \tag{3.40}$$

For this example, none of the existing methods can generate the desired signals with any accuracy tolerance (see Table 3.2) where the related covariance matrix $\mathbf{R}_{AA}$ is neither a positive semidefinite nor a positive definite matrix.

Using GICT, envelopes r_1, r_2, r_3, r_4, r_5, and r_6 of **A** signals are shown in Fig. 3.18 which clearly reflects the desired correlation values. The measured correlations for these envelopes demonstrate the accuracy and effectiveness of GICT as shown below.

$$\boldsymbol{\rho} = \begin{bmatrix} 1 & 0.90 & 0.45 & 0.37 & 0.23 & 0.19 \\ 0.90 & 1 & 0.60 & 0.43 & 0.38 & 0.25 \\ 0.45 & 0.60 & 1 & 0.91 & 0.44 & 0.39 \\ 0.37 & 0.43 & 0.91 & 1 & 0.60 & 0.44 \\ 0.23 & 0.38 & 0.44 & 0.60 & 1 & 0.90 \\ 0.19 & 0.25 & 0.39 & 0.44 & 0.90 & 1 \end{bmatrix} \tag{3.41}$$

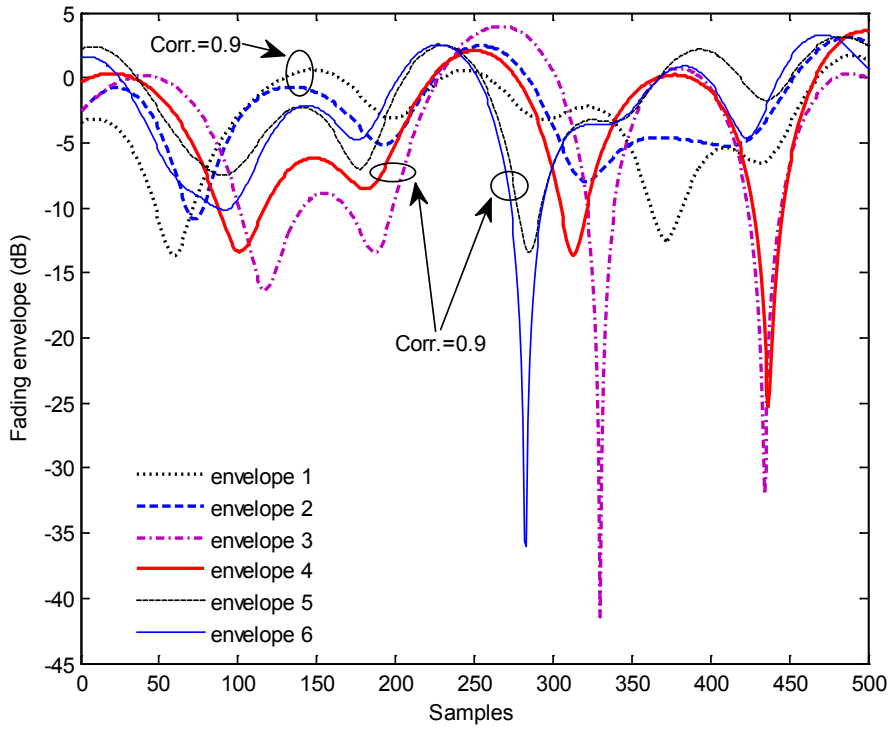

Figure 3.18: Equal power envelopes of **A** generated using GICT for the desired correlation matrix $\boldsymbol{\rho}$ and parameters given in example 3 as; $\sigma_a^2 = 1$ and $\mathbb{k}_{kq} = 1,\ \forall(k,q) = 1,\ldots,6$.

Example 4:

In this representative example, we consider generation of $\mathcal{N} = 3$ correlated flat Rayleigh fading signals as $\widehat{\mathbf{A}} = [\hat{a}_1 \quad \hat{a}_2 \quad \hat{a}_3]$ for unequal power scenario using the following parameters:

Signal power: $\sigma_{\hat{a}_1}^2 = 1$, $\sigma_{\hat{a}_2}^2 = 3$, and $\sigma_{\hat{a}_3}^2 = 9$

Propagation factors: $\mathbb{k}_{12} = \mathbb{k}_{23} = 1.1$ and $\mathbb{k}_{13} = 2.2$

Correlation of signal envelopes: $\hat{\rho}_{12} = 0.9$, $\hat{\rho}_{23} = 0.6$, and $\hat{\rho}_{13} = 0.4$

Using GICT, the first step involves generation of unit power correlated Rayleigh fading signals $\mathbf{A} = [a_1 \quad a_2 \quad a_3]$ with normalized correlations calculated from the desired values using equation (3.35) as $\rho_{12} = 0.519$, $\rho_{23} = 0.115$, and $\rho_{34} = 0.133$. Envelopes (r_1, r_2, r_3) and

phases $(\beta_1, \beta_2, \beta_3)$ of the generated signals $\mathbf{A}$ are depicted in Fig. 3.19 and the measured correlations in this step are $\rho_{12} = 0.52$, $\rho_{23} = 0.113$, and $\rho_{34} = 0.122$.

In the second step, unequal power signals $\widehat{\mathbf{A}}$ are calculated from $\mathbf{A}$ using equation (3.22) and their envelopes $(\hat{r}_1, \hat{r}_2, \hat{r}_3)$ and phases $(\hat{\beta}_1, \hat{\beta}_2, \hat{\beta}_3)$ are depicted in Fig. 3.20. The measured correlations in this step are $\hat{\rho}_{12} = 0.9$, $\hat{\rho}_{23} = 0.6$, and $\hat{\rho}_{13} = 0.39$ which implies the accuracy of the proposed technique.

As can be seen from these figures, envelopes r_2 and r_3 are differ than $\hat{r}_2$ and $\hat{r}_3$ due to the power difference in the first and second steps of generation while r_1 is same as $\hat{r}_1$ since they have equal powers. On the other hand, phases in the first step are similar to that of second and not affected by the power transformation (3.22) as expected.

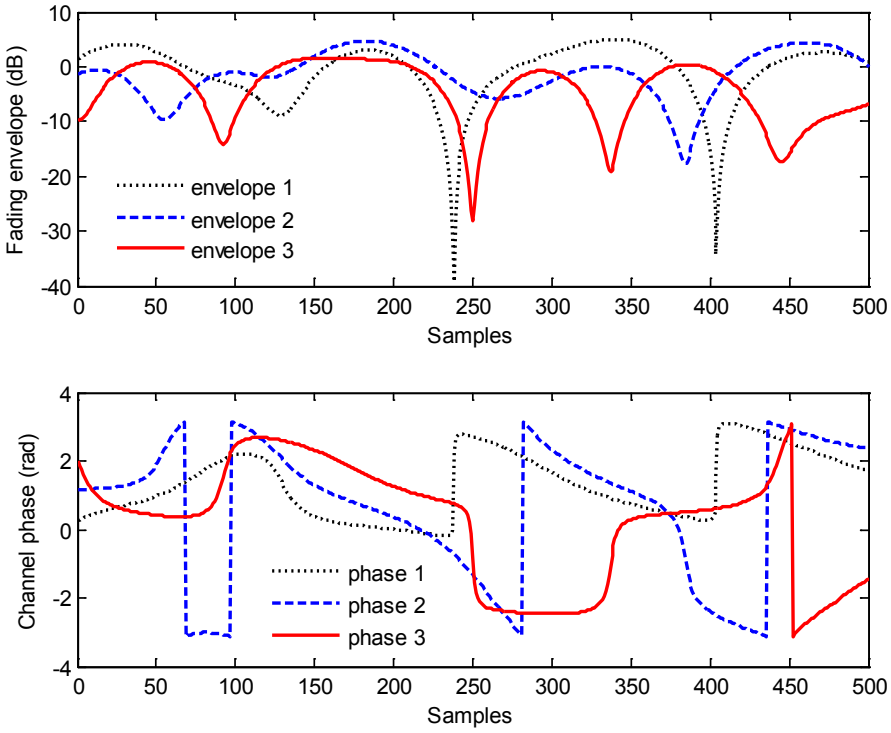

Figure 3.19: Equal unit power envelopes $(\sigma_{a_1}^2 = \sigma_{a_2}^2 = \sigma_{a_3}^2 = 1)$ and phases of $\mathbf{A}$ generated in the first step of GICT for the parameters calculated in example 4 as; $\rho_{12} = 0.519$, $\rho_{23} = 0.115$, and $\rho_{13} = 0.113$.

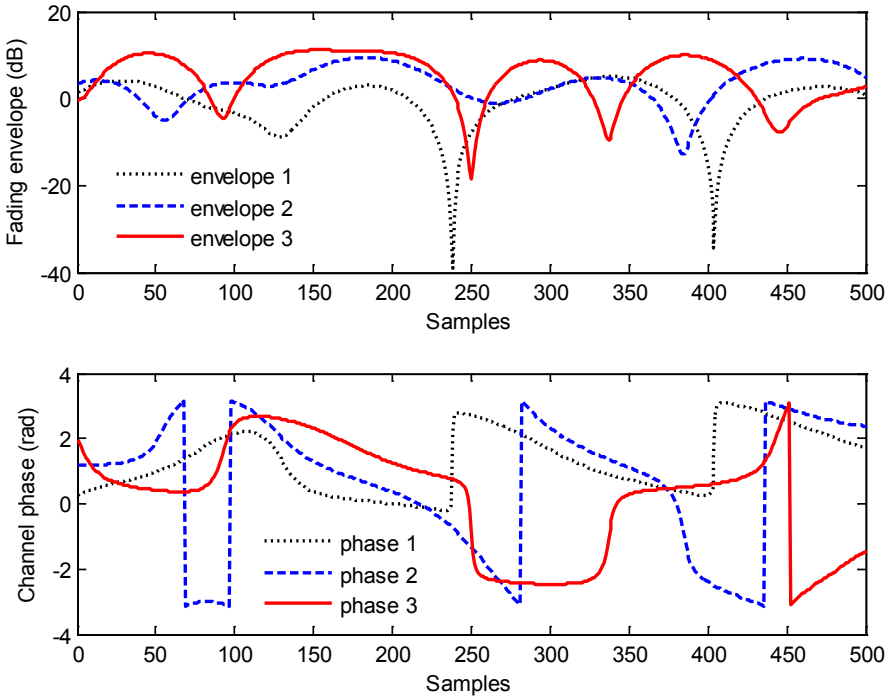

Figure 3.20: Unequal power envelopes and phases of desired $\widehat{\mathbf{A}}$ generated in the second step of GICT for the parameters given in example 4 as; $\sigma_{\hat{a}_1}^2 = 1$, $\sigma_{\hat{a}_2}^2 = 3$, $\sigma_{\hat{a}_3}^2 = 9$, $\hat{\rho}_{12} = 0.9$, $\hat{\rho}_{23} = 0.6$, $\hat{\rho}_{13} = 0.4$, $\mathbb{k}_{12} = \mathbb{k}_{23} = 1.1$, and $\mathbb{k}_{13} = 2.2$.

3.6 Conclusions

In this chapter, two simple techniques have been proposed for accurate generation of equal and unequal power CRFC for multiantenna and multicarrier systems with different propagation conditions. They are designed to overcome the shortcomings of existing methods by avoiding decomposition of complex covariance matrix of the Gaussian samples.

In GSCT, successive coloring of fading signals for all successive pairs is employed by utilizing the real correlation vector of desired signal envelopes. Any number of fading signals with any desired correlations of successive envelope pairs can be simulated accurately while correlations of all other pairs are determined by the related successive pairs. Extensive simulations of practical system scenarios demonstrate the effectiveness of GSCT compared with the conventional methods. It overcomes all shortcomings of existing methods particularly as the number of fading signals increases and/or moderate to high correlations used. For small number of fading signals and/or low correlation levels, GSCT provides high accuracy for the successive pairs of signals similar to conventional methods with significant reduction in computational complexity of $\mathcal{O}(\mathcal{N}^2)$.

In GICT, real correlation matrix of desired signal envelopes is utilized in iterative coloring processes of uncorrelated reference signals to generate any number of correlated fading signals

representing feasible system. Different practical system scenarios are simulated to show the effectiveness of GICT. It overcomes the shortcomings of existing methods when the number of fading signals increased and/or moderate to high correlations is required. For small number of fading signals and/or low correlation levels, GICT provides high accuracy with less computational complexity of $\mathcal{O}(\mathcal{N}^2)$.

Since GSCT utilizes correlation vector of successive envelopes, it is more convenient for generating moderate to large number of correlated signals ($\mathcal{N} > 6$) and less complex compared with GICT. For $\mathcal{N} \leq 6$, the accuracy of GICT outperforms GSCT since it considers the correlations of all signal pairs in the generation process. Analysis of previous methods demonstrates that none of them is able to generate any number of correlated fading signals with any desired correlation. Therefore, simplicity and accuracy of these techniques will help the research community to study and simulate the impact of channel correlations on current and new wireless applications. They are utilized efficiently in the following contributing chapters.

The next chapter focus on new approach to mitigate the effects of channel correlation in multiantenna systems.

Chapter 4

Signal Design for MU-MIMO Correlated Fading Channels

4.1 Introduction

Channels' correlation has the effect to degrade the channel capacity and error performance of MU-MIMO systems considerably. For SU-MIMO, effects of signal constellation design on the capacity and error performance over correlated fading channels have been considered in the literature. However, their applicability on correlated MU-MIMO channels has not been investigated yet.

In this chapter, two transmit signal constellation design methods referred to as unequal power allocation (UPA) and rotated constellation (RC) are proposed to maximize the capacity and error performance of MU-MIMO systems over different correlation levels (ρ) in the interval $[0, 1]$. This novel approach is referred to as constellation constrained MU-MIMO (CC-MU-MIMO) scheme. Based on principles of maximizing d_{min} of the composite received signals, users' data can be recovered using MLJD irrespective of correlation values ρ. Compared with identical constellation (IC) scenario of conventional MU-MIMO, constellation rearrangement of transmitted signals has direct impact to resolve the detection ambiguity when the channel difference is not enough to do, particularly in moderate to high correlations. Extensive analysis and simulation results demonstrate the superiority of proposed techniques to capture the promised gains of multiantenna systems regardless of channel correlations.

This chapter is organized as follows. Literature review on MUMA systems is presented in Section 4.2. System model of CC-MU-MIMO is introduced in Section 4.3. In Section 4.4, signal constellation designs to mitigate fading correlations are presented. It includes two proposed methods, UPA and RC compared with IC design. In Section 4.5, channel capacity analysis including the ergodic sum rate capacity and constellation constrained capacity is presented. In Section 4.6, simulation results of capacity and BER performance of proposed methods are demonstrated over CRFC environment. Finally, chapter conclusions are withdrawn in the last section.

4.2 Literature Review

Wireless digital communication systems are continuously striving for higher data rate. This is particularly a challenging task for power, bandwidth and complexity constrained systems. However, it is well known that spatial dimension can be exploited in rich multipath environment to increase the data rate significantly. This fact is well exploited in SU-MIMO [2, 6, 83, 97, 143-145] and MU-MIMO systems [2, 3, 17, 18, 146] where several transmit and receive antennas are employed to accomplish high spectral efficiency without excess in bandwidth and transmit power [1, 5, 147].

For capacity evaluation promised by MIMO systems in real propagation environment, many research studies have been dealt with the channel correlations due its direct impact rather than the basic assumption of independent fading across different antenna pairs [86, 90, 130-132, 148-151]. For example, high antenna correlations at transmit and/or receive ends may severely degrade the capacity of MIMO to that of SIMO, MISO, or SISO [86, 148]. In [90, 131, 132, 148, 149], intensive investigations have been made on the effects of fading correlation on SU-MIMO channel capacity and BER performance. While correlation in SU-MIMO mainly occurs due to antenna separation at each communication point, additional poor scattering environment may lead to this phenomenon in MU-MIMO systems despite of the natural spatial difference among users [23]. Therefore, unlike SU-MIMO, this correlation will lead to erroneous detection of users' signals or to avoid serving users with high correlated channels which seriously affects the multiuser diversity gain. As a result, the system capacity degrades as the fading channel correlation increases where the separation of users' signals at BS receiver is mainly depends on the channel difference which is considered as a multiple access dimension [18, 21, 99]. Indeed, presence of correlations increases the linear dependence of the transmitted signals which complicates the decoder task.

To mitigate the correlation effects even for extreme levels of full correlation, many techniques have been proposed in the literature such as [86, 152-154]. The key element is not to depend on the fading channel difference alone for signal detection. For example, a precoding technique based on phase and power adjusting of the input constellations has been introduced in [86] for SU-MIMO system with transmit correlation. However, this method assumes the availability of correlation properties at the transmitter side and can not be applied directly for multiuser case without proper modifications. In [154], different scenarios have been presented for signal design of two users equipped with single antenna by applying constellation rearrangement to increase the minimum distance of the composite received signals. The idea of constellation design has been adopted in many studies to improve the performance of wireless systems [158-164]. In [158, 159], rotation of transmitted signal constellations is employed to enlarge the capacity region of different orthogonal and non-orthogonal 2-user Gaussian MAC.

However, for large number of constellation points, relative rotation between the alphabets will not affect the capacity region for any SNR level. In [160], same results and conclusions are found for 2-user Gaussian and fading BC. In [158], signal rotation is utilized also to construct STBC pairs for 2-user MISO and 2-user MIMO fading channel to reduce the detection complexity of ML and SD receivers, respectively. Rearrangement of constellation points is investigated to improve the system performance and bandwidth efficiency of transmit diversity in both Gaussian and fading channels [161-163]. Optimized signal constellation is proposed with network coding for two-way wireless relaying applications [164]. It is applied in the MAC channel with receive diversity to improve the system performance and throughput significantly.

To utilize the available spectrum efficiently, new design approaches for MU-MIMO communications under different channel correlation conditions are of high interest to maintain high data rate and error performance. In this chapter, a novel CC-MU-MIMO scheme to achieve these objectives is presented for cellular system. It is based on the principles of maximizing d_{min} of composite received signal by employing different signal design methods at the users' side. At the receive side, MLJD is employed to recover the users' data irrespective of correlation values ρ. The mutual information formula between transmitted and received signals [143, 145], and the well known Ungerboeck's equation of channel capacity [155] have been modified in this chapter for the purpose of constellation constrained capacity evaluations.

4.3 Constellation Constrained MU-MIMO (CC-MU-MIMO) System Model

4.3.1 Signal Model

Consider CC-MU-MIMO of K active mobile users communicating simultaneously over correlated flat Rayleigh fading MAC with one common BS in one cell cellular system as in Fig. 4.1. Each of the mobile user equipments has a single antenna while the BS receiver equipped with m antennas and utilizes nonlinear MLJD technique for data estimation. Signal constellation of each user is subject to the power control and/or channel phase feedback from BS such that the received composite signals will have maximum d_{min}.

The received signal vector by m receive antennas is represented as

$$\mathbf{r} = \sum_{k=1}^{K} \mathbf{h}_k v_k + \mathbf{n} \tag{4.1}$$

where $\mathbf{r} = [r_1 \quad \cdots \quad r_m]^T \in \mathcal{C}^{m\times 1}$ is $m \times 1$ received signal vector, $\mathbf{h}_k = [h_{k1} \quad \cdots \quad h_{km}]^T \in \mathcal{C}^{m\times 1}$ is $m \times 1$ channel vector of user k whose entries $h_{kl} = x_{kl} + jz_{kl}$, $l = 1, \ldots, m$ are zero

mean unit variance complex fading coefficient between user k and l^{th} receive antenna, x_{kl} and z_{kl} are in-phase and quadrature components of zero mean Gaussian random processes each with variance $1/2$, v_k is transmitted signal of user k subject to power constraint P_k and modulated from equiprobable data b_k, $\mathbf{n} = [n_1 \quad \cdots \quad n_m]^T \in \mathcal{C}^{m\times 1}$ is $m \times 1$ independently identically distributed (i.i.d) complex additive white Gaussian noise (AWGN) vector with elements having zero mean and variance σ_n^2.

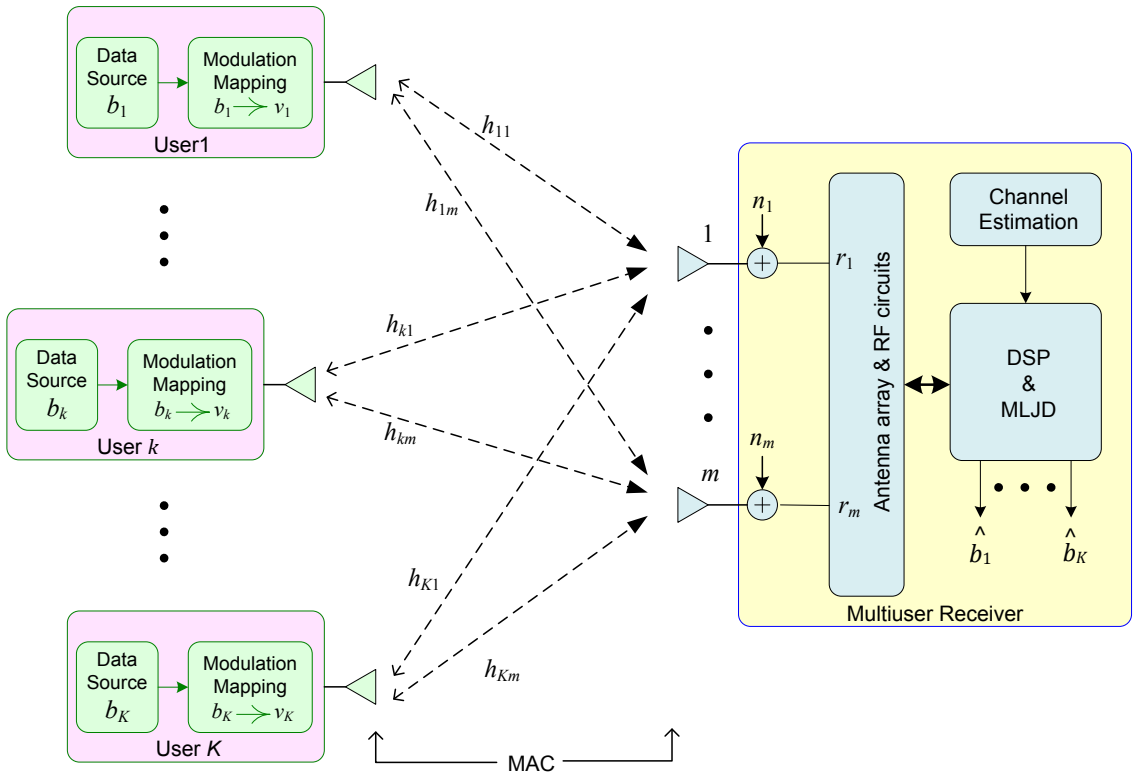

Figure 4.1: CC-MU-MIMO system model of K active mobile users each equipped with one antenna communicating simultaneously over MAC with one common base station receiver having m antennas.

The overall $m \times K$ channel matrix $\mathbf{H} \in \mathcal{C}^{m\times K}$ of considered system can be represented as

$$\mathbf{H} = [\mathbf{h}_1 \cdots \mathbf{h}_k \cdots \mathbf{h}_K] = \begin{bmatrix} h_{11} & \cdots & h_{k1} & \cdots & h_{K1} \\ \vdots & \ddots & \vdots & \ddots & \vdots \\ h_{1l} & \cdots & h_{kl} & \cdots & h_{Kl} \\ \vdots & \ddots & \vdots & \ddots & \vdots \\ h_{1m} & \cdots & h_{km} & \cdots & h_{Km} \end{bmatrix} \tag{4.2}$$

The fading coefficients h_{kl} of **H** can be represented also as

$$h_{kl} = \alpha_{kl}\, e^{-j\beta_{kl}}\ ;\ \ k = 1, \dots, K;\ \ l = 1, \dots, m \tag{4.3}$$

where $\alpha_{kl} = |h_{kl}|$ is the Rayleigh distributed envelope (magnitude) of channel component h_{kl} and $\beta_{kl} = \tan^{-1}(z_{kl}/x_{kl})$ is the uniform distribution phase over the interval $[0, 2\pi]$.

The received signal in equation (4.1) can be rewritten as

$$\mathbf{r} = \mathbf{H}\mathbf{v} + \mathbf{n} = \mathbf{s} + \mathbf{n} \tag{4.4}$$

where $\mathbf{v} = [v_1\ \cdots\ v_k\ \cdots\ v_K]^T \in \mathcal{C}^{K\times 1}$ is the transmitted signal vector of all active users and $\mathbf{s} = [s_1\ \cdots\ s_l\ \cdots\ s_m]^T \in \mathcal{C}^{m\times 1}$ is the vector of superimposed users' signals over their entire channels at the MAC input given as

$$\mathbf{s} = \begin{bmatrix} s_1 \\ \vdots \\ s_l \\ \vdots \\ s_m \end{bmatrix} = \begin{bmatrix} h_{11} & \cdots & h_{k1} & \cdots & h_{K1} \\ \vdots & \ddots & \vdots & \ddots & \vdots \\ h_{1l} & \cdots & h_{kl} & \cdots & h_{Kl} \\ \vdots & \ddots & \vdots & \ddots & \vdots \\ h_{1m} & \cdots & h_{km} & \cdots & h_{Km} \end{bmatrix} \begin{bmatrix} v_1 \\ \vdots \\ v_k \\ \vdots \\ v_K \end{bmatrix} = \begin{bmatrix} h_{11}v_1 + \cdots + h_{k1}v_k + \cdots + h_{K1}v_K \\ \vdots \\ h_{1l}v_1 + \cdots + h_{kl}v_k + \cdots + h_{Kl}v_K \\ \vdots \\ h_{1m}v_1 + \cdots + h_{km}v_k + \cdots + h_{Km}v_K \end{bmatrix} \tag{4.5}$$

where s_l is the superimposed received signal at l^{th} antenna. Hence, the receive composite signal r_l at the l^{th} antenna with the noise component is

$$r_l = \sum_{k=1}^{K} h_{kl}v_k + n_l = s_l + n_l\ ; \quad l = 1, \dots, m \tag{4.6}$$

For the given signal model, the following assumptions are considered:

1) Perfect power control and CSI are assumed at the BS.
2) The channel fading rate (Doppler spread) is assumed to be much less than the data rate. So, the channel remains constant over a frame of hundreds of symbols and changes from one frame to the next independently [29, 37, 144, 146].
3) Due to the use of MLJD at BS receiver, impact of user scheduling is not included and the active users are perfectly synchronized.
4) The total received power constrain of the considered system is $P = \sum_{k=1}^{K} P_k$.
5) The signal path loss from user k to any receive antenna m is identical to the others.
6) CRFC is generated using ICT [141, 142] with correlation matrix of envelopes $\boldsymbol{\rho} \in \mathcal{R}^{Km\times Km}$ whose entries represent the correlation factor ρ_{ij} between i^{th} and j^{th} fading envelope.

4.3.2 Maximum Likelihood Joint Detection (MLJD)

The nonlinear MLJD for the combined received signals is employed at BS receiver. It is optimal in the sense of minimizing the error probability by searching for the most likely transmitted signals. For CC-MU-MIMO system of K active users each equipped with single antenna and using $M_k,\ k = 1, \dots, K$ alphabet size of constellation, there are $D = \prod_{k=1}^{K} M_k$ possible signal vectors at MAC input as

$$\mathbf{v}^{(q)} = \left[v_1{}^{(q)} \ \cdots \ v_k{}^{(q)} \ \cdots \ v_K{}^{(q)} \right]^T ; \quad q = 1, \dots, D \tag{4.7}$$

where $v_k^{(q)}$ is the q^{th} possible transmitted symbol from user k and the total possible signals at the channel input during every symbol interval is $D_i = \sum_{k=1}^{K} M_k$. When all K users utilizes same alphabet size of constellation as $M_k = M,\ k = 1, \dots, K$ then, $D = M^K$ and $D_i = KM$.

From equations (4.5) and (4.7), we have

$$\mathbf{s}_q = \mathbf{H}\mathbf{v}^{(q)} = \left[s_1{}^{(q)} \ \cdots \ s_l{}^{(q)} \ \cdots \ s_m{}^{(q)} \right]^T ; \quad q = 1, \dots, D \tag{4.8}$$

where $s_l{}^{(q)}$ is the q^{th} possible superimposed received signal at l^{th} antenna. Therefore, there are D possible vectors $\{\mathbf{s}_1, \dots, \mathbf{s}_q, \dots, \mathbf{s}_D\} \in \mathbf{S}$ at the MAC input consisting of superimposed users' signals over their entire channels. Highest performance can be achieved if there is no identical elements in $\mathbf{S}$. Therefore, fading channel signatures plays the main role for signal separation as long as the correlation level is very low. For example, all possible vectors $\mathbf{S}$ of 2-user system using $M_1 = M_2 = 4$ of QPSK modulation ($Ae^{j\pi/4}, Ae^{j3\pi/4}, Ae^{j5\pi/4}$ and $Ae^{j7\pi/4}$) and $m = 2$ are shown in Table 4.1. In this example, $D = M^K = 4^2 = 16$ and $D_i = KM = 2 \times 4 = 8$.

Based on the minimum distance criterion, the vector of transmitted users' signals can be estimated as

$$\hat{\mathbf{v}} = \arg \min_{\mathbf{s}_q \in \boldsymbol{S}} \left\| \mathbf{r} - \mathbf{s}_q \right\|^2 ; \quad q = 1, \dots, D \tag{4.9}$$

where $\left\| \mathbf{r} - \mathbf{s}_q \right\|^2$ is the squared distance d_q^2 between received signal vector $\mathbf{r}$ and the possible transmitted signal vector $\mathbf{s}_q$. The estimated signal vector $\hat{\mathbf{v}} = [\hat{v}_1 \quad \cdots \quad \hat{v}_K]^T$ will be remapped then to users' data vector $\hat{\mathbf{b}} = [\hat{b}_1 \quad \cdots \quad \hat{b}_K]^T$.

Table 4.1: All possible composite signal vectors $\mathbf{s}_q \in \mathbf{S}$ at the MAC input of 2-user system ($K = 2$) employing QPSK modulation ($M_1 = M_2 = 4$) and $m = 2$

Signals at MAC input, ${v_k}^{(q)}$		Possible signal vectors at MAC input, $\mathbf{s}_q \in \mathbf{S}$
${v_1}^{(q)}$	${v_2}^{(q)}$	$\mathbf{s}_q = [{s_1}^{(q)} \quad {s_2}^{(q)}]^T \; ; \quad q = 1, \dots, 16$
$Ae^{j\pi/4}$	$Ae^{j\pi/4}$	$\mathbf{s}_1 = \left[A\left(h_{11}e^{j\pi/4} + h_{21}e^{j\pi/4}\right) \quad A\left(h_{12}e^{j\pi/4} + h_{22}e^{j\pi/4}\right)\right]^T$
$Ae^{j\pi/4}$	$Ae^{j3\pi/4}$	$\mathbf{s}_2 = \left[A\left(h_{11}e^{j\pi/4} + h_{21}e^{j3\pi/4}\right) \quad A\left(h_{12}e^{j\pi/4} + h_{22}e^{j3\pi/4}\right)\right]^T$
$Ae^{j\pi/4}$	$Ae^{j5\pi/4}$	$\mathbf{s}_3 = \left[A\left(h_{11}e^{j\pi/4} + h_{21}e^{j5\pi/4}\right) \quad A\left(h_{12}e^{j\pi/4} + h_{22}e^{j5\pi/4}\right)\right]^T$
$Ae^{j\pi/4}$	$Ae^{j7\pi/4}$	$\mathbf{s}_4 = \left[A\left(h_{11}e^{j\pi/4} + h_{21}e^{j7\pi/4}\right) \quad A\left(h_{12}e^{j\pi/4} + h_{22}e^{j7\pi/4}\right)\right]^T$
$Ae^{j3\pi/4}$	$Ae^{j\pi/4}$	$\mathbf{s}_5 = \left[A\left(h_{11}e^{j3\pi/4} + h_{21}e^{j\pi/4}\right) \quad A\left(h_{12}e^{j3\pi/4} + h_{22}e^{j\pi/4}\right)\right]^T$
$Ae^{j3\pi/4}$	$Ae^{j3\pi/4}$	$\mathbf{s}_6 = \left[A\left(h_{11}e^{j3\pi/4} + h_{21}e^{j3\pi/4}\right) \quad A\left(h_{12}e^{j3\pi/4} + h_{22}e^{j3\pi/4}\right)\right]^T$
$Ae^{j3\pi/4}$	$Ae^{j5\pi/4}$	$\mathbf{s}_7 = \left[A\left(h_{11}e^{j3\pi/4} + h_{21}e^{j5\pi/4}\right) \quad A\left(h_{12}e^{j3\pi/4} + h_{22}e^{j5\pi/4}\right)\right]^T$
$Ae^{j3\pi/4}$	$Ae^{j7\pi/4}$	$\mathbf{s}_8 = \left[A\left(h_{11}e^{j3\pi/4} + h_{21}e^{j7\pi/4}\right) \quad A\left(h_{12}e^{j3\pi/4} + h_{22}e^{j7\pi/4}\right)\right]^T$
$Ae^{j5\pi/4}$	$Ae^{j\pi/4}$	$\mathbf{s}_9 = \left[A\left(h_{11}e^{j5\pi/4} + h_{21}e^{j\pi/4}\right) \quad A\left(h_{12}e^{j5\pi/4} + h_{22}e^{j\pi/4}\right)\right]^T$
$Ae^{j5\pi/4}$	$Ae^{j3\pi/4}$	$\mathbf{s}_{10} = \left[A\left(h_{11}e^{j5\pi/4} + h_{21}e^{j3\pi/4}\right) \quad A\left(h_{12}e^{j5\pi/4} + h_{22}e^{j3\pi/4}\right)\right]^T$
$Ae^{j5\pi/4}$	$Ae^{j5\pi/4}$	$\mathbf{s}_{11} = \left[A\left(h_{11}e^{j5\pi/4} + h_{21}e^{j5\pi/4}\right) \quad A\left(h_{12}e^{j5\pi/4} + h_{22}e^{j5\pi/4}\right)\right]^T$
$Ae^{j5\pi/4}$	$Ae^{j7\pi/4}$	$\mathbf{s}_{12} = \left[A\left(h_{11}e^{j5\pi/4} + h_{21}e^{j7\pi/4}\right) \quad A\left(h_{12}e^{j5\pi/4} + h_{22}e^{j7\pi/4}\right)\right]^T$
$Ae^{j7\pi/4}$	$Ae^{j\pi/4}$	$\mathbf{s}_{13} = \left[A\left(h_{11}e^{j7\pi/4} + h_{21}e^{j\pi/4}\right) \quad A\left(h_{12}e^{j7\pi/4} + h_{22}e^{j\pi/4}\right)\right]^T$
$Ae^{j7\pi/4}$	$Ae^{j3\pi/4}$	$\mathbf{s}_{14} = \left[A\left(h_{11}e^{j7\pi/4} + h_{21}e^{j3\pi/4}\right) \quad A\left(h_{12}e^{j7\pi/4} + h_{22}e^{j3\pi/4}\right)\right]^T$
$Ae^{j7\pi/4}$	$Ae^{j5\pi/4}$	$\mathbf{s}_{15} = \left[A\left(h_{11}e^{j7\pi/4} + h_{21}e^{j5\pi/4}\right) \quad A\left(h_{12}e^{j7\pi/4} + h_{22}e^{j5\pi/4}\right)\right]^T$
$Ae^{j7\pi/4}$	$Ae^{j7\pi/4}$	$\mathbf{s}_{16} = \left[A\left(h_{11}e^{j7\pi/4} + h_{21}e^{j7\pi/4}\right) \quad A\left(h_{12}e^{j7\pi/4} + h_{22}e^{j7\pi/4}\right)\right]^T$

4.4 Signal Design for CC-MU-MIMO

Taking the advantage of accurate power control and CSI at BS receiver, UPA and RC signal design methods are proposed in this section for CC-MU-MIMO scheme to mitigate the channel correlation effects. We briefly describe the design and selection of user constellation points having $d_{min\,0}$ to maximize d_{min} of the resulting unique composite points. In such methods, the constrained constellation of transmitted signals will have the effects to resolve the detection ambiguity at the receiver arisen due to high channel dependence (correlation). As a result, channel capacity and BER performance will be maximized irrespective of correlation level ρ. To simplify the analysis and without loss of generality, we consider the composite constellation of $s_l = \sum_{k=1}^{K} h_{kl} v_k$ at l^{th} antenna only assuming that $h_{kl} = 1;\ k = 1, \dots, K$ (i.e. $\alpha_{kl} = 1$ and $\beta_{kl} = 0$). In other words, we assume full channel correlation and the task is to rearrange the composite signal constellation. For comparison purpose, the basic IC design of conventional MU-MIMO system is introduced first.

4.4.1 Identical Constellation (IC)

In this case, IC for all users are used with equal power allocation (EPA) such that the received signals have equal power $P_k = p;\ k = 1, \dots, K$. The possible received symbol s_l will have ambiguity reducing the number of possible received signals D to an actual number of D_{act}. For example, in case of 2-user employing IC-BPSK of $v_k = \mp\sqrt{P_k} = \mp 1$ as a modulation levels, the possible composite received symbol is $s_l = \{+2,\ 0,\ -2\}$. So, there are $D_{act} = 3$ instead of $D = 4$ since the "0" composite symbol can be generated from two different cases ($v_1 = +1,\ v_2 = -1$ or $v_1 = -1,\ v_2 = +1$) as shown in Fig. 4.2.

To give an idea about the composite constellation in case of signal ambiguity ($D_{act} \neq D$), squared average distance (d_{av}^2) is used as a unit metric and given by

$$d_{av}^2 = d_{min}^2 \frac{D_{act}}{D} \tag{4.10}$$

In addition, energy loss factor (γ) in dB represents how much energy needed to achieve the single user performance and can be calculated as

$$\gamma = 10\ log_{10}\left(\frac{d_{min\,0}^2}{d_{av}^2}\right) \tag{4.11}$$

In Table 4.2, some important results are summarized for K-user system employing IC-BPSK. For example, there are $D_{act} = 7$ instead of $D = 64$ for $K = 6$. For this case, cost of $\gamma = 9.68$ dB should be spend to overcome high ambiguity in signal separation. The channel difference may resolve this inherent problem by increasing d_{min} of each received symbol to achieve $D_{act} = D$. However, channels correlation has the opposite function by increasing the linear dependence of transmitted signals causing significant degradation in capacity and system performance. Therefore, the following methods are proposed to reduce the correlation impact by increasing d_{min} of composite signals at the receive side.

Table 4.2: Summary results for K-user system employing IC-BPSK where $M = 2$ and $d_{min\,0}^2 = 4$

K	D_i	D	D_{act}	s_l	d_{min}^2	d_{av}^2	γ
2	4	4	3	-2, 0, +2	4	3	1.24
3	6	8	4	-3, -1, +1, +3	4	2	3.0
4	8	16	5	-4, -2, 0, +2, +4	4	1.25	5.0
5	10	32	6	-5, -3, -1, +1, +3, +5	4	0.75	7.26
6	12	64	7	-6, -4, -2, 0, +2, +4, +6	4	0.43	9.68

4.4.2 Unequal Power Allocation (UPA)

By taking the possibility of accurate power control at BS and according to the path loss advantage inherent in cellular systems due to spatial difference among users, UPA is used for the active users such that the received symbols are maximally separated. Therefore, powers are distributed among users by allocating a fraction η_k of the total power P to user k as

$$P_k = \eta_k P\,; \quad k = 1, \dots, K \tag{4.12}$$

where η_k is power allocation ratio subject to

$$\sum_{k=1}^{K} \eta_k = 1\,; \quad 0 \le \eta_k \le 1 \tag{4.13}$$

For example, the optimal power allocation ratios for 2-user system that maximizes d_{min} of the composite received symbols are found *analytically* as $\eta_1 = 0.8$ and $\eta_2 = 0.2$. These values are valid for any modulation type with any number of levels and will be used throughout this chapter whenever UPA mentioned if not others stated. For UPA-BPSK with $P = 2$ and user 2 has less path loss compared to user 1 (i.e. user 2 is closer to BS than user 1), the optimal assigned powers will be $P_1 = \eta_1 P = 1.6$ and $P_2 = \eta_2 P = 0.4$. Therefore, the transmitted symbols will be $v_1 = \mp\sqrt{P_1} = \mp 1.264$ and $v_2 = \mp\sqrt{P_2} = \mp 0.632$. All possible composite received symbol will be $s_l = \{+1.896,\ +0.632,\ -0.632,\ -1.896\}$ as shown in Fig. 4.3. As can be seen, there are $D_{act} = D = 4$ composite symbols having $d_{min} = 1.264$ which is expected to improve the system immunity against the correlation effects.

4.4.3 Rotated Constellation (RC)

In this method, RC is employed for the active users by taking the possibility of accurate phase control with EPA ($P_k = p;\ k = 1, \dots, K$) at BS. To maximize d_{min} of the composite received signal, a suitable phase difference ξ_k between k^{th} user constellation and reference user constellation must be selected taking into account their channel phases. For CC-MU-MIMO system of $m \geq 2$ with highest SNR at l^{th} antenna, $\xi_k, k = 1, \dots, K$ is calculated according to channel phase β_{kl}. Therefore, procedure of K user system starts with fixing constellation of user 1 as a reference followed by rotating the others based on d_{min} maximization according to channel phases related to the receive antenna with highest SNR as

$$v_k \, e^{j\xi_k} \; ; \quad k = 2, \ldots, K \tag{4.14}$$

For example, the transmitted symbols of 2-user RC-BPSK are given for optimal phase angle rotation $\xi_2 = \pi/2$ and $P_1 = P_2 = 1$ as

$$\begin{aligned} v_1 &= \mp\sqrt{P_1} = \mp 1 \\ v_2 &= \mp\sqrt{P_2} e^{j\xi_2} = \mp j \end{aligned} \tag{4.15}$$

As a result, all possible composite received symbol will be $s_l = \{+1 + j, \; +1 - j, \; -1 + j, \; -1 - j\}$ as shown in Fig.4.4. As can be seen, there are $D_{act} = D = 4$ composite symbols having $d_{min} = d_{min\,0} = 2$ which is better than UPA method at cost of extra overhead represented by the phase control at BS receiver.

To clarify the concept of proposed signal design methods, Fig. 4.5–4.14 show the transmitted and received signal constellations of 2-user system using different modulations (QPSK, 8PSK, 4PAM, 8PAM, and 8QAM). It is obvious that maximizing d_{min} is achieved through rearrangement of users' constellations. In Table 4.3, some important results of the investigated system configurations are summarized.

Table 4.3: Summary results for 2-user system utilizing different modulations

Modulation	M	$d^2_{min\,0}$	Constellation	D_i	D	D_{act}	d^2_{min}	d^2_{av}	γ
BPSK	2	4	IC	4	4	3	4	3	1.24
BPSK	2	4	RC (π /2)	4	4	4	4	4	0.0
BPSK	2	4	UPA	4	4	4	1.6	1.6	0.0
QPSK	4	2	IC	8	16	9	2	1.125	2.5
QPSK	4	2	RC (π /6)	8	16	16	0.53	0.53	5.7
QPSK	4	2	UPA	8	16	16	0.8	0.8	0.0
8PSK	8	0.57	IC	16	64	33	0.34	0.175	5.1
8PSK	8	0.57	RC (π /11)	16	64	64	0.04	0.04	11.5
8PSK	8	0.57	UPA	16	64	64	0.044	0.044	7.2
8QAM	8	0.66	IC	16	64	25	0.66	0.257	4.1
8QAM	8	0.66	RC (π /4)	16	64	64	0.066	0.066	10.0
8QAM	8	0.66	UPA	16	64	40	0.26	0.162	2.0
8QAM	8	0.66	RC (π /4) & UPA	16	64	64	0.09	0.09	4.6
4PAM	4	0.8	RC (π /2)	8	16	16	0.8	0.8	0.0
8PAM	8	0.19	RC (π /2)	16	64	64	0.19	0.19	0.0

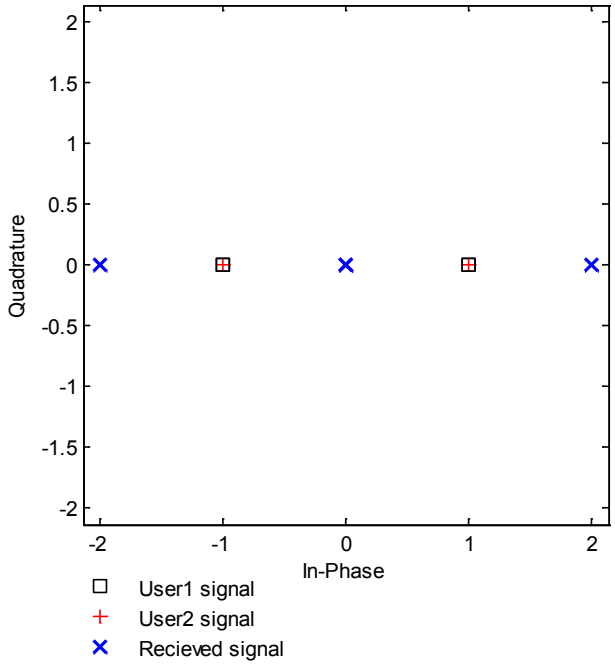

Figure 4.2: Signal constellation of 2-user IC-BPSK ($P_1 = P_2 = 1,\ P = 2$) with the received signals.

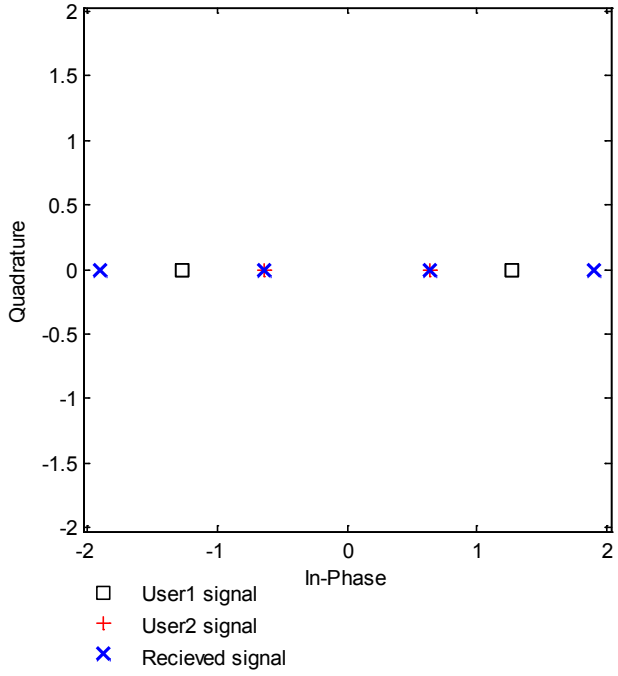

Figure 4.3: Signal constellation of 2-user UPA-BPSK ($\eta_1 = 0.8,\ \eta_2 = 0.2,\ P = 2$) with the received signals.

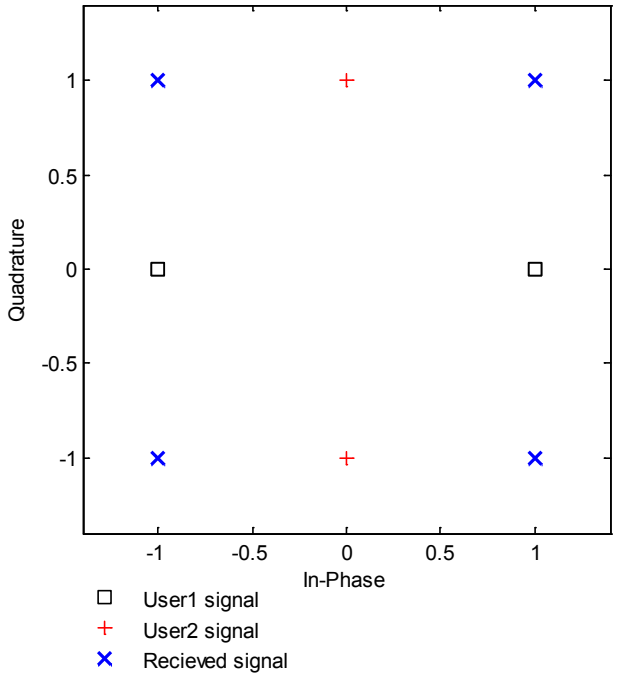

Figure 4.4: Signal constellation of 2-user RC-BPSK ($\xi_2 = \pi/2$) with the received signals where $P_1 = P_2 = 1$ and $P = 2$.

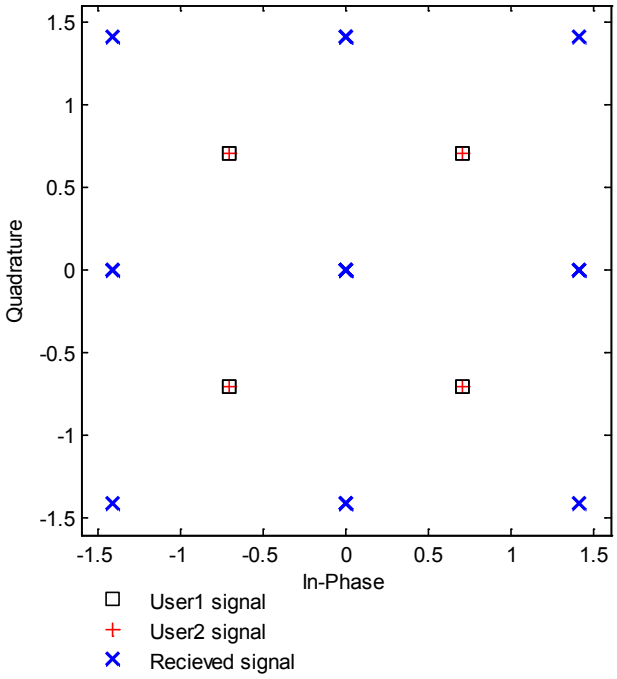

Figure 4.5: Signal constellation of 2-user IC-QPSK ($P_1 = P_2 = 1,\ P = 2$) with the received signals.

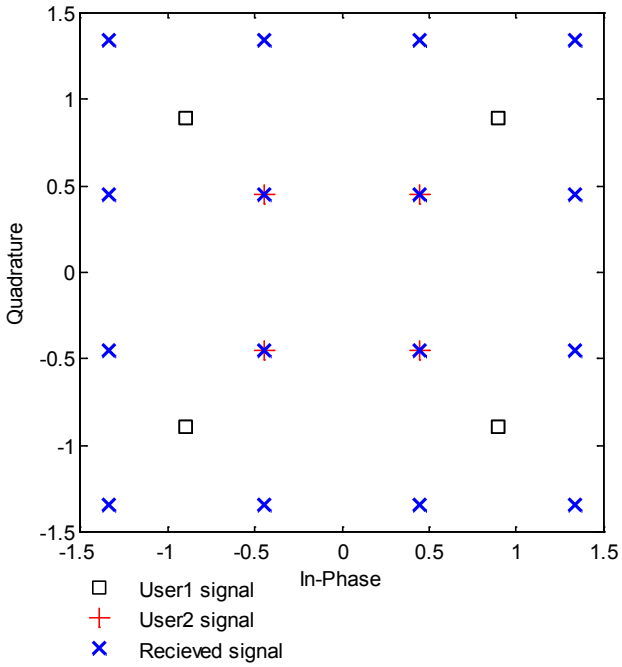

Figure 4.6: Signal constellation of 2-user UPA-QPSK ($\eta_1 = 0.8,\ \eta_2 = 0.2,\ P = 2$) with the received signals.

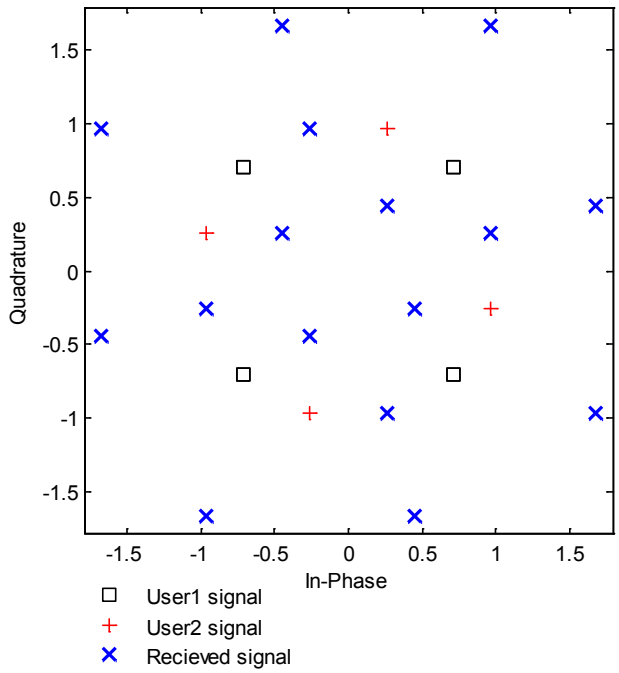

Figure 4.7: Signal constellation of 2-user RC-QPSK ($\xi_2 = \pi/6$) with the received signals where $P_1 = P_2 = 1$ and $P = 2$.

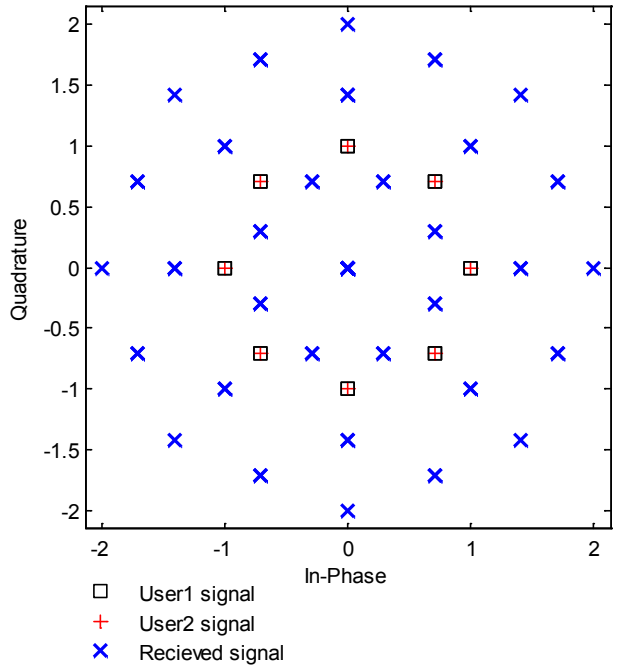

Figure 4.8: Signal constellation of 2-user IC-8PSK ($P_1 = P_2 = 1,\ P = 2$) with the received signals.

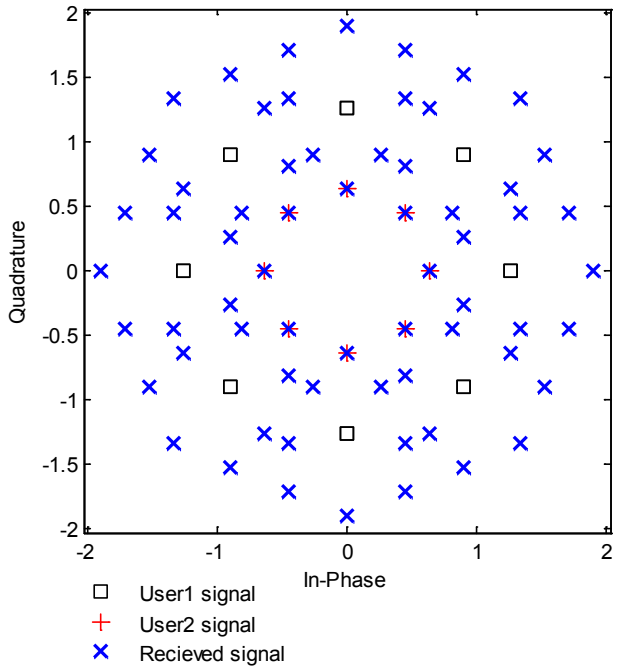

Figure 4.9: Signal constellation of 2-user UPA-8PSK ($\eta_1 = 0.8,\ \eta_2 = 0.2,\ P = 2$) with the received signals.

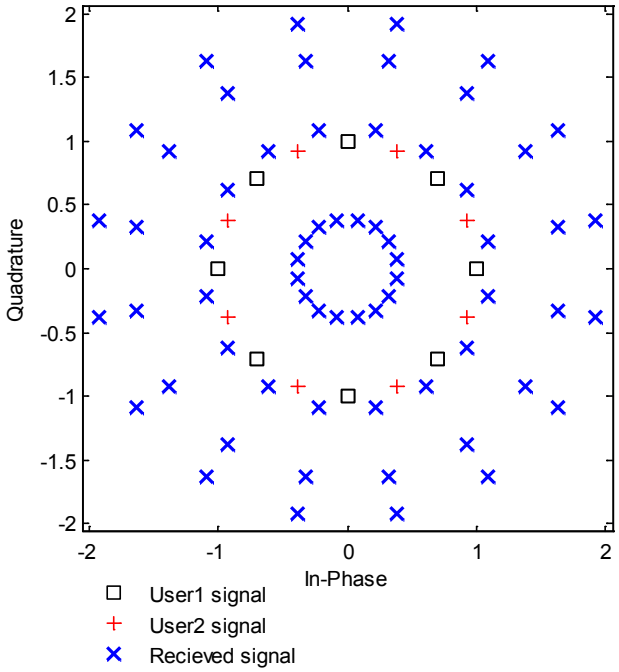

Figure 4.10: Signal constellation of 2-user RC-8PSK ($\xi_2 = \pi/11$) with the received signals where $P_1 = P_2 = 1$ and $P = 2$.

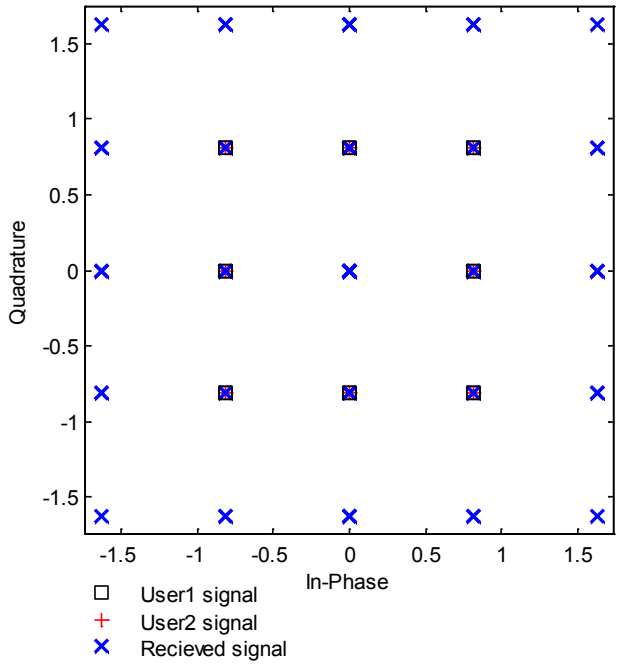

Figure 4.11: Signal constellation of 2-user IC-8QAM ($P_1 = P_2 = 1,\ P = 2$) with the received signals.

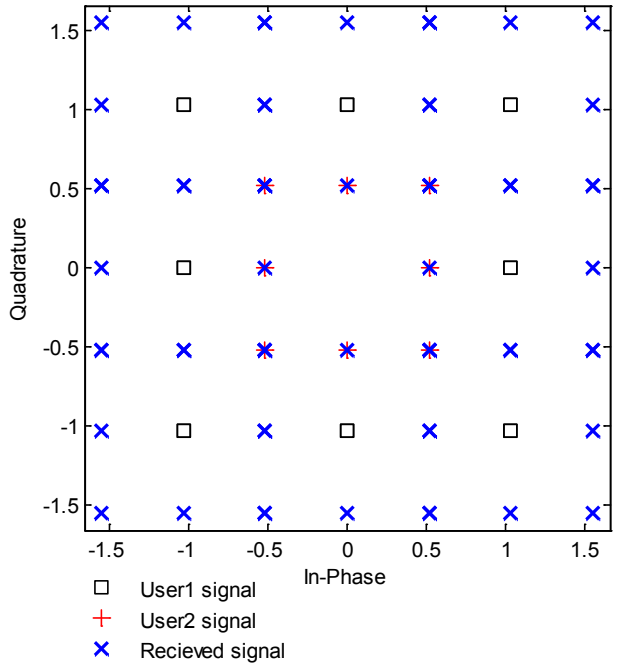

Figure 4.12: Signal constellation of 2-user UPA-8QAM ($\eta_1 = 0.8,\ \eta_2 = 0.2,\ P = 2$) with the received signals.

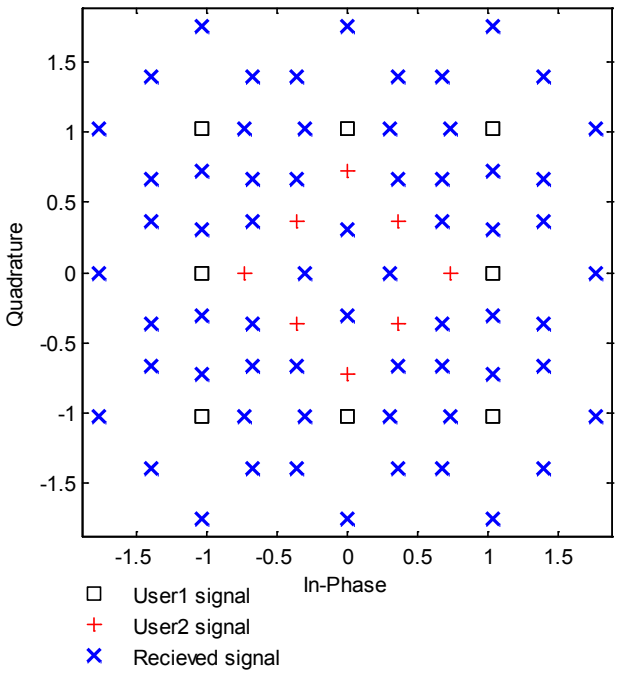

Figure 4.13: Signal constellation of 2-user RC-8QAM ($\xi_2 = \pi/4$) with the received signals where $P_1 = P_2 = 1$ and $P = 2$.

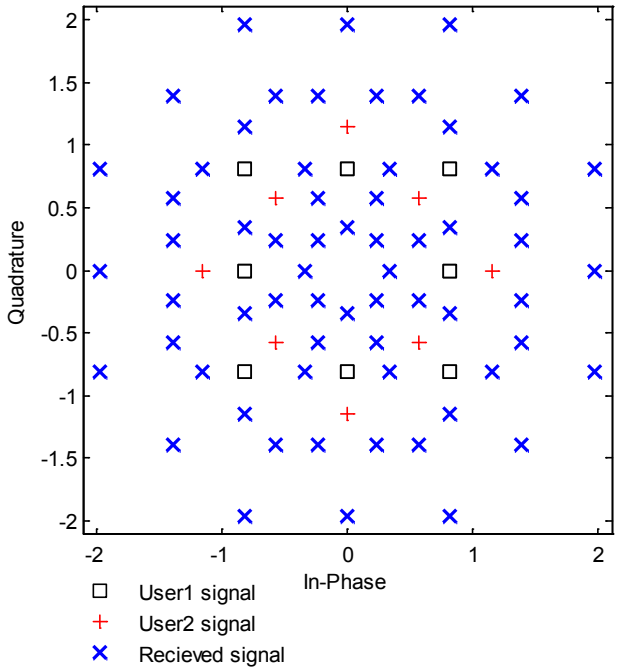

Figure 4.14: Signal constellation of 2-user UPA-RC-8QAM ($\xi_2 = \pi/4$, $P_1 = P_2 = 1$, $P = 2$) with the received signals.

4.5 Channel Capacity Analysis of CC-MU-MIMO

4.5.1 Sum Rate Capacity

Based on the ergodic sum rate capacity of UL Rayleigh fading MU-MIMO channel given in [24, 99], the sum rate capacity for CC-MU-MIMO signal model (4.1) in bit/s/Hz can be written as

$$R_{sum} = \mathrm{E}\left[\log_2\left|\mathbf{I}_m + \frac{1}{\sigma_n^2}\left(\sum_{k=1}^{K}\mathbf{h}_k P_k \mathbf{h}_k^{\mathrm{H}}\right)\right|\right] \tag{4.16}$$

For EPA with $P_k = p = P/K\,;\ k = 1, \ldots, K$, this capacity can be written as

$$R_{sum} = \mathrm{E}\left[\log_2\left|\mathbf{I}_m + \frac{P}{K\sigma_n^2}\left(\sum_{k=1}^{K}\mathbf{h}_k \mathbf{h}_k^{\mathrm{H}}\right)\right|\right] = \mathrm{E}\left[\log_2\left|\mathbf{I}_m + \frac{\Gamma}{K}\mathbf{H}\mathbf{H}^{\mathrm{H}}\right|\right] \tag{4.17}$$

where $\Gamma = P/\sigma_n^2$ is the average SNR.

Since all user equipments are equipped with single antenna, the sum rate capacity of CC-MU-MIMO system grows linearly with $\min[K, m]$. Therefore, any increase of receive antennas m at the BS will lead to linear growth in capacity

4.5.2 Constellation Constrained Capacity

Generally, for the channel model (4.1), any point on the ergodic sum rate capacity curves can be achieved using signal constellation with Gaussian distribution at the MAC input [143, 145, 155, 156]. However, maximum achievable throughput by any practical communication system employing independent and equally likely M modulation levels can be found by calculating the mutual information between transmitted signal vector $\mathbf{v}$ and received signal vector $\mathbf{r}$. It is known as constellation constrained capacity [157] and given in bit/s/Hz by

$$R_c = \mathcal{H}(\mathbf{r}) - \mathcal{H}(\mathbf{r}|\mathbf{v}) = \mathcal{H}(\mathbf{v}) - \mathcal{H}(\mathbf{v}|\mathbf{r}) \tag{4.18}$$

where $\mathcal{H}(x) = -\mathrm{E}[\log_2(x)]$ denotes the entropy function. For CC-MU-MIMO system of K users (transmit antennas) and m receive antennas, we have

$$\mathcal{H}(\mathbf{r}|\mathbf{v}) = m \log_2(\pi e/\Gamma) \tag{4.19}$$

Assuming that all users utilizes same alphabet size of constellation as $M_k = M,\ k = 1, \ldots, K$, the expectation in $\mathcal{H}(\mathbf{r})$ over the sources of randomness $\mathbf{H}, \mathbf{v}$ and $\mathbf{n}$ can be numerically approximated using Monte-Carlo method as

$$\mathcal{H}(\mathbf{r}) = -\mathrm{E}\left[\log_2\left(\frac{\Gamma^m}{D\pi^m}\sum_{q=1}^{D} e^{\left(-\Gamma\|\mathbf{r}-\mathbf{s}_q\|^2\right)}\right)\right] \tag{4.20}$$

where the summation runs over all $D = M^K$ possible signal vectors $\{\mathbf{s}_1, \ldots, \mathbf{s}_q, \ldots, \mathbf{s}_D\} \in \mathbf{S}$. After some mathematical manipulations, R_c can be simplified as

$$R_c = \log_2(D) - \mathrm{E}\left[\log_2\left(e^m \sum_{q=1}^{D} e^{\left(-\Gamma\|\mathbf{r}-\mathbf{s}_q\|^2\right)}\right)\right] \tag{4.21}$$

where the first term can be identified as the entropy $\mathcal{H}(\mathbf{v})$ or the transmitted bits while the second term may represent the loss of information $\mathcal{H}(\mathbf{v}|\mathbf{r})$ due to different transmission schemes.

Ungerboeck's formula of the constellation constrained capacity [155] can be modified as a second method to calculate R_c for CC-MU-MIMO scheme. It can be written for discrete input over the entire channels represented by $\{\mathbf{s}_1, \dots, \mathbf{s}_q, \dots, \mathbf{s}_D\} \in \mathbf{S}$ and continuos output as

$$R_c = \max_{\Pr(\mathbf{s}_1)\dots\Pr(\mathbf{s}_D)} \sum_{q=1}^{D} \Pr(\mathbf{s}_q) \int_{-\infty}^{+\infty} p(\mathbf{r}|\mathbf{s}_q) \log_2 \left[\frac{p(\mathbf{r}|\mathbf{s}_q)}{\sum_{i=1}^{D} \Pr(\mathbf{s}_i)\, p(\mathbf{r}|\mathbf{s}_i)} \right] dr \qquad (4.22)$$

where $\Pr(q)$ is the probability associated with $\mathbf{s}_q$ and $p(\mathbf{r}|\mathbf{s}_q)$ is the conditional probability of received composite symbol given for two dimensional modulation by

$$p(\mathbf{r}|\mathbf{s}_q) = \frac{1}{2\pi\sigma_n^2}\ e^{-\left(\frac{\|\mathbf{r}-\mathbf{s}_q\|^2}{2\,\sigma_n^2}\right)} \qquad (4.23)$$

By assuming equiprobable occurrence of $\mathbf{S}$ elements such that $\Pr(\mathbf{s}_q) = 1/D$, the capacity R_c in bit/s/Hz can be simplified to

$$R_c = \log_2(D) - \frac{1}{D} \sum_{q=1}^{D} \mathrm{E}\left[\log_2 \sum_{i=1}^{D} \exp\left(- \frac{\|\mathbf{s}_q + \mathbf{n} - \mathbf{s}_i\|^2 - \|\mathbf{n}\|^2}{2\,\sigma_n^2} \right) \right] \qquad (4.24)$$

This capacity can be calculated as a function of average SNR represented by $\Gamma = P/\sigma_n^2$.

4.6 Simulation Results

Monte Carlo simulations using MATLAB/7.9 have been carried out in this section to demonstrate and validate the overall performance of $K \times m$ CC-MU-MIMO system using IC, UPA, and RC over CRFC. The first subsection includes the capacity results averaged over 10,000 channel realization. The second subsection demonstrates the results of BER performance considering a frame of 100 symbols from MPSK constellation for each channel realization. In this assumption, the channel still constant over the entire frame length and changes independently from frame to the next. To demonstrate the effects of channel correlation, we consider without loss of generality equal correlation among different fading paths as $\rho_{ij} = \rho\ ;\ \forall i \neq j;\ i,j = 1, \dots, Km$.

Firstly, consider 2×2 CC-MU-MIMO system utilizing QPSK signalling to show the impact of correlation and signal design on the constellation at the receive side and hence, the signal detection. For this purpose, two extreme cases are considered as $\rho = 0.0$ for uncorrelated channels and $\rho = 0.9$ for high correlation.

In Fig. 4.15, constellation points (v_1, v_2) of IC-QPSK ($P_1 = P_2 = 1, P = 2$) is shown with the possible composite received signal s_1 at BS antenna 1 over uncorrelated channel realization of $h_{11} = 0.96 + j0.12$ and $h_{21} = -0.34 + j0.52$. As can be seen, the fading signatures have direct impact to resolve signal ambiguity from 9 to 16 points (see Fig.4.5 for comparison) which enables efficient signal detection. However, fading correlation has the opposite effect as shown in Fig. 4.16 for channel realization of $h_{11} = 0.96 + j0.12$ and $h_{21} = -0.91 - j0.11$ with $\rho = 0.9$. In this case, the recognized signals are 9 which cause severe degradation in spectral efficiency. This problem can be solved efficiently by utilizing the proposed signal design methods.

Results of UPA-QPSK ($\eta_1 = 0.8,\ \eta_2 = 0.2,\ P = 2$) and RC-QPSK ($\xi_2 = \pi/6, P_1 = P_2 = 1,\ P = 2$) are shown in Fig. 4.17 and Fig. 4.18, respectively. As can be see, better constellation is achieved with 16 points and higher d_{min}.

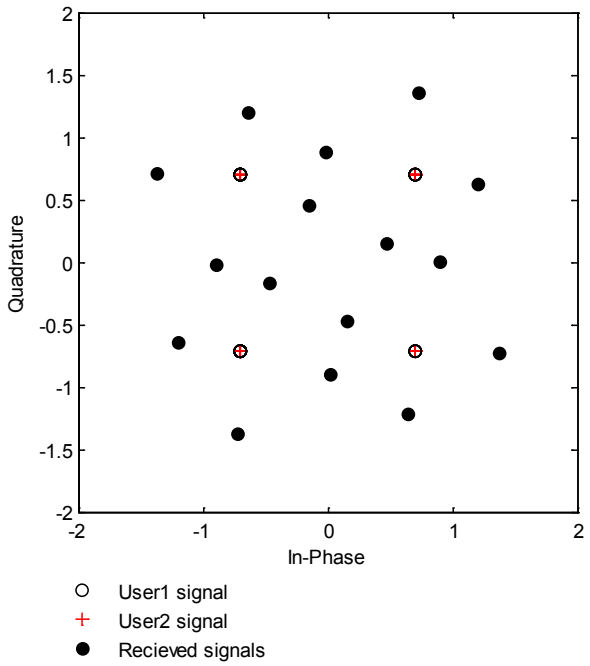

Figure 4.15: Signal constellation points (v_1, v_2) of IC-QPSK ($P_1 = P_2 = 1,\ P = 2$) with the possible composite received signal s_1 over uncorrelated channel realization of $h_{11} = 0.96 + j0.12$ and $h_{21} = -0.34 + j0.52$.

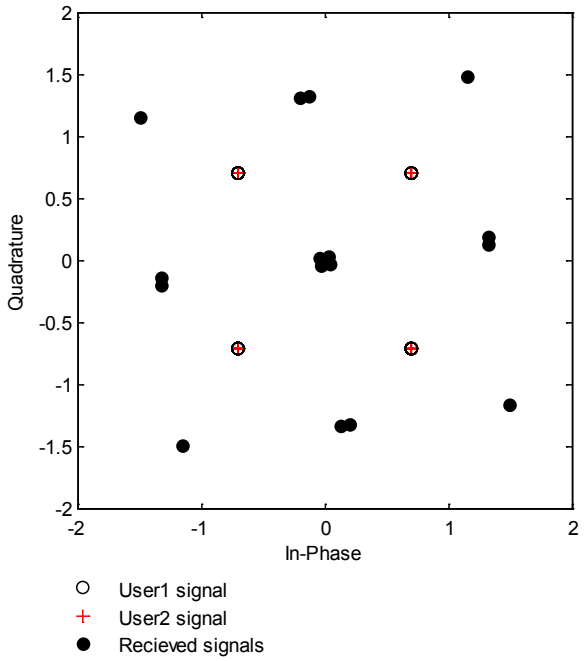

Figure 4.16: Signal constellation points (v_1, v_2) of IC-QPSK ($P_1 = P_2 = 1$, $P = 2$) with the possible composite received signal s_l over correlated channel realization ($\rho = 0.9$) of $h_{11} = 0.96 + j0.12$ and $h_{21} = -0.91 - j0.11$.

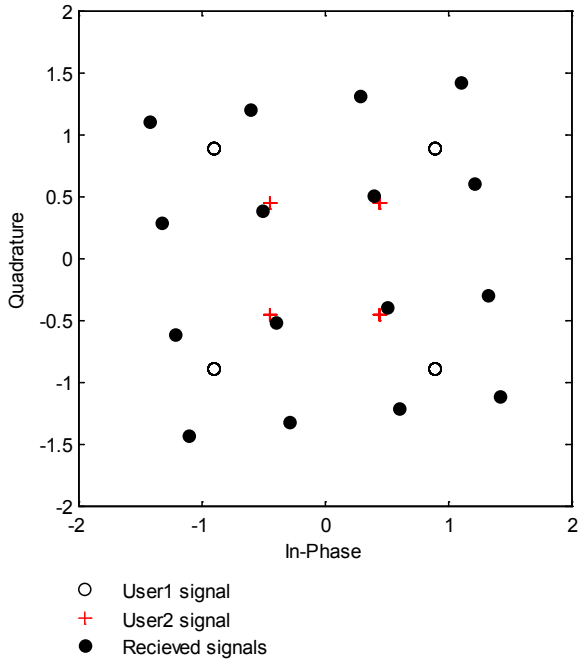

Figure 4.17: Signal constellation points (v_1, v_2) of UPA-QPSK ($\eta_1 = 0.8$, $\eta_2 = 0.2$, $P = 2$) with the possible composite received signal s_l over correlated channel realization ($\rho = 0.9$) of $h_{11} = 0.96 + j0.12$ and $h_{21} = -0.91 - j0.11$.

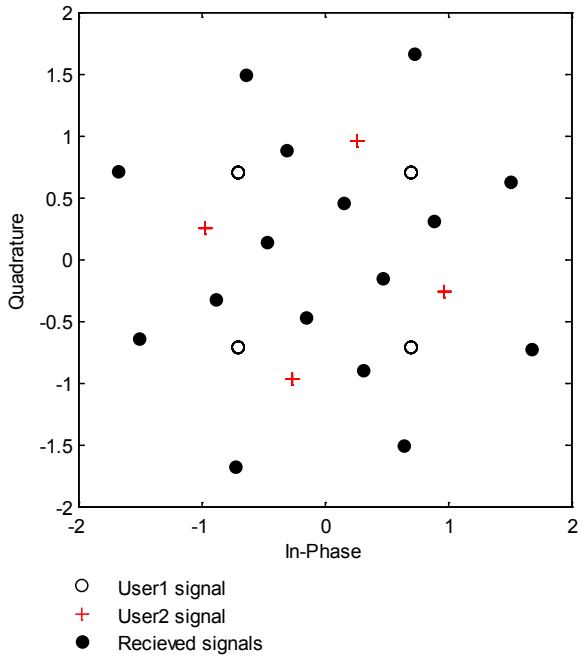

Figure 4.18: Signal constellation points (v_1, v_2) of RC-QPSK ($\xi_2 = \pi/6, P_1 = P_2 = 1, P = 2$) with the possible composite received signal s_l over correlated channel realization ($\rho = 0.9$) of $h_{11} = 0.96 + j0.12$ and $h_{21} = -0.91 - j0.11$.

4.6.1 Channel Capacity

To evaluate the channel capacity of $K \times m$ CC-MU-MIMO system and to show the effectiveness of proposed signal design methods, we consider without loss of generality QPSK signalling and three different cases of channel correlation; $\rho = 0.0$ for uncorrelated channels, $\rho = 0.5$ for moderate correlation, and $\rho = 0.9$ for high correlation. Constellation constrained capacity (maximum achievable throughput) with the ergodic sum rate limit are demonstrated for four system configurations; 2×2, 2×4, 4×4, and 4×2.

Results of 2×2 scheme employing IC-QPSK ($P_1 = P_2 = 1,\ P = 2$), UPA-QPSK ($\eta_1 = 0.8,\ \eta_2 = 0.2,\ P = 2$), and RC-QPSK ($\xi_2 = \pi/6, P_1 = P_2 = 1,\ P = 2$) are shown in Fig. 4.19. It can be seen clearly that constrained capacity of IC, UPA, and RC signalling methods are similar for uncorrelated channel environment. However, as ρ increased, capacity of IC decreases significantly while UPA and RC methods provides stable performance irrespective of ρ values. For example, gain of 6dB in SNR is achieved using UPA or RC compared with IC at maximum capacity of $\log_2(4^2) = 4$ bit/s/Hz when $\rho = 0.9$. At same correlation level and maximum capacity, the achievable gain is increased to 8dB for 2×4 system as shown in Fig. 4.20. In this case, the diversity order is $L = 4$ due to employing 4 receive antennas compared with $L = 2$ for 2×2 scheme.

In Fig. 4.21, results of 4×4 scheme employing IC-QPSK ($P_1 = \cdots = P_4 = 1,\ P = 4$), UPA-QPSK ($\eta_1 = 0.04,\ \eta_2 = \eta_3 = 0.16,\ \eta_4 = 0.64,\ P = 4$), and RC-QPSK ($\xi_2 = \pi/3,\ \xi_3 = \pi/6,\ \xi_4 = \pi/12, P_1 = \cdots = P_4 = 1,\ P = 4$) are depicted. As in the previous system configuration, the constrained capacity of IC, UPA, and RC signalling methods are identical when $\rho = 0.0$. However, the system with IC design suffers from serious capacity degradation as the correlation increased. For example, when $\rho = 0.9$, UPA and RC methods provide 8dB gain in SNR compared with IC at maximum capacity of $\log_2(4^4) = 8$ bit/s/Hz. At same correlation level and maximum capacity, the achievable gain is reduced to 6dB for 4×2 system as shown in Fig. 4.22. In this case, the diversity order is reduced to $L = 2$ compared with $L = 4$ for 4×4 scheme.

From the presented results, CC-MU-MIMO with UPA and RC signal design methods enables robust capacity performance over different channel correlation levels compared with conventional MU-MIMO systems with IC signalling. Furthermore, the achievable gain is increased as the diversity order L increased by utilizing more receive antennas at BS. In this case, more vector elements of **S** can be resolved without ambiguity leading to capacity maximization.

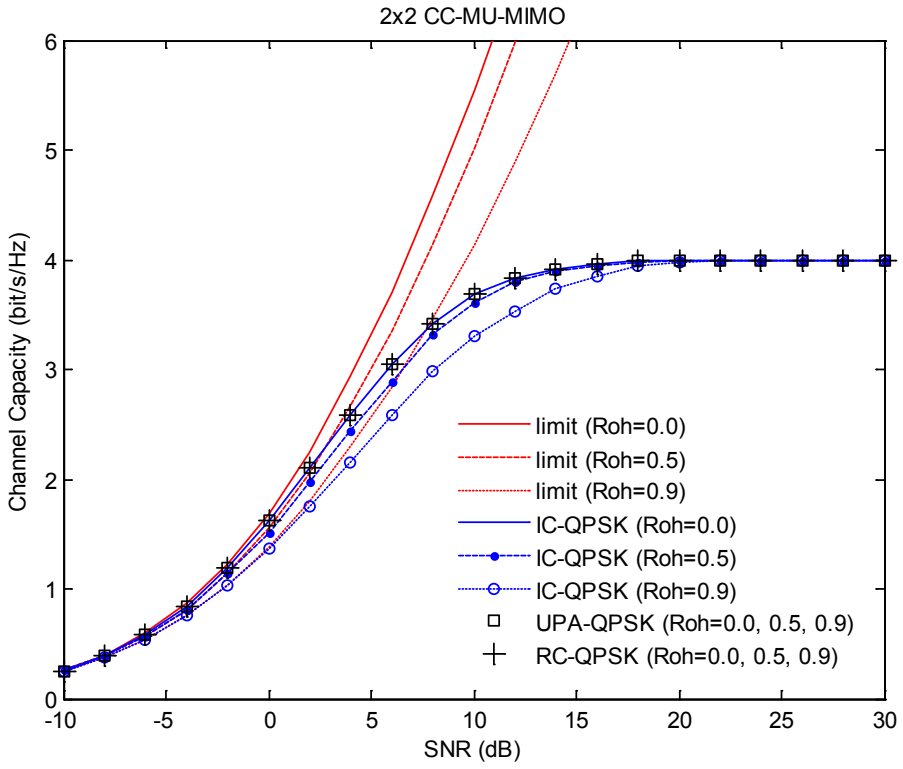

Figure 4.19: Capacity of 2×2 CC-MU-MIMO system over correlated channel with $\rho = 0.0, 0.5,$ and 0.9 for: IC-QPSK ($P_1 = P_2 = 1,\ P = 2$), UPA-QPSK ($\eta_1 = 0.8,\ \eta_2 = 0.2,\ P = 2$), and RC-QPSK ($\xi_2 = \pi/6, P_1 = P_2 = 1, P = 2$).

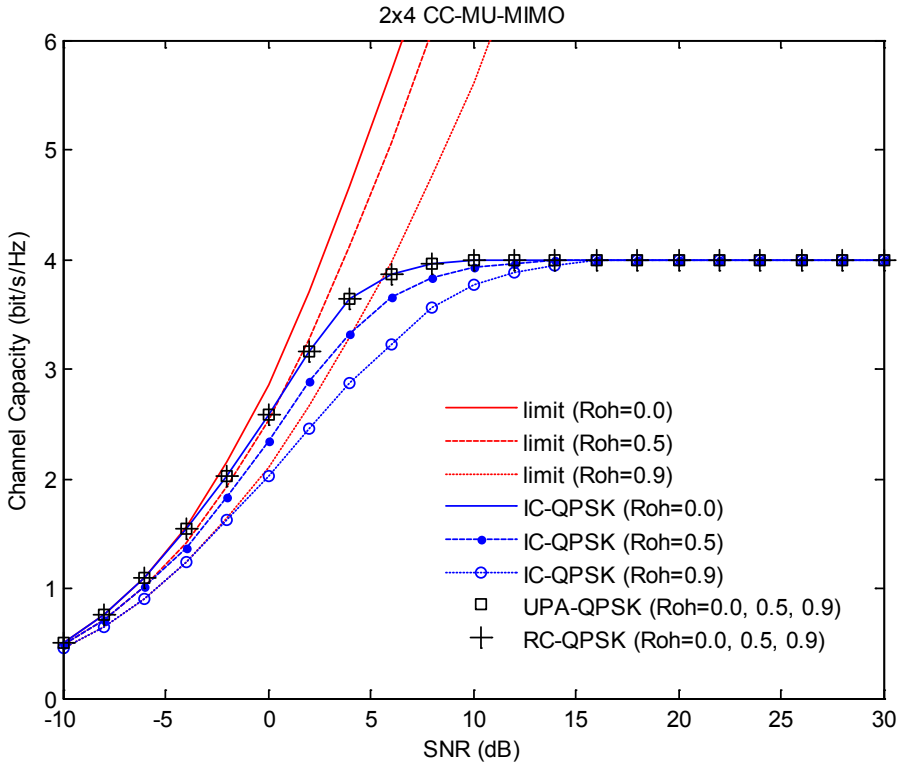

Figure 4.20: Capacity of 2×4 CC-MU-MIMO system over correlated channel with $\rho = 0.0, 0.5,$ and 0.9 for: IC-QPSK $(P_1 = P_2 = 1,\ P = 2)$, UPA-QPSK $(\eta_1 = 0.8,\ \eta_2 = 0.2,\ P = 2)$, and RC-QPSK $(\xi_2 = \pi/6, P_1 = P_2 = 1, P = 2)$.

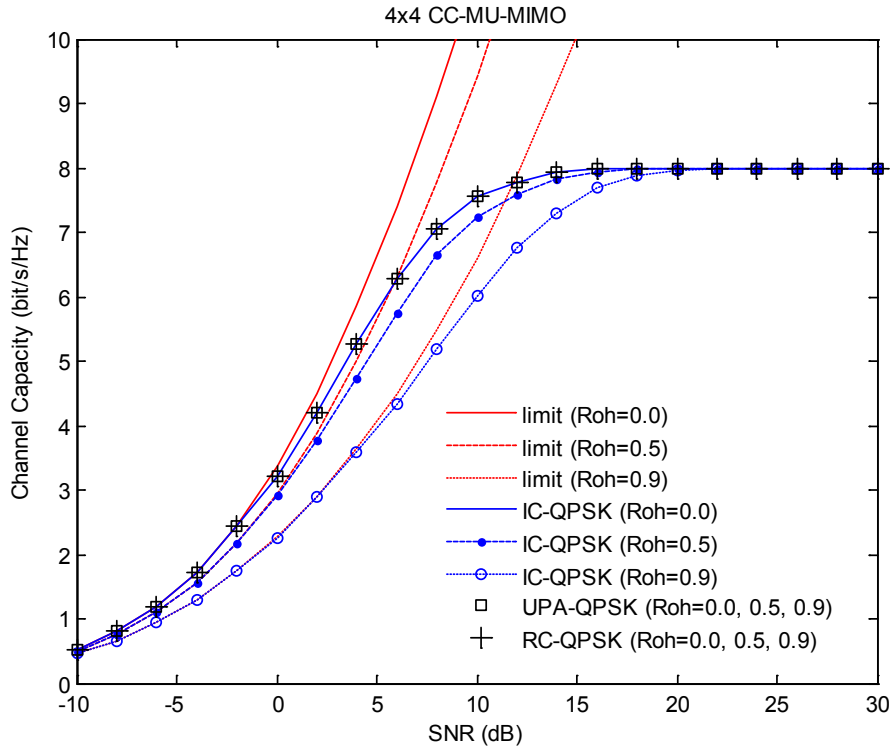

Figure 4.21: Capacity of 4×4 CC-MU-MIMO system over correlated channel with $\rho = 0.0, 0.5,$ and 0.9 for: IC-QPSK $(P_1 = \cdots = P_4 = 1,\ P = 4)$, UPA-QPSK $(\eta_1 = 0.04,\ \eta_2 = \eta_3 = 0.16,\ \eta_4 = 0.64,\ P = 4)$, and RC-QPSK $(\xi_2 = \pi/3,\ \xi_3 = \pi/6,\ \xi_4 = \pi/12, P_1 = \cdots = P_4 = 1, P = 4)$.

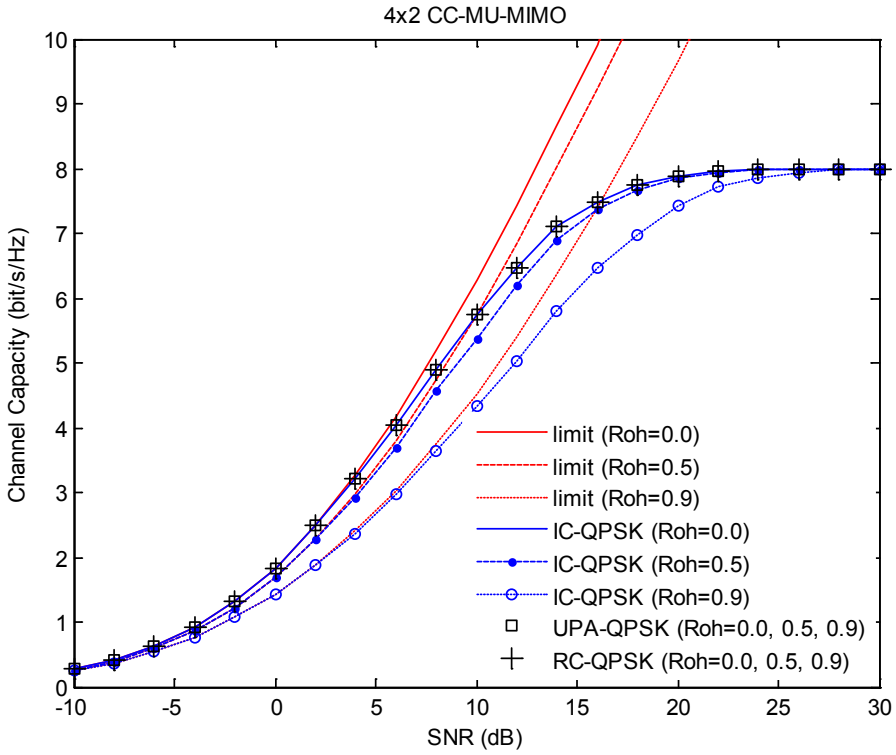

Figure 4.22: Capacity of 4×2 CC-MU-MIMO system over correlated channel with $\rho = 0.0, 0.5,$ and 0.9 for: IC-QPSK ($P_1 = \cdots = P_4 = 1,\ P = 4$), UPA-QPSK ($\eta_1 = 0.04,\ \eta_2 = \eta_3 = 0.16,\ \eta_4 = 0.64,\ P = 4$), and RC-QPSK ($\xi_2 = \pi/3,\ \xi_3 = \pi/6,\ \xi_4 = \pi/12, P_1 = \cdots = P_4 = 1, P = 4$).

4.6.2 BER Performance

To evaluate the average BER performance of $K \times m$ CC-MU-MIMO system and to show the effectiveness of proposed signal design methods, we consider without loss of generality MPSK signalling for same correlation levels used in previous subsection as; $\rho = 0.0, 0.5,$ and 0.9. The results are demonstrated for four representative system configurations as; 2×2, 2×4, 4×4, and 4×2.

Results of 2×2 and 2×4 configurations employing IC-BPSK ($P_1 = P_2 = 1,\ P = 2$), UPA-BPSK ($\eta_1 = 0.8,\ \eta_2 = 0.2,\ P = 2$), and RC-BPSK ($\xi_2 = \pi/2, P_1 = P_2 = 1, P = 2$) are shown in Fig. 4.23. It can be seen clearly that performance of IC, UPA, and RC signalling methods are similar for uncorrelated channel environment. However, as ρ increased, performance of IC decreases significantly while UPA and RC methods provides stable performance irrespective of ρ values. For example, the achieved gain in SNR using UPA or RC compared with IC when $\rho = 0.9$ at target BER of 10^{-5} is 2dB and 5dB for 2×2 and 2×4 schemes, respectively. Due to the spatial diversity, gain of 2×4 with $L = 4$ is higher than 2×2 configuration with $L = 2$.

In Fig. 4.24, performance results of 4×4 and 4×2 schemes employing IC-BPSK ($P_1 = \cdots = P_4 = 1,\ P = 4$), UPA-BPSK ($\eta_1 = 0.04,\ \eta_2 = \eta_3 = 0.16,\ \eta_4 = 0.64,\ P = 4$),

and RC-BPSK ($\xi_2 = \pi/6,\ \xi_3 = \pi/2,\ \xi_4 = 2\pi/3, P_1 = \cdots = P_4 = 1,\ P = 4$) are depicted. As in the previous system configurations, the performance of IC, UPA, and RC signalling methods are identical for uncorrelated channels ($\rho = 0.0$). However, system performance with IC design is significantly decreased as the correlation level increased ($\rho \to 1$). For example, the achieved gain in SNR using UPA or RC compared with IC when $\rho = 0.9$ at target BER of 10^{-5} is 3dB and 7dB for 4×2 and 4×4 schemes, respectively. Due to the spatial diversity, gain of 4×4 with $L = 4$ is higher than 4×2 configuration with $L = 2$.

Finally, performance results of 4×4 system employing IC-QPSK ($P_1 = \cdots = P_4 = 1,\ P = 4$), UPA-QPSK ($\eta_1 = 0.04,\ \eta_2 = \eta_3 = 0.16,\ \eta_4 = 0.64,\ P = 4$), and RC-QPSK ($\xi_2 = \pi/3,\ \xi_3 = \pi/6,\ \xi_4 = \pi/12, P_1 = \cdots = P_4 = 1,\ P = 4$) are demonstrated in Fig. 4.25. In this case, significant gain in SNR of 11dB is achieved for UPA or RC compared with IC at BER of 10^{-5} and correlation level of $\rho = 0.9$.

From the presented results, CC-MU-MIMO with UPA and RC signal design methods enables robust performance compared with conventional MU-MIMO systems with IC signalling irrespective of correlation level. Indeed, correlation has serious impact on the BER performance of conventional MU-MIMO systems. Therefore, receive diversity in such a situation should be increased by increasing the number of receive antennas or reducing the number of served users (user capacity) to maintain a reliable communication. For CC-MU-MIMO scheme, robust and reliable communication is achieved even in extreme level of correlation without need for extra diversity overhead. In Table 4.4, summery results of the achievable SNR gain in dB of proposed system using UPA or RC methods compared with IC for $\rho = 0.5$ and 0.9 are presented. It can be seen that the gain is increased significantly as the correlation ρ, diversity order L, modulation level M, and/or number of fading channels Km increases. In these cases, more vector elements of $\mathbf{S}$ can be resolved without ambiguity leading to highest average BER performance.

Table 4.4: Summary results of achievable SNR gain in dB of CC-MU-MIMO using UPA or RC compared with IC of conventional MU-MIMO for $\rho = 0.5$ and 0.9

CC-MU-MIMO configuration			SNR gain in dB	
K	m	Modulation	$\rho = 0.5$	$\rho = 0.9$
2	2	BPSK	1.2	2.0
2	4	BPSK	2.8	5.0
4	4	BPSK	2.2	7.0
4	2	BPSK	2.0	3.0
4	4	QPSK	4.5	11.0

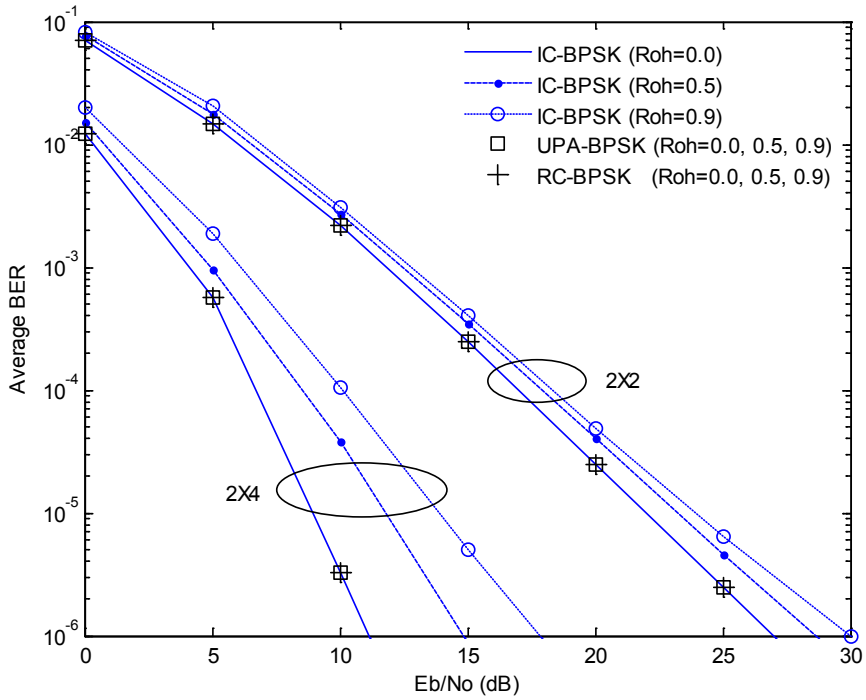

Figure 4.23: Average BER performance of 2×2 and 2×4 CC-MU-MIMO system over correlated channel with $\rho = 0.0, 0.5,$ and 0.9 for: IC-BPSK ($P_1 = P_2 = 1,\ P = 2$), UPA-BPSK ($\eta_1 = 0.8,\ \eta_2 = 0.2,\ P = 2$), and RC-BPSK ($\xi_2 = \pi/2, P_1 = P_2 = 1, P = 2$).

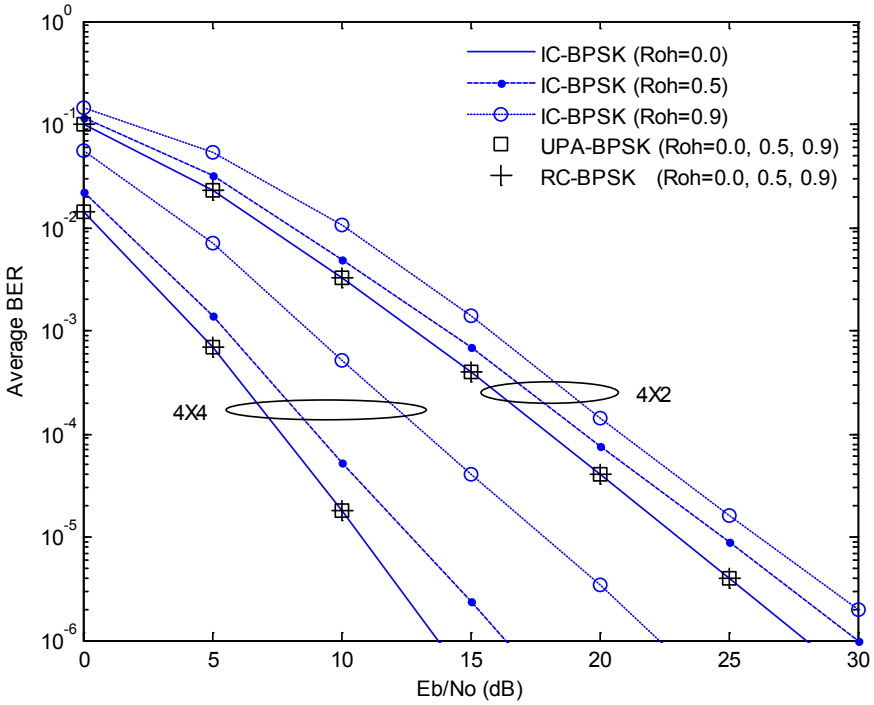

Figure 4.24: Average BER performance of 4×4 and 4×2 CC-MU-MIMO system over correlated channel with $\rho = 0.0, 0.5,$ and 0.9 for: IC-BPSK ($P_1 = \cdots = P_4 = 1,\ P = 4$), UPA-BPSK ($\eta_1 = 0.04,\ \eta_2 = \eta_3 = 0.16,\ \eta_4 = 0.64,\ P = 4$), and RC-BPSK ($\xi_2 = \pi/6,\ \xi_3 = \pi/2,\ \xi_4 = 2\pi/3, P_1 = \cdots = P_4 = 1, P = 4$).

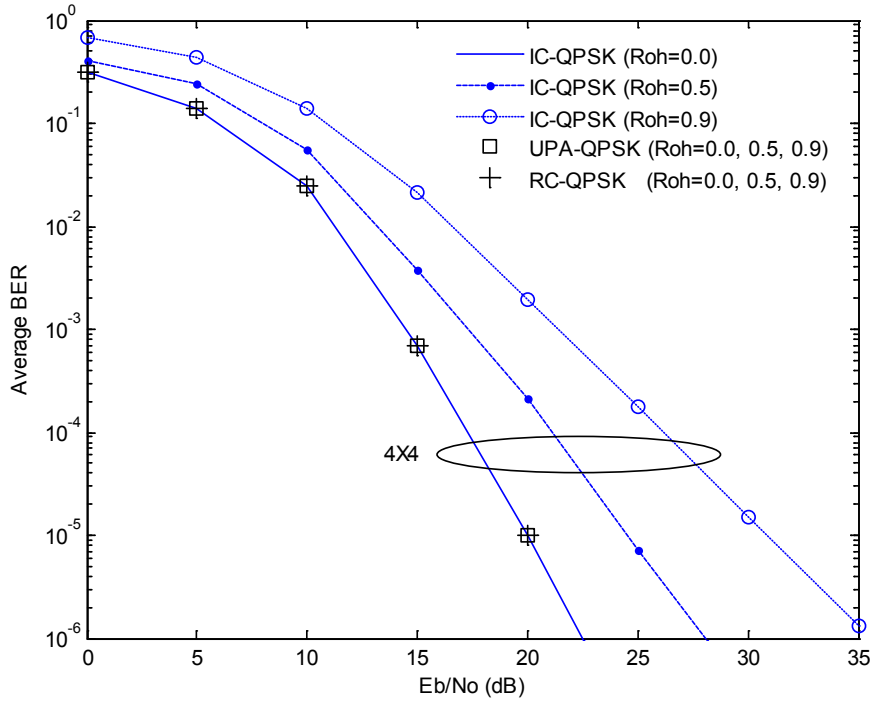

Figure 4.25: Average BER performance of 2×2 CC-MU-MIMO system over correlated channel with $\rho = 0.0, 0.5,$ and 0.9 for: IC-QPSK ($P_1 = P_2 = 1,\ P = 2$), UPA-QPSK ($\eta_1 = 0.8,\ \eta_2 = 0.2,\ P = 2$), and RC-QPSK ($\xi_2 = \pi/6, P_1 = P_2 = 1, P = 2$).

4.7 Conclusions

In this chapter, CC-MU-MIMO scheme is proposed to mitigate the effects of channel correlations using constrained signal constellation and MLJD. It takes the advantages of spatial difference among users to maximize the capacity and error performance of correlated MU-MIMO channels. The proposed UPA and RC methods have the function of maximizing d_{min} of composite received signals to resolve the detection ambiguity caused by channel correlation.

Extensive analysis and simulation results demonstrate the effectiveness of CC-MU-MIMO compared with the conventional MU-MIMO systems. UPA and RC methods show robust and stable performance irrespective of ρ values. The achieved gain in SNR is significant, particularly in moderate to high correlation levels. For example, 11dB gain is achieved for 4×4 system using UPA-QPSK or RC-QPSK compared with IC-QPSK at target BER of 10^{-5} and $\rho = 0.9$. Furthermore, 8dB gain is achieved to reach the maximum capacity of $\log_2(4^4) = 8$ bit/s/Hz. Maximizing channel capacity and BER performance have the effects of maintaining high user capacity even in sever correlation environment without need of extra receive diversity.

In addition to the simplicity of UPA compared with RC method, the possibility of power control at BS makes it more feasible to implement in the available systems. Therefore, this technique provides efficient spectrum utilization and reliable communication in correlated channel environment. In the next chapter, another method is introduced for same targets.

Chapter 5

Receive Antenna Selection (RAS) for Single and Multiuser MIMO Systems

5.1 Introduction

It is well known that channel capacity of SM MIMO systems employing antenna selection can significantly outperform systems without selection for same number of costly RF chains. However, it requires an exhaustive search for the optimal selection (OS) that grows exponentially with the available number of antennas. In this chapter, a new efficient RAS algorithm is proposed for single and multiuser MIMO systems to maximize the channel capacity over CRFC. It utilizes the received signal constellation geometry to select the subset of antennas with highest d_{min} due to its direct impact on the capacity and BER performance. A low complexity algorithm is designed by employing the Euclidean norm of channel matrix rows with their corresponding phase differences.

For any channel correlation and SNR levels, simulation results show that the proposed method outperforms that of norm based selection (NBS) and close to OS with much reduced complexity. Channels' correlation has the effect to reduce the channel capacity of SU-MIMO and MU-MIMO systems considerably. Furthermore, multiple users with highly correlated channels may not be served which reduces the user capacity. In this case, the proposed method enables channel and user capacity maximization at low cost and complexity.

This chapter is organized as follows. In Section 5.2, literature review of receive signal combining techniques for wireless communication systems and antenna selection methods for SU-MIMO and MU-MIMO schemes are presented. RAS for SU-MIMO system is considered in Section 5.3. System model is presented first followed by channel capacity analysis. New low complexity RAS algorithm is proposed with the complexity analysis. Extensive simulation results are carried out to validate and show the superiority of proposed method over CRFC. In Section 5.4, RAS for MU-MIMO is investigated. System model and analysis of sum rate capacity are introduced followed by employing the proposed RAS algorithm for multiuser case. Complexity analysis and simulation results are included also. In Section 5.5, the impact of imperfect channel estimation on the capacity and BER performance of MIMO system employing the proposed algorithms is investigated.

5.2 Literature Review

5.2.1 Receive Signal Combining Techniques

Diversity combining techniques for multiple received copies of the transmitted signal as in SIMO is a classical concept to combat the fading effects in wireless systems by increasing the average received SNR [37-39]. The main combining methods are; the optimal MRC, EGC, SC, and the Generalized SC (GSC). Such a technique can be employed depending essentially on the affordable system complexity, CSI available at the receiver, number of diversity branches L, and target system capacity and BER performance [165-167].

MRC weights each received diversity branch by its complex channel conjugate and then linearly combine them. Although it provides the best possible combined SNR [38], it is very sensitive to the channel estimation errors particularly at low SNR values. Furthermore, it has the highest complexity which is directly proportional to L. In EGC, all available branches L are co-phased and equally weighted then incoherently added. It has the same features of system complexity as MRC since all of L branches are exploited. However, it has less performance due to the *noncoherent combining loss* where adding more signals does not necessarily enhance the performance. On the other hand, SC in which the branch of highest SNR out of L branches is selected for demodulation does not fully exploit the available diversity. It is the simplest combining scheme at the expense of significant performance loss compared with MRC and EGC. However, this technique is suitable for coherent and noncoherent differential detection where the channel estimates are not required [38, 165, 166].

Bridging the gap between the two extremes in diversity combining schemes MRC (or EGC) and SC can be done using GSC schemes by exploiting the fact that most of the *diversity gain* is achieved by combining the strongest L_s branches among the available L ones. GSC schemes refer to the hybrid of SC with MRC for coherent combining and SC with EGC for noncoherent combining [165, 168, 169]. The two extreme values of L_s $(1 \leq L_s \leq L)$ brings GSC back to that of SC when $L_s = 1$ and MRC (or EGC) when $L_s = L$. As a result, efficient trade off between system complexity and performance can be achieved by ignoring the diversity branch which gives significantly small contributions to the overall received SNR.

Methods of signal combining for SU-MIMO systems are depends also on the transmission modes such as transmit diversity, STC, and SM. For transmit diversity and STC modes, the aforementioned MRC, EGC, SC and GSC methods are utilized as in [170-174] whereas hybrid of antenna selection and linear or nonlinear MUD is employed for SM [175-177].

Regardless of the transmission mode, the main problem of any MIMO system with u transmit and m receive antennas is the requirement of $(u + m)$ costly RF chains to be implemented at both link ends. However, additional antenna elements and digital signal

processing are usually inexpensive. Due to this reason, the research community shows great interest in systems that utilizes a subset of available transmit and/or receive antennas which leads to significant saving comes of course at the cost of small performance loss compared with full complexity systems [175, 178]. The major works in this field are mostly involved with the efficient antenna selection algorithms under different channel conditions and hardware shortcomings to achieve the best performance [175-188].

5.2.2 Antenna Selection for SU-MIMO

It is well known that MIMO system with u transmit and m receive antennas can dramatically improve the capacity and reliability in rich fading environments through extra DoF provided by the multiple antenna arrays. This improvement in wireless links can be done using SM for capacity and diversity methods for beamforming gain [6, 86]. However, the need for $(u + m)$ RF chains associated with multiple antennas are costly in terms of hardware requirements, computational complexity, consumed power and size. Therefore, low complexity promising techniques referred to as antenna selection have been proposed as an alternative way to capture most of MIMO system gains [175, 176]. This can be achieved by employing inexpensive antenna elements and RF switches to select the best subset of transmit and/or receive antennas and connect them with the available RF chains.

It has been shown that a MIMO system with OS can significantly outperform a system without selection using same number of RF chains [178]. However, this superior performance requires an exhaustive search for the OS that grows exponentially with available number of antennas, which is computationally prohibitive [185, 186]. For example, selecting optimal subset of $m_s = 6$ from $m = 18$ available receive antennas require $\binom{m}{m_s} = m!/\{m_s!\ (m - m_s)!\} = 18564$ channel capacity calculations. Moreover, if the selection process applied at transmit and receive side, the overall calculations will be more than 344 millions. Therefore, fast selection algorithms based on capacity maximization for SM or highest SNR for diversity were developed for different channel conditions [178-188].

For RAS in SU-MIMO schemes, decremental selection algorithm (DSA) has been proposed in [185] for near-optimal selection based on capacity maximization. It starts from the available m receive antenna elements and one antenna in each step is discarded according to its capacity contribution until the subset of m_s antennas are selected. Incremental selection algorithm (ISA) with lower complexity than DSA is proposed in [186]. This method starts from an empty set of m_s antennas and then one antenna with highest contribution to the channel capacity is added in each step. The computational complexity of these algorithms are reported as of $\mathcal{O}(u^2m^2)$ for DSA and of $\mathcal{O}(umm_s)$ for ISA. Several other algorithms with different complexity requirement are given in [179]. Recently, fast RAS algorithm with global search

function is proposed in [187]. It has better capacity performance than the method of [186] at moderate to high SNR with complexity order of $\mathcal{O}(u^2m)$. Among others, antenna selection based on the received signal power known as NBS with complexity of $\mathcal{O}(um)$ is the simplest selection algorithm which provides best capacity and BER results for diversity systems [175, 181]. However, it has low capacity performance for SM systems compared with capacity optimization based algorithms, specifically at moderate to high SNR.

The other important issue which must be considered is channel correlation. It is a crucial factor in SU-MIMO systems that directly influence diversity and capacity gains [86]. Therefore, spatial correlation based selection (SCBS) algorithm has been proposed in [188] to address this issue. It offers capacity maximization at low complexity of $\mathcal{O}(m^2)$ by utilizing the long-term channel statistics (correlation) rather than instantaneous CSI (ICSI). In [178], correlation based selection (CBS) has been presented to select the channel matrix rows (i.e. receive antennas) with highest power and minimum correlations with the others. It has less complexity of $\mathcal{O}(m^2)$ compared with SCBS due to the use of vector product rather than capacity matrix calculations. In [184], transmit antenna selection (TAS) technique has been proposed based on maximizing SNR margin for linear receivers by assuming independent fading channel. Based on the same assumption, transmit antenna and constellation selection has been investigated in [182] for correlated SU-MIMO fading channels. Cross entropy optimization (CEO) method has been introduced in [181] for RAS to maximize the channel capacity irrespective of the SNR values.

5.2.3 Antenna Selection for MU-MIMO

MU-MIMO systems enable simultaneous transmission between multiple mobile users and BS transceiver by exploiting the spatial dimension [19]. It offers substantial increase in channel and user capacity and reduces users' latency compared with conventional TDMA systems [17, 189, 190]. However, the maximum number of users with multiple antennas that can be supported is limited by total DoF which is defined by the number of BS antennas (m) connected with RF chains. Therefore, different scheduling methods are used to serve the active users and to exploit the inherent multiuser diversity when the sum of users' antennas is larger than m [19, 108]. However, it is seriously affected by channel correlations due to insufficient antenna separation at the communication terminals and/or poor scattering environment [23, 181, 187]. As a result, the sum rate capacity is significantly degraded and users with highly correlated channels may not be served which reduces the user capacity [6, 18].

Compared with SU-MIMO, little work in the field of antenna selection has been done for MU-MIMO systems and most of the available results are for DL channel to maximize the sum rate and/or diversity gains [19, 20, 22, 189-194]. In [189], two TAS algorithms for DL MU-MIMO system with linear precoding of block diagonalization (BD) are proposed based on

symbol error rate (SER) and sum rate capacity optimizations. However, it requires an exhaustive search for the optimal subset of BS antennas to achieve the promised diversity gain. Therefore, two low complexity and sub optimal algorithms are investigated in [190] by utilizing greedy selection mechanism to find the best antenna subset where one antenna with lowest contribution to the system performance is removed at each step. The first algorithm is based on minimizing the post-processing SER for linear multiuser receivers while the second one is based on Frobenius norm to maximize sum rate capacity. Also, optimal and suboptimal TAS algorithms have been proposed for DL MU-MIMO with DPC in [191]. TAS has been considered also in conjunction with the inherent multiuser diversity in MU-MIMO systems. The objective is to overcome the channel hardening caused by large number of antennas, improve the system performance and to reduce the required CSI feedback from users to the BS [20, 193]. In [19], suboptimal algorithms of joint user scheduling and RAS at the users' side are considered for DL MU-MIMO with BD and successive optimization (SO) precoding. The aims are to maximize the sum rate with less complexity compared with exhaustive search methods and to enhance the multiuser diversity gain. In these algorithms and starting from an empty set, one user with highest contribution to the sum rate capacity for BD or Frobenius norm for SO is added each step till the desired number of users have been selected. RAS is performed in conjunction with the user selection to enhance the selection metrics. In [19, 192], further results on sum rate and diversity gains are found when user scheduling with RAS is performed for DL channel.

For the UL MU-MIMO channel, suboptimal joint user and TAS algorithms based on capacity and norm maximization are proposed in [195, 196]. In [197], joint user and RAS based on sequential Monte Carlo optimization is considered to maximize the channel capacity. In [198], a genetic approach is used for joint RAS and symbol detection based on ML criterion. Statistics-based RAS for UL MU-MIMO systems is considered also in [199].

5.3 RAS for SU-MIMO

In this section, a new low complexity RAS algorithm is proposed for SM SU-MIMO systems over CRFC [220]. It is based on d_{min} maximization by utilizing the largest Euclidean norm of channel matrix rows with their corresponding phase differences. In the following, system model of SU-MIMO system with RAS is presented.

5.3.1 System Model

Consider a single SU-MIMO system where the transmitter utilizes all available antennas u while the receiver uses m_s from m receive antennas as shown in Fig. 5.1 [220]. The

correlated $m \times u$ channel matrix $\mathbf{H} \in \mathcal{C}^{m \times u}$ is assumed to be flat Rayleigh fading of zero mean and unit variance complex Gaussian entries given as

$$\mathbf{H} = \begin{bmatrix} h_{11} & \cdots & h_{u1} \\ \vdots & \ddots & \vdots \\ h_{1m} & \cdots & h_{um} \end{bmatrix} = \begin{bmatrix} \mathbf{h}_1 \\ \vdots \\ \mathbf{h}_m \end{bmatrix} \tag{5.1}$$

where, $h_{il} = x_{il} + jz_{il}$ is complex fading coefficient between i^{th} transmit and l^{th} receive antennas, x_{il} and z_{il} are the in-phase and quadrature components of zero mean 0.5 variance Gaussian random processes, and $\mathbf{h}_l, \forall l = 1, \ldots, m$ is the l^{th} row of $\mathbf{H}$. The Rayleigh distributed envelope of h_{il} path is $\alpha_{il} = |h_{il}|$ while $\beta_{il} = \tan^{-1}(z_{il}/x_{il})$ represents the uniform distribution phase over the interval $[0, 2\pi]$.

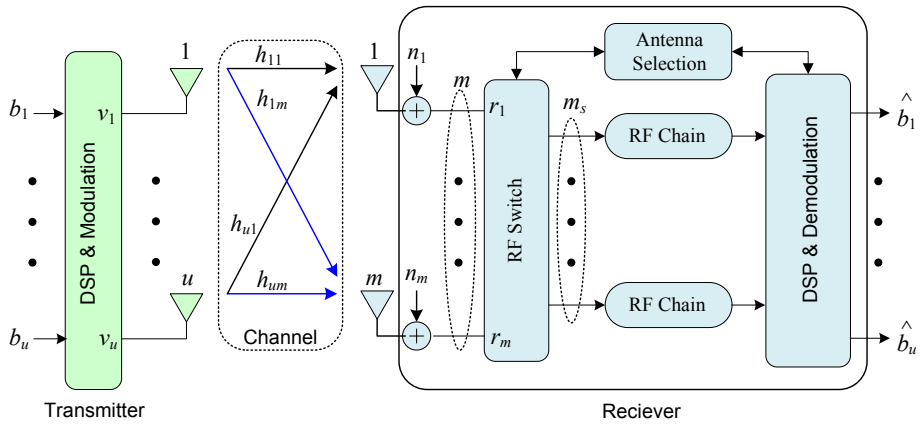

Figure 5.1: System model for $u \times m$ SU-MIMO with RAS.

For the given system model, the following assumptions are considered:

1) The channel fading rate (Doppler spread) is assumed to be much less than the data rate. Therefore, the channel remains constant over a frame of hundreds of symbols [29, 37, 177, 189]. For example, the channel fading rate is approximately 100 Hz for typical channel coherence time of 10 ms. Therefore, a frame of 100 data bits can be transmitted for data rate of 10^4 bits/s for each channel realization and for data rate of 1Mbits/s, the frame length will be increased to 10,000 data bits. Under this condition and for a frame of training phase and data phase, the fading coefficients estimated during the training phase will be constant over the entire data phase and changes from one frame to the next independently [29, 144, 181].

2) Correlated fading signals of $\mathbf{H}$ are generated using ICT [141, 142] with correlation matrix of envelopes $\boldsymbol{\rho} \in \mathcal{R}^{um \times um}$ whose entries represent the correlation factor ρ_{ij} between i^{th} and j^{th} fading signal envelope in the interval $[0, 1]$.
3) Perfect CSI with correlated envelopes and independent phases is assumed at the receiver side.

The corresponding received signal by m receive antennas is given by

$$\mathbf{r} = \mathbf{H}\mathbf{v} + \mathbf{n} \tag{5.2}$$

where $\mathbf{r} = [r_1 \quad \cdots \quad r_m]^T \in \mathcal{C}^{m \times 1}$ is $m \times 1$ received signal vector, $\mathbf{v} = [v_1 \quad \cdots \quad v_u]^T \in \mathcal{C}^{u \times 1}$ is $u \times 1$ transmitted signal vector with equal power distribution modulated from $u \times 1$ equiprobable data vector $\mathbf{b} = [b_1 \quad \cdots \quad b_u]^T \in \mathcal{R}^{u \times 1}$, and $\mathbf{n} = [n_1 \quad \cdots \quad n_m]^T \in \mathcal{C}^{m \times 1}$ is $m \times 1$ i.i.d complex AWGN vector of zero mean and variance σ_n^2 entries.

The received signal vector $\mathbf{r_s} \in \mathcal{C}^{m_s \times 1}$ associated with the selection of m_s from m receive antennas is given by

$$\mathbf{r_s} = \mathbf{H_s}\mathbf{v} + \mathbf{n_s} \tag{5.3}$$

where, $\mathbf{H_s} \in \mathcal{C}^{m_s \times u}$ and $\mathbf{n_s} \in \mathcal{C}^{m_s \times 1}$ denote the selected channel matrix and noise vector, respectively.

MLJD is employed in the considered system. This nonlinear receiver is optimal in the sense of minimizing the error probability by searching for the most likely transmitted signals. For spatial multiplexing SU-MIMO utilizing M modulation levels at the transmitter, there are $D = M^u$ possible signal vectors, $\mathbf{v}_q \in \boldsymbol{V};\ q = 1, \ldots, D$ at the channel input. Therefore, based on the minimum distance criterion, the transmitted signal vector associated with antenna selection is estimated as

$$\hat{\mathbf{v}} = \arg \min_{\mathbf{v}_q \in \boldsymbol{V}} \left\| \mathbf{r_s} - \mathbf{H_s}\mathbf{v}_q \right\|^2 ;\ q = 1, \ldots, D \tag{5.4}$$

The estimated signal vector $\hat{\mathbf{v}} = [\hat{v}_1 \quad \cdots \quad \hat{v}_u]^T \in \mathcal{C}^{u \times 1}$ will be remapped to data vector $\hat{\mathbf{b}} = [\hat{b}_1 \quad \cdots \quad \hat{b}_u]^T \in \mathcal{R}^{u \times 1}$.

5.3.2 Channel Capacity Analysis of SU-MIMO with RAS

For full complexity SU-MIMO system (without antenna selection), the channel capacity C for fixed **H** is given as [17, 24]

$$C = \log_2 \left| \mathbf{I}_m + \frac{\Gamma}{u} \mathbf{H}\mathbf{H}^{\mathrm{H}} \right| \tag{5.5}$$

where, $\mathbf{I}_m$ is $m \times m$ identity matrix, and Γ is the average SNR. Therefore, the maximum capacity associated with RAS can be written as

$$C_s = \max_{\mathcal{s}_i \in \mathbb{S}} \left[\log_2 \left| \mathbf{I}_{m_s} + \frac{\Gamma}{u} \mathbf{H}_{\mathbf{s}}(\mathcal{s}_i) \mathbf{H}_{\mathbf{s}}^{\mathrm{H}}(\mathcal{s}_i) \right| \right] \tag{5.6}$$

where the maximization is over the subset $\mathcal{s}_i \in \mathbb{S}$ for $\mathbb{S} = \{\mathcal{s}_1, \ldots, \mathcal{s}_i, \ldots, \mathcal{s}_{|\mathbb{S}|}\}$ representing the set of all possible subsets of receive antennas whose cardinality is $|\mathbb{S}| = \binom{m}{m_s}$, $\mathbf{I}_{m_s}$ is $m_s \times m_s$ identity matrix, and $\mathbf{H}_{\mathbf{s}}(\mathcal{s}_i)$ is the selected $m_s \times u$ sub-channel matrix according to subset $\mathcal{s}_i$.

For **H** with linearly independent (uncorrelated) rows, the capacity (5.5) can be written as

$$C = \log_2 \left[\prod_{l=1}^{m} \left(1 + \frac{\Gamma}{u} \left\| \mathbf{h}_l^{\mathrm{H}} \right\|^2 \right) \right] \tag{5.7}$$

Therefore, the capacity contributions of all antennas are decoupled and determined by the Euclidian norm of the channel rows. Furthermore, at low SNR or when the rank of **H** is $\min(u, m) = 1$, capacity (5.5) can be approximated as

$$C \approx \log_2 \left[1 + \frac{\Gamma}{u} \mathrm{tr}\left(\mathbf{H}\mathbf{H}^{\mathrm{H}} \right) \right] = \log_2 \left[1 + \frac{\Gamma}{u} \|\mathbf{H}\|_F^2 \right] \tag{5.8}$$

where $\|.\|_F$ is the matrix Frobenius norm.Therefore, channel capacity is determined by the total channel power due to the individual contributions of each antenna to $\|\mathbf{H}\|_F^2$. Hence, the maximum capacity associated with RAS of subset $\mathcal{s}_i \in \mathbb{S}$ can be approximated as

$$C_s \approx \max_{\mathcal{s}_i \in \mathbb{S}} \left[\log_2 \left| 1 + \frac{\Gamma}{u} \|\mathbf{H}_{\mathbf{s}}(\mathcal{s}_i)\|_F^2 \right| \right] \tag{5.9}$$

5.3.3 Proposed Phase Difference Based Selection (PDBS)

5.3.3.1 Principles of PDBS

By employing antenna selection based on the received signal power (Euclidean norm of the channel rows), optimal performance can be achieved for the following specific cases: 1) **H** with orthogonal rows, 2) low SNR, and 3) **H** of rank one. However, this optimality is not maintained at *moderate to high* SNR due to the correlation of some rows even if they have high power [175, 186]. Therefore, it is very important to improve the selection process for this range of SNR and different correlation conditions. This can be achieved by utilizing d_{min} of the combined received signal constellation at each receive antenna. For capacity and BER maximization, geometrical structure of the combined received signal constellation with highest d_{min} is an important factor. In this case, the inherent phase shifts between u transmit antennas will create diverse received constellations having different d_{min} values. This can be explained by the following representative example.

Consider transmission of equal power BPSK signals from two transmit antennas ($u = 2$) in SU-MIMO system of m receive antennas as, $[v_1, v_2] = [\mp 1, \mp 1]$. The received signal r_l at l^{th} antenna is given as

$$r_l = h_{1l}v_1 + h_{2l}v_2 + n_l \tag{5.10}$$

Constellation of r_l without noise component consists four possible points $\{y_1, y_2, y_3, y_4\}$ corresponding to v_1 and v_2 given by

$$\begin{aligned} y_1 &= +h_{1l} + h_{2l}\,, \quad & v_1 &= +1, v_2 = +1 \\ y_2 &= -h_{1l} + h_{2l}\,, \quad & v_1 &= -1, v_2 = +1 \\ y_3 &= -h_{1l} - h_{2l}\,, \quad & v_1 &= -1, v_2 = -1 \\ y_4 &= +h_{1l} - h_{2l}\,, \quad & v_1 &= +1, v_2 = -1 \end{aligned} \tag{5.11}$$

Let's define the phase difference θ_l corresponding to r_l as the resultant phase between h_{1l} and h_{2l} given by

$$\theta_l = \min\{\text{abs}(\beta_{1l} - \beta_{2l}), \quad 2\pi - \text{abs}(\beta_{1l} - \beta_{2l})\} \tag{5.12}$$

where $\beta_{1l} = \tan^{-1}(z_{1l}/x_{1l})$ is the phase of h_{1l} and $\beta_{2l} = \tan^{-1}(z_{2l}/x_{2l})$ is the phase of h_{2l}. It represents with the channel gains ($\alpha_{1l} = |h_{1l}|$ and $\alpha_{2l} = |h_{2l}|$) analogous measure to d_{min}. In correlated channel conditions, the channel gains (α_{1l} and α_{2l}) will be close to each other

depending on the correlation factor while the phases (β_{11} and β_{21}) are independent and can take any value in the interval $[0,2\pi]$. Also, the fading coefficients have more contribution to the received signal r_l than the noise component for moderate to high SNR. Considering these issues, constellation of r_l over possible channel realizations is depicted in Fig. 5.2 for three different possible values of phase difference θ_l. The channel gains α_{1l} and α_{2l} are assumed to be fixed while θ_l can take any value in the interval $[0,\pi]$. The noise component n_l is represented by circular region surrounding the constellation points $\{y_1, y_2, y_3, y_4\}$. From this figure, it is clear that there is one to one correspondence between the phase difference and d_{min}. When $\theta_l = \pi/2$, the constellation has maximum d_{min} compared with when $\theta_l = \pi/7$ and $\theta_l = 3\pi/4$. For $\theta_l = \pi/7$, there is a possibility of signal detection error caused by the noise component and small d_{min} between y_2 and y_4. Thus, the best case that makes l^{th} antenna to be selected is $\theta_l = \pi/2$ which lies in the *middle of phase difference interval* and can be denoted as the *optimal angle* θ_l^*. As a result, there is 50% of phase difference realizations that makes d_{min} large represented by θ_l in the range, $\pi/4 \leq \theta_l \leq 3\pi/4$ and maximum d_{min} is achieved when $\theta_l \to \theta_l^*$.

To generalize this concept for u transmit antennas, the phase difference vector $\boldsymbol{\theta}_l$ for the l^{th} receive antenna is given as

$$\boldsymbol{\theta}_l = \left\{\theta_l(h_{il}, h_{jl})\right\}_{i,j=1;\, i\neq j}^{u} \quad ; \quad l = 1, \dots, m \tag{5.13}$$

where $\theta_l(h_{il}, h_{jl})$ is the phase difference between i^{th} and j^{th} coefficients in the l^{th} row of **H** given as

$$\theta_l\left(h_{il}, h_{jl}\right) = \min\{\text{abs}\left(\beta_{il} - \beta_{jl}\right), \quad 2\pi - \text{abs}\left(\beta_{il} - \beta_{jl}\right)\} \tag{5.14}$$

Therefore, optimal phase difference vector at the l^{th} receive antenna $\boldsymbol{\theta}_l^*$ can be written as

$$\boldsymbol{\theta}_l^* = \left\{\theta_l^*(h_{il}, h_{jl})\right\}_{i,j=1;\, i\neq j}^{u} \quad ; \quad l = 1, \dots, m \tag{5.15}$$

As $\boldsymbol{\theta}_l \to \boldsymbol{\theta}_l^*$, the maximum value of d_{min} will be approached.

Since calculations of $\boldsymbol{\theta}_l$ is less complex than d_{min}, it is considered in this contribution with the Euclidean norm of the channel rows $\|\mathbf{h}_l\|$; $\forall l = 1, \dots, m$ for RAS. In the next subsection, PDBS algorithm is designed and Maximization of the Ergodic capacity is considered rather than constellation constrained capacity of practical signalling due to the utilization of channel properties in the selection process.

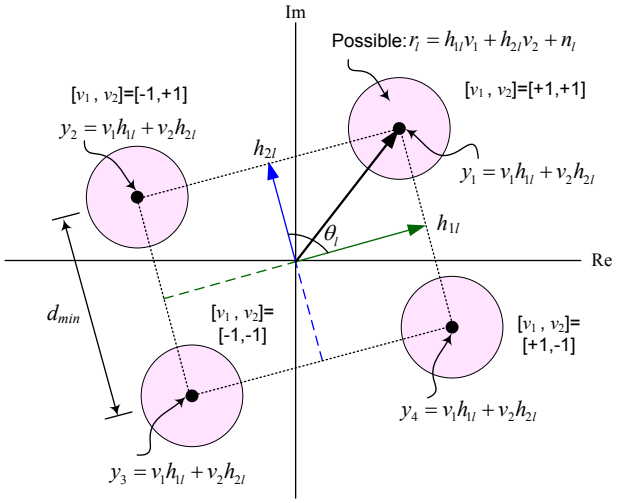

(a): $\theta_l = \pi/2$

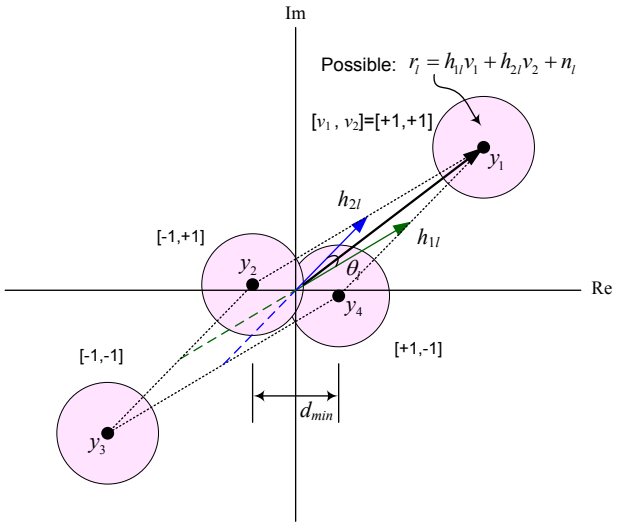

(b): $\theta_l = \pi/7$

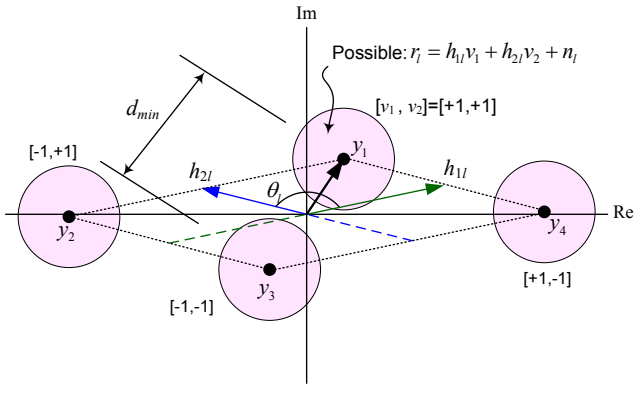

(c): $\theta_l = 3\pi/4$

Figure 5.2: Received signal constellation of r_l at l^{th} antenna over possible channel realizations where the path gains α_{11} and α_{21} are fixed while the phase difference θ_l is; a) $\pi/2$, b) $\pi/7$, and c) $3\pi/4$.

5.3.3.2 PDBS Algorithm

In PDBS algorithm, selection of $\mathbf{H_s}(\mathcal{s}_i)$ is based on the largest Euclidean norms of channel matrix rows $\|\mathbf{h}_l\|;\ \forall l = 1, \dots, m$ with best phase differences $\boldsymbol{\theta}_l \to \boldsymbol{\theta}_l^*;\ \forall l = 1, \dots, m$ for higher contribution to $\|\mathbf{H_s}(\mathcal{s}_i)\|_F^2$. Therefore, maximum capacity associated with antenna selection can be written as

$$C_s = \max_{\substack{\mathcal{s}_i \in \mathbb{S} \\ \boldsymbol{\theta}_l \to \boldsymbol{\theta}_l^*}} \left[\log_2 \left| \mathbf{I}_{m_s} + \frac{\Gamma}{u} \mathbf{H_s}(\mathcal{s}_i) \mathbf{H_s}^{\mathrm{H}}(\mathcal{s}_i) \right| \right] \tag{5.16}$$

where the maximization is over $\mathcal{s}_i \in \mathbb{S}$ and $\boldsymbol{\theta}_l \to \boldsymbol{\theta}_l^*$. For practical signalling, this selection will provide a received vector $\mathbf{r_s}$ to the detection stage with highest SNR and constellations having maximum d_{min}. The proposed algorithm is as follows:

1) Define the set of receive antennas as, $\mathcal{X} = \{1, \dots, l, \dots, m\}$ with $l \in \mathcal{X}$ representing the l^{th} antenna.
2) For all l in $\mathcal{X}$, calculate the phase difference vector $\boldsymbol{\theta}_l$ and the power of channel vector $\mathbf{h}_l$ as $p_l = \|\mathbf{h}_l\|^2$.
3) From $\mathcal{X}$, construct two subsets of receive antennas as $\mathcal{X}_a$ from those satisfying $\boldsymbol{\theta}_l \to \boldsymbol{\theta}_l^*$ and the rest in $\mathcal{X}_b$. For each subset, sort the elements from highest to lowest power.
4) To select the best subset of antennas $\mathcal{s}_i$; choose the first m_s elements from $\mathcal{X}_a$. If the number of elements in $\mathcal{X}_a$ is less than m_s, complete the selection process from $\mathcal{X}_b$.
5) From the selected subset of receive antennas $\mathcal{s}_i$, construct $m_s \times u$ channel matrix $\mathbf{H_s}(\mathcal{s}_i)$ associated with RAS.

5.3.4 Computational Complexity

To demonstrate the computational effort of proposed PDBS algorithm compared with that of OS and NBS, same number of u transmit antennas, m receive antennas and m_s RF chains at the receive side is assumed in all schemes. So, the comparison is based on the selection of m_s from m available receive antennas.

For PDBS algorithm, calculations of um channel Euclidean norms and $m(u!/\{2!\ (u-2)!\})$ phase difference are required. Therefore, total of $m(u^2+u)/2$ calculations are used and the resulting complexity effort is of $\mathcal{O}(mu^2)$.

Using OS algorithm, optimal capacity is achieved by maximizing the following performance function

$$\mathcal{F}_{\mathrm{OS}} := \arg\max_{\mathcal{s}_i \in \mathbb{S}} \left| \mathbf{I}_{m_s} + \frac{\Gamma}{u} \mathbf{H}_{\mathbf{s}}(\mathcal{s}_i) \mathbf{H}_{\mathbf{s}}^{\mathrm{H}}(\mathcal{s}_i) \right| \tag{5.17}$$

Therefore, capacity of $m_s \times u$ selected channel matrix with $\mathcal{O}(m_s^3)$ singular value decomposition (SVD) requirement over all possible $m!/\{m_s!\ (m-m_s)!\}$ combinations of $\mathcal{s}_i \in \mathbb{S}$ has to be calculated. As a result, huge overall computational effort of $\mathcal{O}[m_s^3\ m!/\{m_s!\ (m-m_s)!\}]$ is needed [179, 185].

For NBS algorithm [181], the channel capacity is maximized by maximizing the following performance function

$$\mathcal{F}_{\mathrm{NBS}} := \arg\max_{\mathcal{s}_i \in \mathbb{S}} \|\mathbf{H}_{\mathbf{s}}(\mathcal{s}_i)\|_F^2 \tag{5.18}$$

The complexity of this method is of $\mathcal{O}(um)$ due to the requirement of vector norm calculations over all m channel matrix rows each of u elements.

In Table 5.1, the computational efforts are shown where it should be noted that the main computational burden of OS method comes from matrix rather than vector calculations as in PDBS and NBS. Obviously, PDBS has significant complexity reduction than OS method and more calculations compared with NBS. This will provide important tradeoff between the system performance and complexity (hardware and computational efforts).

Table 5.1: Computational effort for PDBS, OS and NBS algorithms

Algorithm	Total Calculations	Computational Effort
OS	$m_s^3\ m!/\{m_s!\ (m-m_s)!\}$	$\mathcal{O}[m_s^3\ m!/\{m_s!\ (m-m_s)!\}]$
NBS	um	$\mathcal{O}(um)$
PDBS	$m(u^2+u)/2$	$\mathcal{O}(mu^2)$

5.3.5 Simulation Results

In this section, Monte Carlo simulations using MATLAB/7.9 for SU-MIMO system have been carried out in order to validate the capacity and BER performance of PDBS algorithm compared with that of OS and NBS [181, 186]. For simplicity and without loss of generality, $u = 2$, $m = 2, 4, 6$ and $m_s = 1, 2$ are considered and represented for notational convenience as $u \times m/\mathtt{algorithm}$-$m_s$. The reference baseline SU-MIMO without RAS will be represented as $u \times m$ system. To demonstrate the effects of channel correlation, we consider equal correlation

among different Rayleigh fading paths as $\rho_{ij} = \rho\ ;\ \forall i \neq j;\ i,j = 1,\ldots.,um$. In the simulations, three different cases are used; $\rho = 0.0$ for uncorrelated channels, $\rho = 0.5$ for moderate correlation, and $\rho = 0.9$ for high correlation level. The results are averaged using 10,000 channel realization for channel capacity evaluation. For BER performance, a frame of 100 symbols from BPSK constellation is assumed for each channel realization. MLJD detection is employed at the receiver for all considered systems.

5.3.5.1 Channel Capacity

Channel capacity over different correlation levels is shown in Fig. 5.3 for 2×6/PDBS-2 system compared with 2×6/NBS-2 and 2×6/OS-2. Theoretical capacity bounds for the reference baseline 1×1 and 2×2 systems are shown also for comparison. From this figure, it is obvious that the capacity of system employing RAS is higher than 2×2 system for any SNR and correlation levels. At low SNR and low to moderate correlation levels, all selection methods are optimal while at moderate to high SNR with various correlations, the performance is differ from one technique to other. Furthermore, OS algorithm provides stable performance compared with NBS algorithm for all correlation levels. This is due to the fact that for deterministic case and corresponding to one channel realization, the phase shift between channel elements is of high importance as the SNR. Indeed, it represents a crucial factor for system capacity [178]. PDBS algorithm has the property of maintaining highest SNR for RAS while trying to find the best constellation at the same time. Therefore, performance of PDBS is less affected by the correlation while outperform NBS for any SNR, specifically at moderate to high values. For example, at spectral efficiency of 16 bit/s/Hz and compared with 2×2 system for uncorrelated channels, 3.8dB gain is achieved for PDBS while 4dB for OS and 2.8dB for NBS. So, PDBS has only 0.2dB difference in SNR from OS while outperform NBS by 1dB. For high correlation of $\rho = 0.9$ and compared with 2×2 system, 6.9dB gain is achieved for PDBS while 7.4dB for OS and 5.4dB for NBS. Therefore, PDBS has 0.5dB difference in SNR from OS and outperform NBS by 1.5dB. Summery of these results are shown in Table 5.2.

To asses the effects of number receive antennas m on the channel capacity enhancement, Fig. 5.4 show the channel capacity of 2×4/PDBS-2 and 2×6/PDBS-2 over uncorrelated channel with the baseline 1×1 and 2×2 systems. At moderate to high SNR, 1.0dB is achieved by increasing m from 4 to 6 for fixed number of $m_s = 2$ which represents the RF chains. Hence, increasing the number of antennas and using PDBS for the available number of RF chains will provide substantial increase in capacity. For $m = 6$ and different number of m_s RF chains, the capacity is depicted in Fig. 5.5 for 2×6/PDBS-1 and 2×6/PDBS-2 over uncorrelated channel compared with 2×6/OS-1 and 2×6/OS-2. The reference 1×1 and 2×2 systems are shown also in the same figure. As can be seen, performance of PDBS is

similar to OS method for $m_s = 1$. This optimality is due to the fact that, all selection methods are optimal when the rank of channel matrix **H** is one as discussed earlier. Significant increase in capacity is achieved using PDBS by increasing m_s from 1 to 2, as expected. For example, the contribution of second RF chain to the capacity is 6 bit/s/Hz at SNR of 20dB.

Table 5.2: SNR gain in dB for 2×6/NBS-2, 2×6/PDBS-2, and 2×6/OS-2 systems compared with the reference 2×2 at spectral efficiency of 16 bit/s/Hz for uncorrelated ($\rho = 0.0$) and highly correlated channel ($\rho = 0.9$)

Correlation (ρ)	SNR Gain (dB)		
	2×6/NBS-2	2×6/PDBS-2	2×6/OS-2
0.0	2.8	3.8	4.0
0.9	5.4	6.9	7.4

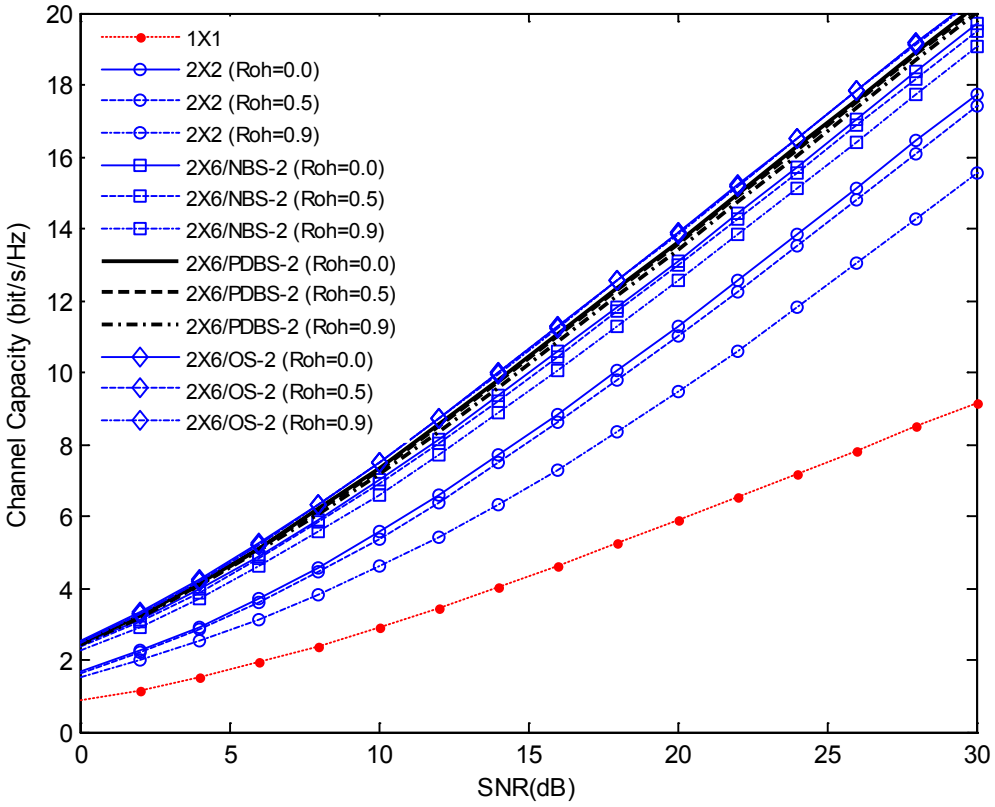

Figure 5.3: Channel capacity of 2×6/PDBS-2 over CRFC compared with, 2×6/NBS-2, 2×6/OS-2, and the reference 2×2 and 1×1 systems.

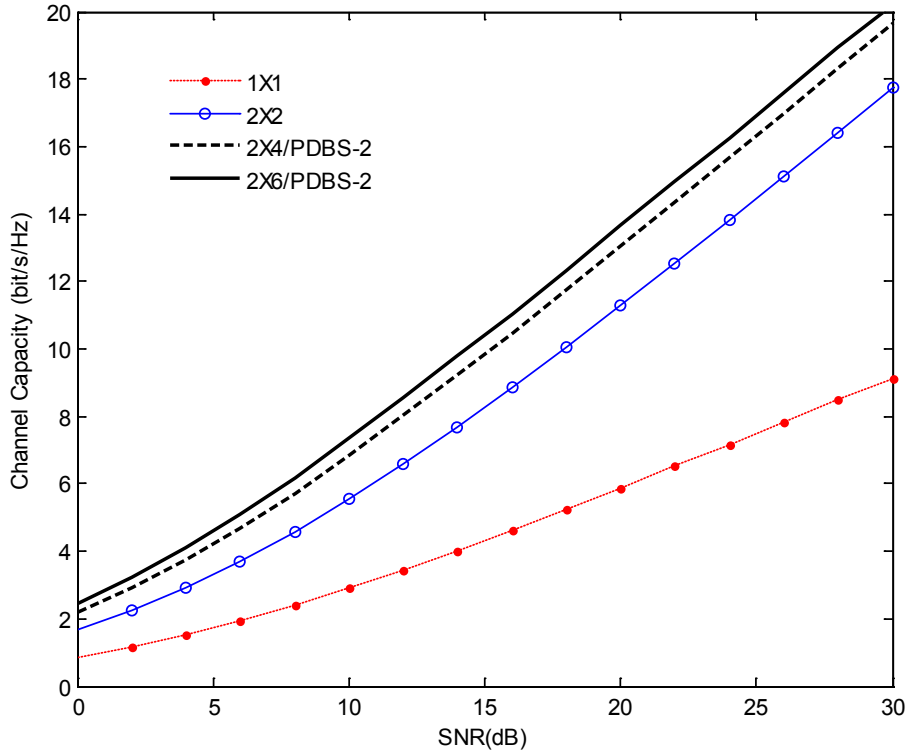

Figure 5.4: Channel capacity of 2×4/PDBS-2 and 2×6/PDBS-2 over uncorrelated Rayleigh fading channel compared with the reference 2×2 and 1×1 systems.

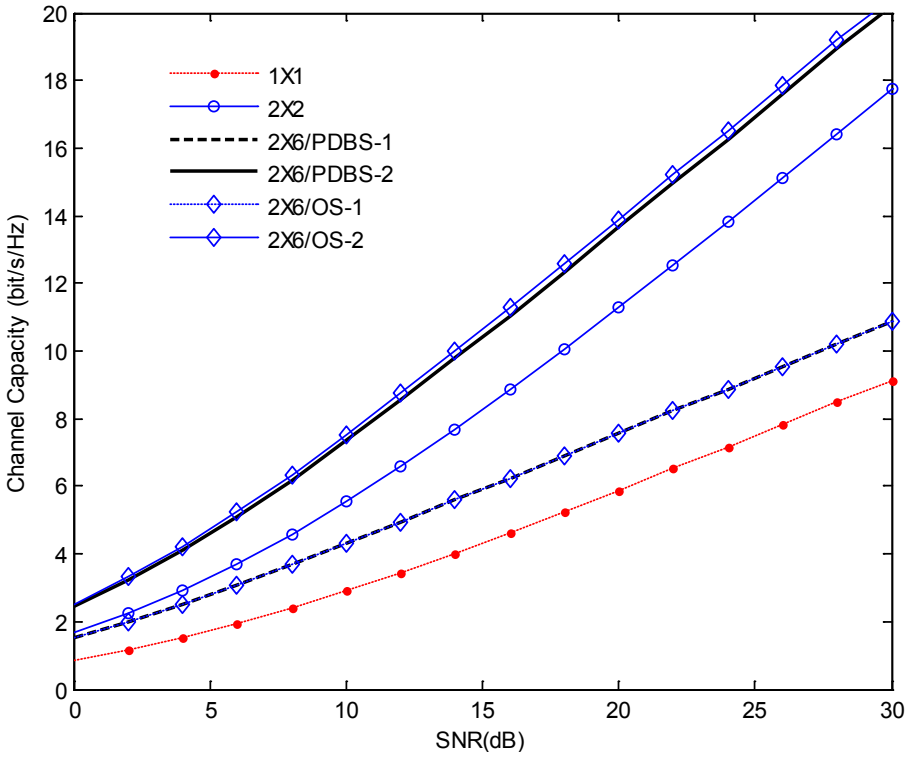

Figure 5.5: Channel capacity of 2×6/PDBS-1 and 2×6/PDBS-2 over uncorrelated Rayleigh fading channel compared with, 2×6/OS-1, 2×6/OS-2, and the reference 2×2 and 1×1 systems.

5.3.5.2 BER Performance

To asses the correlation effects on BER performance, results of 2×4/NBS-2 is shown in Fig. 5.6 compared with the reference 2×2 system. Theoretical performance results of the baseline 1×2 system using MRC (1×2/MRC) are depicted also for completeness. As can be seen, significant gain is achieved for the system with antenna selection compared with 2×2 for all correlation values. The interesting observation is that, while the correlations degrade 2×2 performance, it has the opposite effect for the system with antenna selection. The range of SNR gain at BER of 10^{-5} is approximately from 3.7dB for uncorrelated channels ($\rho = 0.0$) to 10dB for high correlation level of $\rho = 0.9$. The physical interpretation for this behaviour is that the power p_l of $\mathbf{h}_l; l = 1, \dots, m$ may increased with increase of correlation level of its fading path elements and according to their phase difference. With antenna selection, the possibility of increase in p_l as the correlation increases will lead to enhance the error performance. This explanation is enhanced by simulation where it is found that receive antennas are still selected even for the case of high correlation levels in their corresponding fading paths.

For the proposed PDBS algorithm, BER performance of 2×4/PDBS-2 over correlated channel is depicted in Fig. 5.7 compared with 2×4/NBS-2 and the reference 1×2/MRC. System performance using PDBS outperforms that of NBS for all channel correlation levels. As the channel correlation increased, the achieved gain is increased. By increasing the number of receive antennas m from 4 to 6 with fixed number of RF chains $m_s = 2$, the BER performance of 2×6/PDBS-2 is depicted in Fig. 5.8 compared with 2×6/NBS-2 and the reference 1×2/MRC system. As can be seen, for fixed number of m_s antennas, higher gain is achieved as m increased. For example when $m_s = 2$ and $m = 4$ at target BER of 10^{-5}, the achieved gain is 1.1dB at high correlation level of $\rho = 0.9$ compared with 0.8dB for uncorrelated channel ($\rho = 0.0$). For $m_s = 2$ and $m = 6$, the gain is increased to 2dB for $\rho = 0.9$ compared to 1dB for $\rho = 0.0$.

Performance results of PDBS algorithm for different numbers of m and m_s and two extreme cases of correlation ($\rho = 0.0$ and $\rho = 0.9$) are investigated. The reference 1×1 and 1×2/MRC systems are utilized also for completeness. Results of 2×2/PDBS-1, 2×4/PDBS-1, and 2×6/PDBS-1 are shown in Fig. 5.9 with $m = 2, 4,$ and 6 while $m_s = 1$. In Fig. 5.10, BER of 2×4/PDBS-1 and 2×4/PDBS-2 are shown for $m = 4$ while $m_s = 1,$ and 2. In Fig. 5.11, results of 2×6/PDBS-1 and 2×6/PDBS-2 are shown for $m = 6$ while $m_s = 1,$ and 2.

In Fig. 5.9 for $m_s = 1$ and $m = 6$, significant gain of 16.5dB is achieved for high correlation compared with uncorrelated channel. This gain is reduced to 15.4dB when $m = 4$ and approximately 7dB when $m = 2$. By increasing the RF chains from $m_s = 1$ to $m_s = 2$ while keeping $m = 4$ fixed as in Fig.5.10, the gain between two channel conditions ($\rho = 0.0$

and $\rho = 0.9$) is degraded from 15.4dB to 4.5dB. Also, this gain is degraded from 16.5dB to 5.8dB when $m = 6$ as in Fig.5. 11. Hence, higher gain is achieved as m and m_s increased.

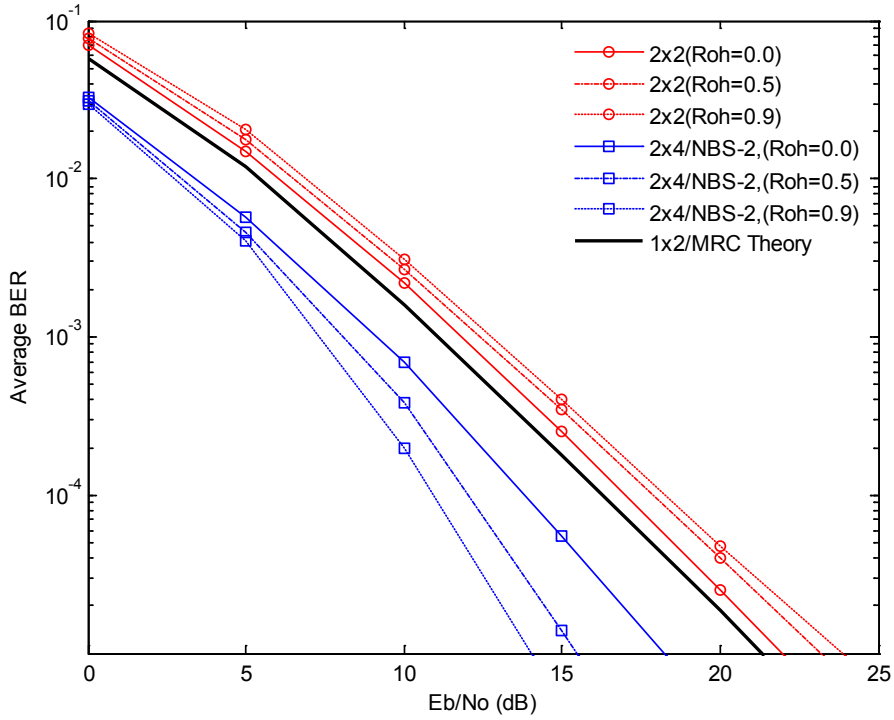

Figure 5.6: BER performance of 2×4/NBS-2 over CRFC compared with the reference 2×2 and 1×2/MRC systems.

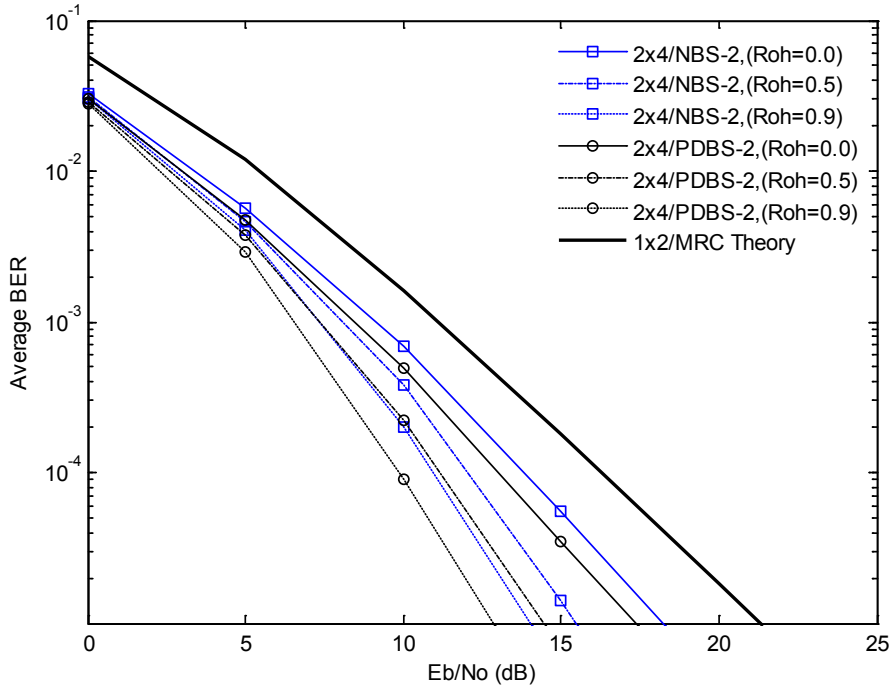

Figure 5.7: BER performance of 2×4/PDBS-2 over CRFC compared with 2×4/NBS-2 and the reference 1×2/MRC system.

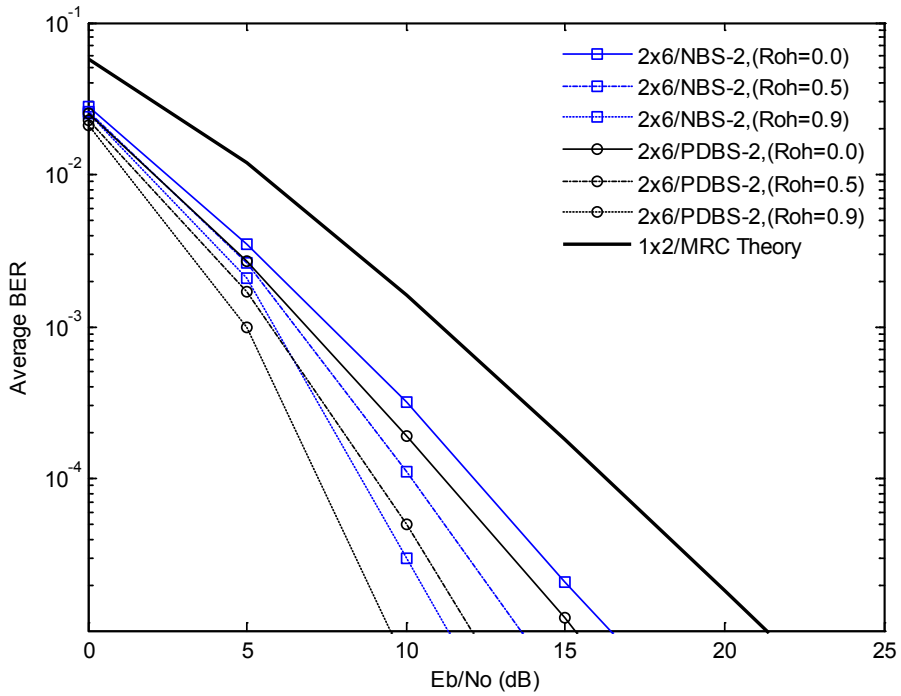

Figure 5.8: BER performance of 2×6/PDBS-2 over CRFC compared with 2×6/NBS-2 and the reference 1×2/MRC system.

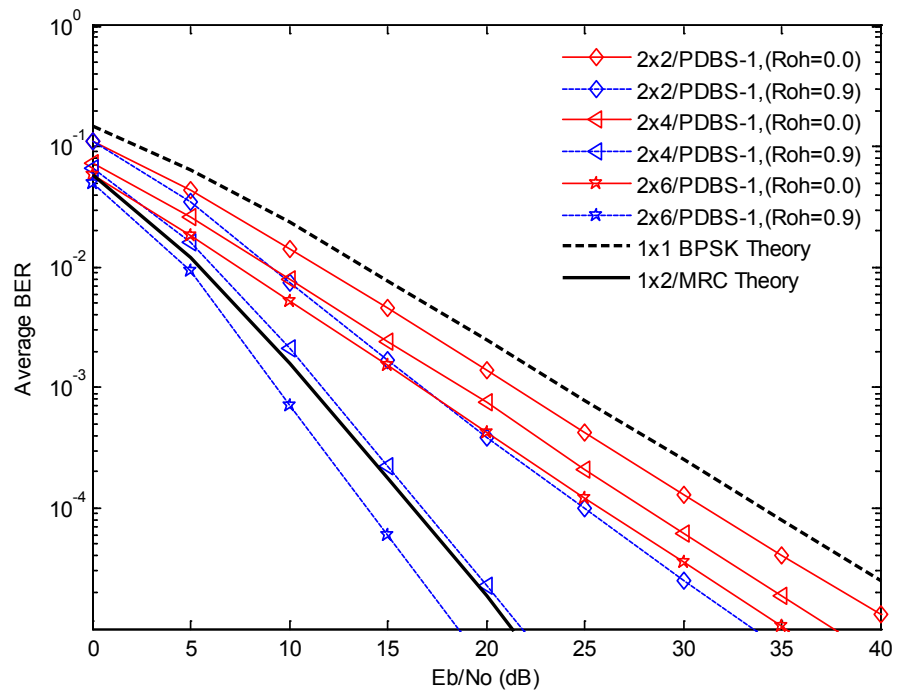

Figure 5.9: BER performance of 2×2/PDBS-1, 2×4/PDBS-1 and 2×6/PDBS-1 over CRFC compared with the reference 1×1 BPSK and 1×2/MRC systems.

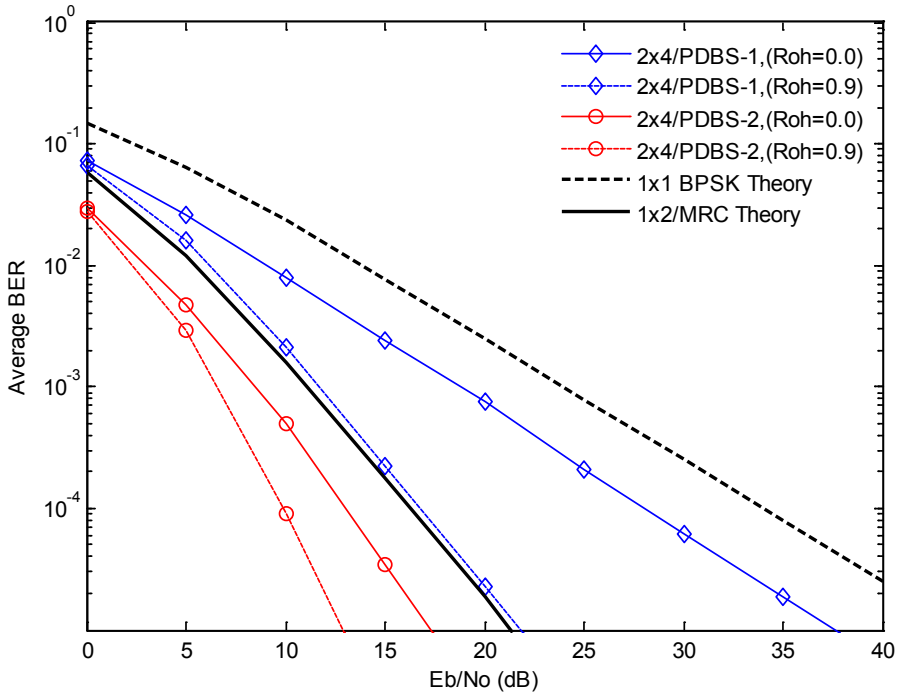

Figure 5.10: BER performance of 2 × 4/PDBS-1 and 2 × 4/PDBS-2 over CRFC compared with the reference 1 × 1 BPSK and 1 × 2/MRC systems.

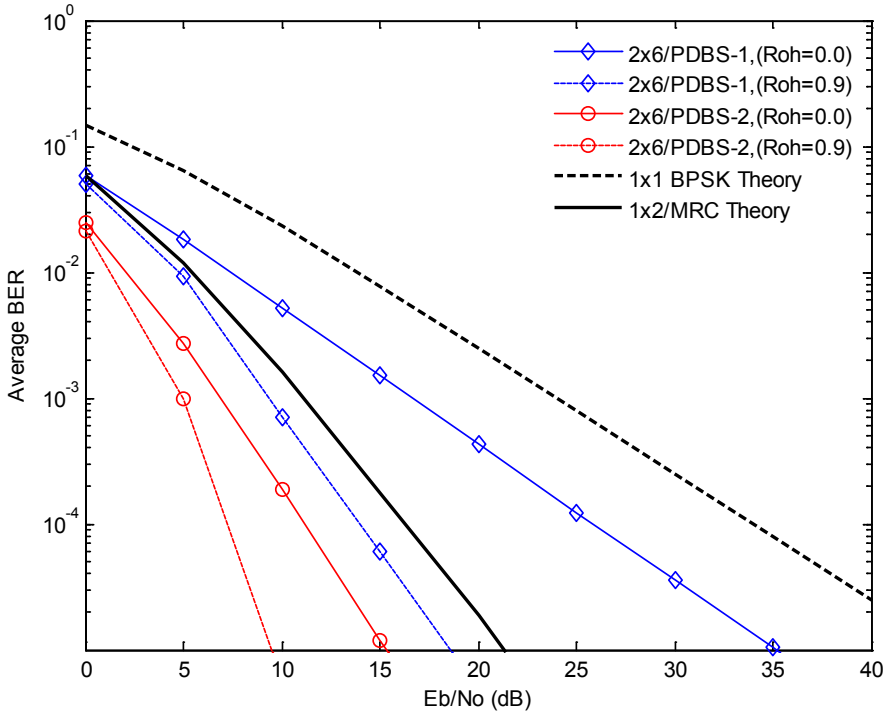

Figure 5.11: BER performance of 2 × 6/PDBS-1 and 2 × 6/PDBS-2 over CRFC compared with the reference 1 × 1 BPSK and 1 × 2/MRC systems.

5.4 RAS for the Uplink MU-MIMO

In wireless MU-MIMO systems, the BS can afford huge capabilities compared with the user equipments due to the limitations on mobile cost, small physical size and battery life [17, 189, 190]. Therefore, RAS for UL MU-MIMO correlated channel is considered in this section motivated by the possibility of accommodating larger number of antennas than available RF chains at BS. The aims are to maximize the sum rate capacity well beyond that achieved by conventional systems (i.e. without antenna selection) and to maintain high user capacity in different correlation conditions at low cost [209]. To the best of our knowledge and compared with the DL channel, little attention has been given to the antenna selection for UL channel. In such systems, NBS algorithms has the least complexity compared with OS based on sum rate capacity maximization at the cost of capacity loss specifically at moderate to high SNR [184, 190, 195, 199]. Since multiple antennas at the users' side can be viewed as virtual transmit antennas as in SU-MIMO [20], the proposed PDBS algorithm for single user is extended for UL MU-MIMO over CRFC [221]. In this case, the inherent phase shifts between multiuser transmit antennas will create diverse received constellations having different d_{min} values which are utilized by PDBS method through the employment of Euclidean norm of channel matrix rows and their corresponding phase difference.

5.4.1 System Model

Consider MU-MIMO system of K active mobile users communicating simultaneously over CRFC with one common BS (e.g. uplink of one cell cellular system) as in Fig. 2.15 [221]. Each of the mobile users utilizes all available $u_k;\ k = 1, \dots, K$ antennas in SM mode while the BS receiver which is equipped with m antennas more than the available m_s RF chains employs RAS to choose the best subset of $m_s \leq m$ antennas according to their channel conditions. The received signal vector at BS antennas can be written as [17, 18, 24, 99]

$$\mathbf{r} = \sum_{k=1}^{K} \mathbf{H}_k \mathbf{v}_k + \mathbf{n} \tag{5.19}$$

where $\mathbf{r} = [r_1 \quad \cdots \quad r_m]^T \in \mathcal{C}^{m\times 1}$ is $m \times 1$ received signal vector, $\mathbf{v}_k = [v_1 \quad \cdots \quad v_{u_k}]^T \in \mathcal{C}^{u_k \times 1}$ is $u_k \times 1$ transmitted signal vector of k^{th} mobile user with equal power distribution and modulated from $u_k \times 1$ equiprobable data vector $\mathbf{b}_k = [b_1 \quad \cdots \quad b_{u_k}]^T \in \mathcal{R}^{u_k \times 1}$, $\mathbf{n} = [n_1 \quad \cdots \quad n_m]^T \in \mathcal{C}^{m\times 1}$ is $m \times 1$ i.i.d complex AWGN vector of entries having zero mean and variance σ_n^2, and $\mathbf{H}_k \in \mathcal{C}^{m\times u_k}$ is the $m \times u_k$ channel matrix of k^{th} user with zero

mean and unit variance complex Gaussian entries. The k^{th} user channel matrix for $k = 1, \ldots, K$ is represented as

$$\mathbf{H}_k = \begin{bmatrix} h_{11}^{(k)} & \cdots & h_{u_k 1}^{(k)} \\ \vdots & \ddots & \vdots \\ h_{1m}^{(k)} & \cdots & h_{u_k m}^{(k)} \end{bmatrix} = \begin{bmatrix} \mathbf{h}_1^{(k)} \\ \vdots \\ \mathbf{h}_m^{(k)} \end{bmatrix} \tag{5.20}$$

where, $h_{il}^{(k)} = x_{il}^{(k)} + jz_{il}^{(k)}$ is the complex fading coefficient between i^{th} transmit antenna and l^{th} receive antenna, $x_{il}^{(k)}$and $z_{il}^{(k)}$ are the in-phase and quadrature components of zero mean 0.5 variance Gaussian random processes, and $\mathbf{h}_l^{(k)}, \forall l = 1, \ldots, m$ is the l^{th} row of $\mathbf{H}_k$. The Rayleigh distributed envelope of $h_{il}^{(k)}$ path is $\alpha_{il}^{(k)} = \left|h_{il}^{(k)}\right|$ while $\beta_{il}^{(k)} = \tan^{-1}\left(z_{il}^{(k)}/x_{il}^{(k)}\right)$ represents the uniform distribution phase over the interval $[0, 2\pi]$.

The received signal vector $\mathbf{r_s}$ associated with the selection of m_s from m receive antennas is given by

$$\mathbf{r_s} = \sum_{k=1}^{K} \breve{\mathbf{H}}_k \mathbf{v}_k + \mathbf{n_s} \tag{5.21}$$

where $\mathbf{r_s} \in \mathcal{C}^{m_s \times 1}$ denotes the selected received signal vector, $\breve{\mathbf{H}}_k \in \mathcal{C}^{m_s \times u_k}$ and $\mathbf{n_s} \in \mathcal{C}^{m_s \times 1}$ denote the selected channel matrix of user$k$ and noise vector, respectively.

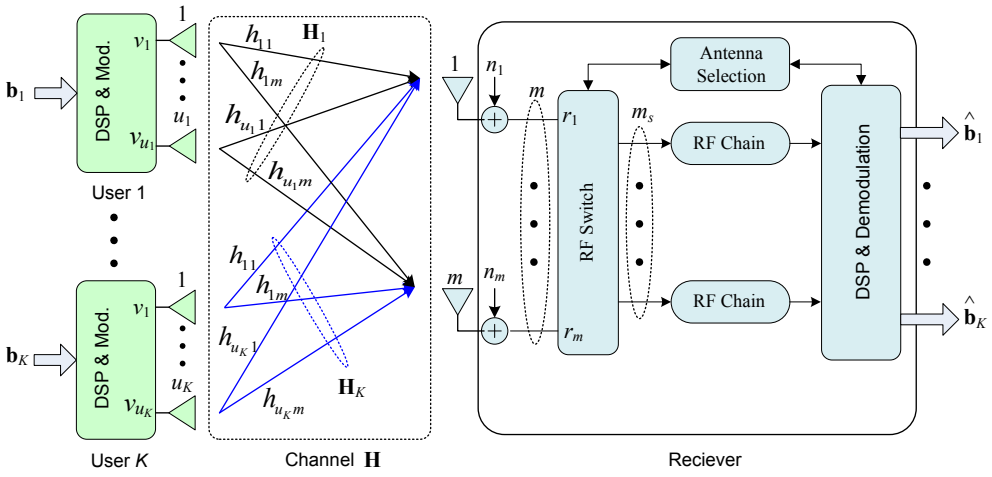

Figure 5.12: System model for MU-MIMO system of K active mobile users and one common BS receiver with RAS.

The overall MU-MIMO channel matrix $\mathbf{H} \in \mathcal{C}^{m\times u}$ can be represented as

$$\mathbf{H} = [\mathbf{H}_1 \quad \cdots \quad \mathbf{H}_k \quad \cdots \quad \mathbf{H}_K] = \begin{bmatrix} \mathbf{h}_1^{(1)} & \cdots & \mathbf{h}_1^{(k)} & \cdots & \mathbf{h}_1^{(K)} \\ \vdots & \ddots & \vdots & \ddots & \vdots \\ \mathbf{h}_l^{(1)} & \cdots & \mathbf{h}_l^{(k)} & \cdots & \mathbf{h}_l^{(K)} \\ \vdots & \ddots & \vdots & \ddots & \vdots \\ \mathbf{h}_m^{(1)} & & \mathbf{h}_m^{(k)} & & \mathbf{h}_m^{(K)} \end{bmatrix} = \begin{bmatrix} \mathbf{h}_1 \\ \vdots \\ \mathbf{h}_l \\ \vdots \\ \mathbf{h}_m \end{bmatrix} \tag{5.22}$$

where $u = \sum_1^K u_k$ is the total number of users' antennas and $\mathbf{h}_l, \forall l = 1, \dots, m$ is the l^{th} row of $\mathbf{H}$. Using the possibility of analyzing SM MU-MIMO as a virtual SU-MIMO system [20], the corresponding received signal vector (5.19) can be rewritten as

$$\mathbf{r} = \mathbf{HV} + \mathbf{n} \tag{5.23}$$

where $\mathbf{V} = [\mathbf{v}_1^T \quad \cdots \quad \mathbf{v}_k^T \quad \cdots \quad \mathbf{v}_K^T]^T \in \mathcal{C}^{u\times 1}$ is the modulated signal vector of users' data vector $\mathbf{b} = [\mathbf{b}_1^T \quad \cdots \quad \mathbf{b}_k^T \quad \cdots \quad \mathbf{b}_K^T]^T \in \mathcal{R}^{u\times 1}$. Therefore, the received signal vector $\mathbf{r_s}$ can be written as

$$\mathbf{r_s} = \mathbf{H_s V} + \mathbf{n_s} \tag{5.24}$$

where $\mathbf{r_s} \in \mathcal{C}^{m_s\times 1}$ denotes the selected received signal vector, $\mathbf{H_s} \in \mathcal{C}^{m_s\times u}$ and $\mathbf{n_s} \in \mathcal{C}^{m_s\times 1}$ denote the overall channel matrix and noise vector after selection.

For system of K active users each equipped with u_k antennas and utilizing M_k alphabet size of constellation, there are $D = \prod_{k=1}^K M_k^{u_k}$ possible signal vectors $\mathbf{V}_q \in \mathcal{C}^{u\times 1}; q = 1, \dots, D$ at the channel input as

$$\mathbf{V}_q = \begin{bmatrix} \mathbf{v}_{1_q}^T & \cdots & \mathbf{v}_{k_q}^T & \cdots & \mathbf{v}_{K_q}^T \end{bmatrix}^T \tag{5.25}$$

where $\mathbf{v}_{k_q} = \begin{bmatrix} v_1^{(q)} & \cdots & v_{u_k}^{(q)} \end{bmatrix}^T \in \mathcal{C}^{\,u_k\times 1}$ and $v_i^{(q)}$ is the q^{th} possible transmitted symbol from i^{th} antenna at user k.

Using MLJD, the transmitted signal vector associated with RAS is estimated based on the minimum distance criterion as

$$\widehat{\mathbf{V}} = \arg\min_{\mathbf{V}_q \in \boldsymbol{V}} \left\| \mathbf{r_s} - \mathbf{H_s V}_q \right\|^2 \;;\; q = 1, \dots, D \tag{5.26}$$

where $\boldsymbol{V} = \{\mathbf{V}_1, \dots, \mathbf{V}_q, \dots, \mathbf{V}_D\}$ is the set of all possible transmitted signal vectors.

The estimated signal vector $\hat{\mathbf{V}} = [\hat{\mathbf{v}}_1 \quad \cdots \quad \hat{\mathbf{v}}_K]^T \in \mathcal{C}^{u\times 1}$ will be remapped to the estimated users' data vector $\hat{\mathbf{b}} = [\hat{\mathbf{b}}_1 \quad \cdots \quad \hat{\mathbf{b}}_K]^T \in \mathcal{R}^{u\times 1}$.

For the considered system model, the following assumptions are considered unless otherwise stated:

1) Perfect power control and CSI are assumed at BS.
2) It is assumed that each user is subject to an individual power constraint of P_k which implies $\mathrm{tr}(\mathbf{Q}_k) \leq P_k$ where $\mathbf{Q}_k \triangleq \mathrm{E}\left[\mathbf{v}_k \mathbf{v}_k^{\mathrm{H}}\right]$ is transmit covariance matrix of k^{th} user.
3) Since CSI is not available at the transmitters, equal power allocation for each user is a robust transmission strategy in UL MU-MIMO system [24]. Then, $P_k = P/K; \forall k = 1, \ldots, K$ where P is the total power constraint and $\mathbf{Q}_k = P_k \mathbf{I}_{u_k}/u_k$.
4) The fading signals of $\mathbf{H}$ with correlated envelopes and independent phases are generated using ICT [141, 142] for desired correlation matrix of envelopes $\boldsymbol{\rho} \in \mathcal{R}^{um\times um}$. The entries of $\boldsymbol{\rho}$ represent the correlation factor ρ_{ij} between i^{th} and j^{th} fading signal envelope in the interval $[0, 1]$.
5) The channel fading rate is assumed to be much less than the data rate, so the channel remains constant over a frame of hundreds of symbols and changes independently from one frame to the next [29, 37, 177, 189].
6) Since the spatial DoF of UL MU-MIMO system associated with RAS is $\mathbb{N} = \min(u, m_s)$, up to $\mathbb{N}$ different data streams can be transmitted simultaneously and any further increase will give little contribution to the sum rate capacity [22, 195]. Therefore, impact of user scheduling is not included in this study by assuming that $u \leq m_s$ and the active users are perfectly synchronized.

5.4.2 Sum Rate Capacity Analysis of MU-MIMO with RAS

The optimal sum rate capacity for UL MU-MIMO system with constant channel is given as [24, 99]

$$R_{sum} = \max_{\sum_{k=1}^{K} \mathrm{tr}(\mathbf{Q}_k) \leq P} \left[\log_2 \left| \mathbf{I}_m + \frac{1}{\sigma_n^2} \sum_{k=1}^{K} \mathbf{H}_k \mathbf{Q}_k \mathbf{H}_k^{\mathrm{H}} \right| \right] \tag{5.27}$$

For equal power allocation, this capacity can be written as

$$R_{sum} = \log_2 \left| \mathbf{I}_m + \sum_{k=1}^{K} \frac{\Gamma}{u_k} \mathbf{H}_k \mathbf{H}_k^{\mathrm{H}} \right| \tag{5.28}$$

where $\Gamma = P/(K\sigma_n^2)$ is the average SNR. Therefore, the sum rate capacity associated with RAS can be written as

$$R_{sum}^{s} = \max_{\mathcal{s}_i \in \mathbb{S}} \left[\log_2 \left| \mathbf{I}_{m_s} + \sum_{k=1}^{K} \frac{\Gamma}{u_k} \breve{\mathbf{H}}_k(\mathcal{s}_i) \breve{\mathbf{H}}_k^{\mathrm{H}}(\mathcal{s}_i) \right| \right] \tag{5.29}$$

where the maximization is over the subset $\mathcal{s}_i \in \mathbb{S}$ for $\mathbb{S} = \{\mathcal{s}_1, \ldots, \mathcal{s}_i, \ldots, \mathcal{s}_{|\mathbb{S}|}\}$ representing the set of all possible subsets of receive antennas whose cardinality is $|\mathbb{S}| = \binom{m}{m_s}$, and $\breve{\mathbf{H}}_k(\mathcal{s}_i)$ is the selected channel matrix of user k corresponding to subset $\mathcal{s}_i$. At low SNR values or when the rank of $\breve{\mathbf{H}}_k(\mathcal{s}_i)$ is $\min(u_k, m_s) = 1$, this capacity can be approximated by

$$\begin{aligned} R_{sum}^{s} &\approx \max_{\mathcal{s}_i \in \mathbb{S}} \left[\log_2 \left(1 + \sum_{k=1}^{K} \frac{\Gamma}{u_k} \mathrm{tr}\{ \breve{\mathbf{H}}_k(\mathcal{s}_i) \breve{\mathbf{H}}_k^{\mathrm{H}}(\mathcal{s}_i) \} \right) \right] \\ &= \max_{\mathcal{s}_i \in \mathbb{S}} \left[\log_2 \left(1 + \sum_{k=1}^{K} \frac{\Gamma}{u_k} \left\| \breve{\mathbf{H}}_k(\mathcal{s}_i) \right\|_F^2 \right) \right] \end{aligned} \tag{5.30}$$

Hence, maximum R_{sum}^{s} is determined by total users' channel power due to individual contributions of each receive antenna. After some mathematical manipulations, it can be proved that

$$\sum_{k=1}^{K} \|\mathbf{H}_k\|_F^2 = \|\mathbf{H}\|_F^2 = \sum_{l=1}^{m} \|\mathbf{h}_l\|^2 \tag{5.31}$$

Therefore, sum rate capacity associated with RAS of subset $\mathcal{s}_i$ is determined by individual contributions of each receive antenna $\|\mathbf{h}_l\|^2$ to the related overall channel power $\|\mathbf{H_s}(\mathcal{s}_i)\|_F^2$. Same conclusion is valid for $\mathbf{H_s}(\mathcal{s}_i)$ with orthogonal rows due to the orthogonality of $\{\mathbf{H}_k\}_{k=1}^{K}$ rows (see Section 5.3.2). In this case, the sum rate capacity is decoupled into m_s antenna contributions and determined by the Euclidian norms of selected rows.

5.4.3 PDBS Algorithm for MU-MIMO

To overcome the shortcoming of NBS and OS algorithms, the proposed PDBS algorithm for SU-MIMO is extended in this subsection by utilizing the overall channel matrix $\mathbf{H} = [\mathbf{H}_1 \quad \cdots \quad \mathbf{H}_K] = [\mathbf{h}_1, \dots, \mathbf{h}_l, \dots, \mathbf{h}_m]^T$ of MU-MIMO. Therefore, selection of $\mathbf{H_s}(\mathcal{S}_i)$ is based on the largest Euclidean norms of channel matrix rows $\|\mathbf{h}_l\|;\ \forall l = 1, \dots, m$ with best phase differences $\boldsymbol{\theta}_l \to \boldsymbol{\theta}_l^*;\ \forall l = 1, \dots, m$ for higher contribution to $\|\mathbf{H_s}(\mathcal{S}_i)\|_F^2$. The maximum capacity associated with antenna selection can be written as

$$R_{sum}^{s} = \max_{\substack{\mathcal{S}_i \in \mathbb{S} \\ \boldsymbol{\theta}_l \to \boldsymbol{\theta}_l^*}} \left[\log_2 \left| \mathbf{I}_{m_s} + \sum_{k=1}^{K} \frac{\Gamma}{u_k} \breve{\mathbf{H}}_k(\mathcal{S}_i) \breve{\mathbf{H}}_k^{\mathrm{H}}(\mathcal{S}_i) \right| \right] \tag{5.32}$$

where the maximization is over $\mathcal{S}_i \in \mathbb{S}$ and $\boldsymbol{\theta}_l \to \boldsymbol{\theta}_l^*$. Due to the inherent phase shift between multiuser transmit antennas, this selection will provide a received vector $\mathbf{r_s}$ to the detection stage with highest SNR and constellations having maximum d_{min}. The proposed algorithm is as follows:

1) Define the set of receive antennas as, $\mathcal{X} = \{1, \dots, l, \dots, m\}$ with $l \in \mathcal{X}$ representing the l^{th} antenna.
2) Given the overall channel matrix $\mathbf{H} = [\mathbf{H}_1 \quad \cdots \quad \mathbf{H}_K] = [\mathbf{h}_1, \dots, \mathbf{h}_l, \dots, \mathbf{h}_m]^T$ where $\mathbf{h}_l;\ \forall l = 1, \dots, m$ is the l^{th} row.
3) For all l in $\mathcal{X}$, calculate the phase difference vector $\boldsymbol{\theta}_l$ and the power of channel vector h_l as $p_l = \|\mathbf{h}_l\|^2$.
4) From $\mathcal{X}$, construct two subsets of receive antennas as $\mathcal{X}_a$ from those satisfying $\boldsymbol{\theta}_l \to \boldsymbol{\theta}_l^*$ and the rest in $\mathcal{X}_b$. For each subset, sort the elements from highest to lowest power.
5) To select the best subset of antennas $\mathcal{S}_i$; choose the first m_s elements from $\mathcal{X}_a$. If the number of elements in $\mathcal{X}_a$ is less than m_s, complete the selection process from $\mathcal{X}_b$.
6) From the selected subset of receive antennas $\mathcal{S}_i$, construct $m_s \times u$ channel matrix $\breve{\mathbf{H}}_k(\mathcal{S}_i)$ associated with RAS for $k = 1, \dots, K$.

5.4.4 Computational Complexity

To evaluate the computational effort of proposed PDBS algorithm for MU-MIMO compared with that of OS and NBS, same total number of transmit antennas u, receive antennas m and RF chains m_s at the receive side is assumed in all schemes. So, the comparison is based on the selection of m_s from m available receive antennas.

For PDBS algorithm, calculations of um channel Euclidean norms and $m(u!/\{2!\ (u-2)!\})$ phase difference are required. Therefore, total of $m(u^2+u)/2$ calculations are used and the resulting complexity effort is of $\mathcal{O}(mu^2)$.

Using OS algorithm, optimal capacity is achieved by maximizing the following performance function

$$\mathcal{F}_{\text{OS}} := \arg\max_{\mathcal{s}_i \in \mathbb{S}} \left| \mathbf{I}_{m_s} + \sum_{k=1}^{K} \frac{\Gamma}{u_k} \breve{\mathbf{H}}_k(\mathcal{s}_i) \breve{\mathbf{H}}_k^{\text{H}}(\mathcal{s}_i) \right| \tag{5.33}$$

In this method, capacity of $m_s \times u_k$ selected channel matrices of K active users with $\mathcal{O}(m_s^3)$ SVD requirement over all possible $m!/\{m_s!\ (m-m_s)!\}$ combinations of $\mathcal{s}_i \in \mathbb{S}$ has to be calculated. As a result, exhaustive computations of $\mathcal{O}[m_s^3\, m!/\{m_s!\ (m-m_s)!\}]$ is needed [179, 185].

For NBS algorithm, selection of m_s receive antennas is based on the corresponding rows of overall channel matrix **H** with the largest Euclidean norm. Therefore, the capacity is maximized by maximizing the following performance function

$$\mathcal{F}_{\text{NBS}} := \arg\max_{\mathcal{s}_i \in \mathbb{S}} \sum_{k=1}^{K} \left\| \breve{\mathbf{H}}_k(\mathcal{s}_i) \right\|_F^2 = \arg\max_{\mathcal{s}_i \in \mathbb{S}} \|\mathbf{H}_{\mathbf{s}}(\mathcal{s}_i)\|_F^2 \tag{5.34}$$

The complexity of this method is of $\mathcal{O}(um)$ due to the requirement of vector norm calculations over all m channel matrix rows each of u elements.

As can be seen, the computational efforts are similar to that shown In Table 5.1 for single user case where the main computational burden of OS method comes from matrix rather than vector calculations as in PDBS and NBS. The complexity of PDBS is significantly less than OS and slightly higher than NBS. Hence, a valuable tradeoff between the system performance and complexity can be achieved.

5.4.5 Simulation Results

Monte Carlo simulations using MATLAB/7.9 for UL MU-MIMO system have been carried out in this section to validate the capacity and BER performance of PDBS algorithm compared with that of OS and NBS. For simplicity and without loss of generality, we consider a system of two users $(K=2)$ each equipped with two transmit antennas $(u_k=2,\ k=1,\ 2)$ communicating simultaneously with one BS equipped with $m=5$ and 6 antennas and $m_s = u = \sum_1^K u_k = 4$ RF chains. It will be represented for notational convenience as $u \times$

$m/algorithm\text{-}m_s$ while the reference baseline MU-MIMO without RAS will be represented as $u \times m$ system. To demonstrate the effects of channel correlation, we consider equal correlation among different Rayleigh fading paths as $\rho_{ij} = \rho\ ;\ \forall i \neq j;\ i,j = 1, \ldots, um$. In the simulations, three different cases are used; $\rho = 0.0$ for uncorrelated channels, $\rho = 0.5$ for moderate correlation, and $\rho = 0.9$ for high correlation level. The results are averaged using 10,000 channel realization for channel capacity evaluation. For BER performance, MLJD detection is employed for all considered systems and a frame of 100 symbols from BPSK constellation is assumed for each channel realization.

In Fig. 5.13, sum rate capacity results over different correlation levels are shown for 4×6/PDBS-4 in bit/s/Hz compared with 4×6/NBS-4 and 4×6/OS-4. Theoretical sum rate bounds for the reference 4×4 system are shown also for comparison. As can be seen, the sum rate capacity with RAS is higher than 4×4 system due to 2 extra receive antennas (spatial dimension). As SNR and/or correlation level ρ increased, the gain is increased substantially. Furthermore, OS algorithm provides stable performance compared with NBS algorithm for all ρ values. In this case, performance of PDBS is very close to OS and very little affected by ρ while outperform NBS for any SNR, specifically at moderate to high values. At low SNR and ρ levels, all RAS methods are optimal while different performance is achieved at moderate to high levels. For example, at spectral efficiency of 26 bit/s/Hz and compared with 4×4 system for uncorrelated channel ($\rho = 0.0$), 1.8dB gain is achieved for PDBS while 1.9dB for OS and 1.2dB for NBS. So, PDBS has only 0.1dB difference in SNR from OS while outperform NBS by 0.6dB. For high correlation of $\rho = 0.9$, the achieved gain is increased to 7.5dB for PDBS compared to 7.8dB for OS and 6.4dB for NBS. Therefore, PDBS has 0.3dB difference in SNR from OS and outperform NBS by 1.1dB. Summery of these results are shown in Table 5.3.

Table 5.3: SNR gain in dB for 4×6/NBS-4, 4×6/PDBS-4, and 4×6/OS-4 systems compared with the reference 4×4 at spectral efficiency of 26 bit/s/Hz for uncorrelated ($\rho = 0.0$) and highly correlated channel ($\rho = 0.9$)

Correlation (ρ)	SNR Gain (dB)		
	4×6/NBS-4	4×6/PDBS-4	4×6/OS-4
0.0	1.2	1.8	1.9
0.9	6.4	7.5	7.8

To investigate the effect of number receive antennas m on the sum rate capacity for fixed number of RF chains (m_s), Fig. 5.14 show the performance 4×5/PDBS-4 compared with 4×5/NBS-4, 4×5/OS-4, and the reference 4×4 system. At spectral efficiency of 26 bit/s/Hz with one additional receive antenna compared with 4×4 system for uncorrelated channel, 1.1dB gain is achieved for PDBS while 1.3dB for OS and 0.7dB for NBS. So, PDBS has only 0.2dB difference in SNR from OS while outperform NBS by 0.4dB. For high correlation of $\rho = 0.9$, the achieved gain is increased to 6.8dB for PDBS while 7.2dB for OS and 6.3dB for NBS. Therefore, PDBS has 0.4dB difference in SNR from OS and outperform NBS by 0.5dB. As seen from these results, PDBS algorithm provides higher gain than NBS and close results to the OS. Hence, higher capacity is achieved by increasing the number of low cost antennas m and using PDBS for the available number of RF chains.

In Table 5.4, sample results of sum rate capacity in bit/s/Hz at SNR of 20dB are shown for 4×6/PDBS-4 compared with 4×6/NBS-4, 4×6/OS-4, and the reference 4×4 system. Capacity gain is shown also with the average user rate $R_{av} = R_{sum}/K$ for 4×4 system of 2 users. For example, the gain in bit/s/Hz of PDBS using $\rho = 0.9$ is 8.7 while 7.2 for NBS and 8.8 for OS. In addition to near optimal performance with low complexity, the achieved gain of PDBS is higher than 7.8 for average user rate in 4×4 system. Therefore, maximum user capacity can be maintained indirectly by exploiting few extra spatial dimensions provided by additional antennas to mitigate the channel correlation effects.

Table 5.4: Sum rate results in bit/s/Hz for MU-MIMO system with and without RAS at SNR = 20dB for different correlation values

Correlation (ρ)	R_{sum} of 4×4	R_{sum}^{s} of 4×6/*algorithm*-4			Gain of 4×6/*algorithm*-4			$R_{av} = R_{sum}/K$
		NBS	PDBS	OS	NBS	PDBS	OS	
0.0	22.2	23.6	24.35	24.4	1.4	2.15	2.2	11.1
0.5	20.6	23.2	24.32	24.4	2.6	3.72	3.8	10.3
0.9	15.6	22.8	24.30	24.4	7.2	8.70	8.8	7.8

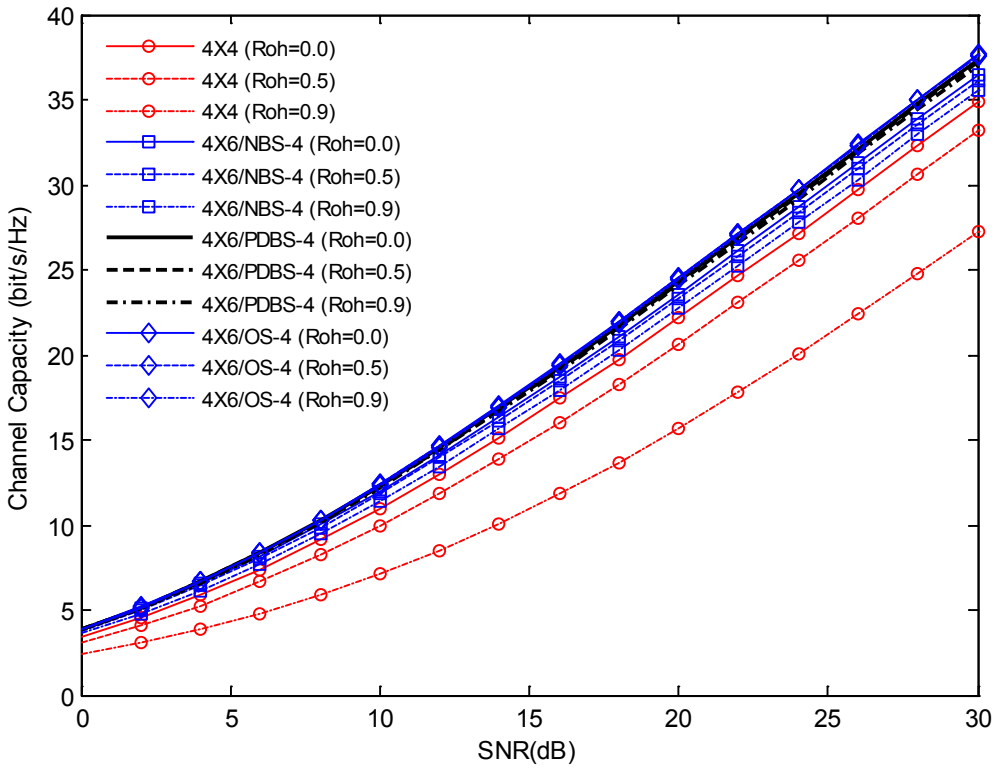

Figure 5.13: Sum rate capacity of 4 × 6/PDBS-4 over CRFC compared with 4 × 6/NBS-4, 4 × 6/OS-4, and the reference 4 × 4 system.

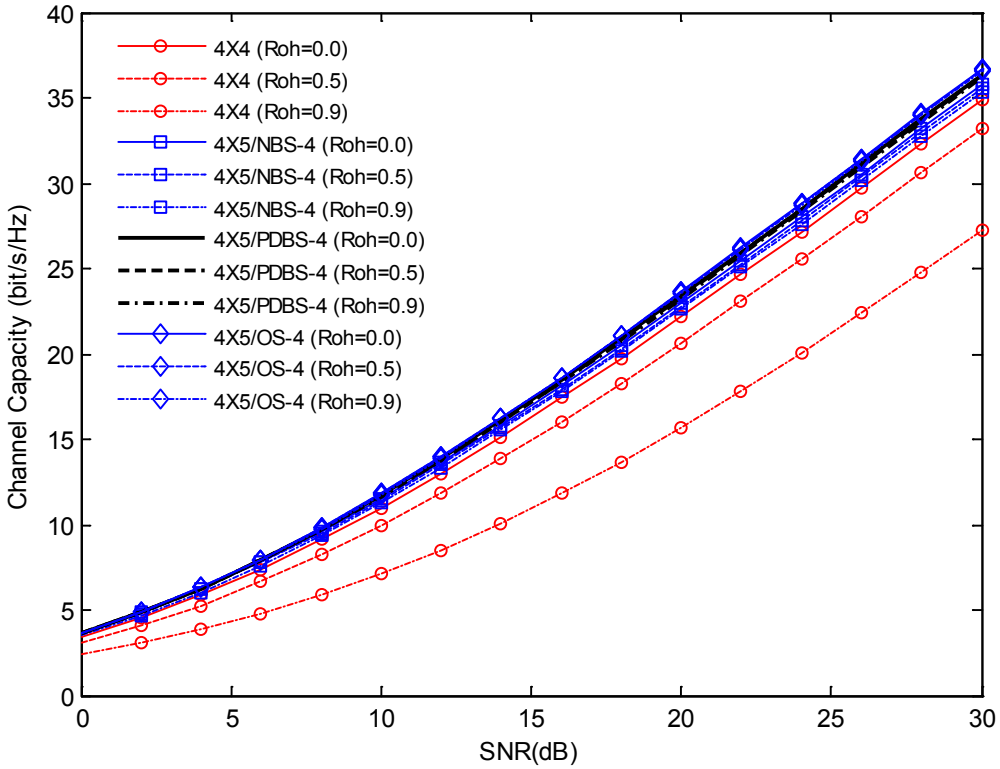

Figure 5.14: Sum rate capacity of 4 × 5/PDBS-4 over CRFC compared with 4 × 5/NBS-4, 4 × 5/OS-4, and the reference 4 × 4 system.

In Fig. 5.15, BER results over different channel correlations for 4×6/PDBS-4 is depicted compared with 4×6/NBS-4 and the reference 4×4 and 1×4/MRC systems. As can be seen, while the correlations degrade the performance of 4×4 system, it has the opposite effect for the system with RAS. For example, at BER of 10^{-6} and compared with the 4×4 system for uncorrelated channel, 4.2dB gain is achieved for PDBS while 3.2dB for NBS. Therefore, PDBS outperforms NBS by 1.0dB. For highly correlated channels of $\rho = 0.9$, gain of 17.2dB is achieved for PDBS while 16.0dB for NBS. Hence, PDBS outperforms NBS by 1.2dB. Performance of PDBS outperforms that of NBS for all channel correlation levels and as the channel correlation increased, the performance gain is increased. From the similarity in results with SU-MIMO systems, higher gain is achieved as m and/or m_s increased.

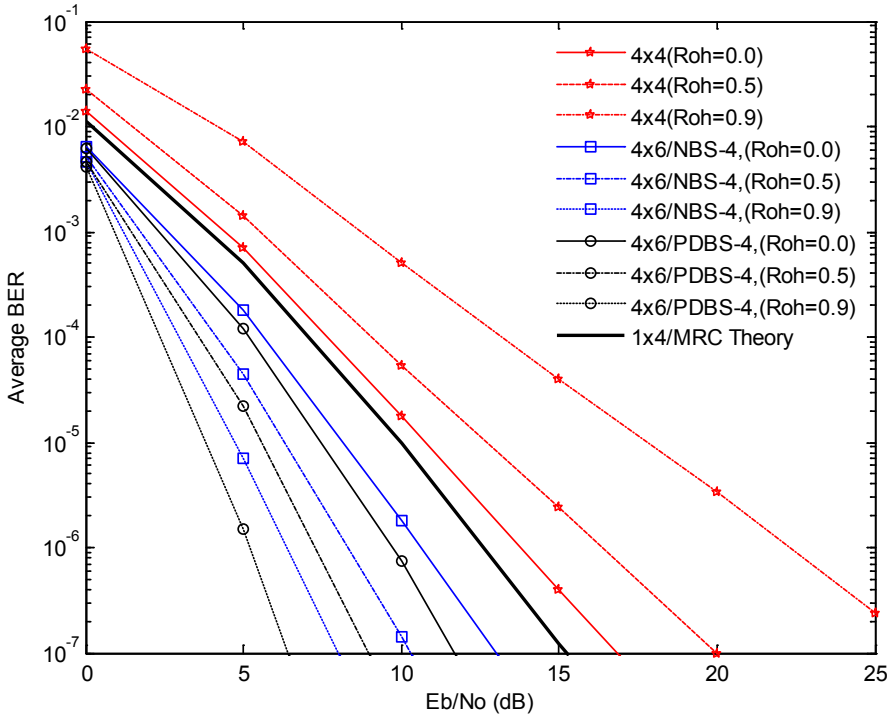

Figure 5.15: BER performance of 4×6/PDBS-4 over CRFC compared with 4×6/NBS-4 and the reference 4×4 and 1×4/MRC systems.

5.5 RAS for MIMO Systems with Imperfect Channel Estimation

Exploiting the advantages offered by wireless MIMO communication systems are crucially depends on the CSI available at the link ends [89, 144, 146, 200]. CSI is usually estimated at the receiver and completely or partially fed back to the transmitter according to the system requirements. In the literature, there are different methods for channel estimation of MIMO systems such as the simple conventional training-based channel estimation [144, 146, 201-203],

blind channel estimation [204], and semi-blind channel estimation [205-208]. To reduce the loss in system throughput due to training overhead, blind techniques for joint channel and data detection are used at the cost of high computational complexity, slower convergence, and/or lower accuracy. Semi-blind techniques are simpler than blind methods at the cost of using few training symbols. Perfect channel estimation using any of the aforementioned methods is a difficult task in multiantenna systems due to the large number of channel parameters to be estimated [208]. Therefore, imperfect CSI at BS receiver is considered in this subsection to investigate its impact on the capacity and error performance of SM multiantenna systems employing PDBS algorithm for RAS.

5.5.1 Channel Model

For SU-MIMO as well as MU-MIMO systems, the overall true $m \times u$ channel matrix $\mathbf{H}$ is considered to represent the fading signals from total u transmit antennas to m receive antennas. The estimated channel matrix will be represented as [89, 189]

$$\widetilde{\mathbf{H}} = \mathbf{H} + \mathbf{E} \tag{5.35}$$

where $\mathbf{E} \in \mathcal{C}^{m \times u}$ is $m \times u$ channel error matrix of complex Gaussian entries with zero mean and σ_{mse}^2 variance. The channel mean square error (MSE) will be represented in dB as

$$\text{MSE} = 10 \log_{10}(\sigma_{mse}^2) \tag{5.36}$$

5.5.2 Channel Capacity

Under equal power allocation conditions when CSI is not available at the transmitter, the lower bound capacity of fixed channel with imperfect estimation can be represented as [89]

$$C^{lower} = \log_2 \left| \mathbf{I}_m + \frac{\Gamma/u}{1 + \sigma_{mse}^2 \Gamma} \widetilde{\mathbf{H}} \widetilde{\mathbf{H}}^{\mathrm{H}} \right| \tag{5.37}$$

Therefore, lower bound of capacity with imperfect channel condition and RAS can be written as

$$C_s^{lower} = \max_{\substack{\mathcal{s}_i \in \mathbb{S} \\ \boldsymbol{\theta}_l \to \boldsymbol{\theta}_l^*}} \left[\log_2 \left| \mathbf{I}_{m_s} + \frac{\Gamma/u}{1 + \sigma_{mse}^2 \Gamma} \widetilde{\mathbf{H}}_{\mathbf{s}}(\mathcal{s}_i) \widetilde{\mathbf{H}}_{\mathbf{s}}^{\mathrm{H}}(\mathcal{s}_i) \right| \right] \tag{5.38}$$

where the maximization is over subset $\mathcal{s}_i \in \mathbb{S}$ and $\boldsymbol{\theta}_l \to \boldsymbol{\theta}_l^*$ for $\mathbb{S} = \{\mathcal{s}_1, \ldots, \mathcal{s}_i, \ldots, \mathcal{s}_{|\mathbb{S}|}\}$ representing the set of all possible subsets of receive antennas, and $\widetilde{\mathbf{H}}_{\mathbf{s}}(\mathcal{s}_i)$ is selected channel matrix according to $\mathcal{s}_i$.

5.5.3 Simulation Results

In order to evaluate the performance of PDBS algorithm with different channel estimation errors, Monte Carlo simulations using MATLAB/7.9 for SM multiantenna system have been carried out in this section. For simplicity and without loss of generality, we consider $m \times u$ uncorrelated channel matrix **H**. The simulated results are averaged using 10,000 channel realization for channel capacity evaluation. For BER performance, MLJD detection is employed for all considered systems and a frame of 100 symbols from BPSK constellation is assumed for each channel realization.

In Fig. 5.16, lower bound capacity (5.38) with perfect and imperfect channel estimation is shown for 2×6/PDBS-2 system. For imperfect channel estimation, MSE of -30dB, -20dB, and -10dB are used. As can be seen, the channel capacity is degraded as the MSE increased, specifically at high SNR. At low to moderate SNR, the noise components at the receiver are more dominant than channel gain components. Hence, the estimation error has less impact to the capacity.

In Fig. 5.17, BER performance with perfect and imperfect channel estimation is shown for 2×6/PDBS-2 system. MSE of -30dB, -20dB, and -10dB are used for imperfect channel estimation. As the MSE increased, the BER performance is decreased, specifically at high SNR. By decreasing the number of receive antennas from $m = 6$ to $m = 4$, the performance loss for same MSE will be more as shown in Fig. 5.18. For example, the performance loss at BER of 10^{-4} and MSE of -20dB is 1.2dB for $m = 6$ compared to 2dB for $m = 4$. Therefore, RAS for a limited m_s RF chains can provide a good immunity to channel estimation errors, specifically as m increased.

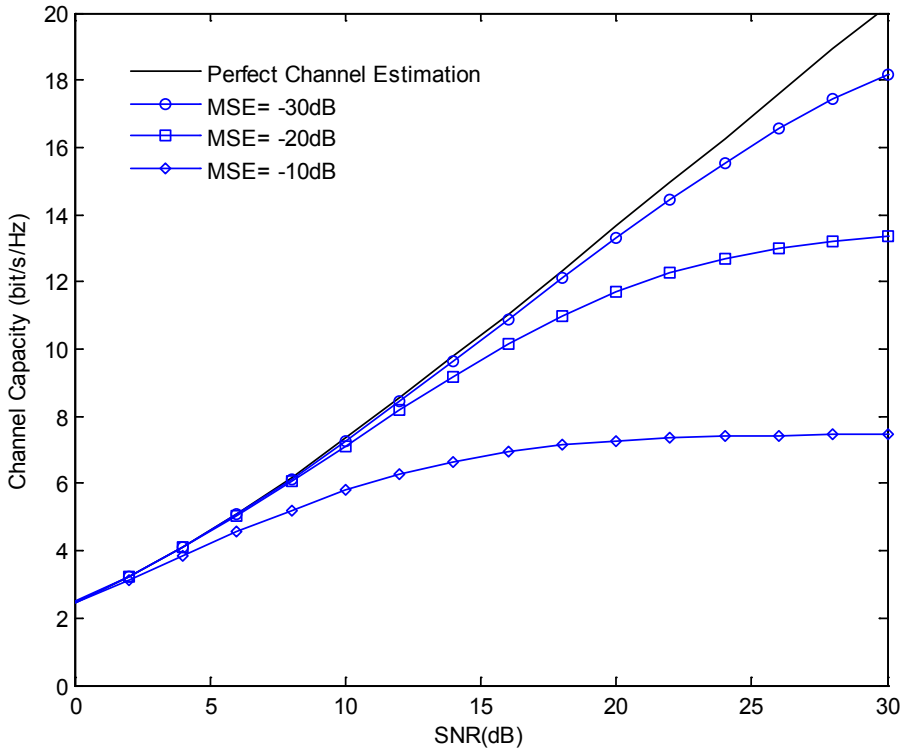

Figure 5.16: Lower bound of 2×6/PDBS-2 system capacity over uncorrelated channel with different values of channel estimation errors.

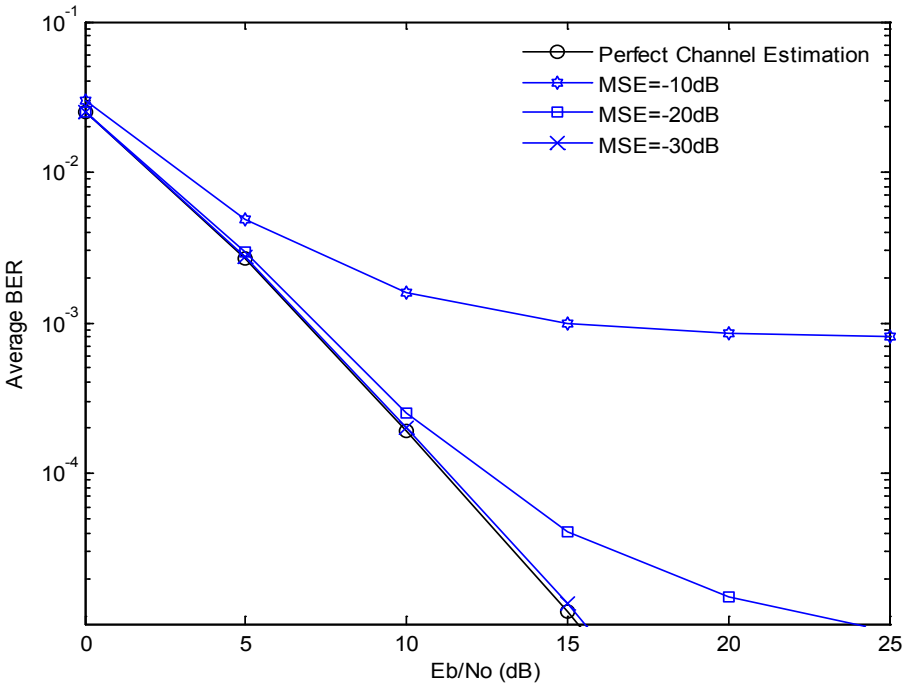

Figure 5.17: BER performance of 2×6/PDBS-2 system over uncorrelated channel with different values of channel estimation errors.

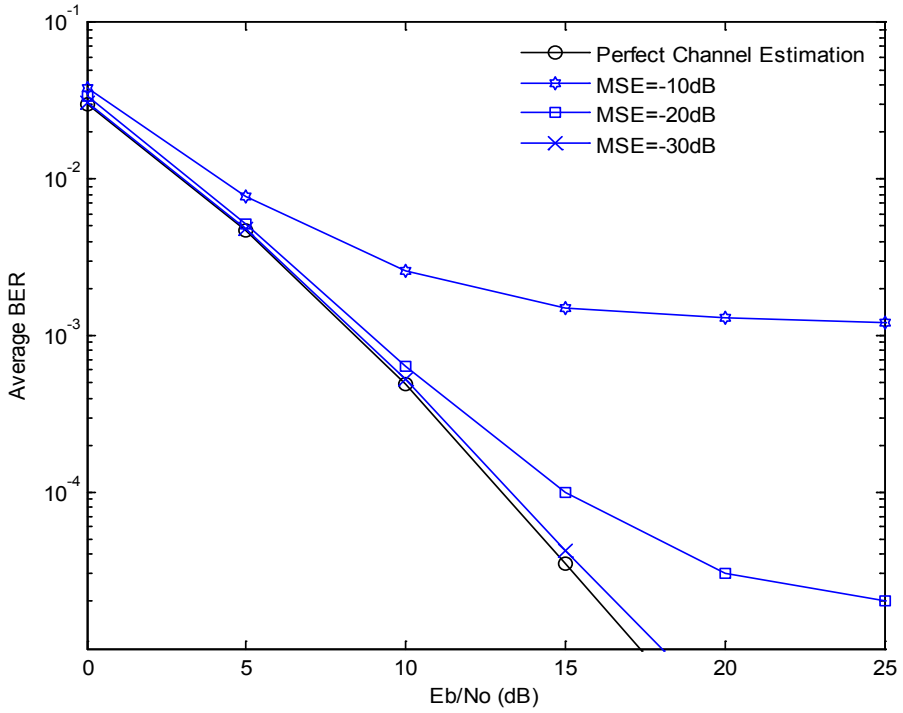

Figure 5.18: BER performance of 2×4/PDBS-2 system over uncorrelated channel with different values of channel estimation errors.

5.6 Conclusions

To meet the increasing demands of modern communication service in bandwidth constrained resource, a novel and efficient RAS algorithm is proposed in this chapter to maximize the channel capacity of single and multiuser MIMO over CRFC environment. The proposed PDBS takes the advantages of NBS and OS methods to provide a competitive performance near to OS with significant reduction in complexity. It exploits the Euclidean norm of channel matrix rows with their corresponding phase difference for the selection task. Without an exhaustive search over all possible antenna combinations and capacity calculations as in OS algorithm, the complexity of PDBS method is of $\mathcal{O}(mu^2)$ vector calculations. Due to this advantage, it is also higher performance and less complex than SCBS method [188] which requires correlation matrix calculations of $\mathcal{O}(m^2)$. Furthermore, it utilizes the principles of signal constellation to tackles the effect of channel correlation on the ergodic capacity rather than maximizing the data rate and error performance of specific linear receivers as in [182].

Extensive analysis and simulations results demonstrate the effectiveness of proposed method. It is shown that the capacity and BER performance using PDBS algorithm outperforms NBS and close to OS algorithm for any SNR and correlation values ρ. Furthermore, it shows more robust performance in correlated environment compared with NBS and conventional systems without RAS. The gain of PDBS is depend on the number of receive antennas m and

number of selected antennas (RF chains) m_s. As m and/or m_s increases, the capacity and BER gains are increased significantly. Furthermore, RAS using PDBS maintains high user capacity for MU-MIMO systems over correlated channels. It provides a robust solution for users with highly correlated channels instead of terminating them as in conventional systems.

For imperfect channel estimation conditions, MIMO systems suffer from high performance degradation, specifically at high SNR. However, providing more receive antennas (m) than the available RF chains (m_s) with RAS has the effect to reduce the performance loss. This low complexity and cost technique provides fast RAS to capture most of the large gains promised by single and multiuser MIMO systems.

In the last contributing chapter, new scheme is introduced to increase the user capacity of MU-MIMO beyond the limit of available number of RF chains with low complexity.

Chapter 6

High User Capacity Group Layered MU-MIMO (GL-MU-MIMO) System

6.1 Introduction

MU-MIMO represent one of the promising and feasible techniques to meet the increasing number of clients and their demands for various wireless services such as internet and media rich applications. However, the maximum number of allowed users is critically limited by the number of receive antennas associated with RF chains at the BS or the high complexity burden of MUD methods.

In this chapter, a novel GL-MU-MIMO scheme is proposed to exploit the available bandwidth for high user capacity with affordable complexity. It takes the advantages of spatial difference among users and power control at BS to increase the number of users beyond the available number of RF chains by dividing them into two groups according to their received power, HPG and LPG. In Rayleigh fading environment, different low complexity GL-MUD configurations, group power allocation, number of receive antennas at BS, and RAS algorithms are utilized to provide a valuable tradeoff between complexity and overall system performance. Through extensive simulations, the results demonstrate the effectiveness of proposed scheme compared with the conventional MU-MIMO systems. It shows a substantial increase in the user and sum rate capacity at target BER performance and SNR values. Furthermore, it provides fair rate distribution among users.

This chapter is organized as follows. Literature review on overloaded MU-MIMO systems are presented in Section 6.2. In Section 6.3, GL-MU-MIMO scheme with the signal model and different GL-MUD configurations with its complexity analysis are given. In Section 6.4, capacity analysis for GL-MU-MIMO scheme is presented. It includes the user capacity, sum rate capacity, and capacity region. In Section 6.5, two proposed algorithms for RAS are introduced with the complexity analysis. Simulation results of GL-MU-MIMO over uncorrelated channel environment with/without RAS are presented in Section 6.6. It includes sum rate capacity, capacity region, and BER performance. In Section 67, GL-MU-MIMO over correlated fading channel is investigated and simulation results for sum rate capacity and BER performance are given. Finally, chapter conclusions are withdrawn in the last section.

6.2 Literature Review

In wireless MU-MIMO systems, the maximum number of users (K) with multiple antennas that can be supported is limited by total DoF represented by the available number of BS antennas (m) connected with RF chains [84]. Therefore, scheduling techniques are employed to exploit the multiuser diversity when the sum of users' antennas is larger than the BS antennas [19, 108]. Moreover, MUD methods employed at BS receiver has direct impact on the maximum number of users that can be supported in the MAC.

By utilizing linear MUD with user equipment equipped with single antenna, up to $K \leq m$ users can be supported simultaneously [12, 17, 18]. In the literature, it is well known that linear MUD schemes such as ZF, MMSE and V-BLAST are capable to provide limited performance at low detection complexity [102, 210, 211, 216, 218]. However, in *rank-deficient* scenario (overloaded systems when $K > m$), the channel matrix becomes noninvertible reducing the DoF required for signal detection.

In contrast, nonlinear MUD schemes such as ML can increase the user capacity by supporting more number of users than BS antennas m with optimal performance [84, 92, 93]. It utilizes the available radio spectrum efficiently at the cost of high computational complexity which increases exponentially with the number of supported users K. Due to the complexity issue, practical implementation of the optimal ML detector in overloaded system scenarios is prohibitive. Therefore, many suboptimal nonlinear MUD schemes have been developed such as SIC [119, 212], PIC [12], SD family [109-112], iterative groupwise detection [213], and MUD techniques based MBER algorithms [113-115] as well as GA [12, 113]. Although complexity of suboptimal MUD methods is less than the optimal ML detection, they are currently still more complex than linear MUD schemes.

To increase the number of DoF represented by m BS antennas for overloaded systems, same number of m costly RF chains is required. Therefore, increasing the number of RF chains to support additional users is practically prohibited in terms of hardware requirements, system complexity, consumed power and size. In relation to this point, however, a promising diversity technique referred to as *antenna selection* has been proposed in the last few years to capture most of the capacity promised by multiantenna systems with low cost [20, 175]. This technique is intensively investigated in the previous chapter for single [179, 181, 187] and multiuser [22, 189, 192] systems to maximize the channel and sum rate capacity, respectively. Since extra antenna elements, RF switches, and digital signal processing are usually inexpensive, the gain of antenna selection can be achieved with additional low cost by choosing the best subset of transmit and/or receive antennas and connect them with the available RF chains. It has been shown that multiantenna system with OS can significantly outperform a system without selection using same number of RF chains [178, 185].

User overloading (or extending cell capacity) based on *users grouping* to share the same signal space dimension (DoF) has been investigated also for different multiple access schemes such as [47, 67, 214, 215, 125, 216-218]. In [47, 214, 215], a higher number of users K than the spreading factor N of OCDMA can be accommodated with small SNR penalty by using OCDMA for the group of first N users and augment it with PN-CDMA or TDMA for the group of additional users. At the receiver, iterative multistage detection is employed to cancel the interference between the two groups. In [67], S-C is employed also by taking the advantage of power disparities among users to share a group of users with single spreading sequence of OCDMA. In [125], improving the user capacity of OCDMA systems has been considered by employing multiple antennas at the transmitters and receiver with linear MUD techniques. Also, collaborative spreading is used recently in [216-218] to share the same spreading sequence among group of more than one user. At the receiver, group despreading followed by low complexity MLJD is carried out to recover the co-spread users' data.

For efficient spectrum utilization, new design approaches for MU-MIMO systems are of high interest to achieve high user capacity with affordable complexity and target BER performance. In the next sections, a novel GL-MU-MIMO scheme is designed to increase the user capacity beyond the available number of RF chains. By taking the possibility of power control at the BS and according to the path loss advantage inherent in the cellular systems due to the spatial difference among users, the total number of active users K is divided into two groups, HPG and LPG. To maintain the channel rank condition, the maximum allowed number of users in each group is determined by the available number of RF chains which leads to duplicate the user capacity compared with conventional MU-MIMO. At the receive side, GL-MUD is utilized for the selected received superimposed group signals in a layered fashion. Signal of HPG are detected in the first stage with high reliability by assuming LPG as interference signals. In the seconde stage, the re-encoded users' data of HPG will be subtracted from the selected received signals using group SIC (GSIC) to remove its interference, which improves the LPG signal detection. RAS diversity is integrated to increase the capacity and improve the error performance by using two antenna selection methods, NBS and novel HPG-PDBS.

6.3 GL-MU-MIMO System

In this section, GL-MU-MIMO is proposed for the following objectives; 1) increase the user capacity for UL MU-MIMO cellular system using the available number of RF chains at BS, 2) substantially reduces the complexity of MUD at BS receiver compared with the optimal ML detection and 3) maintain good error performance for different channel conditions.

6.3.1 Signal Model

Consider an overloaded MU-MIMO system of K active mobile users communicating simultaneously over flat Rayleigh fading MAC with one common BS as in Fig. 6.1. Each of the mobile user equipment has a single antenna while the BS receiver which equipped with m antennas and m_s RF chains employs RAS to select the best subset of antennas $m_s \leq m$ according to their channel conditions. Since the total DoF is limited by m_s RF chains, the considered total number of active users $K \leq 2m_s$ is divided into two groups based on their received signal powers. HPG includes the first $T = m_s$ users with low channel path loss condition (e.g. users near the BS) while LPG contains the additional $U = (K - T) \leq m_s$ users whose channel path loss conditions are high compared with the former (e.g. users near the cell edge). Assuming total average received power constrain of P, the received signal power of HPG users P_H and of LPG users P_L are given as

$$P_H = (1 - \eta)P \tag{6.1}$$

$$P_L = \eta P = \frac{\eta}{1 - \eta} P_H \tag{6.2}$$

$$P = P_H + P_L \tag{6.3}$$

where $\eta;\ 0 < \eta < 0.5$ is the power allocation ratio maintained by the power control at BS.

The received signal vector by m receive antennas is represented as

$$\mathbf{r} = \sum_{k=1}^{T} \mathbf{h}_k v_k + \sum_{k=T+1}^{K} \mathbf{h}_k v_k + \mathbf{n} = \mathbf{s}_H + \mathbf{s}_L + \mathbf{n} \tag{6.4}$$

where $\mathbf{r} = [r_1 \quad \cdots \quad r_m]^T \in \mathcal{C}^{m \times 1}$ is $m \times 1$ received signal vector, $\mathbf{h}_k = [h_{k1} \quad \cdots \quad h_{km}]^T \in \mathcal{C}^{m \times 1}$ is $m \times 1$ channel vector of user k whose entries $h_{kl} = x_{kl} + jz_{kl},\ l = 1, \ldots, m$ are zero mean unit variance complex fading coefficient between user k and l^{th} receive antenna, x_{kl} and z_{kl} are in-phase and quadrature components of zero mean Gaussian random processes each with variance 0.5, v_k is transmitted signal of user k subject to power constraint p_k and modulated from equiprobable data b_k, $\mathbf{n} = [n_1 \quad \cdots \quad n_m]^T \in \mathcal{C}^{m \times 1}$ is $m \times 1$ i.i.d AWGN vector with elements having zero mean and variance σ_n^2, $\mathbf{s}_H \in \mathcal{C}^{m \times 1}$ is $m \times 1$ superimposed signal vector of HPG users over their entire channels, $\mathbf{s}_L \in \mathcal{C}^{m \times 1}$ is $m \times 1$ superimposed signal vector of LPG users over their entire channels.

The overall $m \times K$ channel matrix $\mathbf{H} \in \mathcal{C}^{m \times K}$ of GL-MU-MIMO system can be represented as

$$\mathbf{H} = [\mathbf{h}_1 \ \cdots \ \mathbf{h}_k \ \cdots \ \mathbf{h}_K] = \begin{bmatrix} h_{11} & \cdots & h_{k1} & \cdots & h_{K1} \\ \vdots & \ddots & \vdots & \ddots & \vdots \\ h_{1l} & \cdots & h_{kl} & \cdots & h_{Kl} \\ \vdots & \ddots & \vdots & \ddots & \vdots \\ h_{1m} & \cdots & h_{km} & \cdots & h_{Km} \end{bmatrix} = \begin{bmatrix} \underline{\mathbf{h}}_1 \\ \vdots \\ \underline{\mathbf{h}}_l \\ \vdots \\ \underline{\mathbf{h}}_m \end{bmatrix} \tag{6.5}$$

where $\underline{\mathbf{h}}_l = [h_{1l} \ \cdots \ h_{kl} \ \cdots h_{Kl}] \in \mathcal{C}^{1 \times K}, \forall l = 1, \ldots, m$ is the l^{th} row of $\mathbf{H}$ corresponding to the l^{th} receive antenna. The Rayleigh distributed envelope of channel component h_{kl} is the magnitude $\alpha_{kl} = |h_{kl}|$ and $\beta_{kl} = \tan^{-1}(z_{kl}/x_{kl})$ is the uniform distribution phase over $[0, 2\pi]$. The overall channel matrix $\mathbf{H}$ can be represented also in terms of HPG channel matrix $\mathbf{H}_H \in \mathcal{C}^{m \times T}$ and LPG channel matrix $\mathbf{H}_L \in \mathcal{C}^{m \times U}$ as

$$\mathbf{H} = [\mathbf{H}_H \ \mathbf{H}_L] = \begin{bmatrix} h_{11} & \cdots & h_{T1} & h_{T+1\,1} & \cdots & h_{K1} \\ \vdots & \ddots & \vdots & \vdots & \ddots & \vdots \\ \underbrace{h_{1m} \quad \cdots \quad h_{Tm}} & & & \underbrace{h_{T+1\,m} \quad \cdots \quad h_{Km}} & & \end{bmatrix} = \begin{bmatrix} \mathbf{h}_1^{(H)} & \mathbf{h}_1^{(L)} \\ \vdots & \vdots \\ \mathbf{h}_l^{(H)} & \mathbf{h}_l^{(L)} \\ \vdots & \vdots \\ \mathbf{h}_m^{(H)} & \mathbf{h}_m^{(L)} \end{bmatrix} = \begin{bmatrix} \underline{\mathbf{h}}_1 \\ \vdots \\ \underline{\mathbf{h}}_l \\ \vdots \\ \underline{\mathbf{h}}_m \end{bmatrix} \tag{6.6}$$

where $\mathbf{h}_l^{(H)} = [h_{1l} \ \cdots \ h_{Tl}] \in \mathcal{C}^{1 \times T}$ and $\mathbf{h}_l^{(L)} = [h_{T+1\,l} \ \cdots \ h_{Kl}] \in \mathcal{C}^{1 \times U}$ are the l^{th} rows of $\mathbf{H}_H$ and $\mathbf{H}_L$ corresponding to the l^{th} receive antenna. Therefore, the received signal in equation (6.4) can be rewritten as

$$\mathbf{r} = \mathbf{H}_H \mathbf{v}_H + \mathbf{H}_L \mathbf{v}_L + \mathbf{n} \tag{6.7}$$

where $\mathbf{v}_H = [v_1 \ \cdots \ v_T]^T \in \mathcal{C}^{T \times 1}$ and $\mathbf{v}_L = [v_{T+1} \ \cdots \ v_K]^T \in \mathcal{C}^{U \times 1}$ are the transmitted signal vectors of HPG and LPG users, respectively.

The received signal vector $\mathbf{r_s}$ associated with the selection of m_s from m receive antennas is given by

$$\mathbf{r_s} = \sum_{k=1}^{T} \breve{\mathbf{h}}_k v_k + \sum_{k=T+1}^{K} \breve{\mathbf{h}}_k v_k + \mathbf{n_s} = \breve{\mathbf{H}}_H \mathbf{v}_H + \breve{\mathbf{H}}_L \mathbf{v}_L + \mathbf{n_s} = \breve{\mathbf{s}}_H + \breve{\mathbf{s}}_L + \mathbf{n_s} \tag{6.8}$$

where, $\mathbf{r_s} \in \mathcal{C}^{m_s \times 1}$ denotes the selected received signal vector, $\breve{\mathbf{H}}_k \in \mathcal{C}^{m_s \times 1}$ and $\mathbf{n_s} \in \mathcal{C}^{m_s \times 1}$ denote the k^{th} user channel matrix and the noise vector after selection, $\breve{\mathbf{H}}_H$ and $\breve{\mathbf{H}}_L$ are the HPG and LPG channel matrices associated with antenna selection, $\breve{\mathbf{s}}_H \in \mathcal{C}^{m_s \times 1}$ and $\breve{\mathbf{s}}_L \in \mathcal{C}^{m_s \times 1}$ are

the superimposed signal vector of HPG users and LPG users over their entire channels and associated with antenna selection.

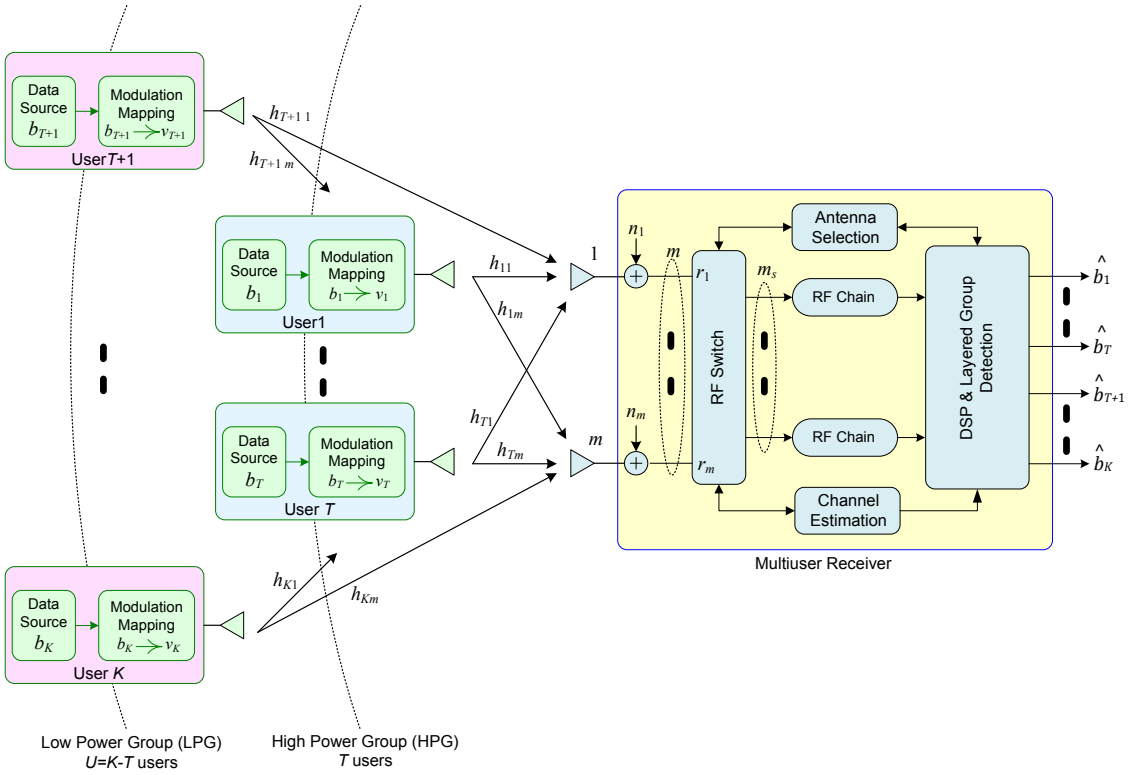

Figure 6.1: System model for GL-MU-MIMO system of K active mobile users and one common BS receiver with RAS technique.

For the given signal model, the following assumptions are considered:

1) Perfect CSI is assumed at the BS receiver.
2) The channel fading rate is assumed to be much less than the data rate. The channel remains constant over a frame of hundreds of symbols and changes independently from one frame to the next [29, 37, 177, 189].
3) Impact of user scheduling is not included by assuming that $K \leq 2m_s$ and the active users are perfectly synchronized.
4) Since CSI is not available at the transmitters, equal power allocation for users in each group is assumed. Hence, $\{p_k = P_H/T\}_{k=1}^{T}$ for HPG users and $\{p_k = P_L/U\}_{k=T+1}^{K}$ for LPG users.

6.3.2 Group Layered MUD (GL-MUD)

Taking the advantage of power disparity between HPG and LPG, GL-MUD is designed for the BS receiver by using different linear/nonlinear group MUD configurations with GSIC as shown in Fig. 6.2. In the first detection layer, the selected received signal $\mathbf{r_s}$ is processed by HPG-MUD using ZF or ML receiver to estimate the data of HPG users $\hat{b}_k, k = 1, \ldots, T$ while treating LPG signals as a background noise. The estimated data of HPG are then re-modulated and multiplied by their channel estimates to calculate the group interference estimate $\hat{\mathbf{s}}_H$. After cancelling $\hat{\mathbf{s}}_H$ from $\mathbf{r_s}$, the input signal $\left(\mathbf{r_s} - \hat{\mathbf{s}}_H\right)$ to LPG-MUD in the second detection layer is processed by ZF or ML receiver to estimate the data of LPG users $\hat{b}_k, k = T+1, \ldots, K$. Highest performance of LPG is achieved when perfect cancellation of HPG interference is accomplished such that the desired signals are disturbed by AWGN only. On the other hand, performance of HPG can be maximized if the interference level of LPG is minimized (i.e. low P_L). For this purpose, appropriate power allocation ratio η should be used to allow reliable communication for different user overloading and number of RF chains.

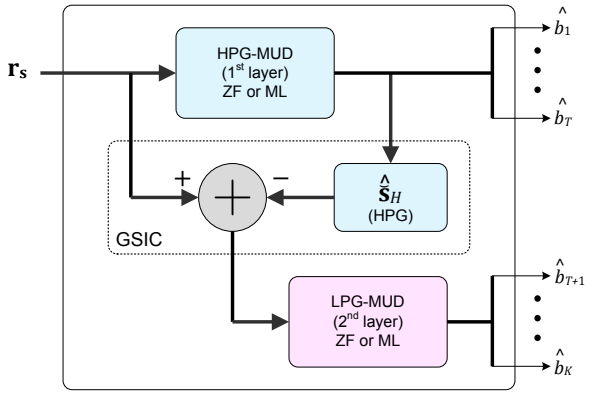

Figure 6.2: GL-MUD for proposed system using linear/nonlinear MUD for HPG and LPG with GSIC.

6.3.2.1 Linear ZF Group Receivers for GL-MUD

In this configuration of GL-MUD, the simple ZF receivers are employed in HPG-MUD and LPG-MUD layers and represented as ZF/ZF-MUD. For HPG-MUD, the linear ZF receiver (as explained in Chapter 2, Section 2.6.2.5) has a front-end $\breve{\mathbf{H}}_H^{\dagger}$ where $\mathbf{A}^{\dagger} = \left(\mathbf{A}^{\mathrm{H}}\mathbf{A}\right)^{-1}\mathbf{A}^{\mathrm{H}}$ denotes the Moore-Penrose inverse of matrix $\mathbf{A}$ with special case of $\mathbf{A}^{\dagger} = \mathbf{A}^{-1}$ when $\mathbf{A}$ is square and invertible [84]. The output of ZF receiver in the first detection layer is given by

$$\hat{\mathbf{v}}_H = \breve{\mathbf{H}}_H^{\dagger}\mathbf{r_s} = \mathbf{v}_H + \underbrace{\breve{\mathbf{H}}_H^{\dagger}(\breve{\mathbf{s}}_L + \mathbf{n_s})} \tag{6.9}$$

where the estimated signal $\hat{\mathbf{v}}_H$ is affected by enhanced noise and other group user interference $\breve{\mathbf{H}}_H^{\dagger}(\breve{\mathbf{s}}_L + \mathbf{n_s})$ which is the cost of low detection complexity. The estimated data of HPG users can be found then by remapping $\hat{\mathbf{v}}_H = [\hat{v}_1 \quad \cdots \quad \hat{v}_T]^T$ to $\hat{\mathbf{b}}_H = [\hat{b}_1 \quad \cdots \quad \hat{b}_T]^T$.

In the second detection layer, the front-end of ZF receiver is $\breve{\mathbf{H}}_L^{\dagger}$. Therefore the output of this receiver in LPG-MUD layer is given by

$$\hat{\mathbf{v}}_L = \breve{\mathbf{H}}_L^{\dagger}\left(\mathbf{r_s} - \hat{\breve{\mathbf{s}}}_H\right) = \mathbf{v}_L + \underbrace{\breve{\mathbf{H}}_L^{\dagger}\left(\breve{\mathbf{s}}_H - \hat{\breve{\mathbf{s}}}_H + \mathbf{n_s}\right).} \tag{6.10}$$

When $\breve{\mathbf{s}}_H = \hat{\breve{\mathbf{s}}}_H$, perfect interference cancellation of HPG users is achieved and the estimated signal vector is influenced by the noise component only which leads to maximize the performance of LPG users. Data estimation of LPG users can be carried out by remapping $\hat{\mathbf{v}}_L = [\hat{v}_{T+1} \quad \cdots \quad \hat{v}_K]^T$ to $\hat{\mathbf{b}}_L = [\hat{b}_{T+1} \quad \cdots \quad \hat{b}_K]^T$.

6.3.2.2 Nonlinear ML Group Receivers for GL-MUD

In this configuration of GL-MUD, the optimal ML receivers are employed in HPG-MUD and LPG-MUD layers and represented as ML/ML-MUD. The nonlinear ML receiver is optimal in the sense of minimizing the error probability by searching for the most likely transmitted signals. For conventional MU-MIMO system of K active users each equipped with single antenna and using $M_k,\ k = 1, \ldots, K$ alphabet size of constellation, there are $D_C = \prod_{k=1}^{K} M_k$ possible signal vectors $\mathbf{v}^{(q)} = \left[v_1^{(q)} \quad \cdots \quad v_K^{(q)}\right]^T \in \mathcal{C}^{K\times 1}\,; q = 1, \ldots, D_C$ at the channel input where $v_k^{(q)}$ is the q^{th} possible transmitted symbol from user k. In the proposed GL-MU-MIMO system, there are $D_H = \prod_{k=1}^{T} M_k$ possible HPG signal vectors $\mathbf{v}_H^{(q)} = \left[v_1^{(q)} \quad \cdots \quad v_T^{(q)}\right]^T \in \mathcal{C}^{T\times 1}\,; q = 1, \ldots, D_H$ and $D_L = \prod_{k=T+1}^{K} M_k$ possible LPG signal vectors $\mathbf{v}_L^{(q)} = \left[v_{T+1}^{(q)} \quad \cdots \quad v_K^{(q)}\right]^T \in \mathcal{C}^{(K-T)\times 1}\,; q = 1, \ldots, D_L$ at the channel input.

For HPG-MUD layer, signal of LPG are considered as a background noise. Therefore, there are only D_H possible signal vectors to the input of first detection layer. Based on the minimum distance criterion, the transmitted HPG signal vector associated with antenna selection is estimated as

$$\hat{\mathbf{v}}_H = \arg \min_{\mathbf{v}_H^{(q)} \in \boldsymbol{V}_H} \left\| \mathbf{r_s} - \breve{\mathbf{H}}_H \mathbf{v}_H^{(q)} \right\|^2 ; q = 1, \dots, D_H \tag{6.11}$$

where $\boldsymbol{V}_H = \left\{ \mathbf{v}_H^{(1)}, \dots, \mathbf{v}_H^{(q)}, \dots, \mathbf{v}_H^{(D_H)} \right\}$ is the set of all possible HPG transmitted signal vectors. The estimated signal vector $\hat{\mathbf{v}}_H = [\hat{v}_1 \quad \cdots \quad \hat{v}_T]^T$ will be remapped to the estimated data vector $\hat{\mathbf{b}}_H = [\hat{b}_1 \quad \cdots \quad \hat{b}_T]^T$.

After applying GSIC of HPG estimated signal from the selected received signal $\mathbf{r_s}$, there are D_L possible LPG signal vectors to the input of LPG-MUD layer and the transmitted signal vector associated with antenna selection is estimated as

$$\hat{\mathbf{v}}_L = \arg \min_{\mathbf{v}_L^{(q)} \in \boldsymbol{V}_L} \left\| \mathbf{r_s} - \hat{\mathbf{s}}_H - \breve{\mathbf{H}}_L \mathbf{v}_L^{(q)} \right\|^2 ; q = 1, \dots, D_L \tag{6.12}$$

where $\boldsymbol{V}_L = \left\{ \mathbf{v}_L^{(1)}, \dots, \mathbf{v}_L^{(q)}, \dots, \mathbf{v}_L^{(D_L)} \right\}$ is the set of all possible LPG transmitted signal vectors. The estimated signal vector $\hat{\mathbf{v}}_L = [\hat{v}_{T+1} \quad \cdots \quad \hat{v}_K]^T$ will be remapped to estimated data vector $\hat{\mathbf{b}}_L = [\hat{b}_{T+1} \quad \cdots \quad \hat{b}_K]^T$.

6.3.2.3 Linear ZF and Nonlinear ML Group Receivers for GL-MUD

Using ZF and ML receivers, the two possible GL-MUD configurations are ZF/ML-MUD and ML/ZF-MUD. In ZF/ML-MUD configuration, ZF receiver is employed in HPG-MUD layer while ML receiver for LPG-MUD layer. As discussed in Section 6.3.2.1, the output of ZF receiver in the first detection layer $\hat{\mathbf{v}}_H$ is given by equation (6.9). In the second detection layer, the output signal vector $\hat{\mathbf{v}}_L$ of ML receiver as discussed in Section 6.3.2.2 is given by equation (6.12). Similarly, for ML/ZF-MUD, ML receiver is employed in HPG-MUD layer while ML receiver for LPG-MUD layer. The output of ML receiver in the first detection layer $\hat{\mathbf{v}}_H$ is given by equation (6.11). In the second detection layer, the output signal vector $\hat{\mathbf{v}}_L$ of ZF receiver is given by equation (6.10). These configurations will provide a tradeoff between complexity and performance compared with ZF/ZF-MUD and ML/ML-MUD. Other low complexity or suboptimal receivers such as MMSE and SD are not considered in this study since their performance is bounded by the proposed detection scheme.

6.3.3 Detection Complexity of Proposed GL-MU-MIMO

In GL-MU-MIMO system with K active users, GL-MUD configurations have different performance and detection complexity. ZF/ZF-MUD has the lowest performance and

complexity while ML/ML-MUD has the best performance at the cost of highest complexity. In this section, complexity of ML/ML-MUD is compared with ML detection of conventional MU-MIMO system assuming that $M_k = M,\ k = 1, \dots, K$ for both schemes and $T = U = K/2$ for GL-MU-MIMO.

The total number of searches required for transmitted signal vectors using GL-MU-MIMO scheme is $D_{GL} = D_H + D_L$ compared with D_C for conventional system. It is represented by

$$D_{GL} = D_H + D_L = M^{K/2} + M^{K/2} = 2M^{K/2} \tag{6.13}$$

For conventional MU-MIMO scheme, the total number of searches required for transmitted signal vectors is

$$D_C = M^K \tag{6.14}$$

Therefore, complexity of GL-MU-MIMO scheme is significantly less than conventional MU-MIMO, specifically as M and/or K increased as shown in Table 6.1. For example, when $M = 4$ and $K = 10$, the total number of required searches is 2048 compared with 1048576 for conventional system.

Table 6.1: Total number of searches required for the transmitted vectors using ML/ML-MUD in GL-MU-MIMO compared with conventional MU-MIMO when ML detection is employed

Number of users (K)	Total number of required searches					
	$M = 2$		$M = 4$		$M = 16$	
	D_C	D_{GL}	D_C	D_{GL}	D_C	D_{GL}
2	4	4	16	8	256	32
4	16	8	256	32	65 536	512
6	64	16	4 096	128	16 777 216	8 192
8	256	32	65 536	512	4.295×10^9	131 072
10	1 024	64	1 048 576	2 048	1.099×10^{12}	2 097 152

6.4 Capacity Analysis of GL-MU-MIMO

6.4.1 User Capacity

The user capacity C_{user} can be defined as the total number of users (K) that simultaneously communicate with common BS receiver in a cell using the available resources (DoF) of time, frequency, space and codes. In the proposed GL-MU-MIMO scheme, one of the main objectives is to increase the user capacity beyond the spatial DoF limit represented by m_s RF chains at BS. Since the HPG is formed from $T = m_s$ high power users and the LPG includes the rest of K users as $1 \leq (U = K - T) \leq m_s$, the user capacity upper bound $C_{user-GL}^{max}$ and lower bound $C_{user-GL}^{min}$ are given as

$$C_{user-GL}^{max} = 2m_s \tag{6.15}$$

$$C_{user-GL}^{min} = m_s + 1 \tag{6.16}$$

In Fig. 6.3, user capacity bounds of GL-MU-MIMO are shown compared with maximum user capacity of conventional MU-MIMO system with linear receiver known as $C_{user-C}^{max} = m_s$. As can be seen, the user capacity is increased by U users of LPG compared with conventional system. Therefore, up to *double* user capacity can be achieved which is significant in terms of serving more user in same available bandwidth resource.

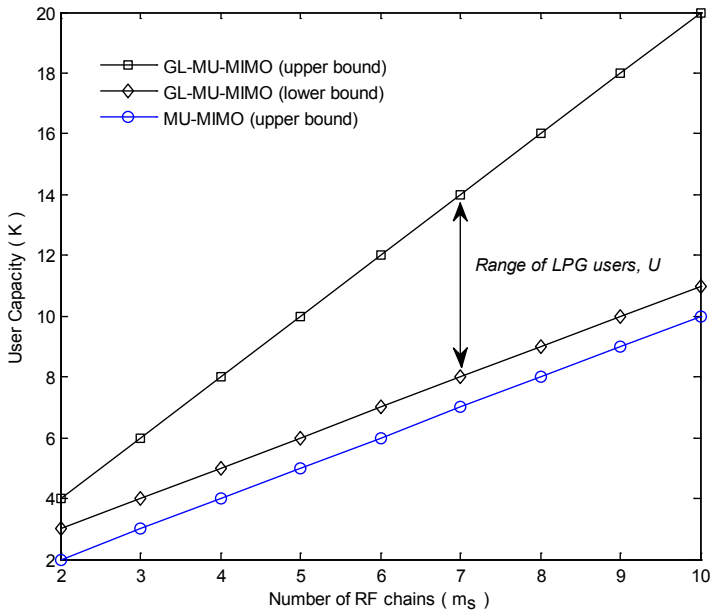

Figure 6.3: User capacity bounds of GL-MU-MIMO system compared with the maximum user capacity of conventional MU-MIMO system.

6.4.2 Sum Rate Capacity

Based on the sum rate capacity of UL MU-MIMO given in [24, 99], the sum rate capacity for GL-MU-MIMO signal model (6.4) with constant channel realization is given as follows

$$\begin{aligned} R_{sum} &= \log_2 \left| \mathbf{I}_m + \frac{1}{\sigma_n^2} \left[\sum_{k=1}^{K} \mathbf{h}_k p_k \mathbf{h}_k^{\mathrm{H}} \right] \right| \\ &= \log_2 \left| \mathbf{I}_m + \frac{1}{\sigma_n^2} \left[\sum_{k=1}^{T} \mathbf{h}_k p_k \mathbf{h}_k^{\mathrm{H}} + \sum_{k=T+1}^{K} \mathbf{h}_k p_k \mathbf{h}_k^{\mathrm{H}} \right] \right| \\ &= \log_2 \left| \mathbf{I}_m + \frac{1}{\sigma_n^2} \left[\frac{P_H}{T} \sum_{k=1}^{T} \mathbf{h}_k \mathbf{h}_k^{\mathrm{H}} + \frac{P_L}{U} \sum_{k=T+1}^{K} \mathbf{h}_k \mathbf{h}_k^{\mathrm{H}} \right] \right| \\ &= \log_2 \left| \mathbf{I}_m + \Gamma \left[\frac{1-\eta}{T} \sum_{k=1}^{T} \mathbf{h}_k \mathbf{h}_k^{\mathrm{H}} + \frac{\eta}{U} \sum_{k=T+1}^{K} \mathbf{h}_k \mathbf{h}_k^{\mathrm{H}} \right] \right| \end{aligned} \tag{6.17}$$

where, $\mathbf{I}_m$ is the $m \times m$ identity matrix, σ_n^2 is the average noise power, and $\Gamma = P/\sigma_n^2$ is the average SNR. In terms of $\mathbf{H}_H$ and $\mathbf{H}_L$, the sum rate capacity can be further simplified to

$$R_{sum} = \log_2 \left| \mathbf{I}_m + \Gamma \left[\frac{1-\eta}{T} \left(\mathbf{H}_H \mathbf{H}_H^{\mathrm{H}} \right) + \frac{\eta}{U} \left(\mathbf{H}_L \mathbf{H}_L^{\mathrm{H}} \right) \right] \right| \tag{6.18}$$

With RAS diversity, the sum rate capacity is therefore given as

$$R_{sum}^{s} = \max_{\mathcal{s}_i \in \mathbb{S}} \left\{ \log_2 \left| \mathbf{I}_{m_s} + \Gamma \left[\frac{1-\eta}{T} \left(\breve{\mathbf{H}}_H(\mathcal{s}_i) \breve{\mathbf{H}}_H^{\mathrm{H}}(\mathcal{s}_i) \right) + \frac{\eta}{U} \left(\breve{\mathbf{H}}_L(\mathcal{s}_i) \breve{\mathbf{H}}_L^{\mathrm{H}}(\mathcal{s}_i) \right) \right] \right| \right\} \tag{6.19}$$

where the maximization is over the subset $\mathcal{s}_i \in \mathbb{S}$ for $\mathbb{S} = \{\mathcal{s}_1, \ldots, \mathcal{s}_i, \ldots, \mathcal{s}_{|\mathbb{S}|}\}$ representing the set of all possible subsets of receive antennas whose cardinality is $|\mathbb{S}| = \binom{m}{m_s}$, and group channels $\breve{\mathbf{H}}_H(\mathcal{s}_i)$ and $\breve{\mathbf{H}}_L(\mathcal{s}_i)$ are the selected channel matrix of HPG and LPG according to the subset $\mathcal{s}_i$, respectively, and $\mathbf{I}_{m_s}$ is the $m_s \times m_s$ identity matrix.

6.4.3 Capacity Region of GL-MU-MIMO

Let R_H and R_L denote the sum rate capacity of HPG and LPG users, respectively. Based on the capacity region of two user UL MU-MIMO investigated in [24, 99], the capacity region of GL-MU-MIMO scheme with constant channel realization is given as the set of all group sum rates (R_H, R_L) satisfying the following three constraints

$$R_H \leq \log_2 \left| \mathbf{I}_m + \frac{P_H}{\sigma_n^2 T} \left(\mathbf{H}_H \mathbf{H}_H^{\mathrm{H}} \right) \right| \tag{6.20}$$

$$R_L \leq \log_2 \left| \mathbf{I}_m + \frac{P_L}{\sigma_n^2 U} \left(\mathbf{H}_L \mathbf{H}_L^{\mathrm{H}} \right) \right| \tag{6.21}$$

$$R_H + R_L \leq \log_2 \left| \mathbf{I}_m + \frac{1}{\sigma_n^2} \left[\frac{P_H}{T} \left(\mathbf{H}_H \mathbf{H}_H^{\mathrm{H}} \right) + \frac{P_L}{U} \left(\mathbf{H}_L \mathbf{H}_L^{\mathrm{H}} \right) \right] \right| \tag{6.22}$$

The capacity region is the pentagon shown in Fig. 6.4. The maximum rate points "A1" for HPG and "B1" for LPG can be achieved as if the other group is absent from the system (see the constraints (6.20) and (6.21)). Constraint (6.22) is on the achievable sum rate when both groups are communicating simultaneously with BS receiver as in point-to-point channel. The corner sum rate points "A" and "B" can be achieved by using GL-MUD which involves groups MUD and GSIC. In the proposed GL-MUD, signals of HPG users are decoded first in the presence of interference from LPG signals followed by GSIC to decode LPG signals without interference from HPG. Therefore, the sum rate point "B" is represented as $(R_H(\mathrm{B}), R_L(\mathrm{B}))$ given by

$$R_H(\mathrm{B}) = \log_2 \left| \mathbf{I}_m + \frac{P_H}{\sigma_n^2 T} \left[\mathbf{I}_m + \frac{P_L}{\sigma_n^2 U} \left(\mathbf{H}_L \mathbf{H}_L^{\mathrm{H}} \right) \right]^{-1} \left(\mathbf{H}_H \mathbf{H}_H^{\mathrm{H}} \right) \right| \tag{6.23}$$

$$R_L(\mathrm{B}) = \log_2 \left| \mathbf{I}_m + \frac{P_L}{\sigma_n^2 U} \left(\mathbf{H}_L \mathbf{H}_L^{\mathrm{H}} \right) \right| \tag{6.24}$$

If the detection process is reversed by decoding signals of LPG users first with the presence of HPG interference and followed by GSIC to decode HPG signals, the sum rate point "A" represented as $(R_H(\mathrm{A}), R_L(\mathrm{A}))$ can be given as

$$R_H(\mathrm{A}) = \log_2 \left| \mathbf{I}_m + \frac{P_H}{\sigma_n^2 T} \left(\mathbf{H}_H \mathbf{H}_H^{\mathrm{H}} \right) \right| \tag{6.25}$$

$$R_L(\mathrm{A}) = \log_2 \left| \mathbf{I}_m + \frac{P_L}{\sigma_n^2 U} \left[\mathbf{I}_m + \frac{P_H}{\sigma_n^2 T} \left(\mathbf{H}_H \mathbf{H}_H^{\mathrm{H}} \right) \right]^{-1} \left(\mathbf{H}_L \mathbf{H}_L^{\mathrm{H}} \right) \right| \tag{6.26}$$

It should be noted that users in each group will have equal rate distribution since they have equal powers by assumption. The capacity region of GL-MU-MIMO scheme will characterize the optimal tradeoff of achievable groups' rate using different power allocations and user overloading.

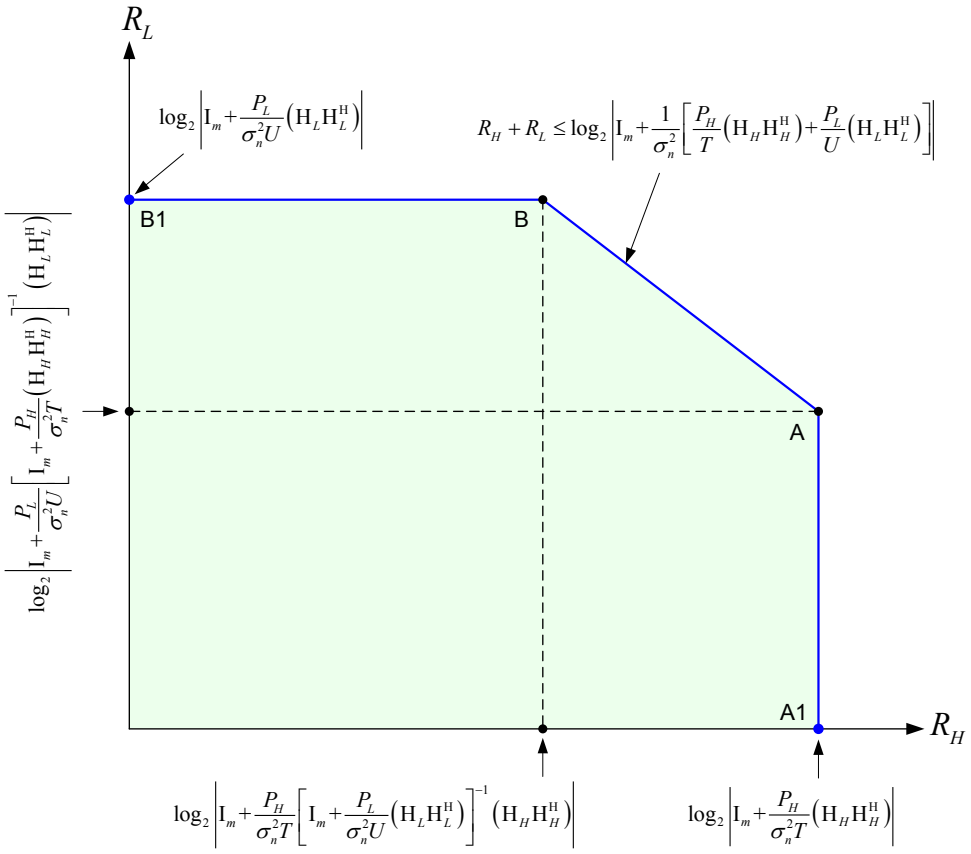

Figure 6.4: Capacity region of GL-MU-MIMO scheme.

When RAS of subset $\mathcal{S}_i$ is utilized, the capacity region of GL-MU-MIMO is similarly given as the set of all rates (R_H^S, R_L^S) satisfying the following three constraints

$$R_H^S \le \max_{\mathcal{S}_i\in\mathbb{S}}\left\{\log_2\left|\mathbf{I}_{m_s}+\frac{P_H}{\sigma_n^2 T}\left(\breve{\mathbf{H}}_H(\mathcal{S}_i)\breve{\mathbf{H}}_H^{\mathrm{H}}(\mathcal{S}_i)\right)\right|\right\} \tag{6.27}$$

$$R_L^S \le \max_{\mathcal{S}_i\in\mathbb{S}}\left\{\log_2\left|\mathbf{I}_{m_s}+\frac{P_L}{\sigma_n^2 U}\left(\breve{\mathbf{H}}_L(\mathcal{S}_i)\breve{\mathbf{H}}_L^{\mathrm{H}}(\mathcal{S}_i)\right)\right|\right\} \tag{6.28}$$

$$R_H^S+R_L^S \le \max_{\mathcal{S}_i\in\mathbb{S}}\left\{\log_2\left|\mathbf{I}_{m_s}+\frac{1}{\sigma_n^2}\left[\frac{P_H}{T}\left(\breve{\mathbf{H}}_H(\mathcal{S}_i)\breve{\mathbf{H}}_H^{\mathrm{H}}(\mathcal{S}_i)\right)+\frac{P_L}{U}\left(\breve{\mathbf{H}}_L(\mathcal{S}_i)\breve{\mathbf{H}}_L^{\mathrm{H}}(\mathcal{S}_i)\right)\right]\right|\right\} \tag{6.29}$$

The corner sum rate points associated with antenna selection "B" represented as $(R_H^S(\mathrm{B}), R_L^S(\mathrm{B}))$ and "A" represented as $(R_H^S(\mathrm{A}), R_L^S(\mathrm{A}))$ are given by

$$R_H^s(\mathrm{B}) = \max_{\mathcal{S}_i \in \mathbb{S}} \left\{ \log_2 \left| \mathbf{I}_m + \frac{P_H}{\sigma_n^2 T} \left[\mathbf{I}_m + \frac{P_L}{\sigma_n^2 U} \left(\breve{\mathbf{H}}_L(\mathcal{S}_i) \breve{\mathbf{H}}_L^{\mathrm{H}}(\mathcal{S}_i) \right) \right]^{-1} \left(\breve{\mathbf{H}}_H(\mathcal{S}_i) \breve{\mathbf{H}}_H^{\mathrm{H}}(\mathcal{S}_i) \right) \right| \right\} \quad (6.30)$$

$$R_L^s(\mathrm{B}) = \max_{\mathcal{S}_i \in \mathbb{S}} \left\{ \log_2 \left| \mathbf{I}_m + \frac{P_L}{\sigma_n^2 U} \left(\breve{\mathbf{H}}_L(\mathcal{S}_i) \breve{\mathbf{H}}_L^{\mathrm{H}}(\mathcal{S}_i) \right) \right| \right\} \quad (6.31)$$

$$R_H^s(\mathrm{A}) = \max_{\mathcal{S}_i \in \mathbb{S}} \left\{ \log_2 \left| \mathbf{I}_m + \frac{P_H}{\sigma_n^2 T} \left(\breve{\mathbf{H}}_H(\mathcal{S}_i) \breve{\mathbf{H}}_H^{\mathrm{H}}(\mathcal{S}_i) \right) \right| \right\} \quad (6.32)$$

$$R_L^s(\mathrm{A}) = \max_{\mathcal{S}_i \in \mathbb{S}} \left\{ \log_2 \left| \mathbf{I}_m + \frac{P_L}{\sigma_n^2 U} \left[\mathbf{I}_m + \frac{P_H}{\sigma_n^2 T} \left(\breve{\mathbf{H}}_H(\mathcal{S}_i) \breve{\mathbf{H}}_H^{\mathrm{H}}(\mathcal{S}_i) \right) \right]^{-1} \left(\breve{\mathbf{H}}_L(\mathcal{S}_i) \breve{\mathbf{H}}_L^{\mathrm{H}}(\mathcal{S}_i) \right) \right| \right\} \quad (6.33)$$

6.5 RAS Diversity

To achieve high user capacity and good BER performance with affordable complexity, RAS diversity is employed in the proposed GL-MU-MIMO system. For this purpose and with the availability of CSI at the receiver, two RAS algorithms are used to select the best subset of m_s from m receive antennas as $\mathcal{S}_i \in \mathbb{S}$. The popular low complexity NBS [181, 186] is considered as the first selection method.

The constellation geometry of combined receive signal with highest d_{min} is a critical factor for system performance. Therefore, higher BER performance can be achieved by using the maximum d_{min} measure or its corresponding in the selection process. To exploit this fact, a new HPG-PDBS algorithm is proposed in this section after brief review of NBS method. It is based on the largest Euclidean norm of HPG channel matrix rows with best corresponding phase difference.

6.5.1 Norm Based Selection (NBS)

In this method, selection of m_s receive antennas is based on the corresponding rows of overall channel matrix **H** with the largest Euclidean norm (power) to maximize the SNR. The complexity of NBS when used in GL-MU-MIMO system is of $\mathcal{O}(Km)$ due to the requirement of vector norm calculations of all m overall channel matrix rows.

NBS Algorithm

1) Define the set of receive antenna elements as, $\mathcal{X} = [1, \dots, m]$ with $l \in \mathcal{X}$ representing the l^{th} antenna.
2) Given the overall channel matrix $\mathbf{H} = \left[\underline{\mathbf{h}}_1, \dots, \underline{\mathbf{h}}_l, \dots, \underline{\mathbf{h}}_m\right]^T$ where $\underline{\mathbf{h}}_l, \forall l = 1, \dots, m$ is the l^{th} row corresponding to the l^{th} antenna.
3) For all l in $\mathcal{X}$, calculate the power of channel vector $\underline{\mathbf{h}}_l$ as $\left\|\underline{\mathbf{h}}_l\right\|^2$.
4) To select the best subset of m_s receive antennas; choose l representing the channel vectors with maximum power.

6.5.2 HPG Phase Difference Based Selection (HPG-PDBS)

The SIC receivers suffers from error propagation due to erroneously detected signals during the consecutive detection stages leading to performance degradation [24]. In GL-MU-MIMO scheme and due to the use of GSIC, signal detection errors of HPG-MUD layer have a direct impact on the system BER performance. Moreover, constellation geometry of the combined receive signals of HPG has the same effect. Therefore, higher BER performance can be achieved by improving the first detection layer using the largest Euclidean norm of overall channel matrix rows $\left\|\underline{\mathbf{h}}_l\right\|^2; \forall l = 1, \dots, m$ in conjunction with the highest minimum Euclidian distance of HPG constellation d_{min}^{HPG} or its equivalent in the selection algorithm. This can be explained by the following example.

Illustrative example

Consider a simultaneous transmission of BPSK signals from $K = 4$ active users to a BS receiver equipped with m antennas and $m_s = T = U = 2$ RF chains in GL-MU-MIMO system (see Fig. 6.1). Let $\eta = 0.2$ such that there is enough power difference between HPG and LPG users. Also, assume that $p_l^{(H)} > \left(p_l^{(L)} + \sigma_n^2\right)$ at the l^{th} antenna where $p_l^{(H)} = \left\|\mathbf{h}_l^{(H)}\right\|^2$ represent the power of l^{th} row in $\mathbf{H}_H$ while $p_l^{(L)} = \left\|\mathbf{h}_l^{(L)}\right\|^2$ is for the l^{th} row in $\mathbf{H}_L$.

At antenna No.1, the combined received signal r_1 is given by

$$r_1 = \underbrace{h_{11}v_1 + h_{21}v_2}_{\text{HPG}} + \underbrace{h_{31}v_3 + h_{41}v_4}_{\text{LPG}} + n_1 = s_H + s_L + n_1 \tag{6.34}$$

The signal constellation of r_1 consists of $2^4 = 16$ possible points corresponding to the superposition of HPG and LPG signals. Since $P_L = 0.25\, P_H$, the power contribution of HPG signals to r_1 is greater than LPG signals. For HPG, the constellation consists of four possible points $\{s_{H1}, s_{H2}, s_{H3}, s_{H4}\}$ corresponding to v_1 and v_2 as

$$\begin{aligned} s_{H_1} &= +h_{11} + h_{21}\,, \quad & v_1 &= +1, v_2 = +1 \\ s_{H_2} &= -h_{11} + h_{21}\,, \quad & v_1 &= -1, v_2 = +1 \\ s_{H_3} &= -h_{11} - h_{21}\,, \quad & v_1 &= -1, v_2 = -1 \\ s_{H_4} &= +h_{11} - h_{21}\,, \quad & v_1 &= +1, v_2 = -1 \end{aligned} \tag{6.35}$$

Similarly, signal constellation of LPG consists of four possible points $\{s_{L_1}, s_{L_2}, s_{L_3}, s_{L_4}\}$ corresponding to v_3 and v_4 as

$$\begin{aligned} s_{L_1} &= +h_{31} + h_{41}\,, \quad & v_3 &= +1, v_4 = +1 \\ s_{L_2} &= -h_{31} + h_{41}\,, \quad & v_3 &= -1, v_4 = +1 \\ s_{L_3} &= -h_{31} - h_{41}\,, \quad & v_3 &= -1, v_4 = -1 \\ s_{L_4} &= +h_{31} - h_{41}\,, \quad & v_3 &= +1, v_4 = -1 \end{aligned} \tag{6.36}$$

Let's define the phase difference θ_1 corresponding to r_1 as the resultant phase between HPG channel coefficients h_{11} and h_{21} given by

$$\theta_1 = \min\{\text{abs}(\beta_{11} - \beta_{21}), 2\pi - \text{abs}(\beta_{11} - \beta_{21})\}. \tag{6.37}$$

Constellation of HPG combined signals in r_1 over possible channel realizations is depicted in Fig. 6.5a while the constellation region of LPG combined signals is shown in Fig. 6.5b.

In Fig. 6.6, signal constellation of r_1 constructed by the superposition of HPG constellation over possible channel realizations and LPG constellation region with low level noise component n_1 is shown for three different possible values of phase difference θ_1. The channel gains α_{11} and α_{21} are assumed to be fixed while θ_1 can take any value in the interval $[0, \pi]$. From this figure, it is clear that there is one to one correspondence between the phase difference and d_{min}^{HPG}. When $\theta_1 = \pi/2$, the constellation has maximum d_{min}^{HPG} compared with when $\theta_1 = 2\pi/3$ and $\theta_1 = \pi/7$. For $\theta_1 = \pi/7$, there is a possibility of signal detection error in HPG-MUD layer due to small d_{min}^{HPG} between s_{H_2} and s_{H_4} which leads to erroneous signal detection in LPG-MUD layer. Thus, the best case that makes antenna No.1 to be selected is $\theta_1 = \pi/2$ which lies in the *middle of phase difference interval* and can be denoted as the *optimal angle* θ_1^*. As a result, there is 50% of phase difference realizations that makes d_{min}^{HPG} large represented by θ_1 in the range, $\pi/4 \leq \theta_1 \leq 3\pi/4$ and maximum d_{min}^{HPG} is achieved when $\theta_1 \to \theta_1^*$.

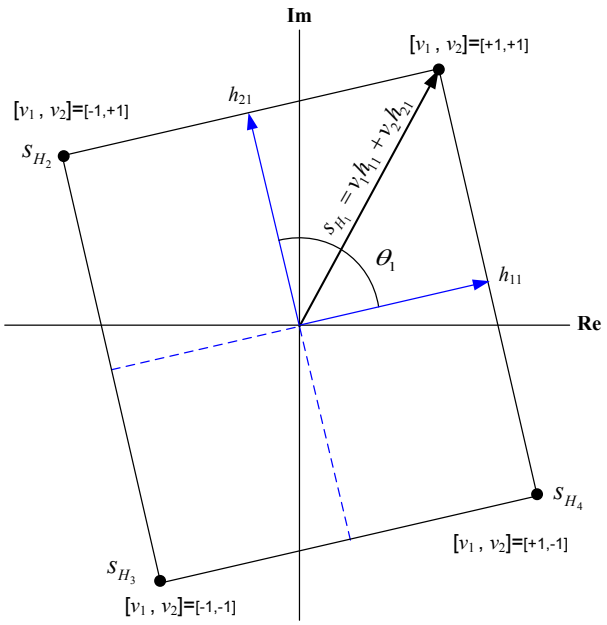

(a) Signal constellation of HPG

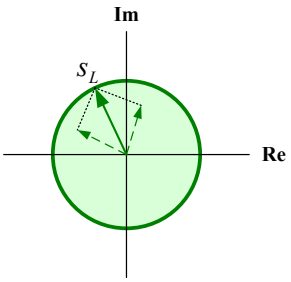

(b) Signal constellation region of LPG

Figure 6.5: a) Constellation of HPG combined signals over possible channel realizations, b) Constellation region of LPG combined signals.

To generalize this concept for T users in HPG, the phase difference vector $\boldsymbol{\theta}_l$ for the l^{th} receive antenna can be found as

$$\boldsymbol{\theta}_l = \left\{\theta_l(h_{il}, h_{jl})\right\}_{i,j=1;\, i\neq j}^{T} \quad , l = 1, \dots, m \tag{6.38}$$

where $\theta_l(h_{il}, h_{jl})$ is the phase difference between i^{th} and j^{th} coefficients in the l^{th} row of $\mathbf{H}_H$ which can be written as

$$\theta_l\left(h_{il}, h_{jl}\right) = \min\{\text{abs}\left(\beta_{il} - \beta_{jl}\right), 2\pi - \text{abs}\left(\beta_{il} - \beta_{jl}\right)\}. \tag{6.39}$$

Good constellation structures at the l^{th} receive antenna with high d_{min}^{HPG} can be achieved when the phase difference between l^{th} row elements of $\mathbf{H}_H$ are within the following interval

$$(\theta^- = \pi/4) \leq \theta_l(h_{il}, h_{jl}) \leq (\theta^+ = 3\pi/4), \tag{6.40}$$

where θ^- and θ^+ are the lower and upper limits of acceptable θ_l. Therefore, optimal phase difference vector at the l^{th} receive antenna $\boldsymbol{\theta}_l^*$ can be written as

$$\boldsymbol{\theta}_l^* = \{\theta_l^*(h_{il}, h_{jl})\}_{i,j=1;\, i\neq j}^{T} \quad , l = 1, \dots, m \tag{6.41}$$

where $\theta_l^*(h_{il}, h_{jl}) = (\theta^- + \theta^+)/2$. Hence, large d_{min}^{HPG} is maintained when $\boldsymbol{\theta}_l$ elements are in the range of equation (6.40) and as $\boldsymbol{\theta}_l \to \boldsymbol{\theta}_l^*$, the maximum value of d_{min}^{HPG} will be approached.

According to the above discussion, antenna selection of a subset $\mathcal{s}_i \in \mathbb{S}, i = 1, \dots, |\mathbb{S}|$ based on the largest Euclidean norm of overall channel matrix rows $\|\underline{\mathbf{h}}_l\|^2; \forall l = 1, \dots, m$ with best corresponding phase differences $\boldsymbol{\theta}_l \to \boldsymbol{\theta}_l^*$ of $\mathbf{H}_H$ rows will provide a received vector $\mathbf{r_s}$ with highest SNR and d_{min}^{HPG}. The proposed HPG-PDBS method enables significant improvement in the first signal detection layer and hence the second layer. Therefore, superior BER performance can be achieved compared with NBS at the cost of extra calculations. In the following, HPG-PDBS algorithm is given.

HPG-PDBS Algorithm

1) Define the set of receive antenna elements as, $\mathcal{X} = \{1, \dots, m\}$ with $l \in \mathcal{X}$ representing the l^{th} antenna.
2) Given the overall channel matrix $\mathbf{H} = [\mathbf{H}_H \ \mathbf{H}_L] = \left[\underline{\mathbf{h}}_1, \dots, \underline{\mathbf{h}}_l, \dots, \underline{\mathbf{h}}_m\right]^T$ where $\underline{\mathbf{h}}_l, \forall l = 1, \dots, m$ is the l^{th} row corresponding to the l^{th} receive antenna.
3) For all l in $\mathcal{X}$, calculate the power of channel vector $\underline{\mathbf{h}}_l$ as $P_l = p_l^{(H)} + p_l^{(L)} = \|\underline{\mathbf{h}}_l\|^2$.
4) Using HPG channel matrix $\mathbf{H}_H$, calculate the phase difference vector $\boldsymbol{\theta}_l, \forall l = 1, \dots, m$ corresponding to the l^{th} receive antenna as in equation (6.38).
5) From $\mathcal{X}$, construct two subset of receive antennas as $\mathcal{X}_a$ from those satisfying $p_l^{(H)} > \left(p_l^{(L)} + \sigma_n^2\right)$ and $\boldsymbol{\theta}_l \to \boldsymbol{\theta}_l^*$ and the rest in $\mathcal{X}_b$.
6) For each subset, sort the elements from highest to lowest power.
7) To select the best subset of antennas $\mathcal{s}_i$; choose the first m_s elements from subset $\mathcal{X}_a$. If the number of elements in $\mathcal{X}_a$ is less than m_s, complete the selection process from subset $\mathcal{X}_b$.

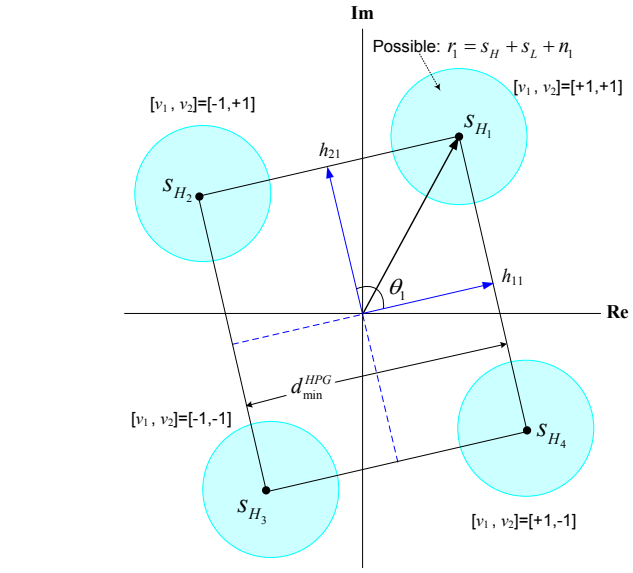

(a): $\theta_1 = \pi/2$

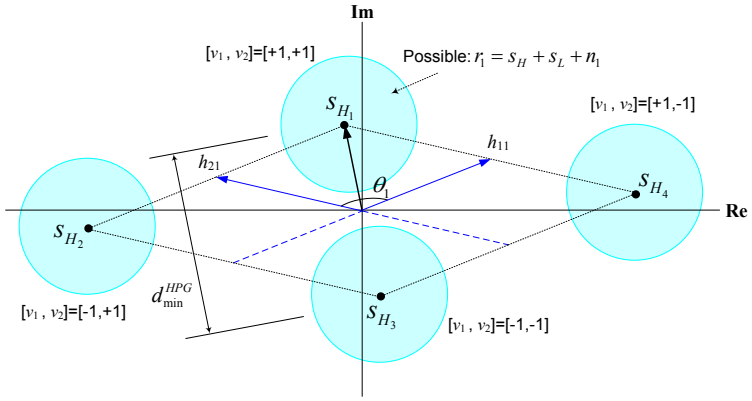

(b): $\theta_1 = 2\pi/3$

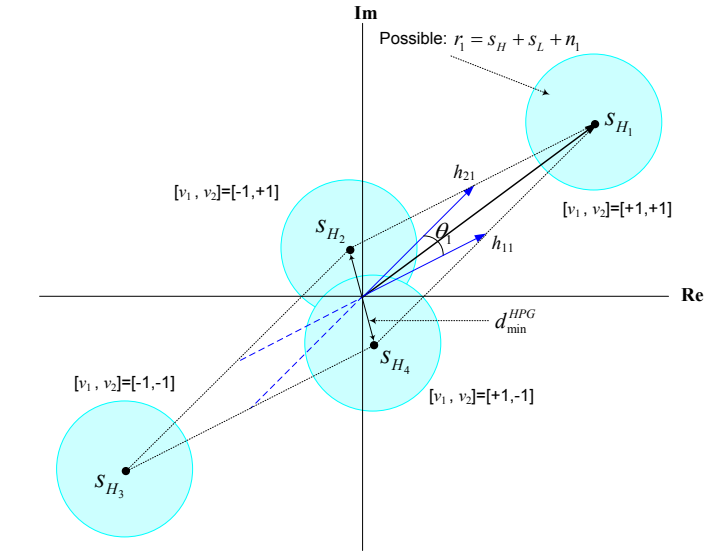

(c): $\theta_1 = \pi/7$

Figure 6.6: Received signal constellation of r_1 over possible HPG channel realizations where the channel gain $\alpha_{11} = |h_{11}|$ and $\alpha_{21} = |h_{21}|$ is fixed while the phase difference is; a) $\theta_1 = \pi/2$, b) $\theta_1 = 2\pi/3$,and c) $\theta_1 = \pi/7$.

Computational Complexity

Using HPG-PDBS algorithm, calculations of Km channel Euclidean norms and $m(T!/\{2!\ (T-2)!\})$ phase difference are required. Therefore, total of $Km + 0.5mT^2 - 0.5mT$ calculations are used and the resulting complexity effort is of $\mathcal{O}(Km + mT^2)$ compared with $\mathcal{O}(Km)$ for NBS algorithm. In Table 6.2, comparison results are shown where HPG-PDBS require extra calculations compared with NBS as a cost of superior performance. This will provide a tradeoff between the system performance and complexity.

Table 6.2: Computational complexity for NBS and HPG-PDBS algorithms

Algorithm	Total Calculations	Computational Effort
NBS	Km	$\mathcal{O}(Km)$
HPG-PDBS	$Km + 0.5mT^2 - 0.5mT$	$\mathcal{O}(Km + mT^2)$

6.6 Simulation Results of GL-MU-MIMO over Uncorrelated Channels

To demonstrate and validate the overall performance of GL-MU-MIMO system over uncorrelated flat Rayleigh fading channel, Monte Carlo simulations have been carried in this section. The first subsection includes the results for GL-MU-MIMO system without RAS diversity ($m = m_s$) while the second subsection demonstrates the results when NBS and HPG-PDBS are employed for $m > m_s$ to enhance the system performance.

The results are averaged using 10,000 channel realization for sum rate capacity evaluation. For BER performance, a frame of 100 symbols from BPSK constellation is assumed for each channel realization where the channel still constant over the entire frame length and changes independently from frame to the next. For notational convenience, GL-MU-MIMO system of K active users and $m = m_s$ receive antennas (i.e. without antenna selection) will be denoted as $K \times m/m_s$. With antenna selection of m_s from m receive antennas using NBS or HPG-PDBS algorithm, the system will be represented as $K \times m/\texttt{algorithm}\text{-}m_s$. For conventional MU-MIMO system, $K \times m$(ML) denote a system of K active users and m receive antennas which employs ML detection whereas $K \times m$(ZF) when ZF detection is used. For completeness, the reference single user MQAM performance is shown with the simulation results and denoted as 1×1(MQAM).

6.6.1 GL-MU-MIMO without RAS Diversity

6.6.1.1 Sum Rate Capacity

To evaluate the sum rate capacity of GL-MU-MIMO system without loss of generality, we consider $4 \times 2/2$ and $6 \times 3/3$ systems (two-fold user capacity) for different power allocation ratios (η). Simulation results using $\eta = 0.2$ and $\eta = 0.1$ are shown in Fig. 6.7 compared with the sum rate capacity of conventional 2×2, 4×2, 3×3, and 6×3 MU-MIMO systems.

As can be seen, the sum rate of $4 \times 2/2$ system is higher than 2×2 and less than 4×2 sum rates. When the power allocation ratio increased as $\eta \to 0.5$ for equal power groups, the sum rate of $4 \times 2/2$ approaches that of 4×2 system. If $\eta \to 0$, the power of LPG approaches zero and hence, the sum rate of $4 \times 2/2$ drops to that of 2×2 system. Therefore, 2×2 and 4×2 systems serve as the upper and lower bounds for $4 \times 2/2$ GL-MU-MIMO system. Similarly, 3×3 and 6×3 systems serve as the upper and lower bounds for $6 \times 3/3$ system. It should be noted that the increase of η will increase the interference level of LPG to HPG which causes low average BER performance. Therefore, careful selection of η values should be maintained. From the presented results, it can be seen that more than 50% of sum rate range between upper and lower bounds can be achieved using $\eta = 0.1$.

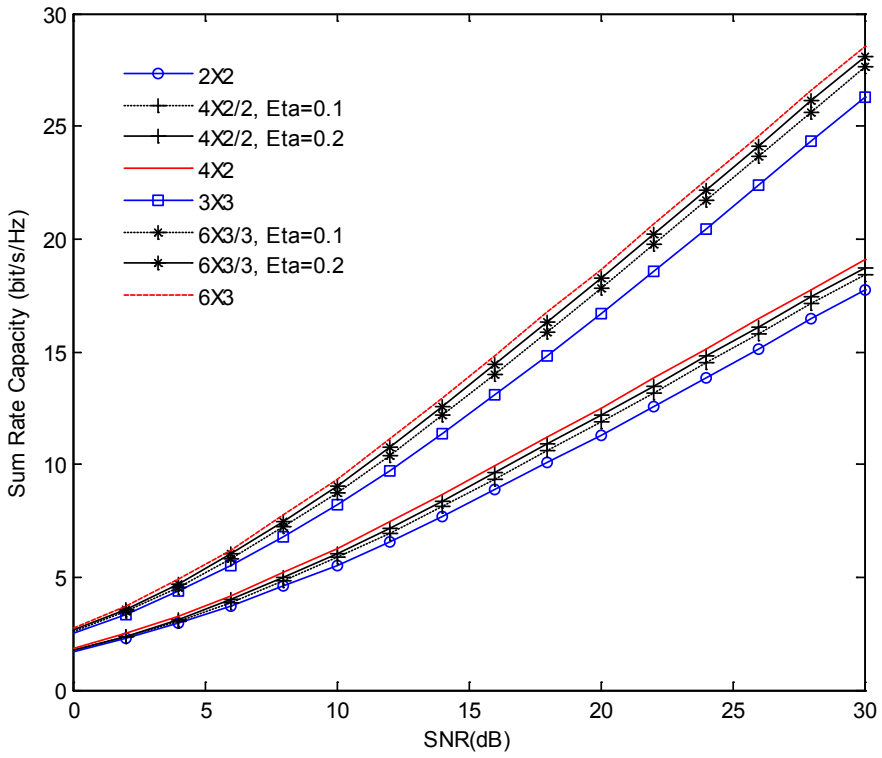

Figure 6.7: Sum rate capacity of $4 \times 2/2$ and $6 \times 3/3$ GL-MU-MIMO system using different group power assignment ($\eta = 0.2,\ 0.1$) compared with conventional 2×2, 4×2, 3×3, and 6×3 MU-MIMO systems.

6.6.1.2 Capacity Region

Capacity region of representative $4 \times 2/2$ GL-MU-MIMO system using $\eta = 0.3,\ 0.2,\ 0.1,$ and 0.05 is shown in Fig. 6.8 for SNR $= 20$ and 30dB compared with the reference 2×2 MU-MIMO systems. Using equations (6.22)-(6.24), the achievable group sum rates $(R_H,\ R_L)$ and sum rate (R_{sum}) in bit/s/Hz are summarized in Table 6.3 for different values of η.

As can be seen, the sum rate of $4 \times 2/2$ system is higher than 2×2 for all SNR values and increases as η increased. Moreover, the achievable group sum rate points $(R_H,\ R_L)$ for given SNR are also depending on η due to the use of GSIC. In Fig. 6.9, the curves of R_H and R_L sum rates are shown as a function of η for different SNR values. For example at SNR $= 20$dB, the point $(R_H = 7.55,\ R_L = 4.12)$ is achieved using $\eta = 0.05$ while point $(R_H = 5.06,\ R_L = 7.13)$ is achieved when $\eta = 0.2$ is used. Therefore, in addition to the increase of user capacity (4 users rather than 2), the proposed system offers a flexible group rate management in a given target SNR through the power allocation ratio η. For instance, LPG users near the cell edge can be served fairly as HPG users near the BS with equal data rate. Hence, we convert the *near-far* problem to our advantage. Recall that in conventional systems, power of the users near the cell edge should be increased to increase their data rate.

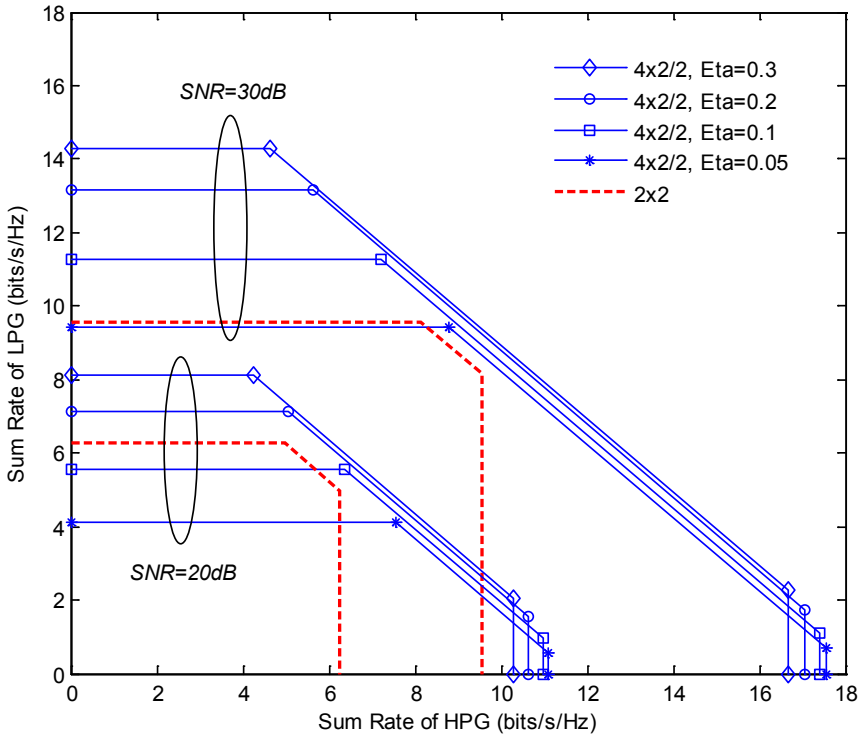

Figure 6.8: Capacity region $(R_H,\ R_L)$ of $4 \times 2/2$ GL-MU-MIMO system in bit/s/Hz at SNR $=$ 20 and 30dB with different power allocation ratio $(\eta = 0.3,\ 0.2,\ 0.1,\ 0.05)$ compared with the reference 2×2 MU-MIMO system.

Table 6.3: Achievable groups and sum rates (R_H, R_L, and R_{sum}) of $4 \times 2/2$ GL-MU-MIMO system in bit/s/Hz at SNR $= 20$ and 30dB with different power allocation ratio (η)

power allocation ratio (η)	SNR $= 20$dB			SNR $= 30$dB		
	R_H	R_L	R_{sum}	R_H	R_L	R_{sum}
0.05	7.55	4.12	11.67	8.80	9.43	18.23
0.1	6.37	5.54	11.91	7.21	11.27	18.48
0.15	5.59	6.49	12.08	6.20	12.45	18.65
0.2	5.06	7.13	12.19	5.61	13.17	18.78
0.25	4.58	7.72	12.30	5.01	13.88	18.89
0.3	4.23	8.12	12.35	4.65	14.30	18.95
0.35	3.94	8.47	12.41	4.31	14.68	18.99
0.4	3.63	8.81	12.44	3.97	15.06	19.03
0.45	3.35	9.11	12.46	3.66	15.39	19.05

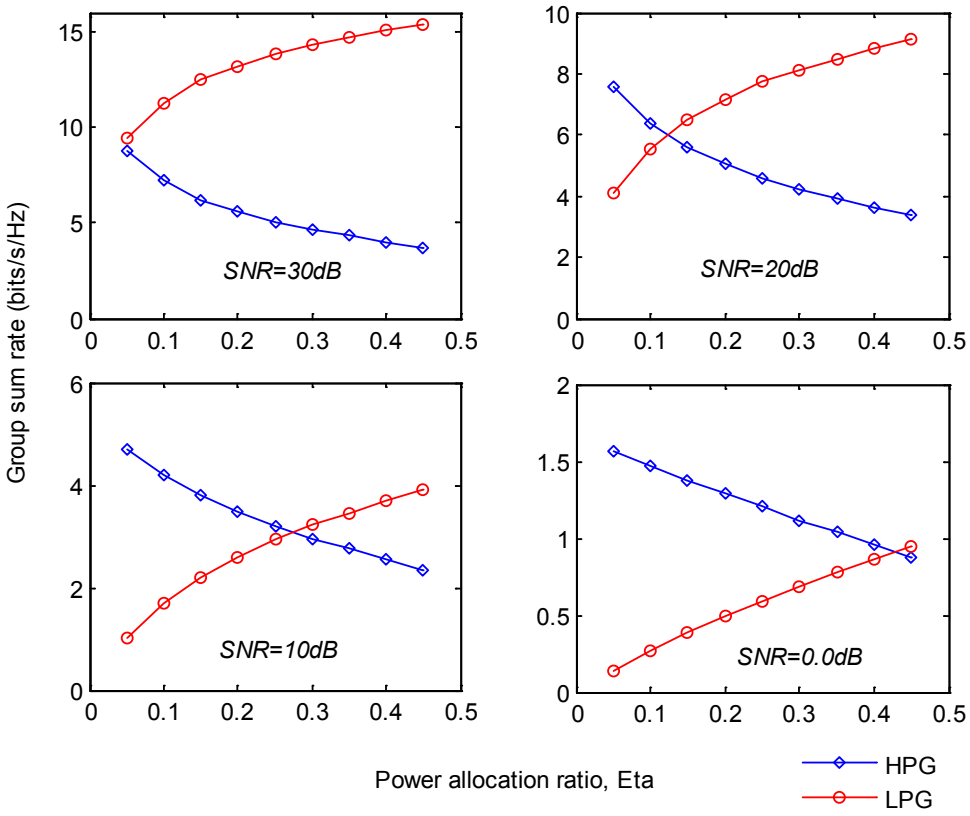

Figure 6.9: Group sum rate (R_H and R_L) of $4 \times 2/2$ GL-MU-MIMO system in bit/s/Hz as a function of power allocation ratio (η) for different SNR.

6.6.1.3 BER Performance

Without loss of generality, we consider representative examples to evaluate the average BER performance of GL-MU-MIMO scheme.

In Fig. 6.10, average BER performance of $4 \times 2/2$ system using ML/ML-MUD and different group power assignment ($\eta = 0.2,\ 0.15,\ 0.1,\ 0.05$) is shown compared with the conventional 4×4 (ZF), 4×2 (ML), and the reference 1×1 (16QAM). Obviously, the system performance over all SNR values is directly affected by the power allocation ratio η. For $\eta = 0.2$ and 0.15, the interference of LPG is high enough to degrade the system performance significantly. Using $\eta = 0.1$, performance of $4 \times 2/2$ system at BER$= 10^{-3}$ outperforms 4×4 (ZF) by approximately 1dB and less than 1×1 (16QAM) by 1dB. For same BER target and SNR ≥ 31dB, the system performance is decreased due to the high contribution of LPG signals to the combined received signal compared with the noise component $\mathbf{n}$. By using $\eta = 0.05$, the power of LPG users will be very little compared with HPG users causing less average BER performance compared with 4×4 (ZF). Therefore, appropriate η values should be selected to allow reliable communication for all served users. The performance results of $4 \times 2/2$ system using low complexity ML/ML-MUD and $\eta = 0.1$ at BER$= 10^{-3}$ compared with the full complexity 4×4 (ZF) system confirm the effectiveness of the proposed technique with significant saving of two receive antennas associated with the RF chains (double user capacity).

In Fig. 6.11, Average BER performance of HPG and LPG for $4 \times 2/2$ system using ML/ML-MUD and $\eta = 0.1$ is shown compared with 2×2 (ZF), 2×2 (ML), and 1×1 (16QAM). Due to the power difference among groups, performance of HPG is higher than LPG which results in unequal error protection. This is very useful to provide different quality of services (QoS) desired in modern wireless applications. For the same system, different values of η are examined and the results are shown in Fig. 6.12. As can be seen, performance of HPG is linearly dependent with η while LPG performance depends on the first detection layer of GL-MUD (i.e. HPG-MUD). The error propagation from HPG-MUD has the main influence on the overall system performance. Therefore, high performance of HPG will result in good error performance of LPG and vice versa. In the proposed GL-MU-MIMO scheme, careful η setting is of high importance to achieve the best system BER performance with most fairness between HPG and LPG performances and sum rates. In Fig. 6.13, BER performance of HPG and LPG with the average BER of $4 \times 2/2$ system is shown as a function of η for SNR $= 20$ and 30dB. As can be seen, $\eta = 0.1$ provides the best performance for this system set up.

To examine different configurations of GL-MUD for the considered $4 \times 2/2$ system compared with 4×4 (ZF) and 1×1 (16QAM), performance results using $\eta = 0.2,\ 0.15,\ 0.1,$ and 0.05 are shown in Fig. 6.14 when ZF/ZF-MUD is employed while Fig. 6.15 for the case of ZF/ML-MUD. For example at BER$= 10^{-3}$ with $\eta = 0.05$, ZF/ML-MUD outperforms

ZF/ZF-MUD by 5.5dB. At the same system setting and from Fig. 6.10 results, performance of ML/ML-MUD outperforms ZF/ML-MUD by 3dB. Since ZF/ZF-MUD is less complex than ZF/ML-MUD which in turns less complex than ML/ML-MUD, the results demonstrate a valuable trade off between system complexity and performance.

To improve the performance of $4 \times 2/2$ system for any GL-MUD configuration, some of the gain in user capacity (saving in antennas) should be sacrificed. In Fig. 6.16, Average BER performance of $4 \times 3/3$ system is shown using $\eta = 0.1$ with ML/ML-MUD, ZF/ZF-MUD and ZF/ML-MUD. In this system setup, the HPG of $4 \times 3/3$ system contains three users while LPG includes one user. Average BER results of conventional 4×4 (ZF), 4×3 (ML), and 1×1 (16QAM) are shown also for comparison. By adding one extra antenna to $4 \times 2/2$, performance of $4 \times 3/3$ is improved significantly due to low interference level of LPG user compared with the power of HPG users. In Table 6.4, SNR results and gain in dB compared with 4×4 (ZF) are given at target BER of 10^{-3} and for different GL-MUD configurations. For example by using ML/ML-MUD, $4 \times 3/3$ system outperforms 4×4 (ZF) by 10dB whereas 1dB gain is achieved for $4 \times 2/2$. Hence, gain of 9dB in SNR is achieved in this case for one extra antenna at the BS. As can be seen, using ZF/ZF-MUD or ZF/ML-MUD in $4 \times 2/2$ system represents infeasible choices for the GL-MUD configuration while they perform well in case of $4 \times 3/3$ according to their complexity.

Table 6.4: SNR and gain results in dB of $4 \times 2/2$ and $4 \times 3/3$ systems at BER of 10^{-3} for different GL-MUD configurations using $\eta = 0.1$ compared with the reference 29dB for 4×4 (ZF).

GL-MUD configuration	$4 \times 2/2$ [Fig. 6.10, 6.14 and 6.15]		$4 \times 3/3$ [Fig. 6.16]	
	SNR (dB)	Gain (dB)	SNR (dB)	Gain (dB)
ML/ML-MUD	28	1	19	10
ZF/ZF-MUD	Not applicable	Not applicable	31	-2
ZF/ML-MUD	38	-9	25	4

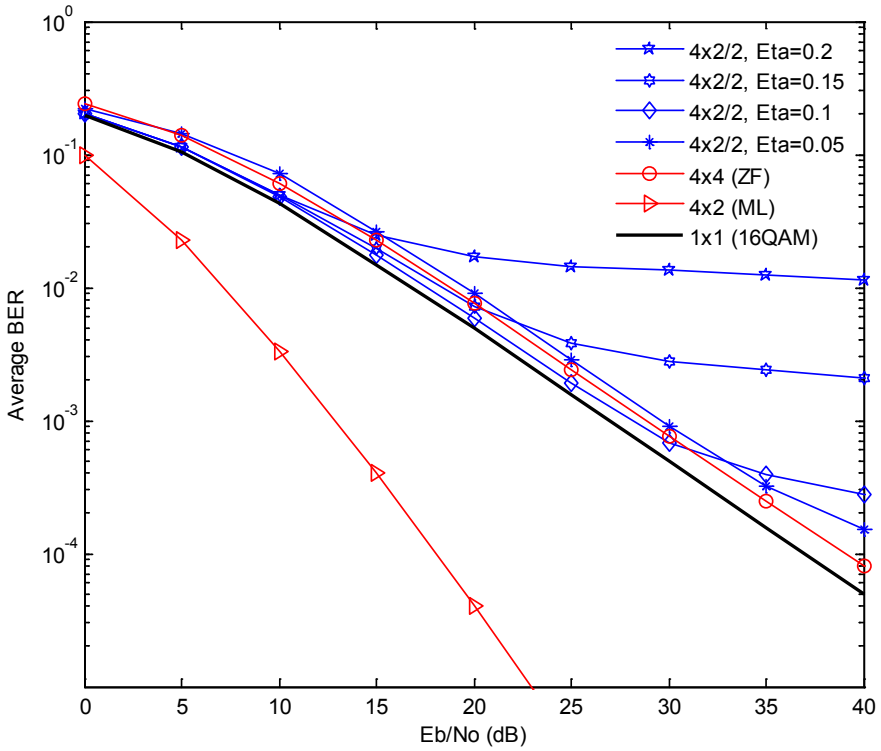

Figure 6.10: Average BER performance of $4 \times 2/2$ system using ML/ML-MUD and different group power assignment ($\eta = 0.2,\ 0.15,\ 0.1,\ 0.05$) compared with conventional 4×4 (ZF), 4×2 (ML), and 1×1 (16QAM).

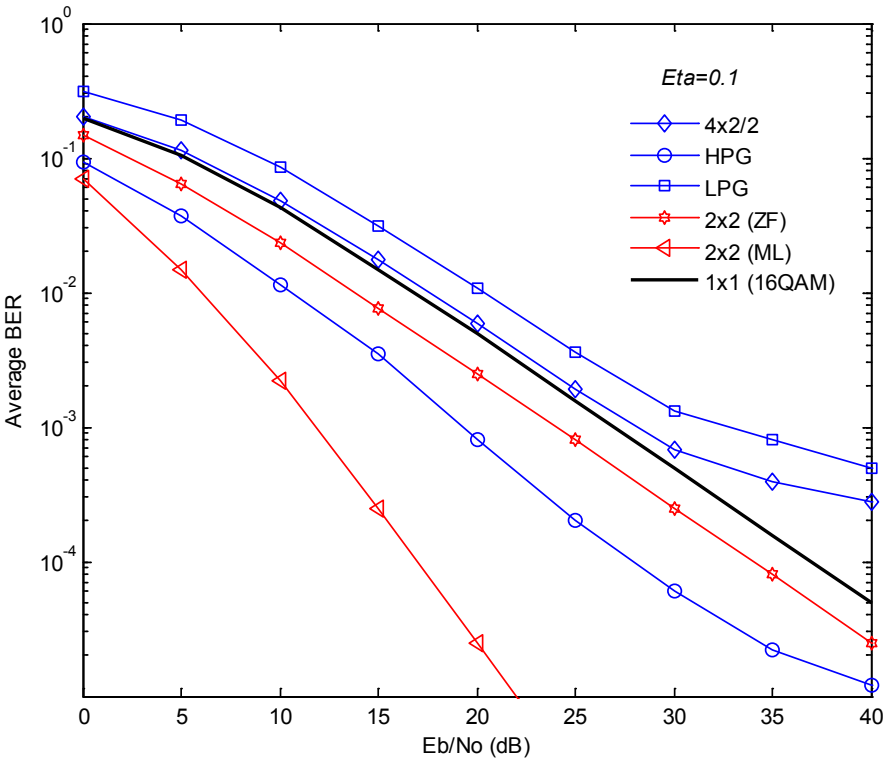

Figure 6.11: Average BER performance of HPG and LPG of $4 \times 2/2$ system using ML/ML-MUD and $\eta = 0.1$ compared with 2×2 (ZF), 2×2 (ML), and 1×1 (16QAM).

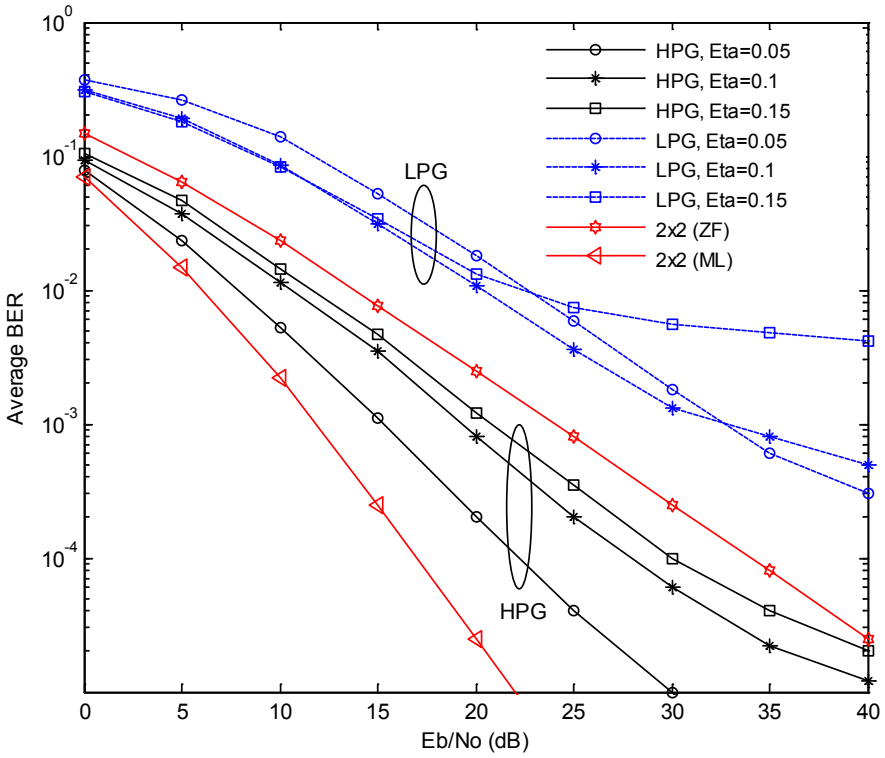

Figure 6.12: Average BER performance of HPG and LPG of $4 \times 2/2$ system using ML/ML-MUD and $\eta = 0.05, 0.1,$ and 0.15 compared with 2×2 (ZF) and 2×2 (ML).

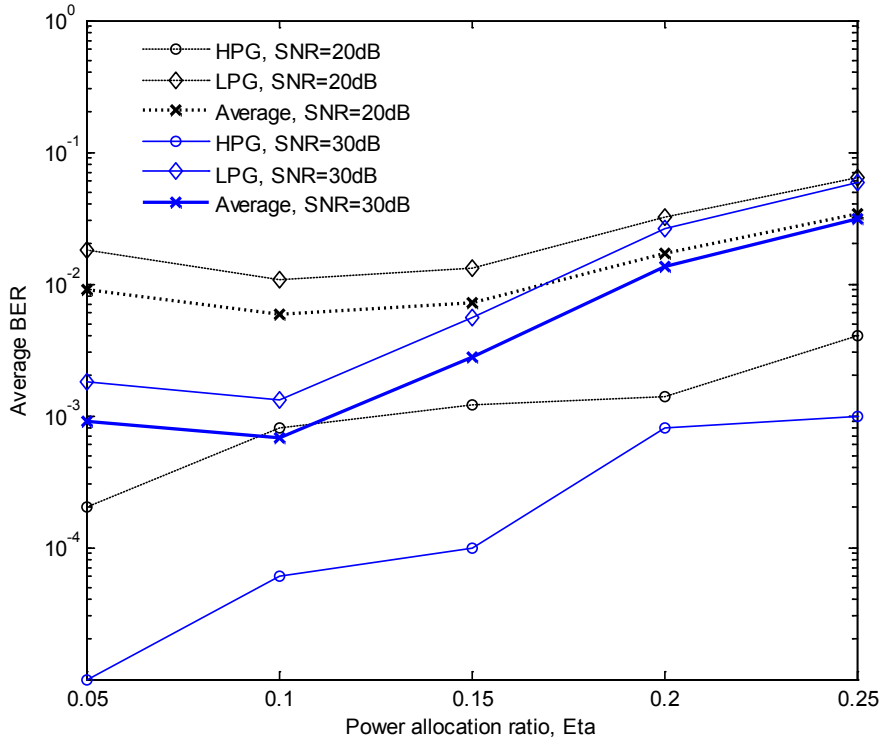

Figure 6.13: Average BER performance of $4 \times 2/2$ system with ML/ML-MUD as a function of power allocation ratio (η) and for SNR $= 20$ and 30dB.

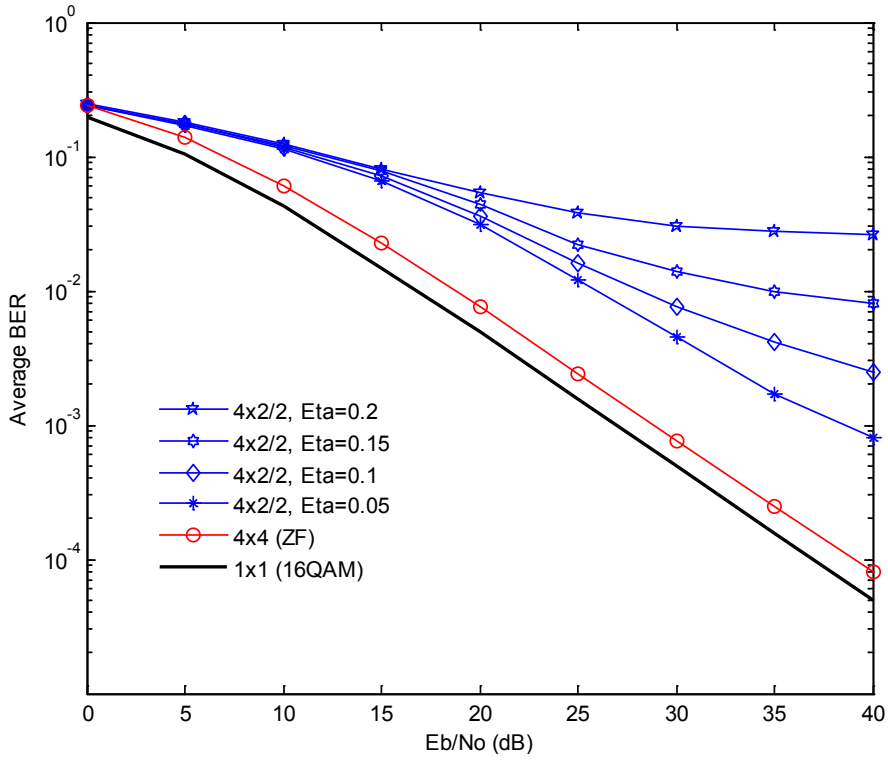

Figure 6.14: Average BER performance of $4 \times 2/2$ system using ZF/ZF-MUD and different group power assignment $(\eta = 0.2,\ 0.15,\ 0.1,\ 0.05)$ compared with conventional 4×4 (ZF), and 1×1 (16QAM).

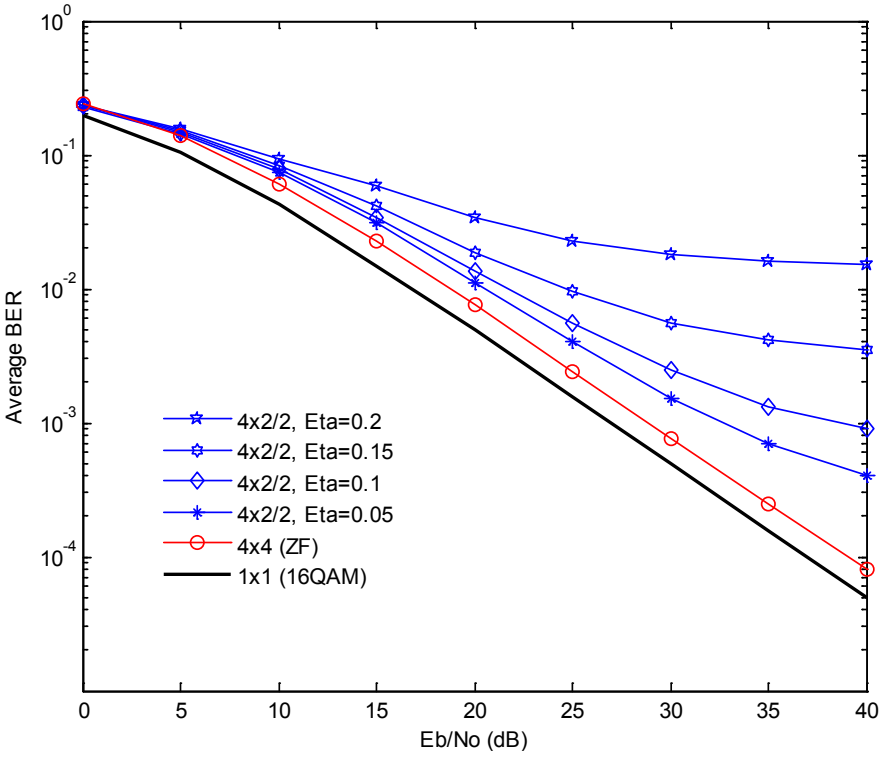

Figure 6.15: Average BER performance of $4 \times 2/2$ system using ZF/ML-MUD and different group power assignment $(\eta = 0.2,\ 0.15,\ 0.1,\ 0.05)$ compared with conventional 4×4 (ZF), and 1×1 (16QAM).

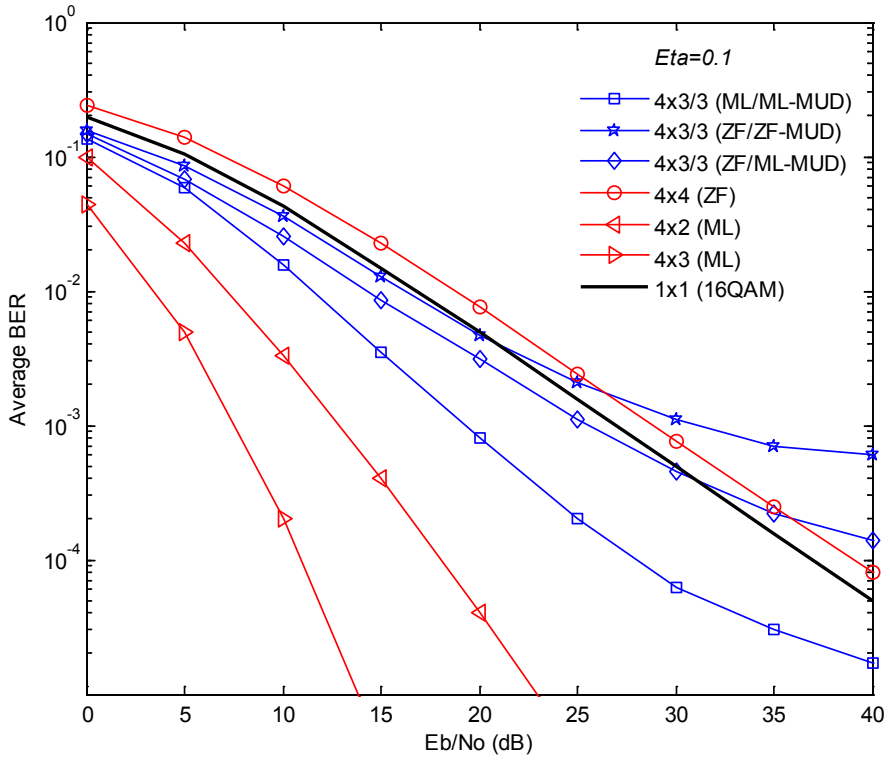

Figure 6.16: Average BER performance of $4 \times 3/3$ system using $\eta = 0.1$ with ML/ML-MUD, ZF/ZF-MUD and ZF/ML-MUD compared with conventional 4×4 (ZF), 4×3 (ML), and 1×1 (16QAM).

6.6.2 GL-MU-MIMO with RAS Diversity

6.6.2.1 Sum Rate Capacity

To evaluate the sum rate capacity of GL-MU-MIMO system with RAS, we consider without loss of generality the following system setup:$K = 4$, $m = 5$, $m_s = 2$ and $\eta = 0.2$. In Fig. 6.17, simulation results of $4 \times 5/$NBS-2 and $4 \times 5/$PDBS-2 are shown compared with $4 \times 2/2$ and 2×2 MU-MIMO systems.

As can be seen, systems with receive antenna selection provides higher sum rate capacity than the systems without selection diversity. Furthermore, sum rate of HPG-PDBS outperforms NBS for all SNR values. For example at spectral efficiency of 16 bit/s/Hz, HPG-PDBS shows 3.5dB gain in SNR compared with $4 \times 2/2$ while outperform NBS by 0.5dB. The gain that achieved with antenna selection diversity is of high importance to increase the groups sum rate and improve the average BER performance.

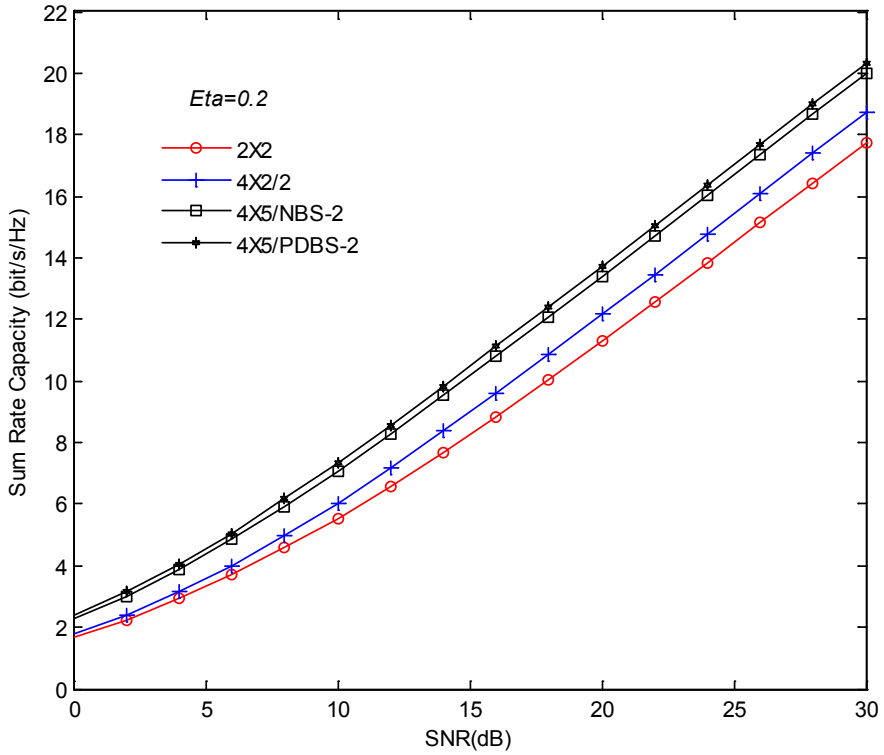

Figure 6.17: Sum rate capacity of 4×5/NBS-2 and 4×5/PDBS-2 GL-MU-MIMO systems using $\eta = 0.2$ compared with $4 \times 2/2$ and 2×2 MU-MIMO systems.

6.6.2.2 Capacity Region

Capacity region of 4×5/NBS-2 and 4×5/PDBS-2 systems with $\eta = 0.2$ are shown in Fig. 6.18 for SNR $= 10, 20$ and 30dB compared with $4 \times 2/2$ system. Using equations (6.29)-(6.31), the achievable group sum rates (R_H^s, R_L^s) and sum rate (R_{sum}^s) in bits/s/Hz are summarized in Table 6.5 for different values of SNR.

As can be seen, the sum rate of 4×5/PDBS-2 is higher than 4×5/NBS-2 which outperforms $4 \times 2/2$ system for all SNR values. Moreover, the achieved HPG sum rate R_H^s using HPG-PDBS is higher than of NBS for all SNR values due to selection process which depends on HPG channels $\mathbf{H}_H$ only. For example at SNR $=$ 20dB, point ($R_H^s = 6.09$, $R_L^s = 7.65$) is achieved using HPG-PDBS while the point is ($R_H^s = 5.34$, $R_L^s = 8.07$) when NBS is employed. In Fig. 6.19, groups sum rate (R_H^s and R_L^s) are shown also as a function of SNR. It can be seen that the equal rate point ($R_H^s = R_L^s$) using the proposed selection algorithms is achieved at different SNR values as 13dB for NBS and 16.2dB for HPG-PDBS. Therefore, selection diversity with different selection algorithms provides more flexibility of group rate management in addition to the substantial increase of sum rate capacity.

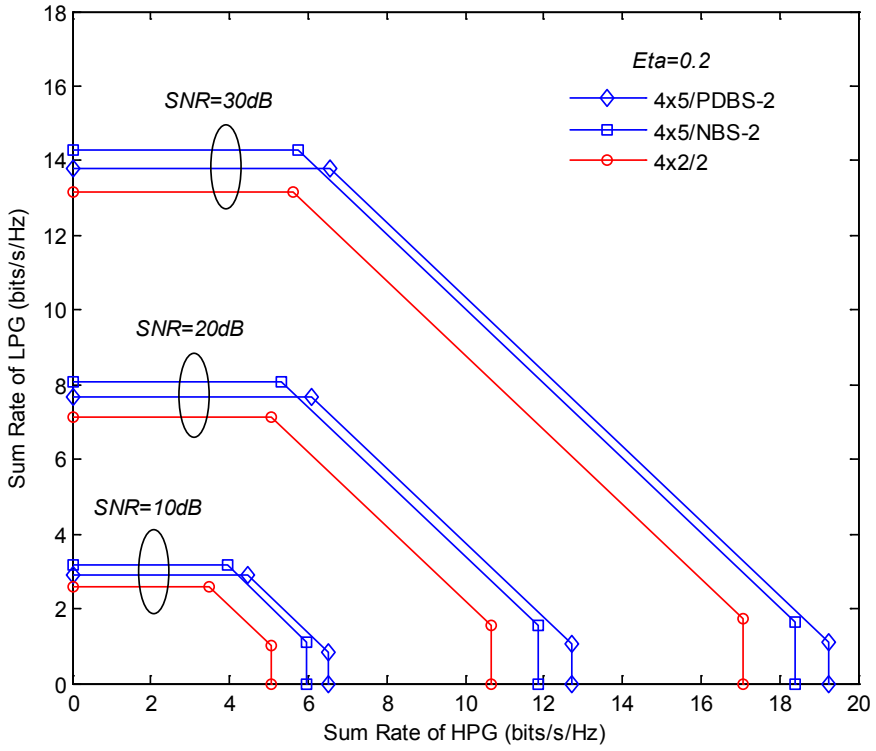

Figure 6.18: Capacity region $(R_H^s,\ R_L^s)$ of 4×5/NBS-2 and 4×5/PDBS-2 systems in bit/s/Hz at SNR $= 10,\ 20$ and 30dB with $\eta = 0.2$.

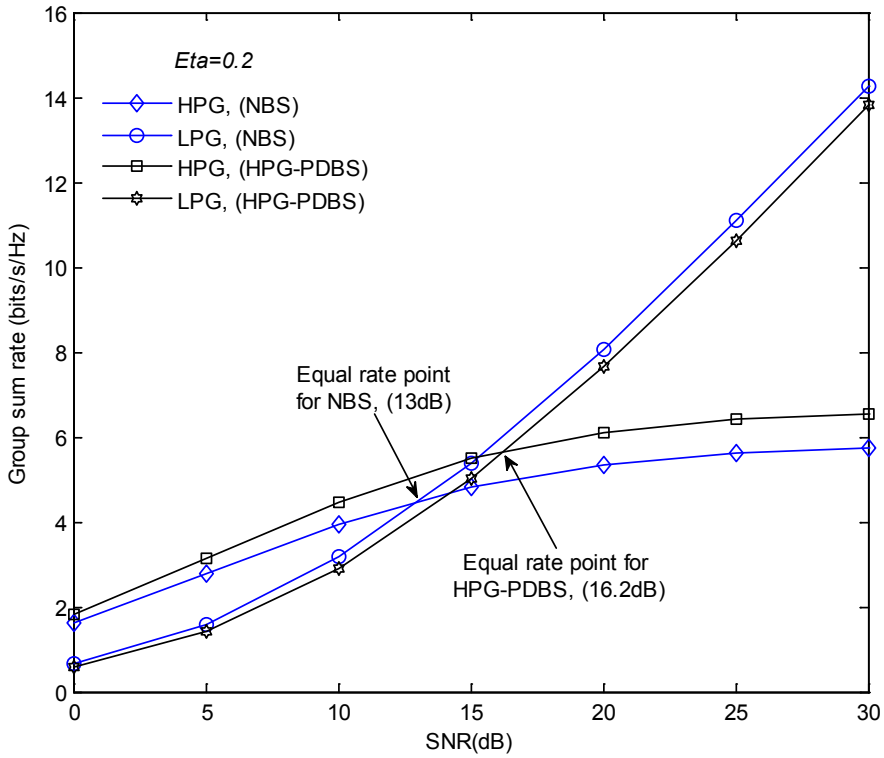

Figure 6.19: Group sum rate (R_H^s and R_L^s) of 4×5/NBS-2 and 4×5/PDBS-2 systems in bit/s/Hz as a function of SNR with $\eta = 0.2$.

Table 6.5: Achievable groups and sum rates (R_H^s, R_L^s, and R_{sum}^s) of 4×5/NBS-2 and 4×5/PDBS-2 systems in bit/s/Hz using $\eta = 0.2$ and different values of SNR

SNR (dB)	4×5/NBS-2			4×5/PDBS-2		
	R_H^s	R_L^s	R_{sum}^s	R_H^s	R_L^s	R_{sum}^s
0.0	1.63	0.65	2.28	1.81	0.57	2.38
10	3.93	3.16	7.09	4.47	2.88	7.36
20	5.34	8.07	13.41	6.09	7.65	13.74
30	5.75	14.26	20.01	6.55	13.80	20.35

6.6.2.3 BER Performance

To evaluate the average BER performance of GL-MU-MIMO system with antenna selection, we consider the following system setup: $K = 4$; $m = 4, 6$; $m_s = 2$; and $\eta = 0.1$.

In Fig. 6.20, average BER performance results of $4 \times 2/2$, 4×4/NBS-2, 4×6/NBS-2, 4×4/PDBS-2, and 4×6/PDBS-2 using ML/ML-MUD are shown compared with 4×4 (ZF), 2×2 (ZF),and 4×2 (ML). For ZF/ZF-MUD and ZF/ML-MUD configurations, the results are shown in Fig. 6.21 and Fig. 6.22 compared with 4×4 (ZF).

Using NBS or HPG-PDBS, the BER performance improved as m increased compared with $4 \times 2/2$ system (without antenna selection) and 4×4 (ZF). Also for a given number of receive antennas m, the performance of ML/ML-MUD configuration outperforms ZF/ML-MUD which in turn outperforms ZF/ZF-MUD. In Table 6.6, SNR and gain results are shown in dB at target BER of 10^{-3} for 4×4/NBS-2, 4×6/NBS-2, 4×4/PDBS-2 and 4×6/PDBS-2 with different GL-MUD configurations compared with 29dB for 4×4 (ZF). From this table, HPG-PDBS outperforms NBS for same m receive antennas and GL-MUD configuration. For example when ZF/ML-MUD is used, HPG-PDBS outperforms NBS by 2.5dB when $m = 4$ while 1.5dB is achieved for $m = 6$. The results of low complexity ML/ML-MUD compared with the full complexity 4×4 (ZF) system confirms and validate the effectiveness of proposed technique with significant saving of two receive antennas associated with the RF chains. Compared with results of $4 \times 2/2$ system (without antenna selection) given in Table 6.4 at BER of 10^{-3}, the achieved SNR gain using NBS is 2dB when $m = 4$ and 3.5dB for $m = 6$. For HPG-PDBS, gain of 3dB is achieved when $m = 4$ and 5dB for $m = 6$. Therefore, antenna selection diversity has a significant impact to improve the average BER performance of GL-MU-MIMO system and its groups.

Table 6.6: SNR and gain results in dB of 4×4/NBS-2, 4×6/NBS-2, 4×4/PDBS-2 and 4×6/PDBS-2 at BER of 10^{-3} with different GL-MUD configurations and $\eta = 0.1$ compared with 29dB for 4×4 (ZF).

MUD configuration	4×4/NBS-2		4×6/NBS-2		4×4/PDBS-2		4×6/PDBS-2	
	SNR (dB)	Gain (dB)	SNR (dB)	Gain (dB)	SNR (dB)	Gain (dB)	SNR (dB)	Gain (dB)
ML/ML-MUD [Fig. 6.20]	26	3	24.5	4.5	25	4	23	6
ZF/ZF-MUD [Fig. 6.21]	Not applicable	Not applicable	39	-10	40	-11	36	-7
ZF/ML-MUD [Fig. 6.22]	34	-5	31	-2	31.5	-2.5	29.5	-0.5

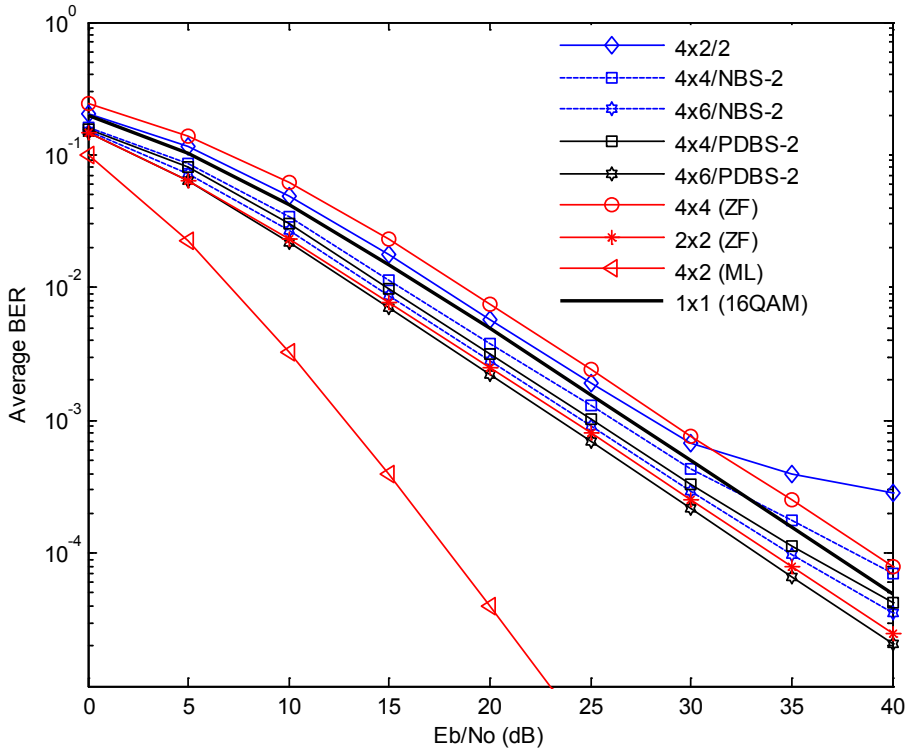

Figure 6.20: Average BER performance of $4 \times 2/2$, 4×4/NBS-2, 4×6/NBS-2, 4×4/PDBS-2, and 4×6/PDBS-2 GL-MU-MIMO using ML/ML-MUD and $\eta = 0.1$ compared with 4×4 (ZF), 2×2 (ZF), 4×2 (ML), and 1×1 (16QAM).

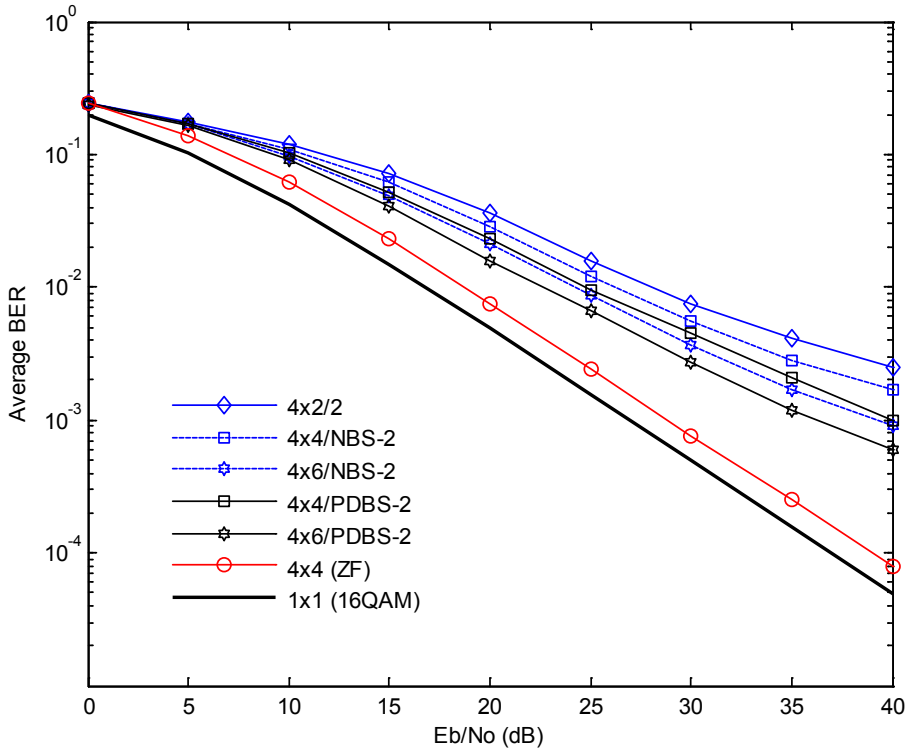

Figure 6.21: Average BER performance of $4 \times 2/2$, 4×4/NBS-2, 4×6/NBS-2, 4×4/PDBS-2, and 4×6/PDBS-2 GL-MU-MIMO using ZF/ZF-MUD and $\eta = 0.1$ compared with 4×4 (ZF), and 1×1 (16QAM).

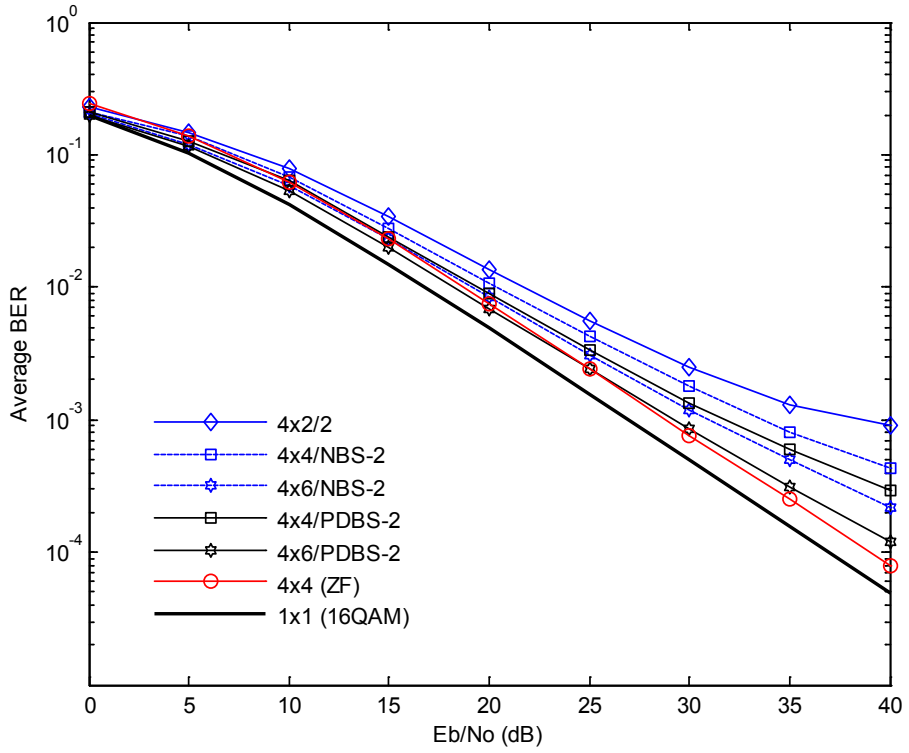

Figure 6.22: Average BER performance of $4 \times 2/2$, 4×4/NBS-2, 4×6/NBS-2, 4×4/PDBS-2, and 4×6/PDBS-2 GL-MU-MIMO using ZF/ML-MUD and $\eta = 0.1$ compared with 4×4 (ZF), and 1×1 (16QAM).

6.7 Simulation Results of GL-MU-MIMO over Correlated Channels

In MU-MIMO systems, users with highly correlated channels due to poor scattering and/ or insufficient antenna spacing at their terminals may not be served which reduces the user and sum rate capacity significantly [18, 23, 86, 181]. In this section, effects of channel correlation on the performance of GL-MU-MIMO system are investigated. For this objective, the fading signals of H with correlated envelopes and independent phases are generated using ICT [141, 142] for correlation matrix of envelopes $\rho \in \mathcal{R}^{\mathrm{Km}\times\mathrm{Km}}$. The entries of ρ represents the correlation factor ρ_{ij} between i^{th} and j^{th} fading signal envelope in the interval $[0, 1]$. To demonstrate and validate the overall performance of GL-MU-MIMO over flat CRFC, Monte Carlo simulations have been carried in this section. The results are averaged using 10,000 channel realization for sum rate capacity evaluation. For BER performance, a frame of 100 symbols from BPSK constellation is assumed for each channel realization where the channel still constant over the entire frame length and changes independently from frame to the next. In all simulations, we consider equal correlation among different Rayleigh fading paths as $\rho_{ij} = \rho\ ;\ \forall i \neq j;\ i, j = 1, \ldots, \mathrm{Km}$.

6.7.1 Sum Rate Capacity

To evaluate the sum rate capacity of GL-MU-MIMO with/without RAS, we consider the following system setup: $K = 4$; $m = 2, 5$; $m_s = 2$; and $\eta = 0.2$. In Fig. 6.23, simulation results of $4 \times 5/$NBS-2 and $4 \times 5/$PDBS-2 are shown compared with $4 \times 2/2$ and 2×2 MU-MIMO systems for moderate correlation level of $\rho = 0.5$. Results of high correlation level of $\rho = 0.9$ are shown in Fig. 6.24. It can be seen that sum rate of systems with RAS are less affected by the correlation level than the systems without selection diversity. Furthermore, as the correlation level increased, HPG-PDBS shows better performance than NBS. For example at spectral efficiency of 14 bit/s/Hz and $\rho_{ij} = 0.5$, HPG-PDBS shows 2.7dB gain in SNR compared with $4 \times 2/2$ while outperform NBS by 1.5dB. For $\rho = 0.9$, HPG-PDBS has 4.2dB gain compared with $4 \times 2/2$ and outperform NBS by 2.0dB. The achieved gain of proposed GL-MU-MIMO with antenna selection diversity is of high importance to enable robust performance over different channel correlation conditions.

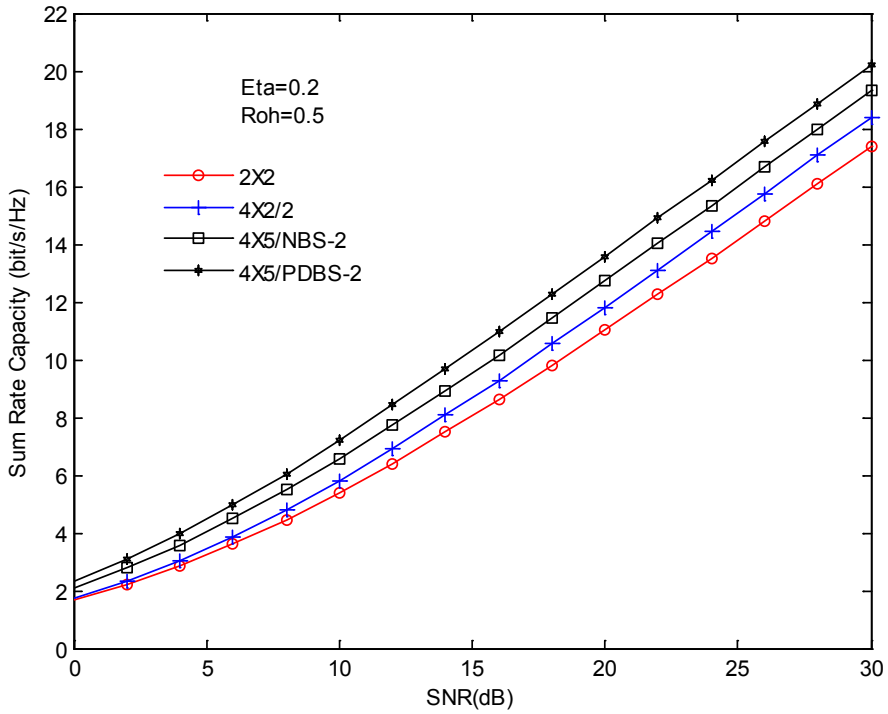

Figure 6.23: Sum rate capacity of $4 \times 5/$NBS-2 and $4 \times 5/$PDBS-2 GL-MU-MIMO systems using $\eta = 0.2$ over CRFC ($\rho = 0.5$) compared with $4 \times 2/2$ and 2×2 MU-MIMO systems.

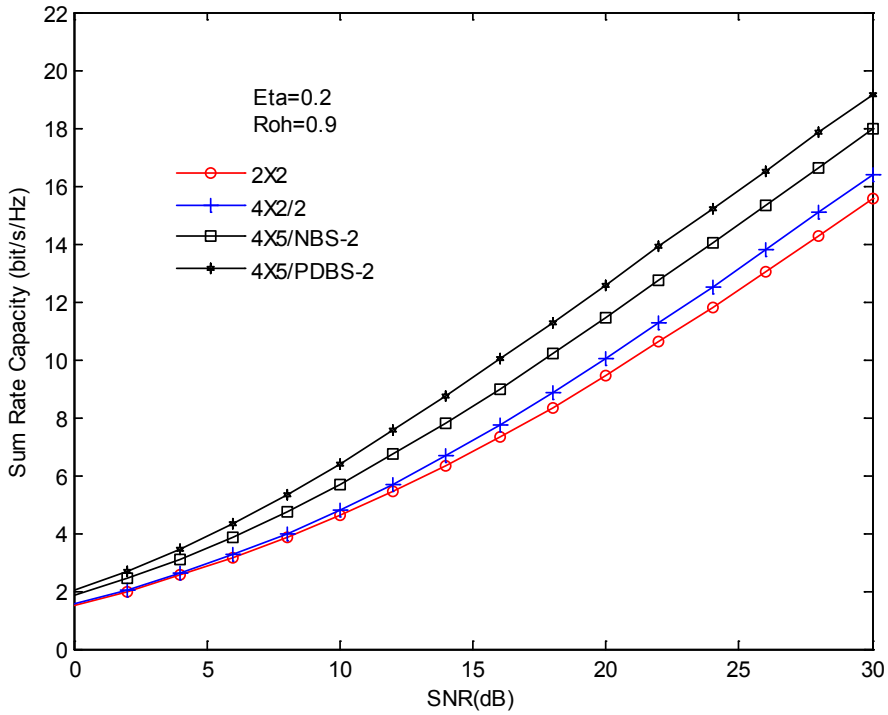

Figure 6.24: Sum rate capacity of $4 \times 5/$NBS-2 and $4 \times 5/$PDBS-2 GL-MU-MIMO systems using $\eta = 0.2$ over CRFC ($\rho = 0.9$) compared with $4 \times 2/2$ and 2×2 MU-MIMO systems.

6.7.2 BER Performance

To demonstrate the effects of channel correlations on the BER performance of GL-MU-MIMO, simulations results are shown in Fig. 6.25 for $4 \times 2/2$, 4×4/NBS-2, and 4×4/PDBS-2 using $\eta = 0.1$ and ML/ML-MUD. To investigate the performance on wide range of correlation levels, two extreme cases are considered as $\rho = 0.0$ for uncorrelated channels and $\rho = 0.9$ for high correlations. The reference performance results of conventional 4×4(ZF) and 4×2(ML) are shown also for comparison.

For conventional MU-MIMO, the correlation has serious impact on the BER when nonlinear ZF receiver is employed compared with ML receiver. For example at BER of 10^{-3}, the SNR loss is approximately 11.5dB for ZF whereas 3dB for ML. Therefore, the receive diversity should be increased by increasing the number of receive antennas or reducing the number of served users (user capacity) to maintain a reliable communication.

For GL-MU-MIMO system without antenna selection at same BER level of 10^{-3}, the SNR loss of $4 \times 2/2$ is 9dB. Therefore, the performance is degraded as the correlation increased. When antenna selection diversity is utilized and as the correlation increased, the proposed system shows a significant gain in SNR of 2dB for 4×4/NBS-2 and 3dB for 4×4/PDBS-2. Interestingly, channel correlation has the effects to increase the performance of GL-MU-MIMO with antennas selection in contrast to the others. As a result for example, the SNR gain of 4×4/PDBS-2 compared with 4×4(ZF) is 4dB for uncorrelated channels and increased to approximately 19dB for high correlation levels. Also, the SNR gap between 4×4/PDBS-2 and 4×2(ML) is 12.5dB for uncorrelated channels and reduced to 6dB for high correlation levels. Therefore, GL-MU-MIMO system with antennas selection provides improved BER performance and maintains robust user and sum rate capacity.

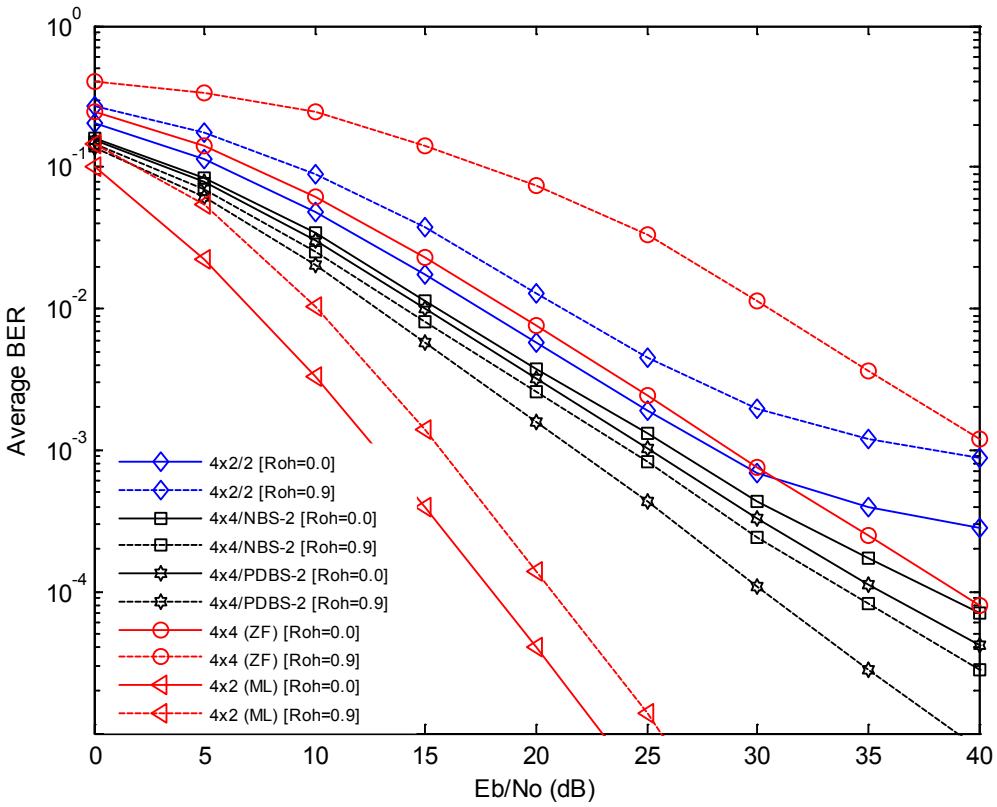

Figure 6.25: Average BER performance of GL-MU-MIMO system using ML/ML-MUD and $\eta = 0.1$ over correlated Rayleigh fading channel.

6.8 Conclusions

In this chapter, a new GL-MU-MIMO scheme is designed to increase the user capacity over Rayleigh fading MAC using the available number of RF chains at BS receiver, low complexity GL-MUD, and RAS diversity. It takes the advantages of spatial difference among users and power control at BS to increase the number of users beyond number of RF chains ($m_s + 1 \leq K \leq 2m_s$) by dividing them into two groups according to their received power. Users near the cell edges are served without need of increasing their power which leads to significant reduction in cochannel interference to neighbouring cells. Furthermore, the proposed technique increases the sum rate capacity and provides fair rate distribution among users with unequal error protection.

Extensive simulation results demonstrate the superiority of proposed scheme compared with conventional MU-MIMO system. By using appropriate power allocation ratio η, it shows higher sum rate capacity and substantial increase in the user capacity up to two-fold at target BER and SNR values. Users of HPG achieve high BER performance and data rate while LPG users are able to maintain high rate and fair error performance due to their path loss. Without RAS diversity ($m = m_s$), high performance is achieved by employing different GL-MUD

configurations and controlling the LPG interference level through its size. When $m > m_s$, the selection diversity through NBS and HPG-PDBS algorithms improves the sum rate and BER performance significantly. For same number of accommodated users K, BER of proposed scheme using HPG-PDBS and ML/ML-MUD outperforms that of MU-MIMO system using ZF receivers with significant saving of receive antennas associated with the RF chains (higher user capacity). Furthermore, in correlated channel environment, it outperforms conventional system in terms of sum rate capacity and BER. As the correlation increased, the achieved gain is increased significantly.

A valuable tradeoff between system complexity and achieved capacity and error performance can be implemented using appropriate value of η, different GL-MUD configurations, number of receive antennas m, and antenna selection methods. Therefore, this technique provides efficient spectrum utilization and reliable communication for high user overloading in practical wireless systems with affordable complexity.

Chapter 7

Conclusions and Future Work

7.1 Conclusions

In this thesis, many contributions have been made to fulfil the increasing demand of high spectral efficiency and user capacity for modern and future wireless communication systems in different channel environment. In chapter 2, extensive analysis on capacity region of Gaussian MAC and the benchmark results of different 2-user multiple access techniques demonstrate that spatial dimension enables significant increase in the channel capacity. It represents one of the best competitive directions to meet the requirement of next generation mobile systems and already adopted by means of SU-MIMO and MU-MIMO in LTE and WiMAX standards. Furthermore, S-C and SIC techniques can be integrated with other multiple access methods for further improvement on the capacity and BER performance with low complexity requirements. Therefore, we specifically utilizes the spatial dimension in multiantenna systems with different techniques such as signal constellation design, antenna selection diversity, user grouping, signal superposition, successive cancellation, and low complexity detection to achieve the targets towards Gigabits communications.

For practical system design and performance evaluations, channel correlation has been considered in this thesis as one of the main channel impurities due its severe influence on diversity, capacity, and multiplexing gains. Therefore, chapter 3 focused on accurate generation methods for CRFC which have been utilized in the rest of the thesis. A new scheme has been proposed in chapter 4 to mitigate the correlation effects on channel capacity and BER performance of MU-MIMO systems. In chapter 5, a novel RAS method has been introduced to maximize the channel capacity of single and multiuser MIMO systems over CRFC. In chapter 6, a new approach was proposed to increase the user and sum rate capacity for MU-MIMO system using the available RF chains at BS with RAS diversity and low detection complexity. The main achievements of this thesis are summarized in the following.

In Chapter 3, two simple techniques refereed to as GSCT and GICT have been proposed for the generation of equal and unequal power CRFC for multiantenna and multicarrier systems. They were designed to overcome the shortcomings of existing methods by avoiding decomposition of desired covariance matrix of the Gaussian samples. Different radio propagation conditions were considered in these techniques.

Successive coloring of uncorrelated reference fading signals for all successive pairs is employed in GSCT by utilizing the real correlation vector of desired signal envelopes. In this technique, any number of fading signals $\mathcal{N}$ with any desired correlations of successive envelope pairs can be simulated accurately while correlations of all other pairs are determined by the related successive pairs. The effectiveness of GSCT compared with existing methods has been demonstrated through extensive simulations of practical system scenarios. This method overcomes the shortcomings of conventional methods particularly as the number of fading signals increases and/or moderate to high correlations is used. For small number of fading signals and/or low correlation levels, it provides high accuracy for the successive pairs similar to existing methods with significant reduction in computational complexity of $\mathcal{O}(\mathcal{N}^2)$.

Iterative coloring of uncorrelated reference signals is employed in GICT by utilizing the real correlation matrix of signal envelopes. Different practical system scenarios have been simulated to show the superiority of GICT for generating any number of fading signals with any desired correlations. It overcomes the shortcomings of conventional methods when the number of fading signals increases and/or moderate to high correlations is required. Furthermore, it provides high accuracy with less computational complexity of $\mathcal{O}(\mathcal{N}^2)$ for the case of generating small number of fading signals and/or low correlation levels. For $\mathcal{N} \leq 6$, GICT provides higher accuracy than GSCT since it considers the correlations of all signal pairs in the generation process. However, GSCT is more convenient for $\mathcal{N} > 6$ since it utilizes the correlation vector of successive envelopes and less complex compared with GICT.

For the generation of realistic fading channels, analysis of conventional methods demonstrates that none of them is able to generate any number of correlated fading signals with any desired correlation. Therefore, simplicity and accuracy of these techniques will help the researchers to study and simulate the impact of channel correlations on various multiantenna and multicarrier systems. Furthermore, the proposed methods enable efficient design, deployment and integration of new techniques into real wireless applications.

In Chapter 4, a novel scheme has been designed to mitigate the effects of channel correlations for MU-MIMO system using constrained transmit signal constellation and MLJD at the receiver. It is referred to as CC-MU-MIMO and takes the advantages of spatial difference among active users with accurate power control at BS to maximize the channel capacity and BER performance for any correlation level. Two signal design methods named as UPA and RC have been utilized to resolve the detection ambiguity caused by channel correlation through maximizing d_{min} of composite received signals.

The effectiveness of proposed scheme has been demonstrated through extensive analysis and simulations compared with the conventional MU-MIMO systems. Both of signal design methods show robust and stable performance irrespective of correlation values ρ. Significant gain in SNR is achieved particularly in moderate to high correlation levels. For example, gain of

11dB is achieved for 4×4 system using UPA-QPSK or RC-QPSK compared with IC-QPSK at target BER of 10^{-5} and correlation level $\rho = 0.9$. Furthermore, 8dB gain is achieved to reach the maximum capacity of $\log_2(4^4) = 8$ bit/s/Hz.

In CC-MU-MIMO, maximizing channel capacity and BER performance have the effects to maintain high user capacity even in sever correlation environment without need of extra receive diversity. Therefore, it provides high spectral efficiency and reliable communication regardless of channel correlation levels. Furthermore, the simplicity of UPA compared with RC method and the possibility of power control at BS makes this method more feasible to be integrated in the available systems.

In Chapter 5, a new PDBS algorithm has been proposed to maximize the channel capacity of single and multiuser MIMO systems employing RAS over CRFC environment. It takes the advantages of NBS and OS methods to provide a competitive performance near to OS with significant reduction in complexity of $\mathcal{O}(mu^2)$ vector calculations. It exploits the Euclidean norm of channel matrix row with their corresponding phase difference for the selection process rather than exhaustive search over all possible antenna combinations and capacity calculations as in OS algorithm. Extensive analysis and simulations demonstrate the superiority of proposed method. It has been shown that channel capacity using PDBS outperform NBS and close to OS for any SNR and correlation values ρ. For fixed ρ and as m and/or m_s increases, the capacity and BER gains are increased significantly. Furthermore, it shows more robust channel capacity in correlated environment compared with NBS and conventional MIMO systems without RAS.

For multiuser systems, RAS using PDBS maintains high user capacity even in sever channel correlations. It provides a robust solution for users with highly correlated channels instead of terminating them as in conventional systems. MIMO systems with imperfect channel estimation suffer from high performance degradation, specifically at high SNR. However, providing more receive antennas than the available RF chains with RAS technique has the effect to reduce the performance loss. This low complexity technique enable fast RAS to capture most of the large gains promised by multiantenna systems over different channel conditions.

In Chapter 6, GL-MU-MIMO scheme has been proposed to increase the user capacity over Rayleigh fading MAC using the available number of RF chains m_s at BS receiver, low complexity GL-MUD, and RAS diversity. The number of users K has been increased beyond the available number of RF chains $(m_s + 1 \leq K \leq 2m_s)$ by taking the advantages of spatial difference among them and power control at BS. They are divided into two groups according to their received power. In this scheme, users near the cell edges are served without increasing their power which leads to significant reduction in cochannel interference to neighbouring cells. Additionally, our scheme increases the sum rate capacity and provides fair rate distribution among served users with unequal error protection advantage.

The effectiveness of proposed scheme compared with conventional MU-MIMO has been demonstrated through extensive analysis and simulations. By using appropriate power allocation ratio η, it shows higher sum rate capacity and substantial increase in the user capacity up to two-fold at target BER and SNR. HPG users achieve high BER performance and rate while LPG users are able to maintain high rate and fair error performance due to their propagation path loss. Without RAS diversity, high error performance is achieved by employing ML/ML-MUD and controlling the LPG interference level through its size. With RAS diversity using NBS or HPG-PDBS, the sum rate and BER performance are improved significantly. For same number of users K, the BER of our scheme using HPG-PDBS and ML/ML-MUD outperforms that of MU-MIMO using ZF receivers with significant saving of receive antennas associated with the RF chains (higher user capacity). Furthermore, in correlated channel environment, it outperforms the conventional system in terms of sum rate capacity and BER. As the correlation level increased, the achieved gain is increased considerably.

In the presented system, a valuable tradeoff between complexity and overall performance improvement can be implemented using suitable value of η, different GL-MUD configurations, number of receive antennas m, and selection methods. Therefore, it provides efficient spectrum utilization and reliable communication for practical wireless applications with affordable complexity and cost.

7.2 Future Work

There are a variety of productive areas for future work on MU-MIMO wireless systems and related topics. In the following, we address some of the important ones related to the subjects presented in this thesis for further consideration.

- **Correlated Channel Modeling:** The problem of generation realistic correlated fading channels for multiantenna and multicarrier systems is tackled in chapter 3 using two methods. The proposed methods are mainly designed for CRFC environment. However, mobile cellular systems may experienced different fading channel environments such as Rayleigh, Rician and Nakagami processes due to their locations and the scattering, reflecting and diffracting objects. Therefore, it is worthwhile to explore a unified approach for generating heterogenous families of fading processes using the proposed successive and iterative coloring techniques. This will enable sufficient testing and performance evaluation of different wireless systems under these circumstances.

- **Signal Constellation Design:** In chapter 4, maximum capacity and error performance of CC-MU-MIMO system is maintained over correlated channels by employing constrained transmit signal constellation and MLJD at the BS receiver. Further

investigations can be carried out using different suboptimal SD methods to reduce the detection complexity and provide a reasonable performance tradeoff according to system requirements. Additionally, it is worthwhile to extend this study by combining the approach of CC-MU-MIMO with that of GL-MU-MIMO for robust and higher user/channel capacity system over different correlation conditions. The broadcast channel of MU-MIMO system with these proposed future works can be investigated also. Based on the availability of CSI at the transmitters' side, the idea of signal constellation design with MLJD can be exploited in future work for new efficient multiple access technique. This can be used in hybrid manner with different conventional multiple access methods for higher capacity multiuser communications.

- **Antenna Selection Diversity:** Channel capacity maximization for single and multiuser MIMO systems over CRFC is investigated in chapter 5 by employing low complexity suboptimal RAS method. The proposed PDBS method utilizes the largest Euclidean norm of channel matrix rows with their corresponding phase differences. As extension of this work, we suggest joint user and RAS for MUMA systems when the total number of active users' antennas is larger than available RF chains. For same situation, TAS at the user side could be included for further investigation to increase the user capacity (i.e. accommodating more users) and/or the achievable sum rate capacity. Constellation constrained capacity for MUMA with TAS and/or RAS could be investigated also in the future work. From another direction, joint channel estimation and antenna selection can be implemented in further studies by utilizing for example the training phase signals. In such a case, OS can be performed by maximizing d_{min} of the composite received constellation of training phase signals (BPSK). Furthermore, user selection can be integrated to achieve the user diversity.

- **High User Capacity Systems:** GL-MU-MIMO scheme is presented in chapter 6 for high user capacity based on users' grouping and low complexity GL-MUD. RAS diversity is utilized also for more improvement. For $K > 2m_s$ and according to the availability of CSI at BS receiver, adaptive user scheduling and group formations to achieve user diversity are left for future research. This will have direct impact on controlling the interference of LPG and hence overall system performance. From the detection side, efficient and low complexity MUD methods using MMSE, SD etc. with interference cancellation would be useful to investigate. In addition, the issue of error propagation from HPG to LPG during the detection process needs more consideration. Based on training phase signals, further investigations on joint channel estimation and selection criteria of user and/or antenna (transmit and/or receive) can be carried out to improve the system performance. For system optimization, different group formation scenarios can be

explored when the users equipped with different number of antennas. This could be based on the selection of best subset of transmit antennas (belong different users) for user and channel capacity maximization or any one of these metrics. Adaptive constrained signal constellation design among users in each group is another direction of future investigation to mitigate the effects of channel correlations. We expect that this approach will maintain high transmission rate and BER performance as found in chapter 4. Last but not least, extension of GL-MU-MIMO scheme to the downlink channel is natural for future studies due to high demands of wireless services such as internet and media applications.

References

[1] S. Parkvall, A. Furuskar, and E. Dahlman, "Evolution of LTE toward IMT-Advanced," *IEEE Commun. Magazin*, vol. 49, no. 2, pp. 84-91, Feb. 2011.

[2] Q. Li, A. Furuskar, G. Li, W. Lee, M. Lee, D. Mazzarese, B. Clerckx , and Z. Li, "MIMO Techniques in WiMAX and LTE: A Feature Overview," *IEEE Commun. Magazin*, vol. 48, no. 5, pp. 86-92, May. 2010.

[3] J. Duplicy, B. Badic, R. Balarj, R. Ghaffar et al., "MU-MIMO in LTE Systems," *EURASIP Journal On Wireless Commun. and Networking,* vol. 2011, ID 496763, pp. 1-13, 2011.

[4] A. Ghosh, R. Ratasuk, B. Mondal, N. Mangalvedhe, and T. Thomas, "LTE-Advanced: Next-Generation Wireless Broadband Technology," *IEEE Wireless Commun.*, vol. 17, no. 3, pp. 10-22, Jun 2010.

[5] S. Ahmadi, "An Overview of Next-Generation Mobile WiMAX Technology," *IEEE Commun. Magazin*, vol. 47, no. 6, pp. 84-98, Jun. 2009.

[6] J. Mietzner, R. Schober, L. Lampe, W. Gerstacker, and A. Hoeher, "Multiple-Antenna Techniques for Wireless Communications – A Comprehensive Literature Survey," *IEEE Commun. Surveys & Tutorials*, vol. 11, no. 2, pp. 87-105, seconed quarter 2009.

[7] H. Li, G. Ru, and H. Liu, "OFDMA Capacity Analysis in MIMO Channels," *IEEE Trans. Inform. Theory*, vol. 56, no. 9, pp. 4438-4446, Sep. 2010.

[8] T. Maciel, and A. Klein, "On the Performance, Complexity, and Fairness of Suboptimal Resource Allocation for Multiuser MIMO-OFDMA Systems," *IEEE Trans. Vehicular Technology*, vol. 59, no. 1, pp. 406-419, Jan. 2010.

[9] P. Chan, E. Lo, V. Lau, R. Cheng, K. Letaief, R. Murch, and W. Mow, "Performance Comparision of Downlink Multiuser MIMO-OFDMA and MIMO-MC-CDMA with Transmit Side Information – Multi-Cell Analysis ," *IEEE Trans. Wireless Commun.*, vol. 6, no. 6, pp. 2193-2203, Jun. 2007.

[10] P. Rossi, "On Throughput of MIMO-OFDM Systems with Joint Iterative Channel Estimation and Multiuser Detection under Different Multiple Access Schemes," *IEEE Commun. Letters*, vol. 15, no. 8, pp. 831-833, Aug. 2011.

[11] L. Hanzo, and B. Choi, "Near-Instantaneously Adaptive HSDPA-Style OFDM Versus MC-CDMA Transceivers for WIFI, WIMAX, and Next-Generation Cellular Systems," *Proc. Of The IEEE*, vol. 95, no. 12, pp. 2368-2392, Dec. 2007.

[12] M. Jiang, and L. Hanzo, "Multiuser MIMO-OFDM for Next-Generation Wireless Systems," *Proc. Of The IEEE*, vol. 95, no. 7, pp. 1430-1469, July 2007.

[13] A. Assra, W. Hamouda, and A. Youssef, " A Channel-Estimation and Data-Detection Scheme for Multiuser MIMO-CDMA Systems in Fading Channels," *IEEE Trans. Vehicular Technology*, vol. 59, no. 6, pp. 2830-2844, July 2010.

[14] S.-M. Tseng, "Sequential Detection for Multiuser MIMO CDMA Systems with Single Spreading Code Per User," *IEEE Trans. Wireless Commun.*, vol. 8, no. 7, pp. 3492-3497, Jul. 2009.

[15] Y. Cai, R. Lamare, and D. Ruyet, " Transmit Processing Techniques Based on Switched Interleaving and Limited Feedback for Interference Mitigation in Multiantenna MC-CDMA Systems," *IEEE Trans. Vehicular Technology*, vol. 60, no. 4, pp. 1559-1570, May 2011.

[16] E. Lo, P. Chan, V. Lau, R. Cheng, K. Letaief, R. Murch, and W. Mow, "Adaptive Resource Allocation and Comparision of Downlink Multiuser MIMO-MC-CDMA and MIMO-OFDMA," *IEEE Trans. Wireless Commun.*, vol. 6, no. 3, pp. 1083-1093, Mar. 2007.

[17] D. Gesbert, M. Kountouris, R. W. Heath Jr., C. CHae, and T. Salzer, "From Single-User to Multiuser Communications: Shifting the MIMO Paradigm," *IEEE Signal Processing Magazin*, vol. 24, no. 5, pp. 36-46, Sep. 2007.

[18] W. Yu, and W. Rhee, "Degrees of Freedom in Wireless Multiuser Spatial Multiplexing Systems With Multiple Antennas," *IEEE Trans. Commun.*, vol. 54, no. 10, pp. 1747-1753, Oct. 2006.

[19] S. Sigdel, and W. Krzymien, "Simplified Fair Scheduling and Antenna Selection Algorithms for Multiuser MIMO Orthogonal Space-Division Multiplexing Downlink," *IEEE Trans. Vehicular Technology*, vol. 58, no. 3, pp. 1329-1344, Mar. 2009.

[20] X. Zhang, Z. Lv, and W. Wang, "Performance Analysis of Multiuser Diversity in MIMO Systems With Antenna Selection ," *IEEE Trans. Wireless Commun.*, vol. 7, no. 1, pp. 15-21, Jan. 2008.

[21] D. Tse, P. Viswanath, and L. Zheng, "Diversity-Multiplexing Tradeoff in Multiple-Access Channels," *IEEE Trans. Inform. Theory*, vol. 50, no. 9, pp. 1859-1874, Sep. 2004.

[22] M. Sadek, A. Tarighat, and A. Sayed, "Active Antenna Selection in Multiuser MIMO Communications," *IEEE Trans. Signal Processing*, vol. 55, no. 4, pp. 1498-1510, Apr. 2007.

[23] W. Xu, S. Zekavat and H. Tong, "A Novel Spatially Correlated Multiuser MIMO Channel Modeling: Impact of Surface Roughness," *IEEE Trans. Antennas And Propagation*, vol. 57, no. 8, pp. 2429-2438, Aug. 2009.

[24] D. Tse, and P. Viswanath, *Fundamentals of Wireless Communication*, Cambridge University Press, 2005.

[25] J. G. Proakis, *Digital Communications*, 4th ed., New York, McGraw-Hill, 2001.

[26] T. Rappaport, *Wireless Communications, Principles and Practice*, 2nd ed., NJ, Prentice Hall PTR, 2002.

[27] G. Prabhu, and P. Shankar, "Simulation of Flat Fading Using MATLAB for Classroom Instructions," *IEEE Trans. Education*, vol. 45, no. 1, pp. 19-25, Feb. 2002.

[28] J. Andersen, T. Rappaport, and S. Yoshida, "Propagation Measurment and Models for Wireless Communications Channels", *IEEE Commun. Magazine*, vol. 33, no. 1, pp. 42 - 49, Jan. 1995.

[29] B. SKLAR, "Rayleigh Fading Channels in Mobile Digital Communication Systems, Part I: Characterization", *IEEE Commun. Magazine*, 1997, vol. 35, no. 7, pp. 90 - 100.

[30] B. SKLAR, "Rayleigh Fading Channels in Mobile Digital Communication Systems, Part II: Mitigation", *IEEE Commun. Magazine*, 1997, vol. 35, no. 7, pp. 102 - 109.

[31] W.C. Jakes, *Microwave Mobile Communications*, New York, Wiley, 1974. Reprinted by the IEEE Press in 1994.

[32] R. Clarke, "A Statistical Theory of Mobile-Radio Reception", *Bell Syst. Tech. J.* , pp. 957–1000, July-Aug. 1968.

[33] Y. Zheng, and C. Xiao, "Improved Models for the Generation of Multiple Uncorrelated Rayleigh Fading Waveforms," *IEEE Commun. Letters*, vol. 6, no. 6, pp. 256 – 258, June 2002.

[34] A. Goldsmith, *Wireless Communications*, Cambridge University Press, 2005.

[35] B. Sklar, *Digital Communications Fundamentals and Applications*, 2nd ed., New Jersey, Prentice Hall, 2001.

[36] R. E. Ziemer, and R. L. Peterson *Introduction to Digital Communication*, 2nd ed., New Jersey, Prentice Hall, 2001.

[37] M. Alouini, and A.J. Goldsmith, "Capacity of Rayleigh Fading Channels Under Different Adaptive Transmission and Diversity-Combining Techniques," *IEEE Transactions on Vehicular Technology*, vol. 48, no. 4, pp. 1165-1181, July 1999.

[38] T. Eng, N. Kong, and L. B. Milstein, "Comparision of Diversity Combining Techniques for Rayleigh-Fading Channels," *IEEE Trans. Commun.*, vol. 44, no. 9, pp. 1117-1129, Sep. 1996.

[39] P. Dighe, R. Mallik, and S. Jamuar, "Analysis of Transmit-Receive Diversity in Rayleigh Fading," *IEEE Trans. Commun.*, vol. 51, no. 4, pp. 694-703, Apr. 2003.

[40] S. Alamouti, "A Simple Transmit Diversity Technique for Wireless Communications," *IEEE Journal on Select Areas in Communications*, vol. 16, no. 8, pp. 1451-1458, Oct. 1998.

[41] J.N. Laneman, D.N.C. Tse, and G.W. Wornell, "Cooperative Diversity in Wireless Networks: Efficient Protocol and Outage Behavior," *IEEE Trans. Inform. Theory*, vol. 50, no. 12, pp. 3062-3080, Dec. 2004.

[42] A. Sendonaris, E. Erkip, and B. Aazhang, "User Cooperation Diversity-PartI: System Description," *IEEE Trans. Commun*., vol. 51, no. 11, pp. 1927-1938, Nov. 2003.

[43] A. Sendonaris, E. Erkip, and B. Aazhang, "User Cooperation Diversity-PartII: Implementation Aspects and Performance Analysis," *IEEE Trans. Commun*., vol. 51, no. 11, pp. 1939-1948, Nov. 2003.

[44] T.E. Hunter, and A. Nosratinia, "Diversity through Coded Cooperation," *IEEE Trans. On Wireless Communications*, vol. 5, no. 2, pp. 283-289, Feb. 2006.

[45] A. Bletsas, A. Khisti, D.P. Reed, and A. Lippman, "A Simple Cooperative Diversity Method Based on Network Path Selection," *IEEE Journal On Selected Areas in Commun*., vol. 24, no. 3, pp. 659-672, Mar. 2006.

[46] T. Cover, and A. El Gamal, "Capacity Theorems for The Relay Channels," *IEEE Trans. Inform. Theory*, vol. 25, no. 5, pp. 572-584, Sep. 1979.

[47] H. Sari, F. Vanhaverbeke, and M. Moeneclaey, "Extending the Capacity of Multiple Access Channels," *IEEE Commun. Magazine*, vol. 38, pp. 74 – 82, Jan. 2000.

[48] A. Jamalipour, T. Wada, and T. Yamazato, "A Tutorial on Multiple Access Technologies for Beyond 3G Mobile Networks," *IEEE Commun. Magazine*, vol. 43, pp. 110 – 117, Feb. 2005.

[49] R. Esmailzadeh, M. Nakagawa, and A. Jones, "TDD-CDMA for the 4th Generation of Wireless Communications," *IEEE WirelessCommun.*, vol. 10, issue 4, pp. 8 – 15, Aug. 2003.

[50] S. Verdu, *Multiuser Detection*, 1st ed. Cambridge University Press, 1998. Reprinted with corrections inUSA in 2003.

[51] P. Bergmans, and T. Cover, "Cooperative Broadcasting," *IEEE Trans. Inform. Theory*, vol. IT-20, no. 3, pp. 317-324, May 1974.

[52] L. Hanzo, M. Munster, B. Choi, and T. Keller, *OFDM and MC-CDMA for Broadband Multiuser communications, WLANs and Broadcasting*, Piscataway, NJ, IEEE Press/Wiley, 2003.

[53] W. Yu, and J. Cioffi, "FDMA Capacity of Gaussian Multiple-Access Channels with ISI," *IEEE Trans. Commun.*, vol. 50, no. 1, pp. 102-110, Jan. 2002.

[54] P. Jung, P. Baier, and A. Steil, "Advantages of CDMA and Spread Spectrum Techniques over FDMA and TDMA in Cellular Mobile Radio Applications," *IEEE Trans. Vehicular Technnology*, vol. 42, no. 3, pp. 357-364, Aug. 1993.

[55] S. Verdu, and S. Shamai, "Spectral Efficiency of CDMA with Random Spreading," *IEEE Trans. Information Theory*, vol. 45, no. 2, pp. 622-640, Mar. 1999.

[56] B. Suard, G. Xu, H. Liu and T. Kailath, "Uplink Channel Capacity of Space-Division-Multiple-Access Schemes," *IEEE Trans. Inform. Theory*, vol. 44, no. 4, pp. 1468 – 1476, July 1998.

[57] T. Kasami, "Coding for A Multiple-Access Channel," *IEEE Trans. Information Theory*, vol. 22, no. 2, pp. 129-137, Mar. 1976.

[58] F. Ali, and B. Honary "Collaborative Coding and Decoding Techniques for Multiple Access Channel," *IEE Proc.-Commun.*, vol. 141, no. 2, pp. 56-62, Apr. 1994.

[59] F.H. Ali, S.A.G. Chandler, and S. Soysa, "Complex-Valued Reciever for Multiuser Collaborative Coding Schemes," *Electronics Letters*, vol. 31, no. 5, pp. 341-342, March 1995.

[60] M. Mattas, and P. Ostergard, "A New Bound for the Zero-Error Capacity Region of the Two-User Binary Adder Channel," *IEEE Trans. Information Theory*, vol. 51, no. 9, pp. 3289-3291, Sep. 2005.

[61] Z. Zhang, T. Berger, and J. Massey, "Some Families of Zero-Error Block Codes for the Two-User Binary Adder Channel with Feedback," *IEEE Trans. Information Theory*, vol. 33, no. 5, pp. 613-619, Sep. 1987.

[62] S. Bross, and I. Blake, "Upper Bound for Uniquely Decodable Codes in A Binary Input *N*-User Adder Channel," *IEEE Trans. Information Theory*, vol. 44, no. 1, pp. 334-340, Jan. 1998.

[63] T. Cover, "An Achievable Rate Region for the Multiple-Access Channel with Feedback," *IEEE Trans. Information Theory*, vol. 27, no. 3, pp. 292-298, May 1981.

[64] T. Cover, "Comments on Broadcast Channels," *IEEE Trans. Inform. Theory*, vol. 44, no. 6, pp. 2524-2530, Oct. 1998.

[65] T. Cover, and J.A. Thomas, *Elements of Information Theory*, 2nd ed., New Jersey, John Wiley & Sons, 2006.

[66] S. Gadkari, and K. Rose, "Time-Division Versus Superposition Coded Modulation Schemes For Unequal Error Protection," *IEEE Trans. Commun. Theory*, vol. 47, no. 3, pp. 370-379, March 1999.

[67] S. Bopping and J.M. Shea, "Superposition Coding in the Downlink of CDMA Celluar Systems," *WCNC2006.IEEE*, vol. 4, pp. 1978-1983, 2006.

[68] F. Etemadi, and H. Jafarkhani, "Rate and Power Allocation for Layered Transmission with Superposition Coding," *IEEE Signal Processing Letters*, vol. 14, no. 11, pp. 773-776, Nov. 2007.

[69] H. Cronie, "Superposition Coding for Power and Bandwidth Efficient Communication over the Gaussian Channel," *Proc. ISIT2007*, Nice, France, pp. 2311-2316, Jun 2007.

[70] C. Manchon, L. Deneire, P. Mogensen, and T. Sorensen, "On the Design of a MIMO-SIC Receiver for LTE Downlink," *Proc. IEEE 68th VTC2008*, Calgary, BC, pp. 1-5, Sep. 2008.

[71] T. Richardson, M. Shokrollahi, and R. Urbanke, "Design of Capacity-Approaching Irregular Low-Density Parity-Check Codes," *IEEE Trans. Information Theory*, vol. 47, no. 2, pp. 619-637, Feb. 2001.

[72] A. Amraoui, S. Dusad, and R. Urbanke, "Achiving General Points in the 2-User Gaussian MAC without Time-Sharing or Rate-Splitting by Means of Iterative Coding," *Proc. IEEE ISIT2002*, Laussanne, Switzerland, pp. 334, Jul. 2002.

[73] A. Roumy, and D. Declercq, "Characterization and Optimization of LDPC Codes for the 2-User Gaussian Multiple Access Channel," *EURASIP Journal on Wireless Communications and Networking*, vol. 2007, ID. 74890, 10 pages, May 2007.

[74] B. Rimoldi, and R. Urbanke, "A rate-splitting approach to the Gaussian multiple-access channel," *IEEE Trans. Inform. Theory*, vol. 42, no. 2, pp. 364-375, Mar. 1996.

[75] B. Rimoldi, and Q. Li, "Potential Impact of Rate-Splitting Multiple Access on Cellular Communications," *Proc. IEEE GLOBECOM'96*, London, UK, pp. 178-182, Nov. 1996.

[76] A. Grant, B. Rimoldi, R. Urbanke, and P. Whiting, "Rate-Splitting Multiple Access for Discrete Memoryless Channels," *IEEE Trans. Inform. Theory*, vol. 47, no. 3, pp. 873-890, Mar. 2001.

[77] J. Cao, and E. Yeh, "Differential Quality-of-Service in Multiple-Access Communication Via Distribted Rate Splitting," *Proc. IEEE GLOBECOM'05*, vol. 3, pp. 1284-1288, Dec. 2005.

[78] J. Cao, and E. Yeh, "Asymptotically Optimal Multiple-Access Communication Via Distribted Rate Splitting," *IEEE Trans. Information Theory*, vol. 53, no. 1, pp. 304-319, Jan. 2007.

[79] X. Xu, and N. Goertz, "Practical Successive Interference Cancellation in the Binary-Input Gaussian Multiple-Access Channel," *Proc. 7th ITG on SCC'08*, Germany, 6 pages, Jan. 2008.

[80] Y. Wu, "RS-CTDMA: A Novel Concept of Multiple Access Design," *IEE Proc.-Communcation*, vol. 150, no. 2, pp. 109-114, Apr. 2003.

[81] L. Ping, L. Liu, K. Wu, and W. Leung, "Interleave-Division Multiple Access," *IEEE Trans. Wireless. Commun.*, vol. 5, no. 4, pp. 938-947, Apr. 2006.

[82] W. Al-Hussaibi, and F. Ali, "On the Capacity Region of Promissing Multiple Access Techniques," *Proc. 12th PGNet2011*, Liverpool, UK, 6 pages, June 2011.

[83] G. Foschini, and M. Gans, "On Limits of Wireless Communications in a Fading Environment when Using Multiple Antennas," *Wireless Personal Commun.*, vol. 6, no. 3, pp. 311-335, Mar. 1998.

[84] A. Paulraj, D. Gore, R. Nabar, and H. Bolcskei, "An Overview of MIMO Communications-A Key to Gigabit Wireless," *Proc. IEEE*, vol. 92, no. 2, pp. 198-218, Feb. 2004.

[85] D. Gesbert, M. Shafi, D. Shiu, P. Smith, and A. Naguib, "From Theory to Practice: An Overvview of MIMO Space-Time Coded Wireless Systems," *IEEE Journal On Selected Areas in Commun.*, vol. 21, no. 3, pp. 281-302, Apr. 2003.

[86] J. Akhtar, and D. Gesbert, "Spatial Multiplexing Over Correlated MIMO Channels With a Closed-Form Precoder," *IEEE Trans. Wireless Commun.*, vol. 4, no. 5, pp. 2400-2409, Sep. 2005.

[87] D. Samuelsson, J.Jalden, P. Zetterberg and B. Ottersten, "Realization of Spatially Multiplexed MIMO System," *EURASIP Journal On Applied Signal Processing*, vol. 2006, ID78349, pp. 1-16, 2006.

[88] H. Bolcskei, D. Gesbert, and A. Paulraj, "On the Capacity of OFDM-BASED Spatial Multiplexing Systems," *IEEE Trans. Commun*., vol. 50, no. 2, pp. 225-234, Feb. 2002.

[89] T. Yoo, and A. Goldsmith, "Capacity and Power Allocation for Fading MIMO Channels with Channel Estimation Error," *IEEE Trans. Inform. Theory*, vol. 52, no. 5, pp. 2203-2214, May 2005.

[90] M. Chiani, M. Win, and A. Zanella, "On the Capacity of Spatially Correlated MIMO Rayleigh-Fading Channels," *IEEE Trans. Inform. Theory*, vol. 49, no. 10, pp. 2363-2371, Oct. 2003.

[91] G. Raleigh, and J. Cioffi, "Spatio-Temporal Coding for Wireless Communication," *IEEE Trans. Commun.*, vol. 46, no. 3, pp. 357-366, Mar. 1998.

[92] R. Nee, A. Zelst, and G. Awater, "Maximum Likelihood Decoding in Space Division Multiplexing System," *Proc. IEEE VTC2000*, Tokyo, Japan, vol. 1, pp. 6-10, May. 2000.

[93] X. Zhu, and R. Murch, "Performance Analysis of Maximum Likelihood Detection in a MIMO Antenna System," *IEEE Trans. Commun*., vol. 50, no. 2, pp. 187-191, Feb. 2002.

[94] A. Gorokhov, "Transmit Diversity Versus SDMA: Analytic and Numerical Comparisons," *Proc. IEEE ICC2000*, New Orleans, USA, vol. 2, pp. 1020-1024, June 2000.

[95] D. Manteuffel, "MIMO Antenna Design Challenges," *Proc. LAPC2009*, Loughborough, UK, vol. 1, pp. 50-56, Nov. 2009.

[96] C. Luxey, "Design of Multi-antenna Systems for UMTS Mobile Phones," *Proc. LAPC2009*, Loughborough, UK, vol. 1, pp. 57-64, Nov. 2009.

[97] I. Telatar, "Capacity of Multi-antenna Gaussian Channels," *Internal Tech. Memo*, AT&T Bell Labs., Murray Hill, NJ, USA, June 1995.

[98] J. Winters, "On the Capacity of Radio Communication Systems with Diversity in Rayleigh Fading Environment," *IEEE Journal On Selected Areas in Commun*., vol. SAC-5, no. 5, pp. 871-878, June 1987.

[99] A. Goldsmith, S.A. Jafar, N. Jindal, and S. Vishwanath, "Capacity limits of MIMO Channels," *IEEE Journal On Selected Areas in Commun*., vol. 21, no. 5, pp. 684-702, June 2003.

[100] H. Weingarten, Y. Steinberg, and S. Shamai, "The Capacity Region of the Gaussian Multiple-Input Multiple-Output Broadcast Channel," *IEEE Trans. Inform. Theory*, vol. 52, no. 9, pp. 3936-3964, Sep. 2006.

[101] Q. Spencer, and A. Swindlehurst, "A Hybrid Approach to Spatial Multiplexing in Multuser MIMO Downlinks," *EURASIP Journal On Wireless Commun. and Networking*, vol. 2004, Issue no. 2, pp. 236-247, 2004.

[102] Z. Pan, K. Wong, and T. Ng, "Analysis of Multiuser MIMO Downlink Networks Using Linear Transmitter and Receivers," *EURASIP Journal On Wireless Commun. and Networking*, vol. 2004, Issue no. 2, pp. 248-260, 2004.

[103] J. Winters, "The Impact of Antenna Diversity on the Capacity of Wireless Communication Systems," *IEEE Trans. Commun*., vol. 42, no. 2/3/4, pp. 1740-1751, Feb./Mar./Apr. 1994.

[104] F. Kaltenberger, M. Kountouris, D. Gesbert and R. Knopp, "On the Trade-Off Between Feedback and Capacity in Measured MU-MIMO Channels," *IEEE Trans. Wireless Commun*., vol. 8, no. 9, pp. 4866-4875, Sep. 2009.

[105] E. Jorswieck, and H. Boche, "Performance Analysis of Capacity of MIMO Systems under Multiuser Interferance Based on Worst-Case Noise Behavior," *EURASIP Journal On Wireless Commun. and Networking*, vol. 2004, Issue no. 2, pp. 273-285, 2004.

[106] K. Josiam, D. Rajan, and M. Srinath, "Diversity Multiplexing Tradeoff in Multiple Antenna Multiple Access Channels with Partial CSIT," *Proc. IEEE GLOBECOM'07*, pp. 3210-3214, Nov. 2007.

[107] D. Mazzarese, and W. Krzymien, "Scheduling Algorithms and Throughput Maximization for the Downlink of Packet-Data Cellular Systems with Multiple Antennas at the Base Station," *Wireless Personal Commun.*, vol. 43, no. 2, pp. 215-260, Oct. 2007.

[108] W. Ajib, and D. Haccoun, "An Overview of Schedualing Algorithms in MIMO-Based Fourth Generation Wireless Systems," *IEEE Network*, vol. 19, no. 5, pp. 43-48, Sep./Oct. 2005.

[109] M. Damen, K. Abed-Meraim, and J-C. Belfiore, "Generalized Sphere Decoder for Asymmetrical Space-time Communication Architecture," *Electronics Letters*, vol. 36, no. 2, pp. 166-167, Jan. 2000.

[110] Z. Yang, C. Liu, and J. He, "A New Approach for Fast Generalized Sphere Decoding in MIMO Systems," *IEEE Signal Processing letters*, vol. 12, no. 1, pp. 41-44, Jan. 2005.

[111] K-K. Wong, A. Paulraj and R. Murch, "Efficient High-Performance Decoding for Overloaded MIMO Antenna Systems," *IEEE Trans. Wireless Commun.*, vol. 6, no. 5, pp. 1833-1843, May 2007.

[112] P. Wang, and T. Le-Ngoc, "A Low-Complexity Generalized Sphere Decoding Approach for Underdetermined Linear Communication Systems: Performance and Complexity Evaluation," *IEEE Trans. Wireless Commun.*, vol. 57, no. 11, pp. 3376-3388, Nov. 2009.

[113] M. Alias, S. Chen, and L. Hanzo, "Multiple-Antenna-Aided OFDM Employing Genatic-Algorthim-Assisted Minimum Bit-Error Multiuser Detection," *IEEE Transactions on Vehicular Technology*, vol. 54, no. 5, pp. 1713-1721, Sep. 2005.

[114] M. Alias, A. Samingan, S. Chen and L. Hanzo, "Multiple Antenna Aided OFDM employing Minimum Bit Error Rate Multiuser Detection," *Electronics Letters*, vol. 39, no. 24, pp. 1769-1770, Nov. 2003.

[115] S. Chen, N. Ahmad and L. Hanzo, "Adaptive Minimum Bit-Error Rate Beamforming," *IEEE Trans. Wireless Commun.*, vol. 4, no. 2, pp. 341-348, Mar. 2005.

[116] C-J. Chen, and L-C. Wang, "On the Performance of the Zero-Forcing Receiver Operating in the Multiuser MIMO system with Reduced Noise Enhancement Effect," *Proc. IEEE GLOBECOM'05*, vol. 3, pp. 1294-1298, Dec. 2005.

[117] L-L. Yang, and L-C. Wang, "Zero-Forcing and Minimum Mean-Square Error Multiuser Detection in Generalized Multicarrier DS-CDMA Systems for Cognitive Radio," *EURASIP Journal On Wireless Commun. and Networking,* vol. 2008, no. 14, pp. 1-13, Jan. 2008.

[118] S. Halunga, and N. Vizireanu, "Performance Evaluation for Conventional and MMSE Multiuser Detection Algorithms in Imperfect Reception Conditions," *ELSEVIER Journal On Digital Signal Processing*, vol. 20, no. 1, pp. 166-178, Jan. 2010.

[119] A. Zanella, M. Chiani, and M. Win, "MMSE Reception and Successive Interferance Cancellation for MIMO Systems with High Spectral Efficiency," *IEEE Trans. Wireless Commun.*, vol. 4, no. 3, pp. 1244-1251, May 2005.

[120] Y. Zhang, J. Zhang, P. Smith, M. Shafi and P. Zhang, "Reduced Complexity Channel Models for IMT-advanced Evaluation," *EURASIP Journal On Wireless Communications and Networking,* vol. 2009, Issue no. 1, pp. 1-13, Feb. 2009.

[121] P. Almers, E. Bonek, A. Burr, N. Czink, M. Debbah, V.Degli-Esposti, H. Hofstetter, P. Kyosti, D. Laurenson, G. Matz, A.F. Molisch, C. Oestages and H. Ozcelik, "Survey of Channel and Radio Propagation Models for Wireless MIMO Systems," *EURASIP Journal On Wireless Communications and Networking,* vol. 2007, Issue no. 1, pp. 1-19, Jan. 2007.

[122] N. Jaber, K. E. Tepe and E. Abdel-Raheem, "Reconfigurable Simulator Using Graphical User Interface (GUI) and Object-oriented Design for OFDM Systems," *ELSEVIER Journal On Simulation Modelling Practice and Theory*, vol. 2011, no. 19, pp. 1294-1317, Feb. 2011.

[123] F. Zabini, B. Masini, A. Conti, and L. Hanzo, "Partial Equalization for MC-CDMA Systems in Non-Ideally Estimated Correlated Fading," *IEEE Transactions on Vehicular Technology*, vol. 59, no. 8, pp. 3818-3830, Oct. 2010.

[124] H. Huang, H. Viswanathan and G. Foschini, "Multiple Antennas in Cellular CDMA Systems: Transmission, Detection, and Spectral Efficiency," *IEEE Trans. Wireless Communcations*, vol. 1, no. 3, pp. 383-392, July 2002.

[125] L.L. Yang, "MIMO-Assisted Space-Code-Division Multiple-Access: Linear Detectors and Performance Over Multipath Fading Channels," *IEEE Journal On Selected Areas in Commun*., vol. 24, no. 1, pp. 121-131, Jan. 2006.

[126] M. Juntti, M. Vehkapera, J. Leinonen, Z. Li, and D. Tujkovic, "MIMO MC-CDMA Communications for Future Cellular Systems," *IEEE Commun. Magazine*, vol. 43, no. 2, pp. 118 – 124, Feb. 2005.

[127] A. Abdi, and M. Kaveh "A Space-Time Correlation Model for Multielement Antenna Systems in Mobile Fading Channels," *IEEE Journal On Selected Areas in Commun*., vol. 20, no. 3, pp. 550-560, April 2002.

[128] R. Ertel, P. Cardieri, K. Sowerby, T. Rappaport and J. Reed, "Overview of Spatial Channel Models for Antenna Array Communication Systems," *IEEE Personal Commun. Mag.*, vol. 5, pp. 10-22, Feb. 1998.

[129] C.-X. Wang, M. Patzold and D. Yuan, "Accurate and Efficient Simulation of Multiple Uncorrelated Rayleigh Fading Waveforms," *IEEE Trans. Wireless Communcations*, vol. 6, no. 3, pp. 833-839, Mar. 2007.

[130] M. Kang, and M.S. Alouini, "Capacity of Correlated MIMO Rayleigh Channels," *IEEE Trans. Wireless Communcations*, vol. 5, no. 1, pp. 143-155, Jan. 2006.

[131] H. Shin, and J. Lee, "Capacity of Multiple-Antenna Fading Channels: Spatial Fading Correlation, Double Scattering, and Keyhole," *IEEE Trans. Inform. Theory*, vol. 49, no. 10, pp. 2636-2647, Oct. 2003.

[132] C-N. Chuah, D. Tse, J. Khan and R. Valenzuela, "Capacity Scaling in MIMO wireless Systems Under Correlated Fading," *IEEE Trans. Inform. Theory*, vol. 48, no. 3, pp. 637-650, Mar. 2002.

[133] L. Tran, T. Wysocki, A. Mertins, and J. Seberry, "A Generalized Algorithm for the Generation of Correlated Rayleigh Fading Envelopes in Wireless Channels," *EURASIP Journal On Wireless Commun. and Networking,* vol. 2005, Issue no. 5, pp. 801-815, Oct. 2005.

[134] S. Sorooshyari, and D. Daut, "On the Generation of Correlated Rayleigh Fading Envelopes for Accurate Simulation of Diversity Channels," *IEEE Trans. Commun.*, vol. 54, no. 8, pp. 1381-1386, Aug. 2006.

[135] R. Ertel, and J. Reed, "Generation of Two Equal Power Correlated Rayleigh Fading Envelopes," *IEEE Commun. Letters*, vol. 2, no. 10, pp. 276 – 278, Oct. 1998.

[136] N. Beaulieu, "Generation of Correlated Rayleigh Fading Envelopes," *IEEE Commun. Letters*, vol. 3, no. 6, pp. 172 – 174, June 1999.

[137] B. Natarajan, C. Nassar, and V. Chandrasekhar, "Generation of Correlated Rayleigh Fading Envelopes for Spread Spectrum Aplications," *IEEE Commun. Letters*, vol. 4, no. 1, pp. 9 – 11, Jan. 2000.

[138] N. Beaulieu, and M. Merani "Generation of Multiple Rayleigh Fading Sequences with Specified Cross-Correlations," *Eur Trans. Telecommun.*, vol. 15, pp. 471 – 476, Sep. 2004.

[139] K. Baddour, and N. Beaulieu, "Accurate Simulation of Multiple Cross-Correlated Rician Fading Channels," *IEEE Trans. Commun.*, vol. 52, no. 11, pp. 1980-1987, Nov. 2004.

[140] W.-H. Chung, R. Hudson and K. Yao, "A Unified Approach for Generating Cross-Correlated and Auto-Correlated MIMO Fading Envelope Processes," *IEEE Trans. Commun.*, vol. 57, no. 11, pp. 3481-3488, Nov. 2009.

[141] W. Al-Hussaibi, and F. Ali, "On the Generation of Correlated Rayleigh Fading Envelopes for Multi-Antenna Systems," *Proc. 7th Innovations'11*, Al Ain and Abu Dhabi, UAE, pp. 12- 17, April 2011.

[142] W. Al-Hussaibi, and F. Ali, "Iterative Coloring Technique for the Generation of Correlated Rayleigh Fading Envelopes for Multi-Antenna and Multicarrier Systems," *Proc. 12th PGNet2011*, Liverpool, UK, pp. 103-108, June 2011.

[143] B. Hochwald, and S. Brink, "Achieving Near-Capacity on a Multiple-Antenna Channel," *IEEE Trans. Commun.*, vol. 51, no. 3, pp. 389-399, Mar. 2002.

[144] A. Soysal, and S. Ulukus, "Joint Channel Estimation and Resource Allocation for MIMO systems—PartI: Single-User Analysis ," *IEEE Trans. Wireless Commun.*, vol. 9, no. 2, pp. 624-631, Feb. 2010.

[145] J. Akhtman, and L. Hanzo, "Closed-Form Approximation of MIMO Capacity," *Electronics Letters*, vol. 45, no. 1, pp. 68-69, Jan. 2009.

[146] A. Soysal, and S. Ulukus, "Joint Channel Estimation and Resource Allocation for MIMO systems—PartII: Multi-User and Numerical Analysis," *IEEE Trans. Wireless Commun.*, vol. 9, no. 2, pp. 632-640, Feb. 2010.

[147] H.-H. Chen, Y.-C. Yeh, Q. Bi, and A. Jamalipour, "On a MIMO-Based Open Wireless Architecture: Space-Time Complementary Coding," *IEEE Commun. Magazin*, vol. 45, no. 2, pp. 104-112, Feb. 2007.

[148] D-S. Shiu, G. Foschini, M. Gans and J. Khan, "Fading Correlation and Its Effects on the Capacity of Multielement Antenna Systems," *IEEE Trans. Commun.*, vol. 48, no. 3, pp. 2363-2371, Mar. 2000.

[149] P. Smith, S. Roy, and M. Shafi, "Capacity of MIMO Systems with Semicorrelated Flat Fading," *IEEE Trans. Inform. Theory*, vol. 49, no. 10, pp. 2781-2788, Oct. 2003.

[150] Q. Zhang, X. Cui, and X. Li, "Very Tight Capacity Bounds for MIMO-Correlated Rayleigh-Fading Channels," *IEEE Trans. Wireless Communcations*, vol. 4, no. 2, pp. 681-688, Mar. 2005.

[151] S. Loyka, "Channel Capacity of MIMO Architecture Using the Exponential Correlation Matrix," *IEEE Commun. Letters*, vol. 5, no. 9, pp. 369-371, Sep. 2001.

[152] R. Nabar, H. Bolcskei, and A. Paulraj, "Transmit Optimization for Spatial Multiplexing in the Presence of Spatial Fading Correlation," *Proc. IEEE GLOBECOM'01*, San Antonio, Tx, vol. 1, pp. 131-135, 2001.

[153] J. Kotecha, and A. Sayeed, "Transmit Signal Design for Optimal Estimation of Correlated MIMO Channels," *IEEE Trans.Signal Processing*, vol. 52, no. 2, pp. 546-557, Feb. 2004.

[154] W. Al-Hussaibi, F. Ali and E. Stipidis, "A Simple 2-User Multiple Access Technique Using Fading Signatures and Space Diversity," *Proc. LAPC2009*, Loughborough, UK, vol. 1, pp. 433-436, Nov. 2009.

[155] G. Ungerboeck, "Channel coding with multilevel/phase signals," *IEEE Trans. Inform. Theory*, vol. IT-28, no. 1, pp. 55-66, Jan. 1982.

[156] S. Ng, and L. Hanzo, "On the MIMO Channel Capacity of Multidimensional Signal Sets," *IEEE Trans. Vehicular Technology*, vol. 55, no. 2, pp. 528-536, Mar. 2006.

[157] F. Brannstrom, T. Aulin, and L. Rasmussen, "Constellation-Constrained Capacity for Trellis Code Multiple Access Systems," *Proc. IEEE GLOBECOM'01*, San Antonio, Tx, 2001, vol. 2, pp. 791-795.

[158] J. Harshan, and B. Rajan, "On Two-User Gaussian Multiple Access Channels With Finite Input Constellation," *IEEE Trans. Inform. Theory*, vol. 57, no. 3, pp. 1299-1327, Mar. 2011.

[159] J. Harshan, and B. Rajan, "Finite Signal-Set Capacity of Two-User Gaussain Multiple Access Channel," *Proc. IEEE ISIT 2008*, Toronto, Canada, pp. 1203-1207, July 2008.

[160] N. Deshpande, and B. Rajan, "Constellation Constrained Capacity of Two-user Broadcast Channel," *Proc. IEEE GLOBECOM'09*, pp. 1-6, Nov. 30-Dec. 4 2009.

[161] C. Wengerter, A. Elbwart, and E. Seidel, "Constellation Rearrangment: Enhancment for Multilevel Modulation Format and Transmit Diversity," *Wireless Personal Communications*, vol. 29, no. 1-2, pp. 35-45, Oct. 2004.

[162] S. Ben Slimane, "Combined Transmitter Diversity and Multi-Level Modulation Techniques," *Wireless Personal Communications*, vol. 39, no. 2, pp. 215-227, Oct. 2006.

[163] M. Khormuji, and E. Larsson, "Improving Collaborative Transmit Diversity by Using Constellation Rearrangment," *Proc. IEEE WCNC*, Hong Kong, pp. 803-807, Mar. 2007.

[164] T. Koike-Akino, P. Popovski, and V. Tarokh, "Optimized Constellations for Two-Way Wireless Relaying with Physical Network Coding," *IEEE Journal On Selected Areas in Commun*., vol. 27, no. 5, pp. 773-787, June 2009.

[165] M.S. Alouini and M. Simon, "Performance Analysis of Generalized Selective Combining Over Rayleigh Fading Channels," *Proc. Communication Theory Mini-Conference 1999*, Vancouver, BC, Canada, pp. 110-114, June 1999.

[166] N. Kong, and L. B. Milstein, "Average SNR of a Generalized Diversity Selection Combining Scheme," *IEEE Commun. Letters*, vol. 3, no. 3, pp. 57-59, Mar. 1999.

[167] L. Yue, "Analysis of Generalized Selection Combining Techniques," *Proc. VTC2000*, Tokyo, Japan, vol. 2, pp. 1191-1195, May 2000.

[168] Y. Ma, and C. C. Chai, "Unified Error Probability Analysis for Generalized Selection Combining in Nakagami Fading Channels," *IEEE Journal On Selected Areas in Commun*., vol. 18, no. 11, pp. 2198-2210, Nov. 2000.

[169] N. Kong, and L. B. Milstein, "Groupwise Generalized Selection Diversity Combining and Its Applications in Wireless Communication," *Proc. MILCOM2009*, Boston, MA, pp. 1-7, Oct. 2009.

[170] D. Love, and R. Heath, Jr. , "Equal Gain Transmission in Multiple-Input Multiple-Output Wireless Systems," *IEEE Trans. Commun.*, vol. 51, no. 7, pp. 1102-1110, Jul. 2003.

[171] M. Li, M. Lin, Z. Gong, J. Ya, Z. Zhang, R. Peng, and D. Li, "Performance Analysis of MIMO MRC Systems," *Electronics Letters*, vol. 43, no. 23, pp. 1-2, Nov. 2007.

[172] K. S. Ahn, "Performance Analysis of MIMO-MRC System in the Presence of Multiple Interferers and Noise over Rayleigh-Fading Channels," *IEEE Trans. Wireless Commun.*, vol. 8, no. 7, pp. 3727-3735, Jul. 2009.

[173] I. Al Falujah, and V. Parbhu , "Error Rate of DPSK Systems with MIMO EGC Diversity Reception over Rayleigh Fading Channels," *IEEE Trans. Commun.*, vol. 56, no. 6, pp. 897-903, June 2008.

[174] W. Li, N. Beaulieu, and Y. Chen, "Generalized Receiver Selection Combining Schemes for Alamouti MIMO Systems with MPSK," *IEEE Trans. Commun.*, vol. 57, no. 6, pp. 1599-1602, June 2009.

[175] A. Molisch, and M. Win, "MIMO Systems with Antenna Selection," *IEEE Microwave Magazine*, vol. 5, no. 1, pp. 46-56, Mar. 2004.

[176] S. Sanayei, and A. Nosratinia, "Antenna Selection in MIMO Systems," *IEEE Commun. Magazine*, vol. 42, no. 10, pp. 68-73, Oct. 2004.

[177] B. Chalise, and L. Vandendorpe, "Performance Analysis of Linear Receivers in a MIMO Relaying System," *IEEE Commun. Letters*, vol. 13, no. 5, pp. 330-332, May 2009.

[178] A. Molisch, M. Win, Y.-S. Choi, and J. Winters, "Capacity of MIMO Systems with Antenna Selection," *IEEE Trans. Wireless Commun.*, vol. 4, no. 4, pp. 1759-1772, Jul. 2005.

[179] M Jensen, and M. Morris, "Efficient Capacity- Based Antenna Selection for MIMO Systems," *IEEE Trans. Vehicular Technology*, vol. 54, no. 1, pp. 110-116, Jan. 2005.

[180] X. Zhang, A. Molisch, and S.-Y. Kung, "Variable-Phase-Shift-Based RF-baseband Codesign for MIMO Antenna Selection," *IEEE Trans. Signal Processing*, vol. 53, no. 11, pp. 4091-4103, Nov. 2005.

[181] Y. Zhang, C. Ji, W. Malik, D. O'Brien and D. Edwards, "Receive Antenna Selection for MIMO Systems over Correlated Fading Channels," *IEEE Trans. Wireless Commun.*, vol. 8, no. 9, pp. 4393-4399, Sep. 2009.

[182] R. Narasimhan, "Spatial Multiplexing with Transmit Antenna and Constellation Selection for Correlated MIMO Fading Channels," *IEEE Trans. Wireless Commun.*, vol. 51, no. 11, pp. 2829-2838, Nov. 2003.

[183] Y. Yang, R. Blum, and S. Sfar, "Antenna Selection for MIMO Systems with Closely Spaced Antennas," *EURASIP Journal On Wireless Communications and Networking,* vol. 2009, ID739828, pp. 1-11, 2009.

[184] R. Heath, Jr., S. Sandhu and A. Paulraj, "Antenna Selection for Spatial Multiplexing Systems with Linear Receivers," *IEEE Commun. Letters*, vol. 5, no. 4, pp. 142-144, April 2001.

[185] A. Gorokhov, D. Gore, and A. Paulraj, "Receive Antenna Selection for MIMO Spatial Multiplexing: Theory and Algorithms," *IEEE Trans. Signal Processing*, vol. 51, no. 11, pp. 2796-2807, Nov. 2003.

[186] M. Gharavi-Alkhansari, and A. Gershman, "Fast Antenna Subset Selection in MIMO Systems," *IEEE Trans. Signal Processing*, vol. 52, no. 2, pp. 339-347, Feb. 2004.

[187] B. Wang, H. Hui, and M. Leong, "Global and Fast Receiver Antenna Selection for MIMO Systems," *IEEE Trans. Commun.*, vol. 58, no. 9, pp. 2505-2510, Sep. 2010.

[188] L. Dai, S. Sfar, and K. Letaief, "Optimal Antenna Selection Based on Capacity Maximization for MIMO Systems in Correlated Channels," *IEEE Trans. Commun*., vol. 54, no. 3, pp. 563-573, Mar. 2006.

[189] R. Chen, R. Heath, Jr., and J. Andrews, "Transmit Selection Diversity for Unitary Precoded Multiuser Spatial Multiplexing Systems With Linear Receivers," *IEEE Trans. Signal Processing*, vol. 55, no. 3, pp. 1159-1171, Mar. 2007.

[190] R. Chen, J. Andrews, and R. Heath, Jr., "Efficient Transmit Antenna Selection for Multuser MIMO Systems with Block Diagonalization," *Proc. IEEE GLOBCOM'07*, Washington, DC, pp. 3499-3503, Nov. 2007.

[191] M. Mohaisen, and K. Chang, "On Transmit Antenna Selection for Multiuser MIMO Systems With Dirty Paper Coding," *Proc. IEEE PIMRC'09*, Tokyo, Japan, pp. 3074-3078, Sep. 2009.

[192] B. Lim, W. Krzymien and C. Schlegel, "Efficient Sum Rate Maximization and Resource Allocation in Block-Diagonalized Space-Division Multiplexing," *IEEE Trans. Vehicular Technology*, vol. 58, no. 1, pp. 478-484, Jan. 2009.

[193] M. Torabi, D. Haccoun, and W. Ajib, "Capacity and Outage Probabilty Analysis of Multiuser Diversity in MIMO MRC Systems with Transmit Antenna Selection," *Proc. PACRIM'09*, Victoria, BC, pp. 59-64, Aug. 2009.

[194] N. Jindal, "Antenna Combining for the MIMO Downlink Channel ," *IEEE Trans. Wireless Commun.*, vol. 7, no. 10, pp. 15-21, Oct. 2008.

[195] W. Zhong, and Y. Xu, "Joint User and Transmit Antenna Selection for Uplink Multi-User MIMO Systems," *Proc. IEEE PIMRC'09*, Tokyo, Japan, pp. 3193-3197, Sep. 2009.

[196] Y. Kim, S. Cho, and D. Kim, "Low Complexity Antenna Selection Based MIMO Scheduling Algorithms for Uplink Multiuser MIMO/FDD System," *Proc. IEEE VTC'07*, Dublin, Ireland, pp. 1663-1667, Apr. 2007.

[197] Y. Zhang, C. Ji, W. Malik, Y. Liu, D. O'Brien and D. Edwards, "Joint Antenna and User Selection Algorithm for Uplink of Multiuser MIMO Systems Using Sequential Monte Carlo Optimization," *Proc. IEEE SSP'07*, Madison, WI, USA, pp. 493-496, Aug. 2007.

[198] K. Huang, and W. Fang, "A Genetic Approach for Joint Receive Antenna Selection and Symbol Detection in the Multiuser MIMO Systems," *Proc. IEEE WiCOM'08*, Dalian, China, pp. 1-5, Oct. 2008.

[199] P. Sudarshan, H. Dai, and B. Hughes, "Statistics-Based Antenna Selection for Multi-Access MIMO Systems," *Proc. 38th Asilomar Conference on SSC'04*, Asilomar, USA, pp. 903-907, Nov. 2004.

[200] A. Assra, and W. Hamouda, "A Channel-Estimation and Data-Detection Scheme for Multiuser MIMO-CDMA Systems in Fading Channels," *IEEE Trans. Vehicular Technology*, vol. 59, no. 6, pp. 2830-2844, July 2010.

[201] B. Hassibi, and B. Hochwald, "How Much Training is Needed in Multiple-Antenna Wireless Links," *IEEE Trans. Inform. Theory*, vol. 49, no. 4, pp. 951-963, Apr. 2003.

[202] M. Biguesh, and A. Gershman, "Training-Based MIMO Channel Estimation: A Study of Estimator Tradeoffs and Optimal Training Signals," *IEEE Trans. Signal Processing*, vol. 54, no. 3, pp. 884-893, Mar. 2006.

[203] E. Karami, "Tracking Performance of Least Squares MIMO Channel Estimation Algorithm," *IEEE Trans. Commun.*, vol. 55, no. 11, pp. 2201-2209, Nov. 2007.

[204] I. Ikhlef, and D. Le Guennec, "A Simplified Constant Modulus Algorithm for Blind Recovery of MIMO QAM and PSK Signals: A Criterion with Convergence Analysis," *EURASIP Journal On Wireless Communications and Networking,* vol. 2007, ID90401, pp. 1-13, 2007.

[205] Y. Zeng, and T.-S. Ng, "A Semi-Blind Channel Estimation Method for Multiuser Multiantenna OFDM Systems," *IEEE Trans. Signal Processing*, vol. 52, no. 5, pp. 1419-1429, May 2005.

[206] S. Shahbazpanahi, A. Gershman and G. Giannakis, "Semiblind Multiuser MIMO Channel Estimation Using Capon and MUSIC Techniques," *IEEE Trans. Signal Processing*, vol. 54, no. 9, pp. 3581-3591, Sep. 2006.

[207] M. Abuthinien, S. Chen and L. Hanzo, "Semi-blind Joint Maximum Likelihood Channel Estimation and Data Detection for MIMO Systems," *IEEE Signal Processing Letters*, vol. 15, pp. 202-205, 2008.

[208] C. Rizogiannis, E. Kofidis, C. Papadias and S. Theodoridis, "Semi-blind Maximum-Likelihood Joint Channel/Data Estimation for Correlated Channels in Multiuser MIMO Networks," *ELSEVIER Journal On Signal Processing,* 90, pp. 1209-1224, 2010.

[209] W. Al-Hussaibi, and F. Ali, "Receive Antenna Selection for Uplink Multiuser MIMO Systems over Correlated Rayleigh Fading Channels," *Proc. 14th WPMC'11*, Brest, France, pp. 388-392, 3-7 October 2011.

[210] M. McKay, I. Collings, and A. Tulino, "Achievable Sum Rate of MIMO MMSE Receivers: A General Analytic Framework," *IEEE Trans. Inform. Theory*, vol. 56, no. 1, pp. 396-410, Jan. 2010.

[211] Z. Wu, and X. Wang, "A New Symbol-Alphabet-Aware Multi-User Detection Scheme," *IEEE Commun. Letters*, vol. 10, no. 8, pp. 582-584, Aug. 2006.

[212] Y. Chun, and S. Kim, "Log-Likelihood-Ratio Ordered Successive Interference Cancellation in Multi-User, Multi-Mode MIMO Systems," *IEEE Commun. Letters*, vol. 12, no. 11, pp. 837-839, Nov. 2008.

[213] B. Zarikoff, J. Cavers, and S. Bavarian, "An Iterative Groupwise Multiuser Detector for Overloaded MIMO Applications," *IEEE Trans. Wireless Commun.*, vol. 6, no. 2, pp. 443-447, Feb. 2007.

[214] F. Vanhaverbeke, M. Moeneclaey, and H. Sari, "DS/CDMA with Two Sets of Orthogonal Spreading Sequences and Iterative Detection," *IEEE Commun. Letters*, vol. 4, no. 9, pp. 289 – 291, Sep. 2000.

[215] H. Sari, F. Vanhaverbeke, and M. Moeneclaey, "Multiple Access Using Two Sets of Orthogonal Signal Waveforms," *IEEE Commun. Letters*, vol. 4, no. 1, pp. 4 – 6, Jan. 2000.

[216] I. Shakya, F. Ali, and E. Stipidis, "Collaborative Space-time Spreading Scheme for Higher than Unity Rate CDMA Downlink," *IET Electronics Letters*, vol. 45, no. 22, pp. 1129-1130, Oct. 2009.

[217] F. Ali, and I. Shakya, "Collaborative Spreading for the Downlink of Overloaded CDMA," *WILEY Wireless Commun. Mob. Comput.*, vol. 10, no. 3, pp. 383 – 393, Mar. 2010.

[218] I. Shakya, F. Ali, and E. Stipidis, "High User Capacity Collaborative CDMA," *IET Commun.*, vol. 5, no. 3, pp. 307-319, Feb. 2011.

[219] W. Al-Hussaibi, and F. Ali, "Generation of Correlated Rayleigh Fading Channels for Accurate Simulation of Promising Wireless Communication Systems," *Submitted in May 2011 to Elsevier: Simulation Modelling Practice and Theory, Revised in Nov.2011.*

[220] W. Al-Hussaibi, and F. Ali, "Fast Receive Antenna Selection for Spatial Multiplexing MIMO over Correlated Rayleigh Fading Channels," *Submitted to Springer: Wireless Personal Communications, Sep. 2011.*

[221] W. Al-Hussaibi, and F. Ali, "Low Complexity Receive Antenna Selection for Uplink Multiuser MIMO Systems over Correlated Rayleigh Fading Channels," *Submitted to IEEE Transaction on Vehicular Technology, Sep. 2011.*